A multi-proxy approach to reconstructing palaeoenvironmental change at Kilombe, Central Rift Valley, East Africa

Sally Hoare

Thesis submitted in accordance with the requirements of the University of Liverpool for the degree of Doctor of Philosophy. I declare that the content of this thesis is my own work and that it has not been submitted for examination at any other university.

24th March 2015

Sally Hoare

Abstract

Linking climate and evolutionary change within the hominin lineage relies on the production of higher resolution records from sites which preserve hominin fossil and/or archaeological occurrences. The Acheulean site of Kilombe in the Central Rift Valley, Kenya is one of the largest handaxe sites in Eastern Africa; its immediate area is now shown to preserve a continuous sedimentary record from the early Pleistocene through to the Holocene. The main Acheulean occurrences at Kilombe date to about one million years, and are preserved in less than one metre of sedimentation. However, renewed research since 2008 has identified a recurring human presence with handaxes found in other parts of the sequence, along with Middle and Later Stone Age materials from late Pleistocene and potentially Holocene deposits.

This thesis presents a record of palaeoenvironmental change extending from 1.07 to 0.487 Ma and coeval with the Acheulean occurrences at Kilombe. A multi-proxy approach was taken here to investigate the nature and impact of both long-term trends of environmental change and those occurring on shorter timescales over a 500,000 year period. The techniques of environmental magnetism and desktop-based major and trace element geochemistry were adopted as a rapid, non-destructive approach which require only small amounts of sample for analyses making them ideal proxies from which to examine environmental change over a long time period with little expense incurred.

A long-term record of environmental change is revealed from the Kilombe sedimentary sequences based on geochemical and magnetic proxies sensitive to chemical weathering intensity and pedogenesis. Overall, results reveal a long-term increasing trend in aridification/cooling at Kilombe throughout the Pleistocene with substantial variability

superimposed upon this trend linked to a range of environmental processes including dissolution and volcanic activity. This research now provides a general environmental setting for the major Acheulean occurrences at Kilombe.

Acknowledgements

I would firstly like to thank my supervisors Professor John Gowlett and Dr Fabienne Marret-Davies for their support, advice and encouragement over the last four years, and for all their help with fieldwork and grant applications. Without their help I may not have been able to compile this thesis.

I have been given strong direction and much needed guidance help in both laboratory methods and my understanding of the techniques used in this thesis and therefore outstanding thanks is offered to the following staff from the School of Environmental Sciences at the University of Liverpool: Dr Jan Bloemendal, Dr John Boyle, Professor Jim Marshall, Professor Frank Oldfield, Dr Elisabeth Rushworth and Professor Ian Stanistreet. I would also like to especially thank Mike O'Connor for all his help and training in laboratory techniques especially in the environmental magnetism laboratory.

I would like to strongly acknowledge National Kenya Museums and the National Council of Science and Technology, Kenya and would also like to thank all members of the Kilombe research team for various forms of advice and assistance in the field, Dr Stephen Rucina, Dr Isaya Onjala, Dr Andy Herries and Dr James Brink. Thanks is also owed to Dr Darren Mark and Dr Leah Morgan from the Scottish Universities Environmental Research Council for all their help and advice on geochronology work.I would also like to thank Jason Hall from the University of Liverpool and Dr Laura Basell from Queens University Belfast for help in the field and with sampling.

I would also like to thank my family for continued support throughout this PhD, and the following postgraduate research students from both archaeology and geography for providing friendship, continued support, suggestions and advice throughout my time a research student; Sam Cook, Peta Bulmer, Joey Gaynor, Shirley Curtis, Jonty Trigg, Pablo Fernandez-Reyes, Pete Norris, Jo Ball, Rachael Lem, Karen Halsall, Chris Oldknow and Onema Odojoh.

I would finally like to thank the Arts and Humanities Research council for financial support for this PhD studentship.

	Table of Contents	
Abstract		2
Acknowledgements		4
Table of Contents		5
List of Figures		12
List of Tables		14
Bibliography		224-237
List of Appendices		238-277
Appendix 1 Environmental magnetism		238
Appendix 2 Major and trace element geochemistry		251
Appendix 3 Loss on Ignition		269
Appendix 4 Granulometry		273
Chapter One Climate and Human evolution		15-23
1.1 Introduction		15
1.2 Cenozoic Climate		17
1.2.1 Linking climate and evolutionary change		17
1.3 Climate forcing and evolutionary theory		19
1.4 Testing extrinsic theories of hominin evolution		20
1.5 Summary and key points for development		21
1.6 Aims and approaches		22
Chapter Two – The context for previous palaeoenvironmental studies in East Africa		24-43
2.1 Introduction		24
2.2 East African Rift System		24
2.3 Previous palaeoenvironmental and palaeoclimate studies from East Africa		28
2.3.1 Palaeoclimate studies		29
2.4 Current approaches to climate and evolutionary theory		32
2.4.1 The Turnover Pulse Hypothesis		33
2.4.2 Variability Selection Hypothesis		34
2.4.3 The Pulsed Climate Variability hypothesis		35
2.4.4 The Accumulated Plasticity Hypothesis		36

2.5 Examining environmental change at the local level		37
2.5.1 Hominin habitats		37
2.5.2 Orbital forcing		38
2.5.2.1 Hadar		38
2.5.2.2 Olduvai Gorge		39
2.5.2.3 Turkana Basin		40
2.5.2.4 Chemeron Formation & Elmenteita		40
2.5.2.5 Olorgesaille		41
2.6 Summary and conclusions		42
Chapter Three Theory and Methodology		44-71
3.1 Introduction		44
3.2 Environmental magnetism and climate reconstruction		44
3.3 Magnetic Force and Behaviour		44
3.4 Mineral Grain size and Domain Structures		45
3.5 Common Magnetic Minerals		48
3.6 Magnetic Parameters		50
3.7 Environmental magnetism and palaeoclimate		51
3.7.1 Deposition & alteration		53
3.8 Chemical weathering indices		55
3.8.1 Chemical weathering indices selection		55
3.8.2 Chemical Index of Alteration		57
3.8.3 Ruxton Ratio		57
3.8.3 CaO/Al		57
3.9 Parent material and changes in provenance		58
3.10 Sediment grain size		58
3.11 Soil forming Factors Jenny (1941		59
3.11.1 Time		60
3.11.2 Relief		60
3.11.3 Parent material		61
3.11.4 Climate		62
3.11.5 Summary		63
3.12 Sampling and provenance		64
3.13 Laboratory methodologies		64
3.13.1 Environmental magnetism		67
3.13.2 Particle size separation		67

3.13.3 XRF analysis		68
3.13.4 Organic matter content analysis (Loss on ignition)		68
3.13.5 Grain size analysis		69
3.14 Statistical analysis		70
3.14.1 Principal component analysis and Pearsons correlation matrix		70
3.14.2 Linear regression analysis		70
Chapter Four Site and study area		72-99
4.1 Introduction		72
4.2 Study area		72
4.2.1 Climate setting		73
4.2.2 Local geological setting		73
4.2.3 Environmental setting		74
4.2.4 History of research		76
4.2.5 Archaeology and Fauna		76
4.2.6 Previous geological and palaeoenvironmental work		77
4.3 New stratigraphic and chronological framework		81
4.3.1 Stratigraphy		81
4.3.2 Facies analysis		93
4.3.3 Establishing chronological controls at Kilombe		95
4.3.3.1 Age depth models		95
4.4 Model of soil/sedimentation and accumulation at Kilombe		95
4.4.1 Autogenic factors		96
4.4.1.1 Time		96
4.4.1.2 Relief		97
4.4.1.3 Climate		98
4.4.1.4 Parent material		98
4.5 Conclusions		99
Chapter Five Major and trace element geochemistry		100-137
5.1 Introduction		100
5.2 Major and trace element geochemistry and mineralogy		100
5.2.1 Statistical analysis		104

5.2.1.1 Pearson’s correlation matrix		105
5.2.1.2 Principal component analysis		106
5.3 Mineralogy		112
5.4 Results stratigraphical variation		117
5.4.1 Lithological units		118
5.4.2 Major and trace element data summary		120
5.4.3 Burial diagenesis		120
5.5 Evaluation of chemical weathering indices		120
5.5.1 Source rock		121
5.5.2 Petrology and mineralogy of Kenya trachytes and trachyphonolites		124
5.5.3 Ti wt % values and source rock composition		124
5.5.4 Ti wt % vs chemical weathering indices		125
5.5.6 Bi-plot Ti versus Al and ratios of (Al/Ti and Ti/Al)		125
5.5.7 Bi-plot Ti versus Zr & Ti/Zr ratio		126
5.5.8 Summary		126
5.6 Immobile element ratios and linear regression analysis		127
5.6.1 Linear regression – provenance		129
5.6.2 Sorting signal (Zr/Rb ratio)		129
5.6.3 Linear regression Zr/Rb		129
5.7 Results - Chemical weathering indices		129
5.7.1 Linear regression analysis of chemical weathering indices		129
5.7.2 Chemical Index of Alteration		129
5.7.3 Ruxton Ratio		133
5.7.4 CaO/Al		133
5.7.5 Chemical weathering indices lithological units		133
5.7.6 Bivariate plot CaO/Al2O3 versus K2O/Al2O3		133
5.7.7 Ternary diagram A-CN-K		134
5.7.8 Summary		135
5.8 Preliminary palaeoclimatic inference		137
5.9 Conclusions		138

Chapter Six Environmental magnetism results		140-188
6.1 Introduction		140
6.2 Magnetic parameters selected		140
6.3 Statistical analysis		141
6.3.1 Inter- relationships among the magnetic parameters		141
6.3.2 Principal component analysis		144
6.3.3 Linear plots		145
6.3.4 Summary		147
6.4 Results - magnetic properties and lithology		147
6.4.1 Plot of Dearing et al., (1997)		164
6.4.2 Summary of results		164
6.5 Sources of fine grained ferrimagnetic magnetite/maghemite		164
6.5.1 Examining the pedogenic origin of fine-grained ferrimagnetic minerals		165
6.5.2 Discussion		166
6.5.3 Volcanic activity		166
6.5.4 Detrital signal or dissolution		167
6.6 Particle size separation		168
6.6.1 Sample selection		168
6.6.2 Results		169
6.6.3 Particle size distribution of the soils and sediments		169
6.6.4 Particle-size specific mineral magnetic measurements		179
6.6.5 Magnetite reduction		180
6.6.6 The loss of the fine grained ferrimagnetic component		180
6.6.7 Sediment accumulation rates		182
6.6.8 Summary of the results of particle-size specific magnetic properties		183
6.7 Paleoclimate signal		184
6.7.1 Results χ_{FD}% and χ_{ARM}/χ_{FD}		184
6.7.1 Long-term trends in χ_{FD}% and χ_{ARM}/χ_{FD}		185
6.7.2 Possible climatic significance of χ_{FD}% at Kilombe		185
6.8 Conclusions		187

Chapter 7 A multi-proxy approach to examining palaeoenvironmental change at Kilombe		189-218
7.1 Introduction		189
7.2 Limitations of context and techniques		190
7.3 A multi-proxy approach		191
7.3.1 Soil forming factors of Jenny (1941		191
7.3.2 Examining the evolution of Quaternary environments at Kilombe		192
7.3.2.1 Geological evolution		192
7.4 Long-term trends of palaeoclimate change at Kilombe		193
7.4.1 Palaeoclimate studies East African Rift System		198
7.4.2 Sediment accumulation rates		199
7.4.3 Pedogenesis and rates of sediment accumulation		200
7.5 Local environments at Kilombe		201
7.5.1 Depositional environments		201
7.5.2 Kilombe Main site		202
7.5.3 Farmhouse Cliff		205
7.5.4 Summary		209
7.6 Discussion		212
7.6.1 Introduction		212
7.6.2 East African aridification trend		212
7.6.3 Mid Pleistocene Revolution and climatic variability 1.1 – 0.7 Ma		214
7.6.4 Identifying selective pressures from local sequences		215
7.6.5.1 Directional change or variability selection		217
Chapter 8 Conclusions and future directions		219-223
8.1 Conclusions		219
8.2 Future directions		222

	LIST OF FIGURES	
Figure 2.1 Schematic figure taken from Potts (2013) showing periods of both high and low climatic variability along with a synthesis of paleoclimate and human evolution over the past 7 million years		32
Figure 3.1 a individual stratigraphic units for Kilombe main site		66
Figure 3.1 b individual stratigraphic units for Kilombe farmhouse cliff		66
Figure 4.1 Topographical maps of Kilombe in relation to other Plio-Pleistocene volcanoes and the Mau escarpment and Aberdares		74
Figure 4.2 Local topographical map of Kilombe in relation to main drainage lines and other geological features		75
Figure 4.3 Original stratigraphic column, Bishop (1978		78
Figure 4.4 Map of Kilombe main site (Gqjh1) in relation to Kilombe Volcano		79
Figure 4.6 (a – g) Stratigraphy at Kilombe main site and Farmhouse Cliff with key stratigraphic and dating marker horizons		85-88
Figure 4.7 Stratigraphic section with age determinations for the Kilombe sequence		89
Figure 4.8 (a) Age-depth model for the Kilombe sedimentary sequence based on $^{40}Ar/^{39}Ar$ dates		94
Figure 4.8 (b) Age-depth model for the Kilombe sedimentary sequence based on $^{40}Ar/^{39}Ar$ and palaeomagetic dates		94
Figure 4.9 Distance (kilometres) and altitudinal differences (metres) between Kilombe main site and Kilombe volcano		97
Figure 5.1 Principal component loading plot showing the distribution of major and trace elements for Kilombe across PC1 and PC2		104
Figure 5.2 a Stratigraphical variation of major elements for the Kilombe sequence		107
Figure 5.2 b Stratigraphical variation of trace elements for the Kilombe sequence		108
Figure 5.3 Bivariate plot of Ti versus Al		122

Figure 5.4 Bivariate plots (linear regression) of Ti versus chemical weathering indices		123
Figure 5.5 Bivariate plot of Ti versus Zr		126
Figure 5.6 Linear regression analysis of Ti/Zr ratio to chemical weathering indices		127
Figure 5.7 Linear regression analysis of Zr/Rb ratio to chemical weathering indices		128
Figure 5.8 Linear regression analysis of chemical weathering indices		131
Figure 5.9 Chemical weathering indices, immobile element ratios, loss-on-ignition and mean grain size for the Kilombe sequence to depth		132
Figure 5.10 Bivariate plot of CaO/ Al_2O_3 versus K_2O/Al_2O_3		134
Figure 5.11 Ternary A-C-K diagram		135
Figure 6.1 Principal component loading plot showing the distribution of magnetic parameters and interparametric ratios for Kilombe across PC1 and PC2		145
Figure 6.2 Linear regression analysis of χ_{LF} versus χ_{FD} and $\chi_{FD}\%$		146
Figure 6.3 Mineral magnetic parameters and interparametric ratios to depth		148
Figure 6.4 Plot of Dearing *et al*., (1997) showing $\chi_{FD}\%$ versus $\chi_{ARM/}$SIRM for the Kilombe sequence		162
Figure 6.5 Plot of Oldfield (1994) showing χ_{ARM}/χ_{LF} versus χ_{ARM}/χ_{FD} for the Kilombe sequence		163
Figure 6.6 (a) Weight percent totals for each individual grain size per sample		170
Figure 6.6 (b) χLF measurements for each particle size fraction for the Kilombe samples		171
Figure 6.6 (c) χFD measurements for each particle size fraction for the Kilombe samples		172
Figure 6.6 (d) HIRM measurements for each particle size fraction for the Kilombe samples		173
Figure 6.6 (e) SIRM measurements for each particle size fraction for the Kilombe samples		174
Figure 6.6 (f) χARM measurements for each particle size fraction for the Kilombe samples		175

Figure 6.6 (g) -300mT measurements for each particle size fraction for the Kilombe samples		176
Figure 6.6 (h) -300mT measurements for each particle size fraction for the Kilombe samples		177
Figure 7.1 a Chemical weathering indices and age depth model for the Kilombe sedimentary sequence		196
Figure 7.1 a Loss-on-ignition, $\chi_{FD\%}$ and χ_{FD}/χ_{ARM} and age depth model for the Kilombe sedimentary sequence		197
	LIST OF TABLES	
Table 4.1 Individual descriptions of units and facies association for the Kilombe sediments including lithology, thickness, colour, mean grain size and loss on ignition % values		83-84
Table 5.1 Pearson's correlation matrix showing the association of major and trace elements at Kilombe		103
Table 5.2 a Major element data for each lithological unit for the Kilombe sedimentary sequence		109
Table 5.2 b Trace element data for each lithological unit for the Kilombe sedimentary sequence		111
Table 6.1 The magnetic parameters and interparametric ratios used in this part of the study, their units and interpretation		142
Table 6.2 Pearson's correlation matrix showing the association of magnetic parameters and interparametric ratios		143
Table 6.3 Average and ranges for magnetic parameters and interparametric ratios for each lithological unit for the Kilombe sequence		149

Chapter One Climate and human evolution

1.1 Introduction

This thesis focuses on the production of a record of palaeoenvironmental change from the Acheulean site of Kilombe, Kenya using a multi-proxy approach (environmental magnetism and major and trace elements geochemistry). This thesis further aims to establish the relationship between this record and other East African records of climate change ca. 1 million years ago, which is an important time frame in hominin evolution.

Climate driven environmental change is considered to have played a key role in the evolution of the hominins from both a biological and behavioural perspective (Potts, 2013). It is however often difficult to examine casual relationships due to the lack of well-dated and high-resolution environmental records that are in direct association with empirical fossil and archaeological data. The archaeological and fossil records of East Africa during the Plio-Pleistocene document major evolutionary changes in the hominin lineage both behaviourally and biologically which include the first appearances of both genera *Homo* and *Paranthropus,* the origins of lithic technology, Oldowan and Acheulean, and the first archaeological sites, significant brain expansion, the dispersal of the hominins into Eurasia, the earliest evidence for the butchery of large mammals and morphological and thermoregulatory adaptations for endurance running (Plummer, 2004). Many of these traits can be linked to climate change, more specifically heightened climatic variability or adaptations to more open environments under progressive and directional climate change (Cerling *et al.,* 1992; Hopley *et al.*, 2007; Potts, 2013; Maslin *et al.,* 2014). One problem in examining causal relationships between evolutionary and climate change, is that most of the available climate data that are either finely resolved in terms of resolution and chronologically come from sources external to the palaeontological and/or archaeological data e.g. marine cores or lake sequences from the Rift Valley lake basins (Potts, 2013). This thesis therefore aims to examine the impact of environmental change at a more local level, by providing a record from the sedimentary sequence at the Acheulean site of Kilombe. Over the last decade the number of climate records produced from archaeological and palaeontological sites has significantly increased and climate and/or palaeoenvironmental records now exist for some key archaeological and fossil hominin sites in East Africa e.g. Olorgesaille, Olduvai, Turkana Basin and Hadar (Owen *et al.*, 2013; Ashley, 2007; Joordens *et al.,* 2011; Campisano & Feibel, 2007). However, these records are generally low-resolution (20-40 cm sampling intervals), often composite and discontinuous or only provide a snapshot of climate e.g. cover short time frames 100,000 – 150,000 Ka. Whilst some of these records are useful for capturing the nature of long-term trends in African climates (Owen *et al.*, 2014), or the nature of orbital forcing and their influence on hominin evolution over shorter time periods (Ashley, 2007), these records rarely capture, over a long-timescale, the nature of both long and short-term trends in climatic variability. Currently, to our knowledge, there are no high resolution records from East African hominin sites that document the nature of both long and short-term episodes of palaeoclimatic/palaeoenviromental change where either both fossil and archaeological occurrences are present. This now demonstrates a need to produce data at a higher resolution in order to further demonstrate causal relationships between evolutionary change and climatic variability at different timescales.

1.2 Cenozoic climate

Changes in African palaeoclimates during the Cenozoic are controlled by a number of processes acting on different timescales, from geological through to millennial scale and decadal, all of which are important in terms of human evolution (Kingston, 2007). Changes in characteristics of the environments where hominins evolved in Africa represent the complex interaction of global climate transitions, changes in tectonics and faulting and local variation in orbitally forced climate change (Maslin & Christensen, 2007). Climatic variability during the Cenozoic, and more specifically the Quaternary, documents both long and short term trends. Occurring on the longest timescales i.e. millions of years and over the longer-term a trend in global cooling is documented which in Africa resulted in more arid conditions, especially in East Africa over the Cenozoic (Kingston, 2007). The expansion and contraction of ice sheets in the Northern Hemisphere linked to orbital forcing were critical in controlling atmospheric circulation hence palaeoprecipitation, and therefore, both the timing and intensity of cycles of aridity and humidity on the African continent. These cycles would have influence the distribution of water and resource availability and created ecological pressures and thus changes in hominins both genetically and behaviourally. Heinrich and El Niño Southern Oscillation like events occurring on much shorter timescales i.e. millennial, centennial and possibly decadal, may have influenced demographics and local extinctions (Kingston, 2007; Maslin & Christensen, 2007).

1.2.1 Linking climate and evolutionary change

The fossil and archaeological records for the hominins is extensive in Africa relative to other lineages e.g. non-human primates. Fossil data are however often spatially and temporally fragmentary, which is also often the case for the environmental context in which they are found. In terms of examining causal relationships between evolutionary and climate change it has been necessary, due to the lack of well-dated continuous terrestrial records in Africa, to examine evolutionary change based on long-term trends of palaeoclimatic change from either global or regional records.

The importance of orbital forcing as a major global driver of climate change has been recognised since the late 1960's (Shackleton, 1967; Emiliani, 1966; Hays *et al.*, 1976). Originally documented from the isotopic analyses of deep-sea cores, oscillations between glacial and interglacial climates are one of the major environmental characteristics of the Quaternary. Forced by changes in the orbital geometry of the earth and variations in earth's orbit due to the gravitational effects of the Sun and other planets, cyclical variations known as Milankovitch cycles are known to occur at regular amplitudes e.g. precession of the equinoxes, which controls seasonality (23 kyr), obliquity or tilt of the Earth, which controls the timing of perihelion and aphelion (41 kyr) and orbital eccentricity around the Sun (100, 400 kyr). Milankovitch cycles affects the amount of solar radiation received by latitude and season, and are therefore the major cause of global, cyclic climate change occurring over the 10 to 100 and 400 thousand year timescales (Hays *et al.*, 1976). From 2.7 Ma – 900,000 Ka, the dominant cycle controlling high latitude forcing of glacial/interglacial cycles is the 41,000 yr obliquity cycle and from 900,000 yr through to present the dominant cycle is eccentricity. However, it is the combination of the different orbital parameters that results in the precessional periodicities of 23,000 and 19,000 years (Maslin & Christensen, 2007).

Data from isotopic analysis from deep-sea cores have been especially pertinent in the recognition of the influence of orbitally forced climate change as a potential driver of evolutionary change (Butzer, 1977; Brain, 1981; Vrba, 1995; deMenocal & Bloemendal, 1995), and the marine core records have been used extensively for this purpose, especially those that serve as a proxy for terrestrial environments e.g. palynology and aeolian dust records (deMenocal, 2004). Data from marine cores generally have a much greater resolution, stronger chronological controls and greater continuity than do terrestrial records; however they do not reveal local conditions especially those in the East African Rift Valley (Rift Valley lake level data will be reviewed in Chapter Two).

The large amplitude climatic variations driven by orbitally forced climate change, recognised from marine core records and lacustrine sequences in East Africa, have however provided data useful to generate models and theories regarding climate and evolutionary change at both continent wide and regional scales (Potts, 2013; Grove, 2011; deMenocal, 2004). These large scale changes have been shown to influence African palaeoenvironments however, due to the lack of localised data it is often difficult to examine the impact of these changes beyond either continent wide or regional scales.

1.3 Climate forcing and evolutionary theory

Climate and environmental change has often been suggested as not only a significant factor but as the primary driving in the evolution of the hominins (Antón, *et al.*, 2014; Maslin *et al.*, 2014; Leroy *et al.*, 2011; Grove, 2011; Potts, 2013). Over the last few decades environmental hypotheses of early hominin evolution have changed focus from theories that predominantly emphasise long-term directional change in habitats e.g. savannah hypothesis (Darwin 1874; Leakey & Harris, 2003) to those that emphasise the role of climatic instability and variability on various timescales (Potts, 1998; Maslin *et al.*, 2014; Grove, 2012; 2014). Theories that emphasise long-term directional change in habitat reconstruction such as the savannah hypothesis are often examined using data gleaned from static habitat reconstruction for individual species, whereas those that emphasise climatic variability utilise climatic data that document trends regionally and globally from marine, speleothem and lacustrine (Maslin *et al.*, 2014; Trauth *et al.*, 2009; Hopley *et al.*, 2007).

The production of new data sets from the analysis of both marine and lake sediment cores in East Africa has caused a major re-evaluation of the relationship between the evolution of the hominins and climate change (e.g. Trauth *et al.*, 2009; Trauth *et al.*, 2010). These data and the theories that utilise them have challenged some of the long-established theories that argued that the dominant environments of early hominin evolution were savannahs or that human evolution was directly being driven by increases in episode of aridity (Vrba, 1995; Reed, 1997; Lee-Thorp *et al.*, 2007). Theories that have been developed since the mid to late 1990s are now in direct contrast to these earlier theories and it is now suggested that the environments of early hominins were constantly shifting driven primarily by orbitally forced climate change. Recent and current research now focuses on how environmental variability driven by climate processes enacting on a number of different timescales, including orbital and suborbital, may have influenced hominin evolution. The main competing theoretical models attempting to explain the external role of climate change and hominin evolution, along with a review of the climate data currently used to support them, will be provided as context in the next chapter.

1.4 Testing extrinsic theories of hominin evolution

Extrinsic theories on the evolution of the hominins (which will be reviewed in Chapter two), have been tested using a variety of approaches and climate data from sources both external and internal to palaeoanthropological and/or archaeological data (Grove, 2011; 2012; Reed, 1997; Faith & Behrensmeyer, 2013). The main sets of climate data used in testing the theories above come from a number of different sources including aeolian dust records, east African lacustrine sequences, benthic oxygen isotope records, stable carbon isotope data from pedogenic carbonates and faunal assemblages; molecular plant biomarkers, pollen, and the Eastern Mediterranean sapropels (deMenocal & Bloemendal, 1995; Trauth *et al.*, 2009; Lisieki & Raymo, 2005; Kingston, 2007; Feakins *et al.*, 2013; deMenocal, 2004). However, the majority of data coming from archaeological or fossil sites are generally either low-resolution or discontinuous in nature and therefore do not always offer a complete view or interpretation of environmental change over time on a more localised scale.

This thesis represents an effort to grapple with two problems by examining how far the impact of changes in both regional and local climates can be evaluated from research into a specific long-term sedimentary sequence, at a local level, at the archaeological site Kilombe in the Central Rift Valley Kenya. The record covers the time periods 1 Ma – 500,000 Ka which is an important time frame for hominin evolution. This thesis does not aim to examine any impact archaeologically of climate change.

1.5 Summary and key points for development

There is an increasing need to understand the climatic processes and environmental drivers of hominin evolution both behaviourally and biologically. However, this is contingent on the production of high-resolution and well dated palaeoenvironmental records. Changes in climate at both a global and regional scale can result in more localised changes in palaeohydrology and palaeovegetation which are likely to influence selective forces whether through directional change or plasticity in terms of speciation, migration and extinction but also in terms of technological change and diversity and encephalisation.

Whilst there is now strong evidence that the most critical events in hominin evolution are associated with periods of prolonged climatic variability and instability, Potts (2013) identifies three reasons that precludes this being taken has a firm conclusion;

- that first and last appearance dates are likely to change and future fossil discoveries may alter the environmental context in which certain species are now located;
- that taphonomic biases, time-averaging and discontinuous sequences can results in difficulties in testing for exact associations between climate change and evolutionary events;
- the essentiality in testing whether climate signal predicted by models, in this case the high/low variability model, are actually recorded as landscape variability in sedimentary basins and strata where evidence of hominin populations are found.

1.6 Thesis aims and approaches

A major current need is to therefore focus on the production of records that provide more detailed characterisation of changing hominin palaeoenvironments over long-time periods and from continuous sequences in order to examine selective pressures in terms of localised changes. These records must come from palaeontological and archaeological sites, rather than externally, in order to more accurately assess the effects of palaeoclimatic change on hominin populations.

This thesis does this by providing a continuous record of environmental and landscape scale changes at the site of Kilombe which will be used to further identify any potential selective pressures on hominin populations at a more localised level. Combined with new age determinations for the Kilombe sedimentary sequence, a multi-proxy approach was taken using geological proxies for precipitation and/or temperature (environmental magnetism and X-Ray fluorescence) in order to investigate the potential effect of climate/environmental change via changes in chemical weathering intensity and pedogenesis. This thesis has three main aims:

1/ to examine, locally, the impact and nature of any long-term trends of environmental change, i.e. the East African aridification trend over 500,000 years at Kilombe;

2/ to examine whether any localised impact of major regional and global climate changes can be identified across the time frame of the study and specifically surrounding the Acheulean occurrence on Kilombe main site i.e. 1.1- 0.9 Ma;

3/ to further examine whether selective pressures occurring on shorter time scales including (climate and volcanism) are apparent in the Kilombe sequence.

4/ to test the potential of geological proxies, environmental magnetism and major and trace element geochemistry as a novel approach to examining palaeoenvironmental change on East African hominin sites.

Chapter Two - The context of previous palaeoenvironmental studies in East Africa

2.1 Introduction

The rich fossil and archaeological record of East Africa is more widely researched than other regions of Africa due to a unique combination of factors. The geological history of the East African Rift System (EARS), faulting and erosion, provides the exceptional opportunity in terms of creating long exposures of sedimentary and lacustrine sequences from the Miocene through to the Holocene. Volcanic deposits and materials within EARS sedimentary sequences permit the application of geochronological techniques such as $^{40}Ar/^{39}Ar$ which enables precise age determinations to be established through long stratigraphic sequences containing palaeontological and archaeological remains. In terms of chronology, the East African record is more finely resolved, temporally, in terms of research into both biological and behavioural adaptation and changes than anywhere else continent wide and beyond. Proxies of palaeoenvironmental and palaeoclimate change are also recorded within these stratigraphic sequences which enables the reconstruction and assessment of both climate dynamics and habitat variability on a range of timescales important for hominin evolution.

2.2 East African Rift System

An understanding of sedimentary stratigraphy and geology is extremely important for a complete understanding of site taphonomy, chronology and palaeoenvironmental reconstruction. There are many reservations that arise over the exact timing and stratigraphic correlation of archaeological events and hominin fossils continent wide. However, the underlying geology and volcanics of East African sites generally offer the chance to resolve continent wide debates on the timing and correlation of archaeological and morphological changes in *Homo* and other hominin lineages. Stratigraphy in EARS can be highly complex due to the complex nature of rift faulting and erosion. Many stratigraphic sequences contain sedimentary hiatuses and/or erosional disconformities and unconformities. In terms of classification, sedimentary sequences in East Africa are generally categorised geologically according to the international stratigraphic guide. Units are generally classified into formal lithostratigraphic units in terms of conventional hierarchy and in the following order i.e. group, formation, member, bed and flow.

Establishing a precise chronology for East African fossil and archaeological sites has proven far less difficult than for South African counterparts due to the abundance of volcanic materials suitable for $^{40}Ar/^{39}Ar$ dating. The two most commonly used dating methods are palaeomagnetism and K/Ar and $^{40}Ar/^{39}Ar$ single crystal laser fusion. Absolute ages for East African sediments are now constrained by the use of mainly $^{40}Ar/^{39}Ar$ of interbedded volcaniclastic sediments and tuffs. New age determinations for a number of sites including Olduvai Gorge and the Olorgesailie Formation have further constrained the dating of key fossils and archaeological horizons and of Plio-Pleistocene climate and palaeoenvironmental change (Deino *et al*., 2006).

The East African rift system occurs as part of series of individual tectonic basins known as rift valleys which are separated from each other by relative shoals and bordered by uplifted shoulders (Chorowicz, 2005). The individual rift valleys form two main lines, the eastern and western branches of the EARS. The eastern branch of the EARS runs over a distance of 2200 km from the Afar triangle, through the Ethiopian rift, Omo-Turkana, the Kenyan Rift and then ends in the basins of the North Tanzanian divergence in the South (Chorowicz, 2005).

The western branch runs over a distance of 2100 km from the north at Lake Albert to the south to Lake Malawi. These successions of graben basins are bordered by high relief in the form of parallel mountain lines and plateaus. The Eastern and western rift branches are both distinct in terms of their individual igneous activity and overall morphologies. The eastern branch can be characterised by extensive volcanism which is surrounded by a broad regional geological feature the Kenya Dome. Volcanic activity in the western branch is scattered and is not surrounded by any major regional plateau. It has been suggested that the differences in volcanic activity and uplift may be related to the way in which the mantle plume is channelled underneath East Africa (Ring, 2014).

In the Eastern branch the Afar triangle occurs between the triple junction of the African, Arabian and Somalian plates. It is floored by both Miocene volcanic rocks dated to 24 to 5.4 Ma and Quaternary volcanic rocks (Baberi *et al*., 1972). In general, elevations are low with some occurring under sea level. In the Afar triangle only the southern half fully belongs to the EARS. The Somalian plateau which lies to the south of the Afar is bounded on the north west by a crest line at an elevation of 3000 m. This plateau then downgrades to the south east. The western site of the Afar is the Ethiopian plateau at elevations of 3600 m. A major depression occurs which comprises a continuous Pliocene to Quaternary rift for around 600 km in the western margin of the Afar. The Afar is suggested to have formed through three major tectonic events from the Miocene, Pliocene through to the Quaternary. The morphology of the Ethiopian plateau differ from the Somalian plateau major shield volcanoes occur and 1000 m thick volume of volcanic rocks. Higher elevations occur especially in the Lake Tana region. The elevations in the Ethiopian plateau are related to uplift forming the Tana dome (Chorowicz, 2005).

The main part of the Ethiopian rift is connected to the southern corner of the Afar triangle. The Ethiopian rift is around 330 km in length and 50 km wide. Elevations are around 700 km in the north east and increase to 1700 m towards the south west. In general, the graben basins in the Ethiopian rift are filled in with lava flows and evaporites with some detritic sediments. The main Ethiopian rift is bordered by two crest lines which overlook the rift valley floor. On the western side elevations of the crest lines vary between 1800 and 3300 m whilst on the eastern side they are between 2500 and 3000 m. The wonji Fault Belt which is a narrow fault zone crosses the main Ethiopian rift from the north to the south (Chorowicz, 2005).

The Ono-Turkana region is characterised by low elevations sometimes as low as 400 m. Thw low areas have no pronounced rifts but a number of north and north east half graben basins occur specifically around Lake Turkana and Chew Bahir. The half graben basins are filled with sediments belonging to the late Cenozoic and the earliest of these basins was formed in the late Oligocene and early Miocene times (Ring, 2014).

The Kenyan (Gregory) rift occurs as part of the eastern branch of EARS and corresponds to the Kenyan dome. The area is dominated by three major volcanoes Elgon at 4321 m, Kilimanjaro at 5964 m and Kenya at 5200 m. The northern Kenya rift is composed of two parallel rift valleys which are at 1050 m elevation. The eastern one extends from the southern part of the half-graben at Lake Turkana whilst the other rift ends at Lake Bogoria. They both have major faults along the western shoulders. The central Kenyan rift begins at the southern end of the northern Kenyan rift valley at the same latitude as Lake Bogoria. The central rift has elevations of more than 3700 m in the eastern side and 3000 m on the western side. On the floor of the central rift elevations rise from 1050 m in the north to

2100 m in the middle and down to 600 m southwards at Lake Natron. Chronology of the formation of the Kenyan rift comprises a number of time periods ranging from 23 to 1.6 Ma (Chorowicz, 2005).

Volcanism in the EARS in the Cenozoic was widespread in the eastern branch. In general, the volcanoes are rooted on open fractures however, volcanoes such as Mount Kenyaare off-axis. Magmas are alkaline to hyperalkaline and have generally evolved from continental tholeiites through alakali to transitional magmas. Magmatism is linked with astehnopsheric ascent. The plume responsible for volcanism in the EARS occurs earliest in Lake Tana and may have migrated southward. Volcanism first began during the Oligocene in the Ethiopian zone at around 30 Ma. In the southern Afar region a number of other volcanic events have been shown to have occurred at 14-11, 11-10, 9-7, 5-4 and after 1.6 Ma. In the northern Kenyan rift in the Oligocene basalts and rhyolites erupted at 33-25 Ma followed by phonolites and nephenlinites 26-20 Ma, hyperalkaline basalts also occur at 15 Ma. In the early Pliocene, trachytic, phonolitic, nephelinitic and basaltic volcanism occurs whilst in the late Pliocene and Quaternary volcanism was mainly trachytic in the rift valley floor and basaltic to the east. Between 20 and 16 Ma Samburu flood basalts erupted in the central Kenyan rift followed by trachytic and phonolitic eruptions between 5 and 2 Ma (Chorowicz, 2005).

2.3 Previous palaeoenvironmental and palaeoclimate studies from East Africa

Numerous investigations on the palaeoenvironments of East African hominin sites during the Plio-Pleistocene have been undertaken. These data fall into three categories: those which serve as a proxy for palaeoclimatic change and capture regional and global changes, those which are primarily concerned with habitat reconstruction, mainly palaeovegetation, and those which focus on palaeoclimatic processes and document more localised conditions from hominin sites.

2.3.1 Palaeoclimate studies

One archive of palaeoclimatic change pertinent to East Africa is the marine core record. These archives, specifically records from the Indian and North Atlantic Oceans, have provided valuable information on the timing of changes in cyclicity (deMenocal & Bloemendal, 1995; deMenocal 2004) and have also enabled the placing of evolutionary events in a palaeoclimatic framework. DeMenocal & Bloemendal (1995) and deMenocal (2004) laid out an evolutionary framework that argued for the link between increasing aridity and early hominin speciation events (*Homo* and *Paranthropus*) which was largely based on analysis of terrigenous dust input to North African marine cores and East African deep sea cores. Both studies documented substantial increase in dust production at 3 – 2.6 Ma, 1.8 – 1.6 Ma and 1.2 – 0.8 Ma concordant with key events in hominin evolution. The idea of the link between increased aridity and Plio-Pleistocene hominin speciation events was also supported by analysis of $\delta^{13}C$ values from plant wax biomarkers and the tooth enamel of fossil herbivores (Bobe & Behrensmeyer, 2004, Cerling, 1992, Feakins, 2005). More recent research from both Bonnefille (2010) and Feakins *et al.,* (2013) has shown that $\delta^{13}C$ values from plant leaf wax biomarkers are decoupled from changes in the proportion of the percentages of grass pollen and that as changes in $\delta^{13}C$ values change significantly from one time interval to the next showing that it is more likely that palaeovegetation changes are being driven by changes in insolation rather than long-term trends of aridity.

An alternative perspective to that offered by the marine core records in East Africa comes from investigations of lacustrine deposits in the Rift Valley, and there have been a number of comparisons of both marine and terrestrial records relevant to hominin evolution (Trauth *et al.*, 2005; 2007;2009; 2010; Deino *et al.*, 2006; Donges *et al*., 2011; Potts, 2013). Trauth *et al.,* (2005) argued for the link between changes in monsoon driven levels of precipitation under orbital precession and the expansion and deepening of rift valley lakes. These authors documented that large and deep lake level phases occur between 2.7 – 2.5 Ma, 1.9 – 1.7 Ma and 1.1- 0.9 Ma.

Whilst these deep lake-level phases appear to partly correspond with increases in dust fluxes and thus the aridity phases documented by deMenocal (2004), a recent reanalysis of terrigenous dust flux from marine sediments (subtropical west Africa; Arabian Sea, eastern Mediterranean Sea) combined with East African lake level records suggests that this is no longer the case. The results of robust statistical analyses document no statistical link between gradual increases in aridity after the initiation of the Northern Hemisphere glaciations, or the eccentricity modulation (100 kyr) of dust fluxes after 1.0 Ma or any step like increase in obliquity modulation of dust fluxes at 2.8 Ma and 1.7 Ma. Rather, their results show that the key periods in hominin speciation and extinction events are coincident with 400 Ka eccentricity maxima which induce periods of high climatic variability on high moisture levels (Trauth *et al.*, 2009).

A further analysis of terrigenous dust fluxes from marine core archives comes from Donges *et al*., (2011) using non-linear statistics, specifically recurrence network analysis. These authors identify three main epochs of interest in which climate tipping points occur at 3.5 – 3.0 Ma, 2.25 – 1.6 Ma and 1.1 – 0.7 Ma and which further correspond to three distinct causal climate mechanisms (major changes in oceanic circulation, 3.5 Ma, intensification of low-latitude Walker circulation, 1.7 Ma, and the Mid-Pleistocene transition 1.1 Ma. It is argued here that all three episodes are characterised by major changes in ocean-atmosphere conditions and therefore the magnitude and style of wet-dry transitions in Africa.

Potts (2013) presents a new framework towards reconciling the results of different environmental indicators of moisture and aridity (i.e. dust records and lake sediments) which he refers to as high and low climate variability framework. Indicators are combined into an environmental framework which emphasises environmental dynamics over time and identifies periods of alternating high/low climate variability based on eccentricity modulated precession. This model also highlights a number of occasions when periods of relative climatic stability are followed by magnified periods of arid to moist climate oscillations and identifies eight periods throughout the Plio-Pleistocene in which major evolutionary events in the hominin lineage are coeval with periods of high amplitude climate variability. Three of the most prolonged intervals documenting high climatic variability are 2.79 – 2.47 Ma, 1.89 – 1.69 Ma and 1.12 – 0.92 Ma. It is these data and proxy archives that have been used to construct and test the main competing theoretical models examining climate and evolutionary theory.

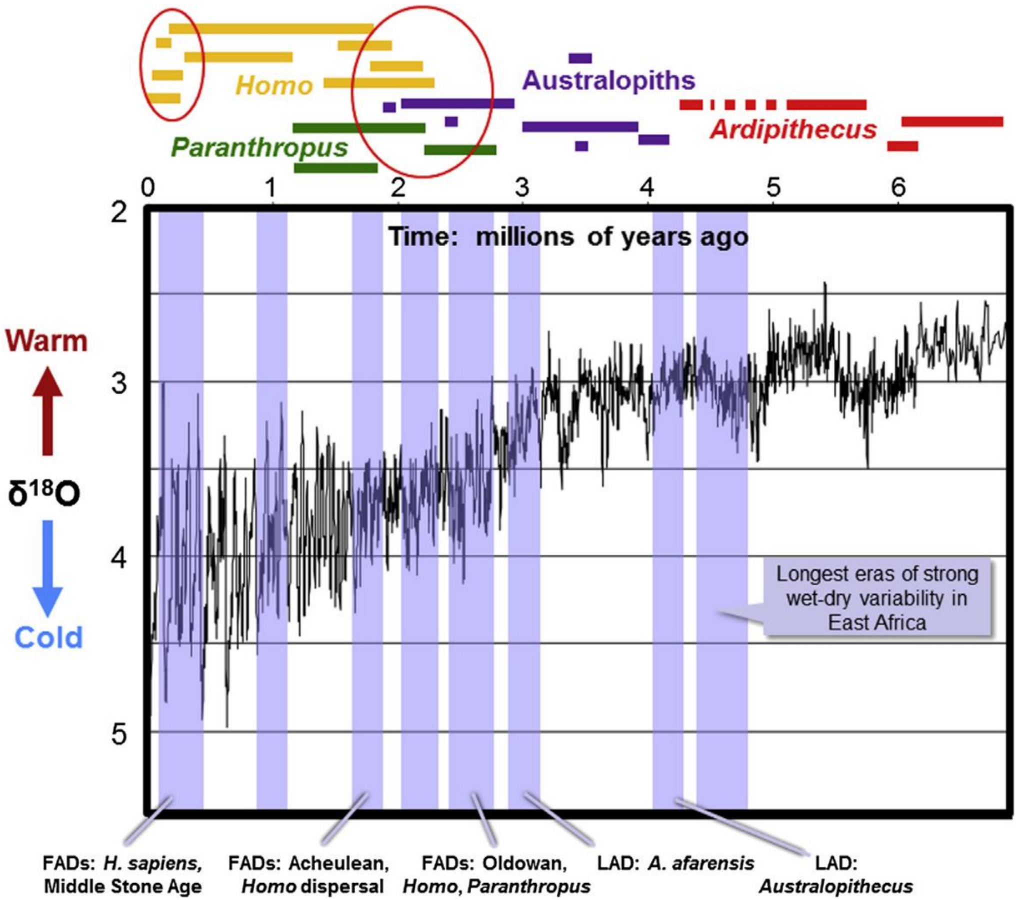

Figure 2.1 Schematic figure taken from Potts (2013) showing periods of both high and low climatic variability along with a synthesis of paleoclimate and human evolution over the past 7 million years.

2.4 Current approaches to climate and evolutionary theory

There are four broad theoretical approaches to examining the role of external climate forcing on the evolution of the early hominins. These are based on/tested with evidence from faunal assemblages, marine and lake-core data.

- The Turnover pulse Hypothesis
- The Variability selection Hypothesis
- The Pulsed climatic variability hypothesis
- The Accumulated Plasticity Hypothesis

2.4.1 The Turnover Pulse Hypothesis

The Turnover pulse hypothesis of (Vrba, 1992; 1997) argues that pulses of macroevolutionary change in lineages of African mammalian fauna occur at times of global cooling, as evidenced in the marine isotope stage record. The term “turnover” is used in a broad sense to include speciation, extinction and migration events that simultaneous increase above background rates due to climate change. Vrba (1997; 1992 and 1995) has tested this hypothesis using data from faunal assemblages, mainly the African bovids and found that a significant period of increased turnover in bovid species occurred 2.5 Ma which is suggested to be in response to the onset of the Northern Hemisphere glaciation (Vrba, 1995). Vrba (1995) further links the onset of the NHG to an increase in the diversity of hominin species and to the appearance of the Oldowan tools which also occur around this time.

The validity of this model was called in to question by Behrensmeyer *et al.,* (1997) who criticised the use of faunal data from South Africa, due to poor chronological controls and taphonomic biases, however further tested this approach and demonstrated that the largest and most significant increase in faunal turnover during the Plio-Pleistocene occurred in Africa between 2.5 and 1.7 Ma. White (1995) also found no evidence for possible turnover pulses in patterns of hominin speciation. The Turnover Pulse hypothesis has been further tested by Grove (2011) and Faith & Behrensmeyer (2013). Faith & Behrensmeyer (2013) have recently tested the Turnover Pulse Hypothesis in South Africa using records of Quaternary ungulates from the Cape Floristic Region combined with sea-level data and palaeovegetation records. These authors found no correlation between speciation and TPH, however results suggested a link between climate change and pulses of migration and extinction within the ungulate lineages.

2.4.2 Variability Selection Hypothesis

The Variability selection Hypothesis of Potts (1996; 1998) of hominin evolution reflects an alternate view of Plio-Pleistocene climate change, to TPH, based on a continuum of climatic fluctuations ranging from millennial scale through to the much longer climatic cycles produced by orbital forcing rather than increased global cooling. This hypothesis suggests that the evolution and adaptation towards generalism in the hominins, or ecological flexibility, is in response to both long and short term climate oscillations such as Milankovitch cycles. Potts (1998) applies this term to account for the evolution of adaptive traits within populations, as they experience highly variable environments over a number of generations. If more than one form of genetic variation would promote reproductive and survival success in any given environment then VS would select for both adaptive traits e.g. one trait may be more advantageous in a new environment whereas a second trait, or genetic variation, would be more advantageous in the previous environment in which it first appeared. Therefore the second trait would survive environmental change and persist in a population over long time scales. Grove (2011) was the first to explicitly test the assumptions of the Variability Selection Hypothesis by demonstrating the genetic basis via allele frequencies using a series of tests from theoretical biology. Grove (2011) identifies the period 2.5 – 1.2 Ma as being concordant with large amplitude changes in climatic variability evident in the benthic oxygen isotope records, and that this variability would be the most crucial phase in human evolution favouring plasticity and versatility. Grove (2011) further demonstrates that between 2.7 – 2.5 Ma climatic variability rather than climatic change would have favoured greater selection for plasticity, or variability selection rather than Vrba (1995) predicted turnover pulse.

2.4.3 The Pulsed Climate Variability hypothesis

The Pulsed Climate Variability Hypothesis of Maslin and Trauth (2009), and Maslin *et al.*, (2014) is a development of both TPH and VSH. This theory highlights the role that short but extreme periods of climatic variability specifically occurring in East Africa may have had on hominin speciation events and hominin evolution in general. These pulses of Maslin & Trauth (2009) refer to short periods of extreme climatic variability, that alternate between the appearance and disappearance of the large and deep Rift Valley lakes which are primarily forced by orbital precession in East Africa. These pulses are however ultimately governed by global climate events such as NGC (2.7-2.5 Ma) the onset of Walker circulation (1.9-1.7 Ma), and the Mid-Pleistocene revolution (1.1-0.9 Ma). Based on data from East African lake records and those documenting high-latitude climate transitions these authors observed that the periods of extreme climatic variability in the late Cenozoic, or pulses, appear to correlate with 400 kyr eccentricity maxima up to 2.7 Ma. After 2.7 Ma wetter but highly variable phases appear every 800 kyr. Three other periods of eccentricity maxima occur during the late Cenozoic however do not correspond to the formation of large-deep lake phases in Africa, these other periods of eccentricity maxima in Africa do not correlate with times of significant global climate transitions leading to the conclusion that major changes at high latitudes are resulting in regional climate sensitivity in East Africa during the Pleistocene. These authors found that the first appearance of 12 out 15 hominin species corresponds to one of these extreme wet/dry periods in Africa, and that the presence of the large ephemeral lakes in the East African Rift Valley coincides with major events or changes in hominin evolution.

2.4.4 The Accumulated Plasticity Hypothesis

The accumulated plasticity model of Grove (2014) tests, via an evolutionary algorithm, the link between temporally unstable environments, the evolution of plasticity and evolutionary dispersals. Grove (2014) argues that whilst many authors have linked climatic variability with behaviour versatility prior to his work there has been no suggestion of links between plasticity and dispersals. The evolutionary algorithm employs latitudinal gradients in temperature and population tolerance ranges and dispersals windows and was run using two different environmental scenarios designed to examine the effects of climate change i.e. patterns of directional change or climate variability i.e. quasi-oscillatory patterns. This approach therefore allows the tracking of the evolution of plasticity and directional selection in a variety of climatic systems. The results suggest that dispersals are most likely to occur when a period of extended high climatic variability is followed by period of low climatic instability. Although tested here in the context of the dispersal of biological organisms the application of this theory is directly relevant to other aspects of early hominin evolution such as brain expansion.

2.5 Examining environmental change at the local level

2.5.1 Hominin habitats

Outside of the major lake basins in East Africa, the majority of data produced for fossil and archaeological sites has mainly been concerned with the reconstruction of hominin habitats via palaeovegetation records. One of the most abundant sources of data comes from $\delta^{13}C$ values from pedogenic carbonates preserved in palaeosols and from the tooth enamel of fossil herbivore assemblages. Both of these proxies enable the relative proportions of C3 and C4 vegetation types to be determined over time. Interpretation of $\delta^{13}C$ values from both these sources are however limited by both the selective feeding of mammalian species and by the sometimes large stratigraphic distances between preserved palaeosol horizons at hominin sites (Kingston, 1999; Kingston, 2007). A further problem, although highlighted in the context of South Africa, is the concept of climate averaging in mammalian faunal assemblages (Hopley & Maslin, 2010) in which many of these assemblages are argued to contain species adapted to different ends of the precessional cycle in one assemblage resulting in misleading palaeoclimatic/palaeoenvironmental interpretations.

These issues aside, existing data sets have proven useful in examining the nature of long-term trends of environmental change in East Africa and generally demonstrate that during the Plio-Pleistocene habitats became less wooded and more open as part of a long-term trend, however habitats were heterogeneous with a mix of both C3 and C4 environments (Plummer *et al.,* 1999; Wynn, 2004; Bobe *et al.*, 2002).

More detailed reconstructions on palaeovegetation changes from hominin sites come from palaeofloral evidence, specifically pollen and phytoliths. Bonnefille (1995; 2010) has provided reviews of palaeovegetation change based on compilations over 100 palynological assemblages from East African hominin localities during the Plio-Pleistocene. However, no obvious trends towards aridification were apparent (Bonnefille, 1995). These studies did document both complex and diverse habitats over time and indicated periods of high environmental variability with changes from open grasslands to forested and woodland habitats possibly driven by changes in orbital forcing. Phytolith assemblages have also been recovered from a number of sites including Olduvai Gorge (Barboni *et al.*, 2010). Both phytolith and palynological evidence taken from hominin fossil and archaeological sites together show that hominins were utilising a diverse range of habitats. These data however are limited and may reflect biases, at times, towards the preservation of taxa representing specific habitat types.

2.5.2 Orbital forcing

A number of studies of fossil hominin and archaeological sites have attempted to link local environmental sequences to global patterns of climate change driven by changes in orbital parameters, thus allowing the selective pressures associated with orbitally forced climate change and driving palaeontological/archaeological changes at these localities to be further and more fully examined.

2.5.2.1 Hadar

The stratigraphic sequence at the Hadar Formation of Ethiopia extends from 3.5 to 2.2 Ma. This site also preserves an important record of hominin palaeoenvironments and hominin fossils including the abundant remains of *Australopithecus afarensis* and has so far yielded over 370 specimens from 90 localities within the formation (Campisano & Feibel, 2007; Aronson *et al.*, 2008). Campisano & Feibel (2007) provide high resolution sedimentalogical and palaeontological records from Hadar combined with other climate proxies taken from dust flux, sapropel and marine core isotope data and observe cyclical changes between fluvial and lacustrine deposits linked to orbital forcing prior to 2.9 Ma. These authors note that a period of relative high-amplitude climatic variability occurs between 3.15 and 2.95 Ma that is concordant with morphological changes in the *A. afarensis* lineage, relating to size. Aronson *et al.,* (2008) use proxies of $\delta^{13}C$ and $\delta^{18}O$ values from palaeosol carbonates at Hadar to examine changes in paleo-rainfall estimates and palaeovegetation dynamics in the context of the Ethiopian monsoon and identify two historical regimes. Both approaches were able to examine environmental change at this site against external climate processes.

2.5.2.2 Olduvai Gorge

Olduvai Gorge is well known for its rich palaeotological and archaeological records which occur within a 100 metre sedimentary sequence of fluvial, wetland and lake margin sediments. At Olduvai Gorge there have been a number of studies placing environmental proxy data and palaeoenvironments within a framework of orbitally forced climate change (Ashley, 2007; Ashley *et al.,* 2009; Stanistreet, 2012). Ashley (2007) document five lake level cycles of expansion and contraction occurring on sub-orbital timescales within a 50,000 year period between 1.84 and 1.74 Ma. Their insolation time series analysis shows five cycles of solar radiation concordant with lake level changes. This study also documented an increase of up to one third between the wet and dry periods of the 21 kyr cycles in rainfall estimates. A further study by Ashley *et al.,* (2009) between 1.79 and 1.74 Ma documents three wet periods with two intervening dry periods in 50,000 year periods. No notable change was noted in the Oldowan tool kit at spring water sites during this period reflecting a sustained use of these resources despite persistent environmental change.

2.5.2.3 Turkana Basin

More detailed records of palaeoclimatic change from lacustrine sequences come from the Turkana basin (Brown & Feibel, 1991; Feibel, Harris & Brown, 1991; Lepre *et al.*, 2007). These authors document lacustrine conditions in the Turkana basin at 4.2 – 4, 3.5 and 3 Ma. Brown & Feibel (1991) also report a period of lake-level instability at 1.7 Ma. A more recent study by Joordens *et al.,* (2011) suggests that between 2 – 1.85 Ma the Turkana basin may have provided a refugium for hominins due to its stable lake-levels and well-watered conditions, conditions which contrast with other lake basins in the Rift Valley during the same period. These authors further argue that stable lake-level conditions persisted in the basin for 150,000 years. Directly following this period strong fluctuations between lake-level high stands and low stands are observed which persist until 1.7 Ma (Fiebel, Harris & Brown, 1991). Lepre *et al.,* (2007) present a record from the KBS member (1.9 – 1.6 Ma) of changing lake levels. This study used depositional environments and sedimentation rates to interpret lake-level changes in the context of variations in the intensity of the monsoon systems. Changes in lake-levels at this site were argued to be driven by both orbital precession and obliquity.

2.5.2.4 Chemeron Formation & Elmenteita

A number of records are available from the Central Kenyan Rifts that document changing lake levels and the palaeoclimatic processes controlling them. A diatomite sequence from the Chemeron formation in the Tugen Hills documents changing sedimentation patterns and lake forming between 2.7 and 2.55 Ma (Deino *et al.*, 2006; Kingston *et al.*, 2007). The lake forming episodes fluctuate between wet and dry predominantly driven by orbital precession (Kingston *et al.*, 2007). More recent data produced at a much higher resolution for this sequence indicate that the wet-dry cycles were occurring, on average, every 1400 years, which gives a previously undocumented record of millennial scale and a valuable insight on the nature of short-term fluctuations in Plio-Pleistocene climate (Wilson *et al.*, 2010 published abstract). A 30 metre diatomite from the Nakuru-Elmenteita basin in the Central Rift documents the presence of large- deep freshwater lake several hundreds of metres deep dated to 0.977 Ma (Evernden & Curtis, 1965).

2.5.2.5 Olorgesailie

From the southern Rift the archaeological site of Olorgesailie yields an 80 metre thick diatomite sequence providing a long-term record of lake forming episodes and palaeoclimatic change (Behrensmeyer *et al.*, 2002; Owen *et al.*, 2008; 2012; 2014). Behrensmeyer *et al* (2002) document a major lake-forming episode at around 0.992 Ma and Owen *et al.,* (2008) document changing lake level fluctuations that alternate between wetter and drier conditions along with changes in variation and complexity of habitats during the Pleistocene. More recent records from Olorgesailie, Munya wa Gicheru, document eight lake level high stands and low stands between 1.9 and 1.65 Ma which are argued to reflect periodicities on two different timescales – orbital and ENSO type climate (Owen *et al.*, 2012). Documenting long-term changes in palaeoclimatic conditions, a 1.2 Ma record comes from the Kedong-Olorgesailie sections of Olorgesailie. This record shows a distinctive long-term trend towards increasing aridity in the basin, using geochemical analysis, and from lacustrine to fluvial conditions during the Pleistocene. This record also documents the influence of rift faulting on the palaeoclimate record (Owen *et al.*, 2014).Taken together studies linking environmental change within the Olorgesailie basin clearly document both climatic variability and longer-term trends toward aridity.

2.6 Summary and conclusions

There are numerous global and regional proxy records for palaeoclimate change which are relevant when examining evolutionary change at East African hominin sites. For the most part these are coming from marine cores and more recently from lacustrine deposits from rift valley lake sequences. Whilst these records provide an important context for examining evolutionary change occurring on different timescales, only approaches taken to examine the effect of orbitally forced climate change on a site by site basis are useful when attempting to link change in hominin lineages both behaviourally and biologically to climate change. However, only a few sites have produced such records and provide a causal link e.g. Hadar the link between size increase in *A. afarensis* being concordant with high climatic variability and at Olorgesaille when a change in landscape use is noted between 1.1 and 0.9 Ma also concordant with climatic instability.

Aside from the more difficult problems of stratigraphic gaps in sequences and geological unconformities and disconformities when examining long sequences in East Africa other problems are apparent. Preservation of biological proxies such as pollen and diatomites also present a problem in terms of analysing long sequences at a high resolution and both these proxies along with phytoliths and as stable isotope analysis are time consuming and expensive to utilise. Alongside the wider aims of the thesis in Chapter one, this PhD will further explore the potential of geological proxies, environmental magnetism and major and trace element geochemistry (desktop based), in reconstructing palaeoenvironmental and palaeoclimatic change at Kilombe. Both techniques are rapid, inexpensive, non-destructive, can be applied to bulk sediments and only require a small amount of sample for analysis making them ideal for examining long stratigraphic sequences at a high resolution. The theory and methodology for both techniques will be fully outlined, including strengths and limitations in the following chapter.

Chapter Three Theory and methodology

3.1 Introduction

This chapter will provide the theoretical and methodological background to the main techniques used for palaeoenvironmental analysis in this study, environmental magnetism and major and trace element geochemistry. The first part will provide a literature review on applications of both techniques and the second part will outline the sampling strategy and laboratory methods used.

3.2 Environmental magnetism and climate reconstruction

Environmental magnetism was primarily developed during the 1980s from theories of rock magnetism that had previously been used in combination with standard palaeomagnetic investigations. Previous studies concerning magneto-climatology have primarily focused on loess sequences (e.g. Zhou *et al.*, 1990), lake-sediments (e.g. Thompson *et al.*, 1980), and cave sequences (e.g. Herries & Latham, 2003). The application of environmental magnetism to archaeological problems has also become much more frequent over the last decade and applications include investigations of taphonomic, behavioural and environmental processes and modelling (e.g. Dalan & Banerjee, 1998). All types of rocks and sediments contain varied quantities and types of magnetic minerals, the most common being iron oxides. A variety of mineral magnetic analyses can be used to investigate the amount, shape and size of the various magnetic minerals present in a sample, the simplest being magnetic susceptibility, MS or χlf (Thompson &Oldfield, 1986).

In terms of examining environmental change there is a wide application of the technique in terrestrial environments especially to lake, alluvial and fluvial sediments, soils & palaeosols and Aeolian sediments (Liu *et al*, 2012). A number of studies have shown that changes in magnetic mineralogy, concentration and grain size can be influenced by a number of external processes other than climate and as such basic parameters such as magnetic susceptibility are not so straightforward in terms of a proxy for palaeoclimatic change. In terms of measuring the magnetic properties of bulk sediments, changes in lithology, depositional environments and sediment grain size can also be reflected in changes in magnetic properties (Liu *et al.*, 2012). In sequences that comprise a number of different lithological units and potentially different depositional environments it is firstly necessary to evaluate changes in the magnetic properties of bulk sediment samples against changes in lithology. If the lithology is homogenous then variations in magnetic properties are generally related to palaeoclimatic change or changes in provenance. In lithologies that are heterogeneous e.g. sands, clays and silts changes in the magnetic properties can be related to changes in sediment grain size, especially those occurring across transitional boundaries (Basavaiah *et al.*, 2004). A number of other factors that can affect the magnetic signal include dissolution, or loss of the signal through burial diagenesis and the presence of bacterial magnetotactic bacteria (Liu *et al.*, 2012; Oldfield & Crowther, 2007).

3.3 Magnetic Force and Behaviour

The following section is largely based on information drawn from (Dunlop & Ozdemir, 1997; Thompson & Oldfield, 1986; Evans & Heller, 2003; Walden, Oldfield & Smith, 1999). Magnetic behaviour of some form occurs in all materials and arises from electron and orbital spins within atoms of particular elements. Movements of electrons has been demonstrated to cause a magnetic field. In atoms electrons spin in two ways, around their nuclei and also their axis which results in two types of motion which together create a magnetic field. When a substance is placed in a magnetic field of strength, *H* (units Am^{-1}), the magnetisation, *J* (the magnetic moment of the sample per unit volume, (Am^{-1}), is related to *H* by the magnetic susceptibility, К*,* of the substance e.g. $J = K H$. Magnetic susceptibility is generally expressed either in terms of mass, χ (m^3/Kg^{-1}) or volume (area), as К (Am^{-1}/Am^{-1}).

The magnetic properties of an atom arise as a result of interactions between the spin moments of the electron and also the orbital moment. Arrangements of electrons within the atomic shell of an atom differ between materials and this results in the production of different magnetic fields in different materials.

There are a number of different forms of magnetism:

Diamagnetism

This is the rudimentary property of all substances and involves a small repulsion by a magnetic field. Electron shells are full so spins are precise and cause a magnetic field in the opposite direction to the field which has been applied. Thus diamagnetism has an overall weak and also negative magnetism. All atoms and molecules show this form of magnetism. Pure diamagnetic effects are founds in commonly in minerals such as quartz (SiO_2), calcite ($CaCO_3$) and gypsum ($CaSO_4.2H_2O$). The magnetic susceptibility of a diamagnetic substance is small, negative and independent of temperature.

Paramagnetism

In materials or substances that are paramagnetic substances are attracted towards a magnetic field. Electron shells are also incomplete and this results in each atom within the electron shell has a magnetic moment. When an electric field is applied to the magnetic moments of the electrons, the electrons then align along the applied field creating a positive but weak magnetic field. Some form of paramagnetic behaviour is exhibited in most natural mineral assemblages. Paramagnetic substances include iron sulphides such as pyrite (FeS_2).

Some atoms contain electrons that are unpaired, interactions with neighbouring spins causes partial alignment, even in the absence of an external magnetic field and a number of different types of magnetisation are caused:

Ferromagnetism

Electron shells are incomplete (similar to paramagnetic materials) but in this case the electron shells are magnetically coupled with quantum exchange forces (mechanical), which results in alignment along the same direction. These materials are magnetic without any application of an external applied field. As such ferromagnetic materials can therefore acquire strong and spontaneous magnetisations. Ferromagnetism is the strongest known form of magnetism and includes materials such as Iron (Fe) and Nickel (Ni) that are not generally found in the natural terrestrial environment.

Naturally occurring materials that are magnetic without an applied field are known as imperfect:

Anti-ferromagnetic

Anti-ferromagnetic materials have a zero force because alternating layers within the crystal lattice have become magnetise in the opposite direction due to the coupling of an intermediate oxygen atom in iron oxides. When there are an equal number of unpaired electrons within a sample, there is no spontaneous magnetisation and is therefore, anti-ferromagnetic.

Ferrimagnetic

When a substance has an unequal number of unpaired electrons the magnetic moment of the atom is also unequal and so what is known as a net magnetisation is produced. Ferrimagnetic materials are the strongest naturally occurring terrestrial magnetic materials and also have a strong positive magnetisation. Ferrimagnetic materials include iron oxides such as magnetite (Fe_3O_4) and maghemite (γFe_3O_3).

Canted anti-ferromagnetic

When the sub-lattice in an otherwise anti-ferromagnetic mineral is imperfect a relatively weak positive magnetisation can exist known as canted anti-ferrimagnetism. Canted anti-ferromagnetic minerals include some iron oxides such as hematite (α Fe_2O_3) and iron hydroxides such as goethite (FeOOH).

3.4 Mineral Grain size and Domain Structures

The type of magnetisation is controlled by the mineralogy of a substance or material. Therefore, mineralogy is one of the important factors which controls magnetic remanence acquisition. The other important factor is the magnetic grain size or domain, which controls the behaviour of both ferri and anti-ferromagnetic minerals. Magnetic grain size is of particular importance in climate reconstruction.

Various domain categories can be identified that influence the stability and strength of the magnetisation present within a particular mineral:

Multidomain (MD).

MD grains are formed in large mineral grains. As the sample is magnetised the excess energy leads to the creation of more domains. At a critical point, all domains align via a gradual process that evolves from low to high magnetisation. Such minerals are easy to magnetise and demagnetise and this is known as magnetically SOFT behaviour.

Psuedo-single domain (PSD).

These are minerals that are large enough to be MD grains but still display SSD behaviour because of their inability to minimise to a zero energy state. They represent the boundary between the two domain states SSD and MD.

Stable-Single Domain (SSD).

In smaller grains there is only one domain as there is insufficient space and/or energy to create more domains. High magnetic fields are generally required to change the magnetisation, especially if the grain is elongated. It is difficult to magnetise and demagnetise these minerals and this is what is known as magnetically HARD behaviour. Single domain grains can be subdivided into both SSD grains and also ultra-fine superparamagnetic grains.

Super-paramagnetic grains (SP).

Superparamagnetism arises as a result of magnetic anisotropy. SP grains are very small (< 20-30 nm), and due to their small size, energy is inherently unstable and so the thermal energies in the mineral randomise any magnetic field that exist. The size difference at the boundary between SSD/SP grains is very slight and SP grains display viscous behaviour as they lose more magnetisation over time. SP grains can be identified because at certain high frequencies and low temperature they behave as SSD grains. SP grains are extremely important in environmental reconstruction as they are often formed during pedogenesis.

3.5 Common Magnetic Minerals

Iron oxides are the most common magnetic minerals that occur in the natural environment. In both terrestrial and marine environments the formation of iron oxides involves aerobic weathering of surface magmatic rocks. The most common magnetic minerals are described below:

Magnetite (Fe_3O_4) is the most important magnetic mineral in environmental systems and it occurs in both primary and secondary forms in sedimentary and igneous rocks. Magnetite contains both Fe^{II} and Fe^{III} and is black in colour. At temperatures below $575^{0}C$ (its curie temperature) it is ferrimagnetic. Magnetite also has the strongest spontaneous magnetisation of any magnetic mineral.

Maghemite (γFe_2O_3) occurs as a weathering product of magnetite as a result of low temperature oxidisation and it can also occur as an end product of other Fe oxides during heating. This mineral occurs widely in soils and is important in environmental reconstruction. Due to maghemite having a similar chemical composition to haematite and a similar structure to magnetite is can often prove difficult to distinguish between them although maghemite has a much lower spontaneous magnetisation.

Haematite (αFe_2O_3) is widely distributed in soils and is highly stable. It is often the end product of transformations of other iron oxides. Haematite can prodcue a red colouration when it is finely divided or it can appear black in colour when it is highly crystalline. It has a canted anti-ferromagnetic atomic structure and produces a weak magnetisation. It is grain size dependant with SD grains having very high coercivities and SP grains generally being non-magnetic.

Goethite ($\alpha FeOOH$) occurs widely in soils as a weathering product of other iron bearing minerals. It is weakly magnetic with a canted anti-ferromagnetic atomic structure. At ambient temperatures goethite is one of the most thermodynamically stable iron oxides and is the first oxide to form. As temperatures increase it can dehydrate to form the mineral haematite. It can be difficult to distinguish between hematite and goethite however, goethite's coercivity is generally much higher than that of hematite. Goethite is dark brown or black in colour when occurring in large crystal aggregates and yellow when occurring in its powdered form.

Greigite (Fe_3S_4) occurs in a reducing environment and is a ferromagnetic iron sulphide. It oxidises to various iron oxides leaving the paramagnetic pyrite as the sulphide component. Recently the importance of greigite has increased in environmental applications however it is still uncommon for greigite to dominate the magnetic properties of a substance.

3.6 Magnetic Parameters

Mineral magnetic parameters refer to the properties and concentration of iron oxides and sulphides in any soil, rock or sediment. In addition to magnetic susceptibility a number of other parameters are used to characterise materials within a sample. These techniques originally derive from the disciplines of rock magnetism and palaeomagnetism (Evans & Heller, 2003).

Concentration parameters

- **Initial susceptibility or low-field χ_{LF} and χ_{HF}** measurements are rapid and often used as a proxy for magnetic mineral concentration usually magnetite.
- **SIRM** concentration of remanence holding materials usually ferromagnetic grains.

Magnetic domain state

- **X_{FD}** indicates concentration of superparamagnetic ferrimagnetic grains (SP grains form pedogenically in soils/palaeosols) which can increase with increasing annual rainfall.
- **$X_{FD\%}$** indicates the proportional contribution of SP grain to the bulk measurement.
- **χ_{ARM}** concentration of ultra-fine particles of magnetite near the SD/SP domain boundary.
- **χ_{ARM}/χ_{LF}** SSD ferromagnetic grains.
- **χ_{ARM}/SIRM** relative grain size of magnetite – higher values indicate SP grains and lower. values suggest coarse MD grains.
- **χ_{ARM}/χ_{FD}** ratio of SD magnetite to SP magnetite.

Magnetic mineralogy

- **IRM ratios (%)** percentage of SIRM acquired at a specific field.
- **HIRM** reflects the concentration of imperfect antiferromagnetic minerals.
- **SOFT** reflects the proportional contribution of low coercivity magnetic mineral to the SIRM.

- **S-RATIOS, IRM -100_{mT} /SIRM** and **IRM -300_{mT} /SIRM** ratio of saturated to non-saturated minerals at 100Mt. Low negative values are dominated by “soft” minerals and higher negative values are indicate coarse MD ferrimagnets.
- **SIRM/χ_{lf}** proportion of ferromagnetic materials – lower ratios indicate greater proportion of paramagnetic and diamagnetic minerals and values > 30 indicate presence of greigite.

3.7 Environmental magnetism and palaeoclimate

Mineral magnetic studies of soil and sedimentary sequences can provide information in palaeoclimate for a number of reasons. Primary Iron is incorporated into soils and sediments in the form of secondary iron oxides which come primarily from weathering of parent rocks in the source area. The main source of Fe for soils comes from the chemical weathering of Fe silicates resulting in the release of Fe^{2+} which is then oxidised into Fe^{3+} in an aerobic soil environment. The neoformation of specific iron oxides i.e. magnetite or hematite is the end result of the complex interaction of a number of environmental factors which not only includes climate and rainfall but also organic matter and the age of the soil (Evans &Heller, 2003. Maher (1998) has demonstrated that in topsoils, pedogenic processes such as hydrolosis, fermentation and biologically induced mineralisation act in the conversion of primary and secondary iron into magnetite, and through oxidation and reduction cycle’s maghemite is formed. This process is known as both pedogenic and magnetic enhancement as it produces a dominance of strongly magnetic magnetite/maghemite. The degree to which pedogenic enhancement enacts is controlled by the amount and type of iron oxides, sulphides and amorphous iron in parent material.

Magnetic enhancement through the formation of secondary iron oxides, via pedogenic processes, has been shown to occur in both modern soils and palaeosols (Maher, 1998). Although, there are five main factors that account for pedogenic enhancement (source rock composition, relief, time, biota and climate) the influence of past climate change on the magnetic enhancement of soils has been well researched (Dearing *et al*., 1996; Zhou *et al*., 1990). The majority of work has been conducted on the Chinese loess/palaeosol sequences and which have provided a major contribution in examining changes in the intensity of the East Asian Monsoon systems (Maher, 1998; Liu *et al*., 2012). In this respect, characteristics of soil magnetic iron oxide assemblages have been linked to climatic factors, mainly temperature and rainfall, which provide a direct proxy for changes in the monsoon and orbital precession (Torrent *et al*,. 2007). The idea that changes in magnetic susceptibility are linked to rainfall or wet/dry cycles via pedogenic processes was first proposed by Maher & Thompson (1991), although other models exist proposing changes in dust flux as a mechanism for magnetic enhancement (Kukla, *et al*., 1988). A number of other studies have suggested the link between magnetic enhancement and pedogenic processes via a combination of both physical, chemical and biological activities (Sun & Liu, 2000; Torrent *et al.,* 2007).

The correlation between magnetic enhancement, pedogenesis and mean annual rainfall and palaeorainfall estimates is well researched (Balsam *et al.*, 2011). In well-drained soils for example, surface soil layers have been shown to contain significant quantities of secondary magnetic minerals, ultrafine SP and SD magnetite/maghemite, formed via pedogenic processes (Blundell *et al*., 2009; Maher & Thompson, 1991). Studies have also shown that as mean annual rainfall increases so does pedogenic and magnetic enhancement. In general, the neoformation of ultrafine pedogenic magnetic minerals is greatest in tropical environments or were climate is governed by the monsoon systems i.e. environments that experience seasonal wet/dry cycles (Balsam *et al*., 2011). However, a number of studies have also demonstrated that once mean annual rainfall > 1200 mm/yr magnetic enhancement can decrease due to the dissolution of ferrimagnetic minerals and transformation of magnetite into iron sulphides (Balsam *et al*., 2011).

3.7.1 Deposition & alteration

Environmental magnetism has been widely applied in studies of palaeoclimate in a range of settings lake, marine and terrestrial (Liu *et al*., 2012). In terrestrial settings the main applications are to loess/palaeosol sequences were pedogenic alteration occurs in situ. In contrast, sedimentary rock sequences in terrestrial settings are likely to contain information from a variety of sources which may include pedogenic alteration at source, during transportation and occurring post-depositionally.

3.8 Chemical weathering indices

Various geochemical proxies have been proposed to examine the intensity of chemical weathering on continents (Duzgoren-Aydin & Malpas, 2002; Ao *et al.*, 2011). These indices are generally applied to bulk samples and incorporate the values of major elements into one single metric measurement, the variation of which can then be used to examine changes in chemical weathering intensity in a weathering profile (Price & Velbel, 2003). In terms of selecting which indices are most useful/reliable in a specific environment a variety of criteria can be used which depend on source rock type e.g. mafic, felsic or intermediate and as to whether the source rock is either homogenous or heterogeneous in the case of metamorphic rocks.

Most chemical weathering indices have been proposed for felsic and or intermediate rocks (Ruxton, 1968; Nesbitt & Young, 1982) whilst only a few are judged applicable to all rocks such as basic and metamorphic (Colman, 1982; Parker, 1970). The main assumption in the formulation of chemical weathering indices is that changes in the behaviour of major elements are controlled, primarily by the degree of chemical weathering under conditions of humidity and aridity. For example, as chemical weathering intensity increases certain major elements such as Al_2O_3, TiO_2 and Fe_2O_3 are generally considered to be immobile and therefore remain constant in a weathering profile whilst certain other major elements are considered to be mobile such as Si_2O, Na_2O, MgO, CaO and Na_2O. These elements are expected to decrease as chemical weathering intensity increases in relation to the immobile elements. Chemical weathering indices are normally conveyed as weight percent or molecular ratios.

Studies that utilise chemical weathering indices generally focus on changes in specific indices with depth in an attempt to quantify changes in bulk geochemistry as chemical weathering progresses. This therefore assumes that all the samples in a weathering profile have the same initial geochemical composition i.e. source material and that samples from the deepest part of the weathering profile are subject to less extensive weathering than those in closer proximity to the surface.

It is generally considered that chemical weathering indices are not overly influenced by sediment grain size (Garzanti *et al.*, 2010). However, a number of studies have shown this not to be the case and that changes in grain size can, at times, have a significant effect on the behaviour of major elements used in calculating weathering indices (Shao *et al.*, 2012; Xiong *et al.,* 2010). Profiles subject to intense chemical weathering can see the destruction of primary minerals and the formation of secondary minerals such as fine-grained clays therefore sorting and grain size can influence to some degree values obtained for chemical weathering indices.

3.8.1 Chemical weathering indices selection

The following chemical weathering indices were selected:

3.8.2 Chemical Index of Alteration

One of the most widely and accepted index is the chemical index of alteration of Nesbitt and Young (1982) or CIA and was applied initially to examine quantitatively examine chemical weathering in sediments and sedimentary rocks. Over the last few decades the CIA has been used in a variety of contexts including sedimentary rocks, palaeosols and river drainage basins (Owen *et al.*, 2014; Mclennan, 1993; Price & Velbel, 2003). This index is essentially a measure of the conversion of feldspars into clays during chemical weathering. CIA is defined using molar proportions, as CIA = $(Al_2O_3 / (Al_2O_3 + CaO^* + Na_2O + K_2O)) \times 100$ with CaO^* being the CaO content present in the silicate proportion of the bulk sample. This index has been utilised in numerous palaeopedological studies.

3.8.3 Ruxton Ratio

In 1968 Ruxton proposed a simple index of weathering (SiO_{2}/ Al_2O_3) now termed the Ruxton ratio. This index is best suited for weathering profiles developed on uniform acid to intermediate bedrock. The Ruxton ratio relates loss of silica to total element loss and considers aluminium to be immobile during weathering. Ruxton (1968) tested this ratio on weathering profiles from both igneous and metamorphic rocks globally in humid regions and found that this ratio correlated well with total element loss.

3.8.3 CaO/Al_20_3

This ratio is similar to the Ruxton ratio and is shown to increase as chemical weathering decreases. This ratio related the loss of CaO to Al_2O_3 and again considers aluminium to be immobile during the weathering process.

3.9 Parent material and changes in provenance

The geochemical composition of sediments is primarily dependent on the geochemical composition of the source rock or parent material from which the sediments derive during chemical or physical weathering. Therefore, it is vital to not only identify source rock but also to recognise any potential changes in parent material. Any change in parent material must therefore be ruled out as a possible influence on the palaeoclimate or palaeoenvironmental proxy signal.

The major and trace elements of Al, Nb, Ti, and Zr can generally be treated as immobile in soils and sediments because of their low solubility in low temperature aqueous solutions (Hayashi *et al.*, 1997). Ratios of all four elements in soils and palaeosols are generally very similar to those of the source rock (Maynard, 1992; Young & Nesbitt, 1998). In unweathered igneous rocks Ti generally resides in mafic minerals such as biotite and chlorite whereas Al resides in residual feldspars, micas and clays such as kaolinite, smectite and illite (Hayashi *et al.*, 1997). Although the ratios of all these elements have been shown to be similar to source rock composition in soils and palaeosols fractionation can occur during transportation in sediments most notably in stream sediments due to the larger density of Zr (Cullers *et al.*, 1988). A detailed study was implemented by Wintsch and Kvale (1994) in which the different mobility's of Ti and Al under burial diagenesis was examined. This study showed that both elements are stable under most environmental conditions and would either reprecipitate as hydroxides or oxides or be incorporated into the clay minerals. Therefore, they could be used to identify soils and sediments of originally uniform composition. The ratio of the oxides of Ti/Al and Al/Ti have been used in a variety of studies as an indicator of provenance (Young & Nesbitt, 1998; Maynard, 1992; Ashley & Driese, 2000). A comparative study by Young & Nesbitt (1998) has shown that higher Ti/Al ratios generally correspond to more mafic igneous rocks and bivariate plots of Ti versus Al can be used to examine to examine a variety of environmental processes such as weathering and sorting along with provenance.

Zirconium and niobium as high field strength elements are generally associated with fractionation of the heavy minerals and are also not subject to transport in aqueous solutions. Heavy minerals are not known to be influenced to any degree by changes in palaeoclimatic conditions during chemical weathering processes and therefore their distribution in soils/sediments is primarily governed by the original geochemical composition of the source rocks (Scheffler *et al.*, 2006). A variety of geochemical studies have demonstrated that igneous rock types can be clearly differentiated by their Zr/Nb, Ti/Zr and Zr/Ti ratios (Hayashi *et al.*, 1997).

3.10 Sediment grain size

The ratio of trace elements Zr and Rb has been widely used as a proxy for both changes in grain size and chemical weathering in a variety of environmental settings (Dypvik & Harris, 2001; Chen *et al.*, 2006; Zabel *et al.*, 2001). Zr is commonly used in element ratios as an immobile element to examine the relative stability of other elements in soils and sediments as zircon as a mineral is strongly resistant to chemical weathering processes. Zr is generally concentrated in the heavy minerals present in sediments specfically Zircon. In sedimentary rocks Zircon is most often contained within the coarser grained, specifically silt sized fractions and can therefore provide a good indication of changes in concentration of silt sized materials. Rb is not generally associated with any minerals that are Rb bearing, and is mainly present in potassium bearing minerals such as the micas, clay minerals and K-feldspars and specifically in the finer grain sized fractions. Rb is not as stable an element in weathering systems as Zr and can be removed under the extensive weathering of K-feldspars. Zr/Rb ratios therefore show significant increase as grain size increase from fine to coarse grained in a sedimentary sequence.

3.11 Soil forming Factors Jenny (1941)

Jenny (1941) outlines the factors influencing soil formation which can be used as framework when considering variability in the properties of soils/sediments in terrestrial environments. The main factors identified include climate, organisms/vegetation, relief, parent material, climate and time. Blundell *et al.,* (2009) also further note the interdependency of these factors.

3.11.1 Time

In terms of examining both magnetic enhancement and chemical weathering intensity via pedogenic processes, time is shown to be a key dependent factor on the changing properties of both proxies in soils and sediments (Singer *et al.,* 1992; Ao *et al.*, 2011). Studies on both the Chinese loess/palaeosol sequences and marine environments demonstrate the importance of the link between magnetic enhancement and time (Singer *et al.*, 1992), whilst other studies document substantial magnetic enhancement of modern soils due to longer exposure/duration times to pedogenesis (Maher & Thompson, 1995).

Vidic *et al.,* (2004) also report the significance that both duration of pedogenesis and climate have on the magnetic enhancement of loess/palaeosols in China. This study clearly demonstrates the effects of longer residence times in palaeosols than loess units and shows the complex relationship between climate, duration of pedogenesis and magnetic enhancement.

In studies of chemical weathering intensity and specifically the application of chemical weathering indices, both time and duration of pedogenesis are also argued to be key and interdependent factors (Dosseto & Vigier, AGU abstract 2010; Rudnick *et al.*, 2004). Both these studies suggest that as greater erosion can occur under conditions of higher rainfall, this can leads to a reduction in chemical weathering intensity on sediments as time for weathering is also reduced to less time spent in the basin. Conversely, chemical weathering has been shown to intensify under conditions of decreased erosion and longer exposure times to weathering. In a derived sequence residence times are likely to undergo much longer exposure time to pedogenesis given weathering at source, during transport and post-depositionally.

3.11.2 Relief

Whilst studies above document the importance of time, duration of pedogenesis and climate, a further factor of relief must also be considered. In tectonically active and volcanic regions, it is generally argued that chemical weathering rates are much lower due to the shorter residence times of soils and sediments. This is seen as a function of both high relief and low soil depth which in effect leads to increased rates of erosion (Dixon *et al.*, 2012; Ferrier & Kirchner, 2008). This particular effect is common on hillslopes in tectonically active regions and has been demonstrated by Dixon *et al*., (2012) who document and increase in chemical weathering intensity in hillslopes with lower slope gradients than those with higher slope gradients in California. These authors also note the interplay between increased elevation and decreasing temperature on chemical weathering intensity along with relief. In the context of Australian palaeolandscapes Wilford (2012) notes the influence of low relief and low slope angle as a factor promoting increased chemical weathering intensity along with climate.

3.11.3 Parent material

There are a number of factors to consider as to the influence of parent material on soil/sediment forming factors. In terms of soil magnetism, Blundell *et al.*, (2009) identify four key factors which include concentration of Fe, the occurrence of primary ferrimagnetic minerals in soils of igneous origin, resistance of certain rock types to weathering and parent material influence on local soil conditions i.e. texture and drainage. In terms of soil/sediment geochemistry, their geochemical and mineralogical composition is determined by the mineralogy of the parent material. Wilford (2012) notes that parent material particularly resistant to chemical weathering can often influence degrees of weathering i.e. contribute to reduction of weathering in an environment. Enrichment and depletion factors in the concentration of major and trace elements in soils/sediments has been shown to vary significantly according to rock type i.e. mafic, basic, ultrabasic (Galan *et al.*, 2008). A study by Woodruff *et al.*, (2009) has demonstrated that abrupt changes can occur in soil mineralogy concordant with abrupt changes in parent material. However, these authors also note that the geochemical influence of changing parent materials can sometime be obscured by climatic conditions.

3.11.4 Climate

There have been many attempts to identify the main climate controls on the magnetic and geochemical properties of soils and sediments. In studies of soil magnetic properties, precipitation, specifically rainfall, has been identified as one of the main factors leading to the magnetic enhancement of top soils on modern environments and also in palaeosols (Balsam *et al.,* 2011; Dearing *et al.,* 2001). Peaks in magnetic susceptibility have been documented by Singer *et al.,* (1996) which suggested that the relationship between higher rainfall and increased humidity is the causal factors for magnetic enhancement in some Hawaiian soils. Less attention has been paid to the influence of temperature as a factor in magnetic enhancement of soils and sediments. However, there are a number of studies suggesting temperature to be a significant factor (Barron *et al.*, 2003; Song *et al.*, 2014). Barron *et al*., (2003) have argued that temperature is a key factor in the magnetic enhancement of soils with laboratory experiments demonstrated the link between temperature and the conversion of ferrihydrites to maghemite. On the Chinese Loess Plateau, Song *et al.,* (2003) suggest that although dominant control on magnetic enhancement of surface soils is rainfall, temperature is also a significant factor.

In studies of chemical weathering intensity a complex relationship between temperature and precipitation is also documented. In general, tropical regions experience the most intense chemical weathering conditions due to the much higher levels of precipitation and temperatures. Ernest (2000) suggests that as some temperate regions with high rainfall levels experience less intense chemical weathering, temperature must also be a key factor. Ernst (2000) has also noted the important also of evapotranspiration which can act to increase precipitation levels via a feedback loop with higher temperatures resulting in intense chemical weathering.

3.11.5 Summary

In summary, the factors influencing magnetic and geochemical properties of soils and sediments in response to chemical weathering and pedogenesis are complex and also interdependent. Factors leading to intensely weathered soils and sediments include situations where:

1. Landscapes have been exposed to the above weathering agents for considerable time which would result from low rates of erosion (relief and duration of weathering) and also over long-timescales.
2. Situations where the parent rock or source material is highly weatherable.
3. When climate conditions, specifically rainfall and temperature, would promote intense chemical weathering and soil formation.

3.12 Sampling strategy and provenance

During the July 2011 to 2013 field seasons 228 samples were extracted from GqJh1 (AH) at 5 cm and Farmhouse Cliff at 10 cm intervals from the Kilombe sedimentary sequence (19 meters) using geology hammers and chisels and approximately 30 grams of material were taken for each sample. Samples were placed immediately into pre-labelled plastic sample bags for transportation back to the laboratory. A step trench was dug approximately 1 metre into the sediments to create a uniform vertical surface, eliminate surface contamination and enable the extraction of fresh material. A further 9 samples (200 grams) were taken from the centre of each unit from the main site GqJh1 (AH) for particle size separation in 2013. A resolution of 5 and 10 cm was selected with the aim of capturing the nature of climate change on different timescales (long-term trends and orbital/sub-orbital).

Figure 3.1 shows photographs of the stratigraphic sequence at Kilombe main site (a) and farmhouse cliff (b), whilst Figure 4.7 shows the standard composite stratigraphic section along with key dates for the entire Kilombe sequence. Full detail of the sedimentological attributes for each stratigraphic unit, including sorting, Munsell and sedimentary structures, are presented in Table 4.1 and further detail on facies association is given in section 4.3.2. The sedimentary sequence at Kilombe comprises 16 lithostratigraphic units belonging to four facies associations. The geochemical, rock magnetic, granulometry and loss-on-ignition values for each sample is listed in the appendices and the provenance, including sample numbers for individual samples per lithologic unit is as follows; unit 1 yellowish red claystone (KL1-KL53, 32 samples), unit 2 grayish brown claystone (KL57 – K15, 19 samples), unit 3 pale yellow claystone (K16-K22, 7 samples), unit 4 grey clay/diamictite (K23-K32, 10 samples), unit 5 palaeosol pale brown (K33-K39, 7 samples), unit 6 white tuff (K40, 1 sample),unit 7 tuffaceous pale brown claystone (K41-K47, 7 samples), unit 8 pale yellow tuff (K48, 1 sample), unit 9 Three banded tuff (K50, 1 sample), unit 10 dark brown tuffaceous clays (1-9, 8 samples), unit 10 (A) orange clay band (5, 1 sample), unit 11 very pale brown clayey tuff (10 -26, 17 samples), unit 11 A white tuff (21 1 sample), unit 12 brown clay series (27-49, 22 samples), unit 13 orange clay series (50-69, 18 samples), unit 14 brown banded tuff with clay deposits (70-83,14 samples), unit 15 pink earthy tuff (84-126, 43 samples), unit 16 orange brown earthy tuff (127-144, 18 samples).

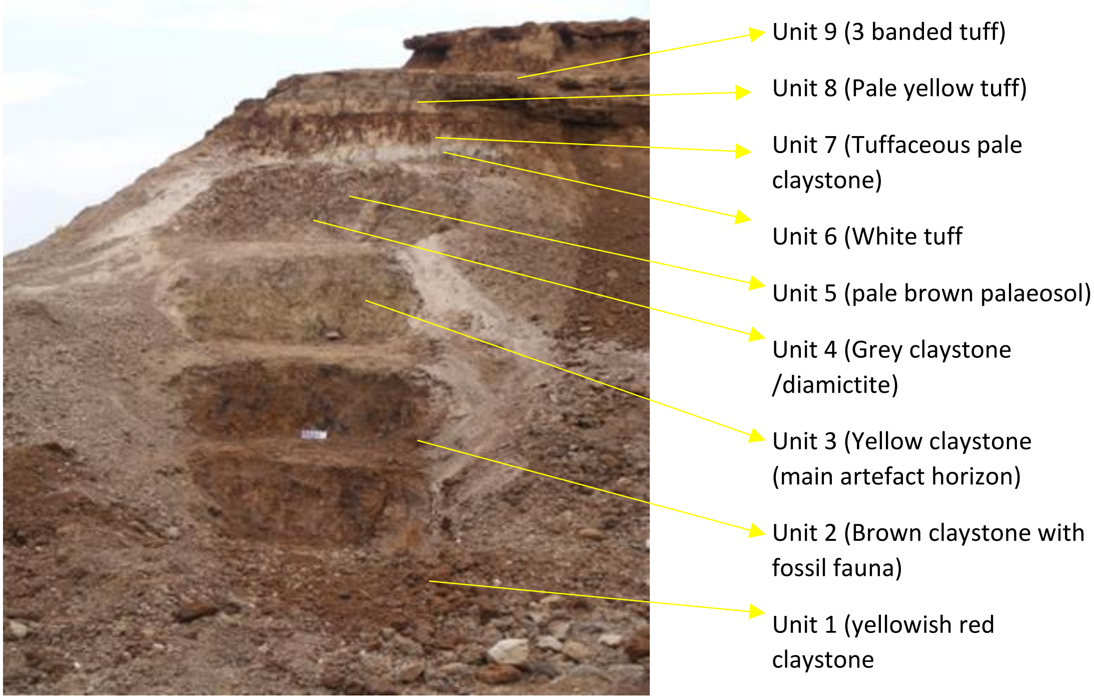

Figure 3.1 a individual stratigraphic units for Kilombe main site

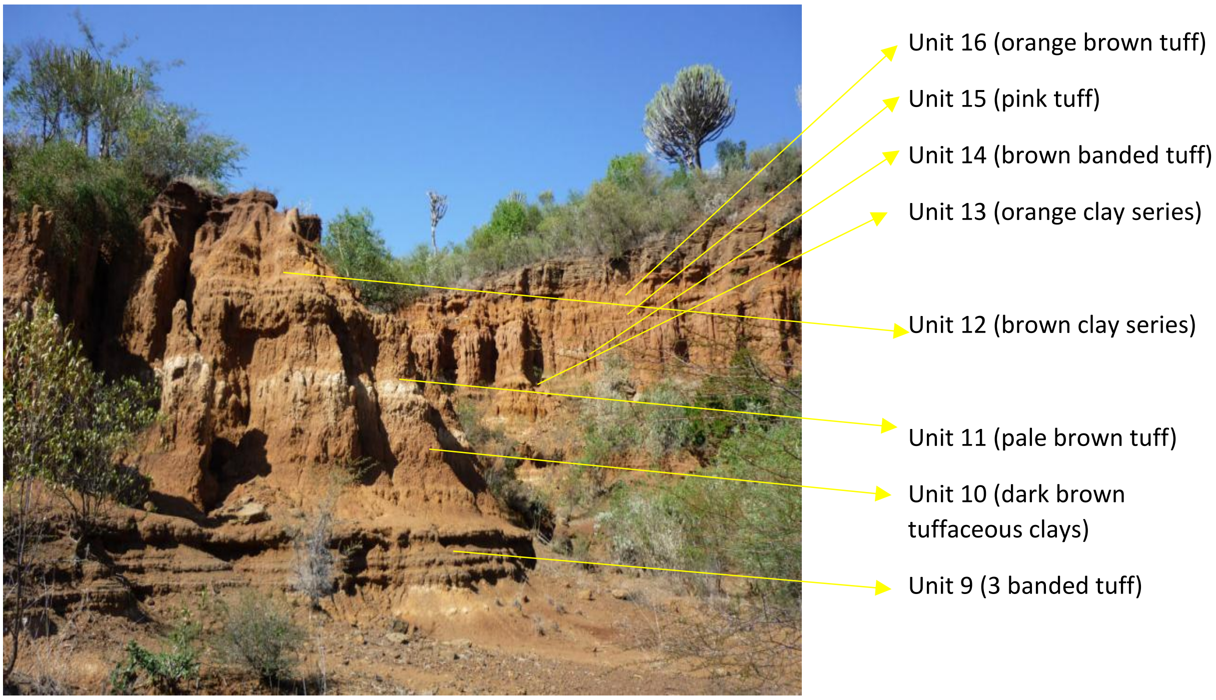

Figure 3.1 b individual stratigraphic units for Kilombe farmhouse cliff

3.13 Laboratory methodologies

3.13.1 Environmental magnetism

All the samples were freeze-dried for 24 hours and were then disaggregated using a mortar and pestle before packing into 10ml plastic pots. All 228 samples from GqJh1 (AH) and Farmhouse Cliff were subject to the following sequence of magnetic measurements:

Low frequency magnetic susceptibility (χ_{LF}) measured at 0.47 kHz and high frequency magnetic susceptibility (χ_{HF}), at 4.7 kHz, using a Bartingdon MS2 meter. The difference between the two measurements gives the frequency dependent susceptibility expressed as either mass specific property (χ_{FD}) or as a percentage of $\chi_{LF,}$ $\chi_{F\%.}$

Anhysteretic Remanent Magnetisation (ARM) was imparted using a DTECH alternating field demagnetizer with a peak alternating field of 100 mT and a DC biasing field of 0.1 mT. Plotted values have been normalised for the DC biasing field and expressed as $\chi_{ARM.}$

Saturation Isothermal Remanent Magnetisation (SIRM) using a 1 T field generated by an MMPM5 Pulse Magnetiser. Reverse field demagnetisation at fields of –20 $_{mT,}$ -40 $_{mT}$, - 100 $_{mT}$ and – 300 $_{mT}$ was then performed and samples were directly exposed to IRM reverse immediately after SIRM. All remanence measurements were made using a Molspin fluxgate spinner magnetometer with a noise level of 0.1 x 10 $^{-8}$ A m^2.

S-ratio, and Hard and Soft isothermal remanent magnetisation were subsequently calculated to characterise different grain size fractions and mineralogies in the samples. (HIRM = (SIRM+IRM$_{-300mT}$)/2, SOFT = (SIRM-IRM$_{-20mT}$)/2. S-ratios expressed as % reverse saturation, S$_{-20mT}$=(((-IRM$_{-20mT}$/SIRM)+1)/2)x100, S$_{-40mT}$=(((-IRM$_{-40mT}$/SIRM)+1)/2)x100, S$_{-100mT}$=(((-IRM$_{-100mT}$/SIRM)+1)/2)x100, S$_{-300mT}$=(((-IRM$_{-300mT}$SIRM)+1)/2)x100.

The following interparametric ratios χ_{ARM}/χ_{LF}, χ_{ARM}/SIRM, SIRM/χ_{LF} and χ_{ARM}/χ_{FD} were also calculated from pre-processed data.

3.13.2 Particle size separation

8 samples were selected for particle size analysis (for further magnetic analysis due to suspected dissolution) using a water tank and siphoning tube with settling times based on Stoke's Law. One hundred grams of each sample was processed by firstly ultrasonically dispersing and then shaking for 24 hours in an automatic shaker in calgon solution. After dispersal each sample was then wet-sieved through a 63 micron brass sieve which was used to separate the samples into coarse and fine fractions. The < 63 micron fraction was then transferred into 500 ml settling tubes filled with deinoized water and placed in a constant temperature bath (28 C). The sediments were then separated into seven particle size fractions < 2, 2-4. 4-8, 8-16, 16-32, 32-63 and > 63 microns based on settling velocities in water according to Folk (1965). At designated intervals based on settling times of Stoke's law 20 ml of the suspension was siphoned from the settling tubes. This was repeated 3 times to improve accuracy. Samples were then centrifuged at 400 rpm for 20 minutes and then freeze dried to remove water content. Samples were then weighed and subject to the full sequence of magnetic measurements outlined above.

3.13.3 XRF analysis

The major and trace element composition of the bulk sediment samples from Kilombe main site and farmhouse cliff were analysed using a Bruker Axis S2 Ranger energy dispersive X-Ray Fluorescence (XRF) to identify the amount of each major and trace element present in each sample. Sediments were gently disaggregated using a mortar and pestle. Disaggregated sediment (~0.5g) was packed into polythene containers and a Polypropylene film was stretched across the base of the container. The sediment was lightly pressed using a plunger. Standard reference materials were used to check the accuracy of the XRF (Buffalo River Sediment, San Joaquin Sediment, Pond Sediment and Stream Sediment). The four standard samples were run every 28 samples and the machine was calibrated using copper disc after every 28 samples also. As the samples were organic poor it was not necessary to adjust for organic matter content.

3.13.4 Organic matter content analysis (Loss on ignition)

Organic matter content for the Kilombe samples were calculated using the loss on ignition method (LOI) at 10 cm resolution. To remove the sediments moisture content approximately 0.5 g of the samples were weighed into 10ml porcelain crucibles and then oven dried at 105^{o} C overnight and then reweighed to determine moisture content. The samples were then placed into a furnace for a further four hours to remove all the organic matter present. The samples were then re-weighed again and then percentage of organic matter was subsequently calculated using a preformatted spreadsheet using moisture loss and the loss on ignitions results

3.13.5 Grain size analysis

Grain size analysis was carried out on sub samples from the Kilombe samples at 50 cm resolution and the grain size distributions of the samples were measured using a Coulter Laser Granulometer (LS200). As the samples were very low in organic matter it was not necessary to remove this before grain size analysis was carried out. Samples were first ultrasonically dispersed and then heated gently on a hotplate to reduce the samples into a slurry. A small amount of sediment from each of the dispersed samples was then mixed on a watch glass with calgon to disaggregate the sediment. Once smooth, the disaggregated sediment was added to the granulometer and the grain size was measured when satisfactory obscuration had been reached. The data was processed using the program GRADISTAT (Blott & Pye, 2001).

3.14 Statistical analysis

Statistical analysis was carried out for the different data sets individually with the same approach used throughout.

3.14.1 Principal component analysis and Pearson's correlation matrix

Principal component analysis is a multivariate statistical method that allows the study of a number of variables together. The primary function of principal component analysis is to reduce the dimensionality of data. In general the first three principal components can account for the majority of variation within a given data set. It also functions to assign source identity to each principal component analysed. PCA has been widely used in palaeoenvironmental studies in terms of palaeoenvironmental reconstruction and palaeoclimatology. Using eigenvalues and Pearson's correlation matrix relationships between data are generally classified as weak, <0.4, moderate, 0.5 - 0.7 and strong, >0.7. Eigen values also account for the percentage or proportion of variance explained by the factors in the raw data sets. In Pearson's correlation matrix two tailed tests of significance are applied with r values accounting for the strength of a given correlation and p values denoting statistically significant relationships (Hill & Lewicki, 2006).

3.14.2 Linear regression analysis

Linear regression analysis is a statistical approach that can be used to rapidly quantify basic associations among variables, which are usually represented on bivariate plots. In palaeoenvironmental studies this technique is often used to denote the relationship in a sedimentary sequence between two parameters or elements. A regression line is fitted to the set of data points, with the technique providing the best-fitting straight line through the points. Plots of residuals can also be used to examine points that fall away from the regression line and are not statistically significant as part on an overall trend or relationship (Hill & Lewicki, 2006).

Chapter Four Site and study area

4.1 Introduction

The first part of this chapter will provide background to the study area and history of research into the Acheulean site of Kilombe. The second part of the chapter will describe the new stratigraphic and chronological framework along with the model of soil forming factors based on Jenny (1941) that will form the basis of the palaeoenvironmental work in Chapters Five, Six and Seven.

4.2 Study area

The Central Rift Valley of Kenya is part of the East African Rift system an area which has been exposed to constant volcanic activity from the Miocene through to the Holocene and present day (King *et al.*, 1972; Baker *et al.*, 1970; Brotzu *et al.*, 1984; Strecker *et al.,* 1990; Spiegel *et al.*, 2007). Most of the volcanic activity is centred on the Kenya dome and the volcanic rocks extend for over a 1000 km along the Kenya Rift (King & Chapman, 1972). The Rift is characterised by intense faulting, which are normal and the displacements of which can vary from several metres up to several thousands of metres (King *et al.*, 1972). As a result of the Rift formation this area has a moderate altitude and forms a catchment for the drainage of two major forest stands to the east and west; the Nyandarua Mountains and the Mau Escarpment both of which lie at altitudes of 3960 m and 3000 m respectively. This area of the central Rift includes three large lakes: Elmenteita, Nakuru and Naivasha.

4.2.1 Climate setting

Present day climate patterns in East Africa are governed by several convergence zones and major airstreams which are superimposed on a number of regional influences including topographic, maritime and lacustrine (Nicholson, 2000). Wind and air pressure patterns include the Congo air stream and the north east and south east monsoon systems which are classed as dry monsoons. The major airstreams are separated by the Intertropical Convergence Zone, and this area is therefore strongly influenced by its seasonal migration and coinciding patterns of precipitation (Nicholson, 2000). Annual rainfall patterns are bimodal with most precipitation received in April and May and shorter rains occurring in November. These rainfall patterns follow the highest suns in March and September (Nicholson, 1996; 2000). Changes and variation in the intensity of precipitation are linked to east – west changes in Walker circulation and El Nino Southern Oscillation.

4.2.2 Local geological setting

The site of Kilombe lies ca.6 km south of the Equator at a junction between the Kavirondo Rift Valley and the Western side of the Central Rift (Jones, 1979). The geology of this area was first described by Gregory (1921) with further systematic geological mapping taking place in the 1960's and 70's by Jennings (1964; 1971), Mcall (1964) and Jones (1975) and Jones and Lippard (1979). The immediate area, shown in Figure 4.1, is dominated by the Plio-Pleistocene trachytic volcanoes of Londiani, Kilombe and Menengai which have altitudes of 3010, 2380 and 2278 metres respectively. Kilombe volcano, which is approximately 4 km from the study site, is a caldera volcano with a volume of 15 km^3 (McCall, 1964; Ridolfi *et al.*, 2006). The underlying geology of the local area consists of a series of alkali basalt lavas ranging in type from hawaiites and mugearite, and known as the Saos Mugearites, suggested to the products of Miocene eruptions (Jones, 1981). The basalts are now completely overlain by trachytes and trachyphonolite flows at Kilombe but do penetrate the trachytic flows at Londiani (Jones, 1981).

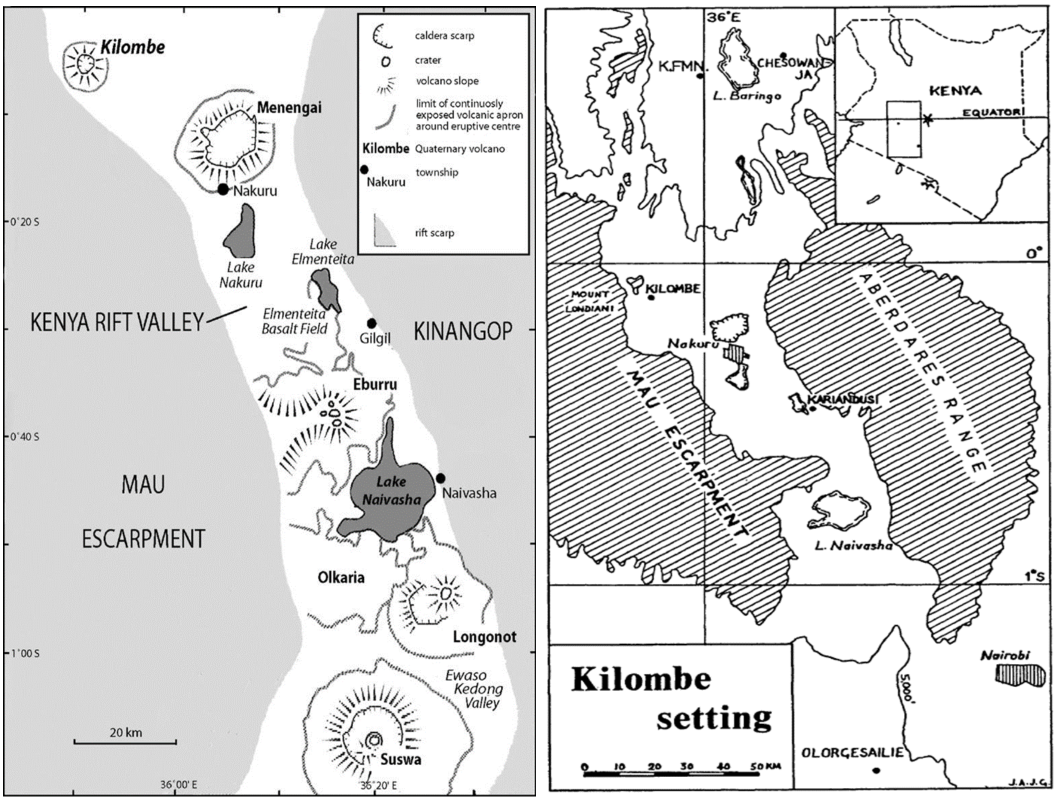

Figure 4.1 Topographical maps of Kilombe in relation to other Plio-Pleistocene volcanoes and the Mau escarpment and Aberdares (from Gowlett *et al*, 2015).

4.2.3 Environmental setting

The site of Kilombe lies approximately 4 km southeast of Kilombe volcano and 6 km south of the Equator co-ordinates 0^{o} 06'S, 35^{o} 53'E. Drainage is provided by two rivers, the Molo and Rongai, both of which rise from the Mau escarpment ca. 50 km to the south west of Kilombe then descend over 1500 m flowing north towards Lake Baringo 100 km further away. The rivers are fixed deeply into their valleys and although both are modern features it is likely that the main lines of drainage during the early to middle Pleistocene at Kilombe were ever far from the main site area (Figure 4.2). Today the area is well-vegetated and dominated by secondary acacia and euphorbia bush (Jennings, 1971; Gowlett *et al.*, 2015). Mean annual rainfall at Kilombe is around 917 mm (Rongai weather station).

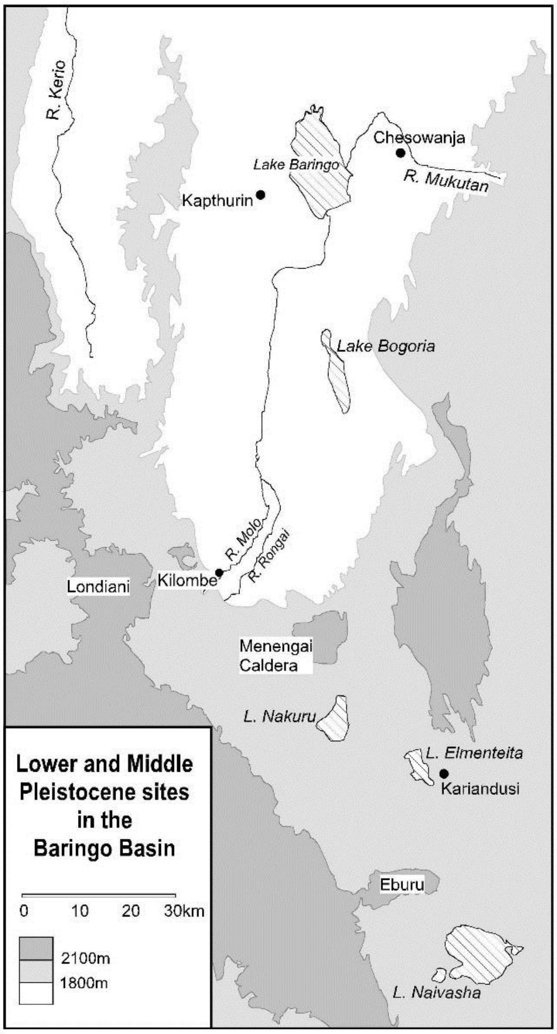

Figure 4.2 Local topographic map of Kilombe in relation to main drainage lines and other geological features (from Gowlett et al, 2015).

4.2.4 History of research

Geologist W. B. Jones, during the course of geological mapping conducted as part of the EAGRU project, first discovered the Acheulean site complex of Kilombe in 1972. The first full geological and archaeological research was carried out by W. W. Bishop and J. A. J. Gowlett in 1978, (Bishop, 1978; Gowlett, 1978). One of the main features of Kilombe is the extensive main artefact horizon occurring on a clayey surface and allowing the study of over 700 Acheulean handaxes in a single occupation and also allowing comparison of site formation and taphononmic processes (Gowlett, 1978; Gowlett, 1988; Gowlet & Crompton, 1994; Gowlett *et al.*, 2015). New research since 2008 has aimed to develop a much stronger context for archaeological interpretation including improved chronology for the site and the first detailed palaeoenvironmental research conducted through this PhD.

4.2.5 Archaeology and Fauna

One of the most distinctive feature archaeologically at Kilombe is the occurrence of hundreds of Acheulean bifaces that are exposed across a land surface for around 200 metres in all directions (Gowlett *et al.*, 2015). The archaeology of Kilombe offers an almost unique opportunity to study variation among contemporaneous bifaces within a single site complex. Bifaces studies so far have come from both surface collection and excavation with bifaces commonly occurring at the contact point between the dark brown clays and pale pumiceous tuff (now re-named the grayish brown claystone and pale yellow claystone (units, 2 and 3). The dominant raw materials used in manufacture are the local trachyphonolite lavas which comprise around 93% of raw material used. The bifaces have been subject to chemical weathering to a pale grey colour but were originally black (shown from broken bifaces). Almost all the remaining bifaces were manufactured from trachyte which was available locally at Kilombe volcano c. 3-4 km away. During the January 2011 field season two handaxes of trachyte were also found at the foot of Kilombe gorge which leads out from Kilombe volcano caldera. In the course of recent field research numbers of handaxes have also been found at higher levels now including levels towards the top of Farmhouse Cliff and also in lower units within the four meters above the three-banded tuff (3BT). The 3BT is one of only two primary airfall tuffs at Kilombe and therefore a key dating horizon for the site. The 3BT has been previously dated to > 780,000 Ka via the identification of a palaeomagnetic reversal (Bishop, 1978; Gowlett, 1978) and has now yielded a more constrained age of 1.03 Ma via $^{40}Ar/^{39}Ar$ (discussed further in section 4.3.3).

Faunal remains at Kilombe are not prolific however, at least 12 individual taxa are now recorded and examined by J. S. Brink. Faunal remains are only observed at the north end of the main site from the lower units of brown clays and more specifically at the contact area between the lower RBC and upper DBC (now re-defined as the yellowish red claystone and brown claystone). Local preservation of these remains only occur in a certain area and has been interpreted as being representative of an area where the clays were accumulating rapidly. The most common animal represented at Kilombe is hippopotamus and there is a range of bovids including giant buffalo and gazelle (Gowlett *et al.*, 2015).

4.2.6 Previous geological and palaeoenvironmental work

The fullest and clearest local stratigraphy in the region is preserved around Kilombe (GqJh1) and Farmhouse Cliff and was first described by Bishop (1978). Previous work on the geology and palaeoenvironments at Kilombe was undertaken by Jennings (1971) Jones (1979). Bishop's work categorised and surveyed the lithological units at Kilombe main site and farmhouse cliff and identified 8 major stratigraphic units starting with the weathered trachyphonolite lavas finally capped by a massive ashflow tuff. Figure 4.3 from Bishop (1978) shows the stratigraphic section starting with Kilombe main site and then Farmhouse cliff.

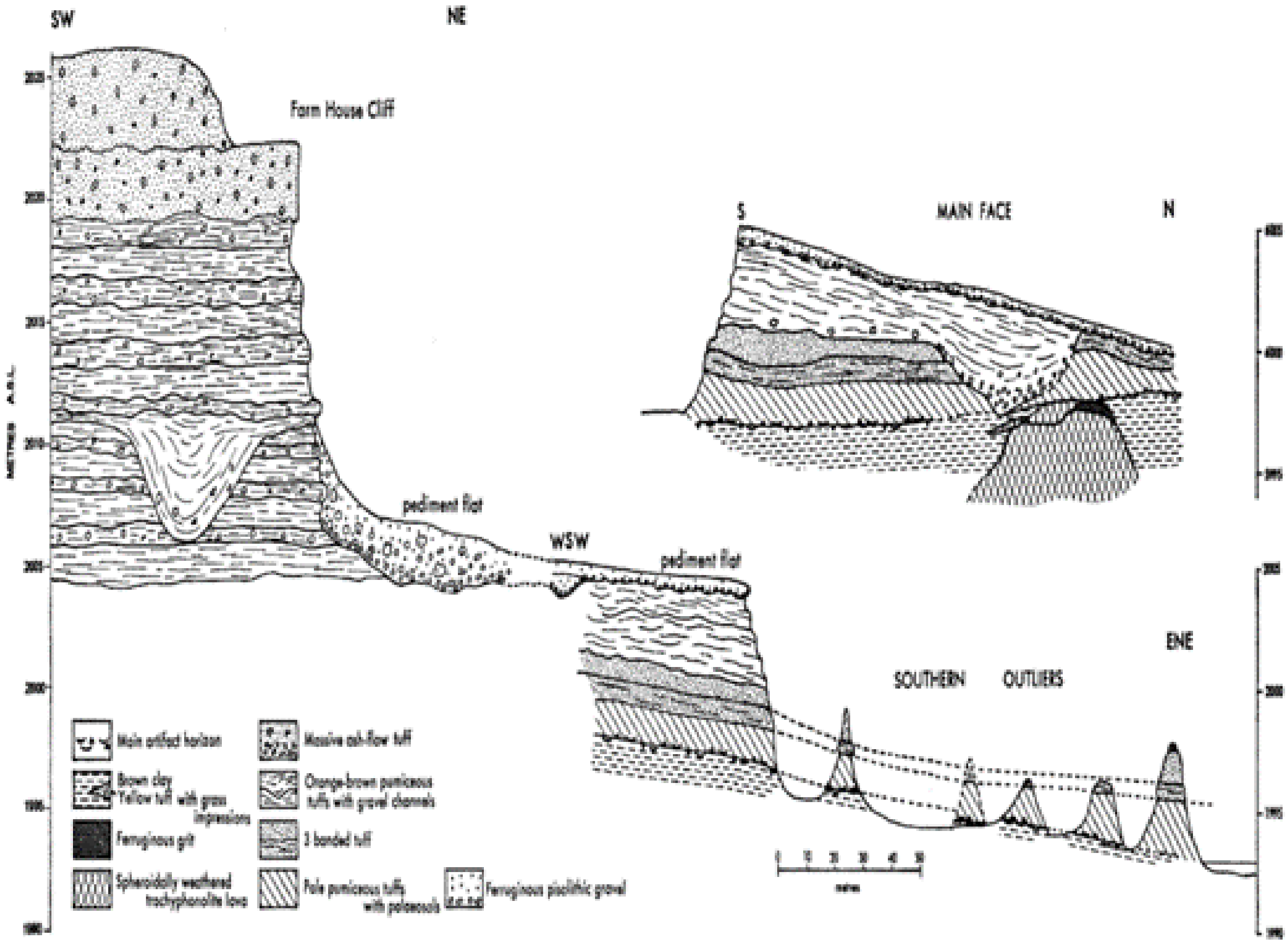

Figure 4.3 Original stratigraphic column, Bishop (1978).

Bishop (1978) demonstrated that the Pleistocene sediments have become exposed through at least two cycles of erosion. An early cycle of pedimentation is argued to have produced extensive flats with notch cliffs surviving at the back of the flats protected by the ashflow tuff. Beneath the pediments a series of badland amphitheatres occur in an erosional gully system within which the main archaeological horizons occur (Bishop, 1978; Gowlett, 1978).

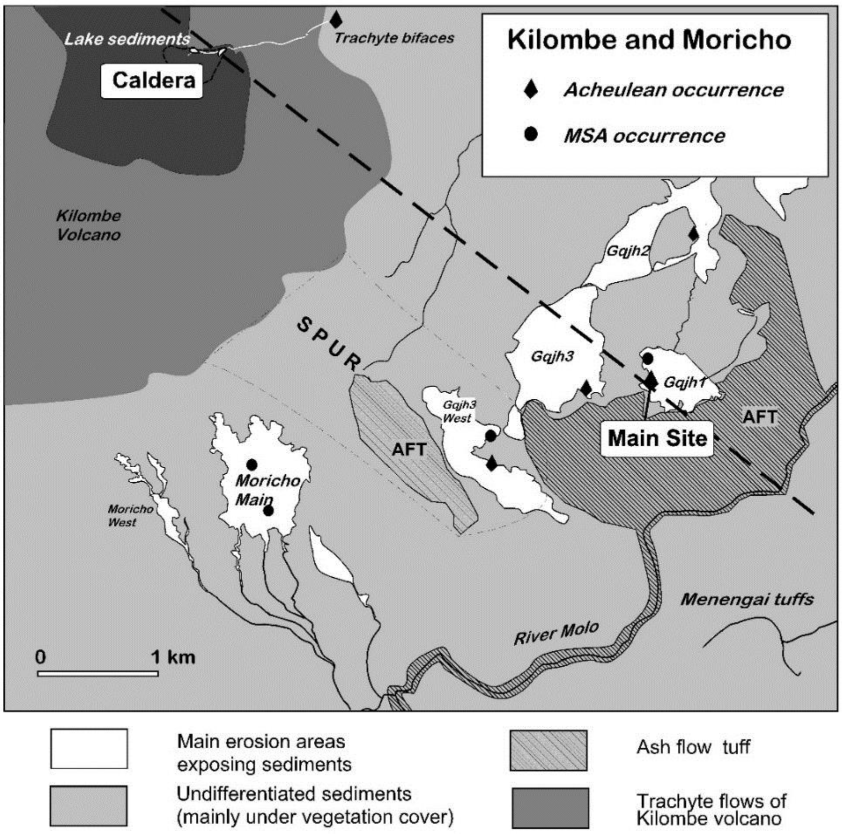

Figure 4.4 Map of Kilombe main site (Gqjh1) in relation to Kilombe Volcano (from Gowlett *et al*, 2015).

The sequence at the main site starts with the lowest unit of trachyphonolite lavas previously dated to 1.7 +/- 0.05 Ma by K-Ar (Bishop, 1978), and suggested by Jones (1979) to be contemporary with the later trachyte flow from Kilombe volcano dated to c. 1.9 +/- 0.15 Ma.

Figure 4.4 shows the location of Kilombe main site (Gqjh1) in relation to Kilombe volcano. The trachyphonolite lavas are extensive across the region south of the volcano and both the irregular surface and ridges formed during deposition may have helped to cause ponding in some local areas (Gowlett *et al*, 2015).

On the main site Bishop (1978) suggested that the clays are the weathering products of the trachyphonolite lavas. Bishop further argued that, aside from its occurrence in clefts and hollows in the lava, the clays were not in situ weathering products and the sequence was colluvial via the mechanism of soil creep. Bishop (1978) suggested that the source rock for the Kilombe sediments is a ridge of trachyphonolite lava located at Kilombe volcano. Soils are argued to have formed from chemical weathering of the lavas with transportation occurring via a combination of lubrication of the regolith with water and subsequent movement downslope via soil creep. In terms of depositional history of the sediments and soils Bishop suggests that a phase of deep weathering and subaerial erosion directly followed the deposition of the lava flows from Kilombe volcano and that the weathering products were subsequently re-deposited as clays in the hollows of the lava. The main artefact horizon is suggested to occur on a clay wash surface within which lens of grit and sand may indicate the presence of shallow channels and ephemeral runnels. The pale pumice tuffs with root casts and palaeosols were held to indicate subaerial conditions and these palaeosols also indicate intervals of soil development. Although minor corrections have been made to Bishop's stratigraphic framework, almost all of these early interpretations have been supported by recent fieldwork and thin section analyses presented in section 4.3 and further detail on relief and topography is presented in Chapter 3.

4.3 New stratigraphic and chronological framework

4.3.1 Stratigraphy

Previous investigations Bishop (1978) had defined lithofacies for Kilombe from fieldwork. The stratigraphy was redefined by Gowlett *et al*., (2015) and has been subsequently refined during the course of this PhD based on new field descriptions and supplemented by some laboratory thin section analysis (Kilombe main site by Professor Ian Stanistreet, University of Liverpool) to confirm field descriptions. This work expands on the lithofacies results and conclusions of Bishop (1978) and now places the sedimentary sequence at Kilombe into a well-defined sequence stratigraphic framework. The strata at Kilombe were designated into individual lithologic units and sub-units, and subsequently facies association, which were then used to characterise and interpret the various depositional environments, to develop the sequence-stratigraphic framework at Kilombe for palaeoenvironmental analyses.

During the July 2011 to 2013 field seasons 228 samples were extracted from GqJh1 (AH) at 5 cm and Farmhouse Cliff at 10 cm intervals using geology hammers and chisels and approximately 30 grams of material were taken for each sample. Samples were placed immediately into pre-labelled plastic sample bags for transportation back to the laboratory. A step trench was dug approximately 1 metre into the sediments to create a uniform vertical surface, eliminate surface contamination and enable the extraction of fresh material. A further 9 samples (200 grams) were taken from the centre of each unit from the main site GqJh1 (AH) for particle size separation in 2013. A resolution of 5 and 10 cm was selected with the aim of capturing the nature of climate change on different timescales (long-term trends and orbital/sub-orbital).

The sedimentary sequence at Kilombe is comprised of primary and re-worked volcanic ash and pumice tuffs, colluvial claystones and palaeoesols. The 25 metre thick measured sequence at Kilombe is now sub-divided into 16 sedimentary units based on the characteristic sedimentologic attributes for lithofacies reconstruction. The individual descriptions of units and facies including lithology, thickness, colour, sedimentary structures, and fossils, bedding characteristic and post-depositional features are presented in Table 4.1 and described in section 4.3.2, Facies analysis, and Figure 4.6 shows photographs of the sedimentary sequence for Kilombe with new age determinations and key marker horizons. Figure 4.7 shows the new sequence stratigraphy with the new age determinations yielded through both $^{40}Ar/^{39}Ar$ and palaeomagnetic dating.

Redating of the basal trachyphonolite lava via $^{40}Ar/^{39}Ar$ has yielded a new age determination of 1.57 Ma. This age therefore rules out any normal polarity periods occurring after this age such as Olduvai subchron (1.95-1.78 Ma). The confirmation of the recording of a normal polarity in both the yellowish red and brown clays coupled with the identification of Brunhes-Matuyama recorded in unit 15, the pink earthy tuff, suggest this to be the Jaramillo subchron occurring between 1.07 and 0.99 Ma (Ashton, 2013). This gives a maximum age of 1.07 Ma for the basal yellowish red claystone. The $^{40}Ar/^{39}Ar$ of 1.03 Ma from the three-banded tuff would appear to be in conflict with the palaeomagnetic age of 0.99 obtained for the brown claystone, however, the associated error margin of 0.12 Ma for the $^{40}Ar/^{39}Ar$ age allows a strong correlation of both dates within the error margin. A further period of normal polarity occurs in unit 11, the pale brown clayey tuff, which is now identified in the sequence as Santa Rosa at 0.932 Ma (Ashton, 2013).

Unit number & name	**Number of samples & sample codes**	**Thickness (cm)**	**Facies association**	**Granulometry (sediment type, textural group & mean grain size μm)**	**LOI %**	**Munsell colour**	**Sorting**	**Sedimentary structures - bedding**	**Roundness**
1 Yellowish red claystone	32 (KL1-KL53	1830 - 1670 cm	1	Fine silt (mud) (2.5)	7	5 YR 5/5/8 (Yellowish red)	Poorly	Very thickly	Sub-rounded/sub-angular
2 Grayish brown claystone	19 (KL57 – K15)	1670 – 1575 cm	1	Clay (mud) (1.9)	7.6	10 YR 5/5/2 (Grayish brown)	Moderate	Very thickly	Sub-rounded
3 Pale yellow claystone	7 (K16-K22)	1575 - 1540 cm	1	Mud (mud) (1.8)	5.8	5 Y 7/7/3 (Pale yellow)	Poorly	Medium	Sub-rounded
4 Grey clay/diamictite	10 (K23-K32)	1540 - 1490 cm	1	Mud (mud) (1.9	6.2	5 Y 6/6/1 (gray)	Poorly	Medium	Sub-rounded-sub-angular
5 Palaeosol pale brown	7 (K33-K39)	1485 – 1455 cm	2	Mud (mud) (2)	5	10 YR 6/6/3 (Pale brown)	Poorly	Medium	Angular/sub-angular
6 White tuff	1 (K40)	1455 - 1440 cm	4	Mud (mud) (2)	1	10 YR 1 (White)	Moderate	Thinly	Rounded-sub-rounded
7 Tuffaceous pale brown claystone	7 (K41-K47)	1445 – 1410 cm	1	Mud (mud) (1.7)	7.7	10 YR 7/7/4 (Very pale brown)	Moderate	Medium	Sub-rounded
8 Pale yellow tuff	1 (K48)	1410 cm	4	Very fine silt (mud) (3.9)	8.8	2.5 Y 2 (Pale yellow)	Poorly	Thinly	Rounded-sub-rounded
9 Three banded tuff (1 metre deposit represented by one sample here)	1 (K50)	1405 cm	3	Fine sandy silt (sandy mud) (15)	7.8	10 YR (6/6/4)	Very poorly	Thickly	Angular-sub-angular
10 Dark brown tuffaceous clays	8 (1-9)	1400 – 1320 cm	3	Very fine silt (mud) (4)	7.2	10 YR 3/3 (Dark brown)	Poorly	Thickly	Sub-rounded
10 (A) Orange clay band	1 (5)	1360 cm	4	Mud (mud) (3.5)	10	10 YR 7/8	Poorly	Thinly	Sub-rounded
11 Very pale brown clayey tuff	17 (10 - 26)	1310- 1150 cm	4	Very fine silt (mud) (4)	8.4	10 YR 7/3 Very pale brown	poorly		Sub-rounded/sub-angular
11 **A** White tuff	1 (21)	1200 cm	4	-		5 Y 8/1 white	-	Thinly	Sub-rounded
12 Brown clay series (5 sub units)	22 (27-49)	1140 – 930 cm	4	-	-				
A light gray tuff	6 (27-32)	1140 - 1090	4	Very fine silts (mud) (4.4)	12	10 YR 7/7/1 light gray	Poorly	Medium	Sub-angular/sub-rounded

Unit number & name	**Number of samples & sample codes**	**Thickness (cm)**	**Facies association**	**Granulometry (sediment type, textural group & mean grain size μm)**	**LOI %**	**Munsell colour**	**Sorting**	**Sedimentary structures - bedding**	**Roundness**
B yellowish brown tuffaceous clays	3 (33-35)	1080 - 1060 cm	4	Very fine silt (mud) (4.4)	9.7	10 YR 6/4 Light yellowish brown	Poorly	Thinly	Sub-rounded/sub-angular
C brownish gray tuffaceous clay	3 (36-38)	1050-1030 cm	4	Very fine silt (mud) (2.6)	4.6	10 YR 6/2/ light brownish gray	Poorly	Thinly	Sub-rounded/sub-angular
D yellowish brown tuffaceous clays	5 (39-44)	1020-980 cm	4	Fine silt (mud) (5.1)	8.3	10 YR 5/4 yellowish brown	Poorly	Medium	Sub-rounded/sub-angular
E yellow tuff	5 (45-49)	970 – 930 cm	4	Fine silt (mud) (5.1)	15	10 YR 7/8 yellow	Poorly	Medium	Sub-rounded
13 Orange clay series (6 sub-units)	18 (50-69)	920 -750 cm		-	-				
A white tuff	1 (50)	920 cm	4	-	15	2.5 Y 8/1 white	-	Thinly	Sub-rounded
B yellow clay	2 (53-54)	910 – 900 cm	4	Fine silt (mud) (6.2)	13	10 YR 7/8 yellow	Poorly	Thinly	Sub-rounded/sub-angular
C white clayey tuff	2 (55-56)	890 – 880 cm	4	-	14.1	2.5 Y 8/1 white	Poorly	Thinly	Sub-rounded/sub-angular
D yellow clay	5 (57-61)	870 -830 cm	4	Fine silt (mud) (5.4)	12.1	10 YR 7/8 yellow	Poorly	Medium	Sub-rounded/sub-angular
E white tuff	4 (62-65)	820-790 cm	4	Fine silt (mud) (7.7)	13.1	10 YR 8/1 white	Poorly	Medium	Sub-rounded
F brownish yellow clay	4 (66-69)	780 – 750 cm	4	Very fine sandy silt (sandy mud) (7.7)	14	10 YR 6/8 brownish yellow	Poorly	Medium	Sub-rounded/sub-angular
14 Brown banded tuff with clay deposits	14 (70-83)	740-610 cm	4	Very fine silt (sandy mud) (10)	8.7	7.5 3/3 YR dark brown	Poorly	Thickly	Sub-rounded/sub-angular
15 Pink earthy tuff	43 (84-126)	600 – 180 cm	4	Very fine silt (mud)(5.3)	7.7	5 YR 6/2 pinkish gray	Poorly	Thickly	Sub-rounded/subangular
16 Orange brown earthy tuff	18 (127-144)	170 – 0 cm	4	Very fine sandy silt (sandy mud((6.9)	5.6	7.5 YR 6/8 reddish yellow	Poorly & very poorly	Thickly	Sub-rounded/sub-angular

Table 4.1 Individual descriptions of units and facies association for the Kilombe sediments including lithology, thickness, colour, mean grain size and Loss on ignition % values

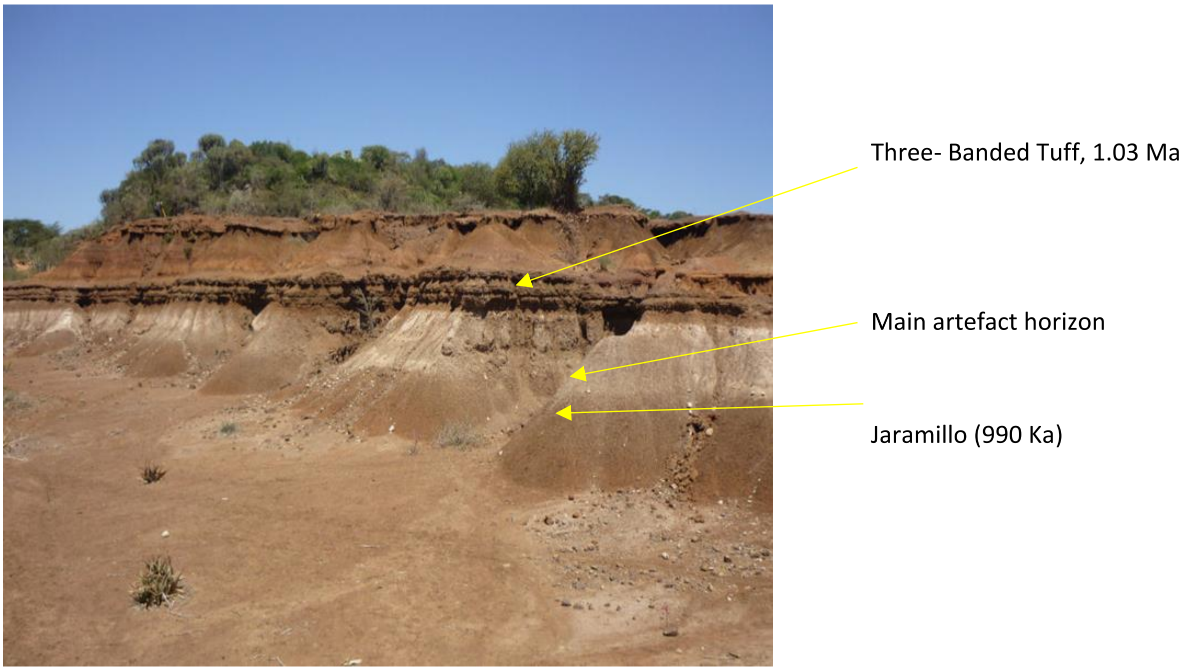

Figure 4.6 (a) stratigraphy at Kilombe main site with key marker horizons. Figures b and c show individual strata

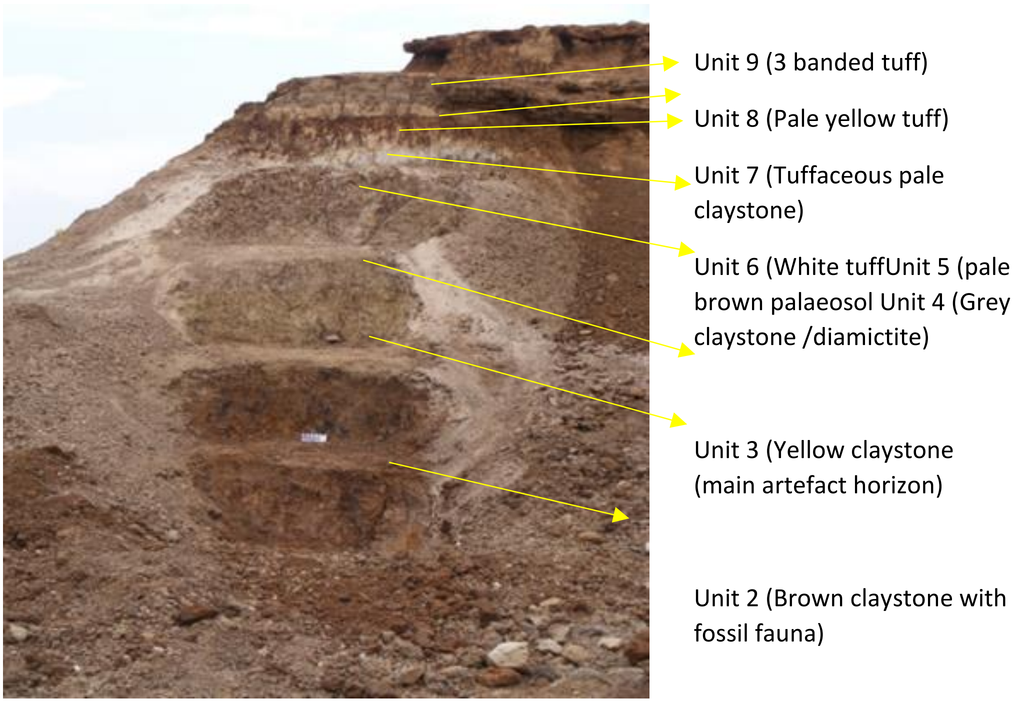

Figure 4.6 (b) Kilombe main site

Figure 4.6 (d) Farmhouse Cliff
Figure 4.6 (c) Kilombe main site

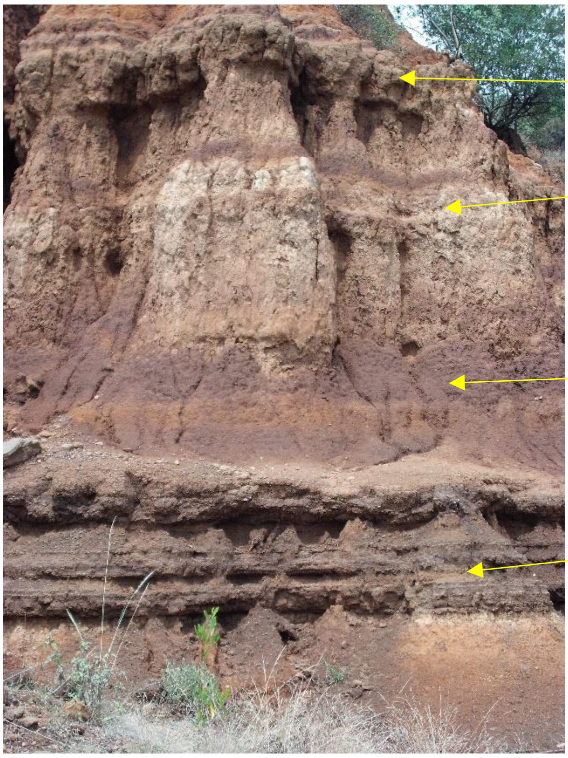

Figure 4.6 (e) Farmhouse Cliff

Figure 4.6 (f) Farmhouse Cliff

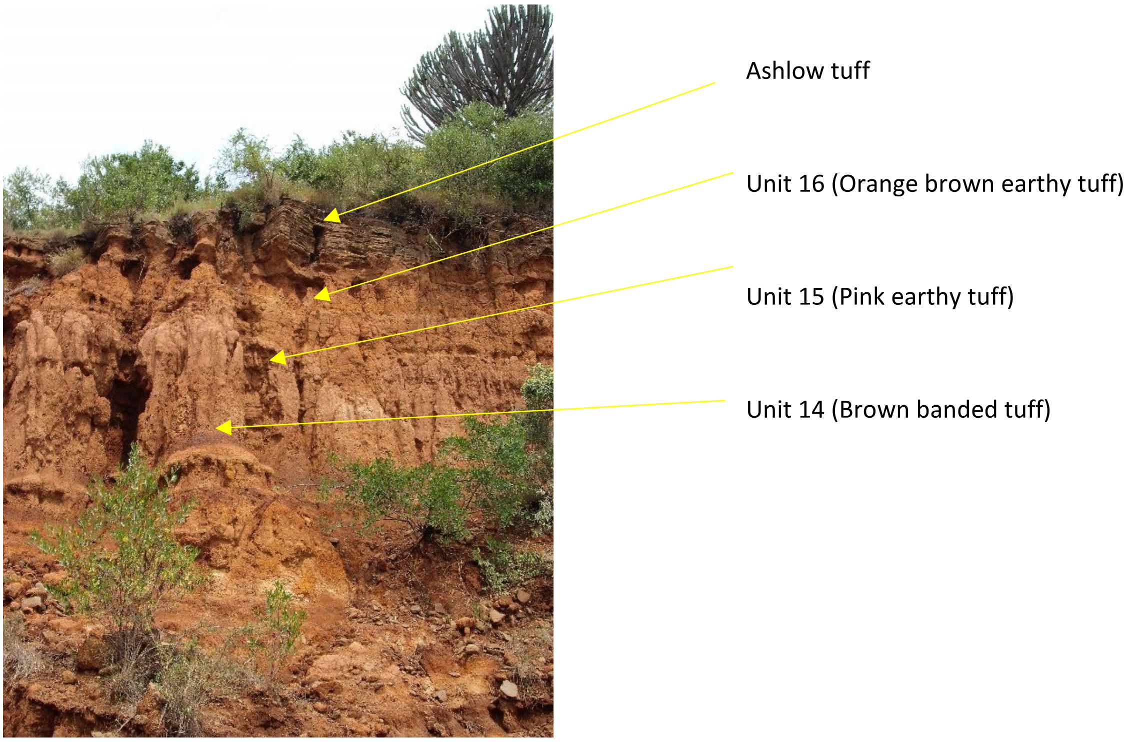

Figure 4.6 (g) Farmhouse Cliff

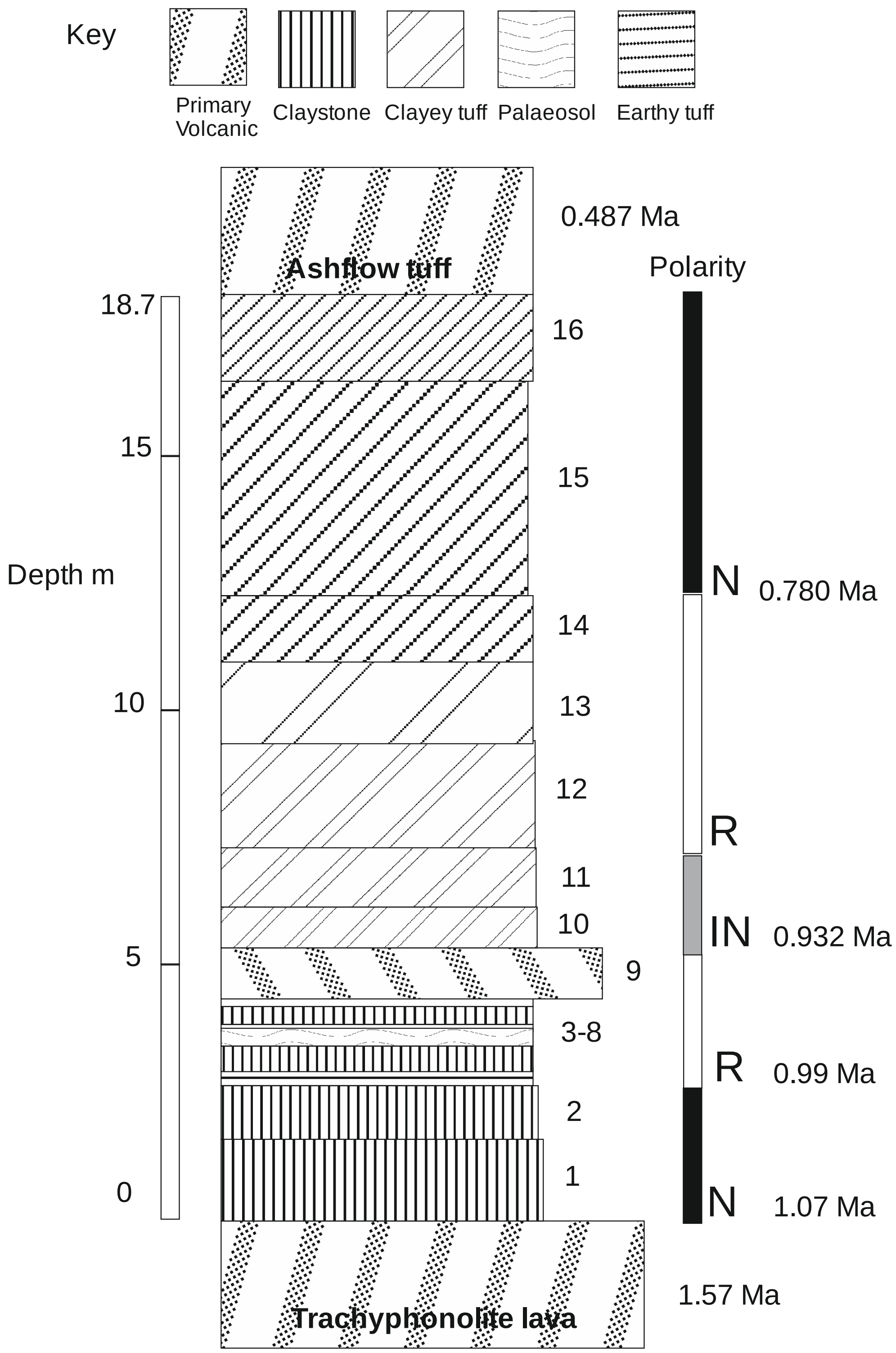

Figure 4.7 Composite stratigraphic section with age determinations for the Kilombe sequence

4.3.2 Facies analysis

Claystone Facies (1)

<u>Description</u>

The claystone facies correspond to Bishop's (1978) brown clays, palaeosol and pale pumiceous tuffs. This facies now corresponds to units 1, 2, 3, 4 and 7 listed in table 4.1. The claystone facies consist of various forms from sandy (unit 2) to tuffaceous (unit 7) claystones. The colours vary significantly ranging from brown to red, grey and yellow. In section, thickness ranges from 1.5 metres to 35 centimetres. Sedimentary features are generally structureless and upper and lower contacts are either gradational to other claystones or sharp to some of the tuffs. The claystone facies contain no organic remains or fossils aside from unit 2 (brown claystone) which contain fossil fauna remains. The micro-structure is commonly either subangular-blocky or angular blocky and may be post-depositional. Manganese veins occur within most of the units as do small orange, black and yellow inclusions. These inclusions are prominent in units 2- 5 on the main site than in unit 1.

<u>Interpretation</u>

The processes of deposition and formation of the claystone facies are soil development at source rock, Kilombe volcano, and subsequent transportation via colluvial processes and sheet wash to the sedimentary basin (Bishop, 1978). Processes of formation most likely include compaction and all show evidence for pedogenic overprinting in the field and in thin section.

Palaeosol Facies (2)

Description

Only one unit, 5, within the Kilombe main site sequence corresponds to this facies association and corresponds to Bishop's (1978) palaeosol. This facies is recognised by the development of interstitial clay overlain by a resedimented tuff and overprints unit 4 (diamictite/clay). It is generally poorly sorted with a clay matrix. The thickness of this unit is 35 cm. The sedimentary structures are post-depositional based on cross-cutting relationships and these include large blocky angular and subangular-blocky peds which can be 3 cm long/wide, which become smaller towards the top of the unit and may indicate weak horizons. Other post depositional features include manganese veins and clay coating on the peds. Abundant redoximorphic features are observed such as hard black rounded Fe–Mn concretion

Interpretation

Palaeosols are generally identified using three defining characteristics either soils structures and horizons or root traces. Using these characteristics unit 5 is interpreted as a palaeosol which has formed from chemical weathering and pedogenesis during a process of subaerial exposure. This may represent a hiatal surface with a substantial time gap for soil development to have taken place. The palaeosol appears to have been preserved in this instance by deposition of a resedimented tuff which overlies this unit.

Primary airfall tuff (3)

Description

Only one unit, 9, in the sequence corresponds to this facies association. However, there are number of units at FHC which may also represent primary ashfall and would need to be confirmed by thin sections analysis. This unit, 9, which occurs as three distinct beds and exhibit graded bedding and laminations. This unit is 1 metre thick and is a brown lapilli tuff, coarse-grained with abundant K-Feldpars which are visible in section and hand specimens. This unit corresponds to Bishop's (1978) three-banded tuff argued to represent either primary airfall tuff or deposition within still water environment.

Interpretation

The sedimentary structures and abundant, pristine, unaltered K-feldspar crystals suggest a primary tephra deposit deposited by a concentrated air current and mechanical transportation. This deposit is underlain by a beige re-worked tuff which may represent the more acidic phase of a continuous eruption.

Re-worked tuffs (4)

Description

The re-worked tuffs correspond to Bishop's (1978) pale pumice tuffs and orange-brown pumiceous tuffs and now include tuffaceous clays and clayey tuffs. Units (6, 8, 10, 11, 12, 13, 14, 15 and 16) correspond to this facies association and they range in thickness from 10 to 400 cm. The colours range from white, yellow, dark brown, pink and orange brown. The tuffs vary from fine to coarser grained, are generally crystal poor, most are structureless (Kilombe main site) whilst others on FHC classed as clayey tuffs preserve features such Mn concretions and clay coated peds.

Interpretation

The re-worked tuffs appear to have been deposited through similar processes to the claystone facies and some are argued to show re-working in fluviatile channels (Bishop, 1978). Crystals, were preserved, are rounded and show evidence of re-working. FHC tuffs (units, 14, 15 and 16) show evidence of pedogenic overprinting with redoxomorphic features being more prominent in the upper six metres of FHC. Some tuffs attributed to this facies association may represent some primary ash deposits (unit 12 a) and will need to be further investigate using micromorphology.

4.3.3 Establishing chronological controls at Kilombe

The new age determinations at Kilombe presented in Figure 4.8 (a and b) are based on dates using geomagnetic polarity reversals (palaeomagnetism) and also the timing of volcanic eruptions ($^{40}Ar/^{39}Ar$ single crystal laser fusion). Two age depth models were produced for Kilombe. The first being based on $^{40}Ar/^{39}Ar$ dates alone, and the second being based on the results of both $^{40}Ar/^{39}Ar$ and palaeomagnetism. The new $^{40}Ar/^{39}Ar$ dates were provided by Dr Leah Morgan and Dr Darren Mark from the Scottish Universities Environmental Research Council (SUERC laboratories, East Kilbride). Three samples from the archaeological site were selected for dating, the trachyphonolite lava, the 3BT (lithological unit 9) and the ashflow tuff. The implications of these new age determinations are discussed more fully in Chapter 7, section 7.3.2.1. A further sample of trachyte lava was also dated from Kilombe volcano.

Figure 4.8 (a) Age-depth model for the Kilombe sedimentary sequence based on $^{40}Ar/^{39}Ar$ dates

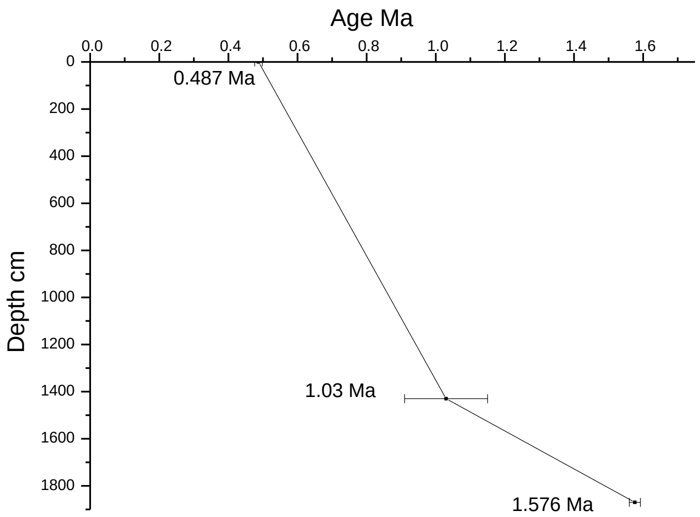

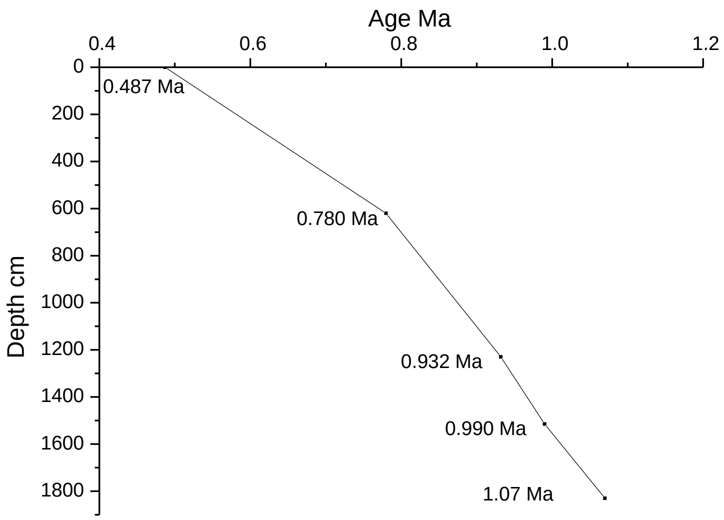

Figure 4.8 (b) Age-depth model for the Kilombe sedimentary sequence based on $^{40}Ar/^{39}Ar$ and palaeomagetic dates

4.3.3.1 Age depth models

A variety of approaches can be taken in producing age-depth models. In terms of the limited number of absolute ages available at Kilombe the most appropriate model was deemed to be linear interpolation. Figure 4.8 a depicts the first age-depth model for Kilombe based on just the $^{40}Ar/^{39}Ar$ dates. This model alone would suggest the Kilombe sedimentary sequence at the main site and Farmhouse cliff to be approximately 1 million years in duration. This is unlikely given the length of the entire sequence, which is continuous and contains no obvious major hiatuses or erosional surfaces, and including the ashflow tuff is only around 25 metres. The second age-depth model, Figure 4.8 b, takes into account the palaeomagnetic ages and boundaries of the reversals. This second model would suggest that the Kilombe sequence has a duration of approximately 500,000 kyr. The combination of both dates yields a more accurate chronology and the second age-depth model is therefore selected.

4.4 Model of soil/sedimentation and accumulation at Kilombe

4.4.1 Autogenic factors to consider (formation of the Kilombe sequence)

In terms of understanding the climatic/environmental factors which may be controlling changes in the Kilombe data sets (Chapters 5 and 6) and specifically the acquisition of geochemical and magnetic properties in the soils/sediments, as well as the lithological variation presented in Figure 4.7, there are a number of other important autogenic factors to consider, as outlined in Chapter three, by Jenny (1941). These factors, specifically time, relief, climate and parent material and examine how the interplay between these factors may either act to promote or inhibit intensity of chemical weathering and pedogenesis at Kilombe.

4.4.1.1 Time

The combined age model in figure yields a maximum age of 1.07 Ma at the base of the sedimentary sequence (yellowish red claystone) and a minimum age of 487 Ka at the top of the sequence (ashflow tuff). This suggests that the duration of sedimentation in this part of the basin was approximately 500,000 years which gives a substantial time frame in which pedogenic processes and chemical weathering intensity can enact. The effects of changes in sedimentation rates are discussed more fully in Chapter 7 however, sedimentation rates between established ages in the sequences shows that accumulation rates are quite variable at this site. The lower part of sequence at Kilombe main site has been subject to rapid sedimentation rates of approximately 4 cm per/Ka, whilst sedimentation rates across the upper part of FHC are much lower at 2 cm per/Ka which suggests that the soils/sediments in this part of the record would have had a substantial time to undergo chemical weathering processes under long exposure times and duration of weathering.

4.4.1.2 Relief

Relief at Kilombe can be classed as low (Figure 4.9) Attitudinally there is only 3 metres difference between the base of Kilombe volcano (1823 m), and Kilombe main site (1820m) with a difference between the two points of approximately 4 km. Heights do vary significantly with topography on a SW-NE axis. However, to be noted is that there is a 300 metre difference attitudinally between the crater rim of Kilombe resulting in high relief at the volcano. The trachyphonolite ridge, argued by Bishop (1978) to represent the source rock for sediments on Kilombe main site, is around 100 metres higher than FHC and the main site and the resulting slope angle (transportation path) is low, with changes in altitude occurring gradually along the valley. The gradient of the slope is low and therefore the resulting slope angle can also be classed as low. In terms of low relief and low slope angle the likely result would be decreased rates of erosion resulting in much longer exposure to chemical weathering intensity at Kilombe. However, there are significant changes in altitude which depending on the path of transportation from Kilombe volcano could indicate high relief at times and increased erosion.

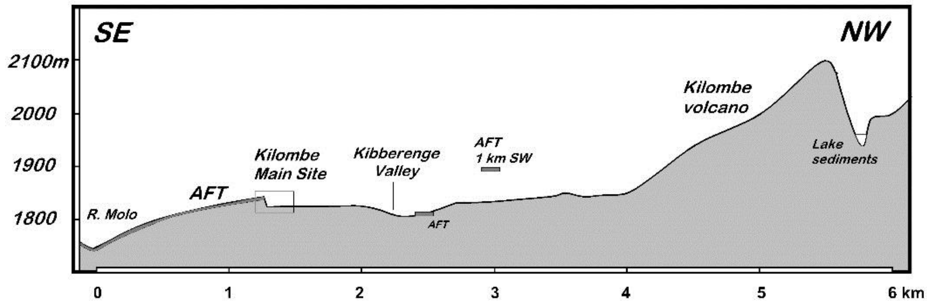

Figure 4.9 Distance (kilometres) and altitudinal differences (metres) between Kilombe main site and Kilombe volcano (from Gowlett *et al*, 2015).

4.4.1.3 Climate

The sedimentary sequence at Kilombe covers the time span 1.07 Ma – 487 Ka, although the basal trachyphonolite lavas date to 1.57 Ma. Very few localised climate records are available aside from Elmenteita, Olorgesaille and the Kapthurin Formation from which to examine the potentially effects of local climates across this time frame. However, a number of records are available from the wider East African Rift and also the marine core archives. In terms of wider trends in Palaeoclimatic change 1 Ma – 500 ka, climate data from both marine, lacustrine and Δc^{13} for East Africa suggest a long-term trend towards aridification punctuated by periods of climatic variability resulting in much wetter (but highly variable) phases and the occurrence of large deep lake phases in the Rift Valley and driven by changes in eccentricity modulated precession (deMenocal, 2004; Trauth *et al*., 2005).In effect, it is likely that prevailing climates across the 500,000 year duration of the Kilombe sequence were highly variable effecting both levels of precipitation and temperature driven by changes in the East African Monsoon systems and at times major global climate change.

4.4.1.4 Parent material

Bishop (1978) described the resistance of the trachyphonolite lavas to chemical weathering. In general, igneous rocks formed at the surface are more in equilibrium with surface conditions and therefore more resistant to chemical weathering conditions (Ernst, 2000).At Kilombe both the trachyte and trachyphonolite flows are formed at the surface in this area which would results in resistance to chemical weathering intensity for sediments derived from their weathering, specifically the claystones on Kilombe main site.

4.4.1.5 Model

In summary the factors of time, relief, and climate and parent material, examined in the context of the Kilombe data present a model which would favour enhancement of rather than reduction of chemical weathering and pedogenic intensity. The relationship between the above factors at Kilombe is however complex. In general, low relief and slope angle leads to decreased erosion, low sedimentation rates and long exposure times resulting in enhanced chemical weathering with accumulation rates on site also affecting rates of post-depostional alteration and pedogenic activity, whereas high relief and increased erosion reduces time for weathering. However, climate and specifically rainfall and temperature are also major factors controlling rates of erosion. East African climate records, particularly those recording the behaviour of the East African monsoon systems shows the period 1 Ma to 500,000 to record pronounced variability between wet/dry conditions driven by changes in orbital precession. Variation between high and low levels of precipitation could potentially act at Kilombe to increase rates of erosion at time of higher rainfall, reducing chemical weathering intensity, and could further act to reduce chemical weathering intensity even at times were decreased levels of erosion and long exposure times were influenced by lower rainfall. In effect, resulting in a complex model for examining environmental/climate change at this site.

4.5 Conclusions

The Acheulean site of Kilombe is extremely important archaeologically due to the possibilities of study allowed by the number of handaxes from a single horizon (Gowlett, 1978; Gowlett *et al.*, 2015). Kilombe is also one of the few archaeological sites which preserves a continuous record of sedimentation and potentially palaeoenvironmental change over a long time period. New research since 2008 resulting in the discovery of handaxes from higher levels suggests that there may have been a continuous or recurring human presence in the local area. New age determinations and refinements of the stratigraphic column for the Kilombe presented in this chapter, along with the model based on Jenny (1941) now provide a strong chronological and lithological framework within which to examine palaeoenvironmental/palaeoclimatic change for this long term human occupation.

Chapter Five Major and trace element geochemistry

5.1 Introduction

This chapter presents the results of X-ray fluorescence (major and trace elements geochemistry). Chapter three Theory and methodology highlighted a number of issues in terms of evaluating the response of geochemical data sets to palaeoclimatic change. Two of the main issues apparent are the influence of changes in source rock or parent material and the influence of sorting signal or changes in grain size. A further complication is that changes in the data can often be the result of changes in lithology. It is therefore necessary to evaluate both the individual major and trace element data and chemical weathering indices in terms of response to lithology at Kilombe and also in terms of any possible response to changes in source rock or sorting signal.

The first part of this chapter will present the results of major and trace element data and chemical weathering indices for each lithological unit at Kilombe with the support of statistical analyses and will then present the defining geochemical characteristics of each lithological unit. A summary of the mineralogy will then be provided. The second part of the chapter will examine geochemically any potential changes in source rock and then evaluate chemical weathering indices against source rock and sorting signal. A preliminary palaeoclimatic interpretation of the link between chemical weathering intensity and climate at Kilombe is provided before summary and conclusions.

5.2 Major and trace element geochemistry and mineralogy

A description of the individual lithological units is presented in Chapter 4 along with graphic sedimentary log. The statistical summary of PCA and Pearson correlation matrix is given below and presented in Figure 5.1 and Table 5.1 The major and trace element data is graphically presented in Figure 5.2 a and b and detail is given in Appendix 2. Average values and ranges are presented for each lithological unit in Table 5.2.

5.2.1 Statistical analysis

The use of multivariate statistics can provide information, in a broad sense, on the controlling factors in changes in element concentrations in a geochemical data set.

5.2.1.1 Pearson's correlation matrix

The major and trace elemental correlations were determined for the Kilombe samples by calculating Pearson's correlation matrix. The inter-elemental relationships showed that Si shows only a statistically significant and positive relationship with K ($r = 0.46$, $p<0.05$) which is in turn only positively correlated with Rb (0.74, $p<0.05$) and Sr (0.58, $p<0.05$). Si also shows a strong but negative relationship with Fe (-0.90, $p<0.01$) and Al (-0.82, $p<0.01$). Whilst Al is only moderately correlated with Fe (0.56, $p<0.01$) and negatively correlated with K (-0.47, $p<0.05$). Fe shows a moderate correlation with Ti (0.57, $p<0.01$) and Mn (0.60, $p<0.01$) and with V, Cu, Zn and Ga (0.55, 0.63, 0.46 and 0.47, all at $p<0.05$). Titanium is moderately to strongly correlated with Ca, V, Cu and Ni (r = 0.63, 0.76, 0.67 and 0.62, $p<0.01$). Calcium is only positively correlated with Ti (r = 0.63, $p<0.01$). Mn exhibits moderate to strong positive correlations with Fe and Ba (0.53, $p<0.05$ and 0.73, $p<0.01$). Ba is also correlated moderately with Rb, Sr, Ni, Cu, V and Ti (0.42, 0.52, 0.46, 0.46, 0.58 and

0.41, all at $p<0.05$). Ga is moderately to strongly correlated, positively with Pb, Zr and Nb ($r = 0.61$, 0.78 and 0.70, $p<0.01$). Vanadium shows a moderate to strong statistical correlation with Fe, Ni, Ti and Cu ($r = 0.55$, 0.61, 0.76 and 0.70, $p<0.05$). Zn is only correlated with Nb ($r = 0.54$, $p<0.05$) which in turn also correlates with Ga, Pb, Zr and Sr ($r = 0.78$, 0.75, 0.94, $p<0.01$ and 0.54, $p <0.05$). Zr correlates strongly and positively with both Pb, Ga and Nb ($r = 0.75$, 0.70, 0.94, $p<0.01$).

	Si	Al	Ca	K	Fe	Mn	Ti	Ba	V	Cu	Ga	Pb	Ni	Nb	Rb	Sr	Y	Zn	Zr
Si	1	**-0.82857**	-0.29302	0.46238	-0.90622	-0.46933	-0.58089	-0.2467	-0.50239	-0.62185	-0.46188	-0.35255	-0.38894	-0.2898	0.20161	0.15891	-0.02628	-0.4221	-0.27107
Al	**-0.82**	1	0.13256	-0.49621	0.56163	0.23705	0.31017	0.08754	0.22848	0.47707	0.47373	0.31342	0.34794	0.24873	-0.3568	-0.1482	-0.08468	0.33347	0.26997
Ca	-0.29	0.39897	1	0.11134	0.20625	-0.02545	0.63105	0.28739	0.30905	0.21312	-0.30645	-0.32629	0.20608	-0.44915	0.07669	0.42456	-0.0175	-0.08987	-0.45162
K	**0.46238**	-0.04061	0.11134	1	-0.48151	-0.19194	0.00615	0.23835	0.13538	-0.16336	-0.38516	-0.12242	0.06875	-0.22689	0.74721	0.58585	-0.28635	-0.50511	-0.21077
Fe	-0.90622	0.13256	0.20625	-0.48151	1	0.53932	0.57222	0.22305	0.55772	0.63246	0.47855	0.38467	0.32709	0.35131	-0.11973	-0.26569	0.1134	0.46622	0.29739
Mn	-0.46933	-0.49621	-0.02545	-0.19194	0.53932	1	0.17647	0.73357	0.43485	0.44075	0.26086	0.36786	0.27709	0.25681	0.09959	-0.01987	0.0431	0.20731	0.19954
Ti	-0.58089	0.56163	0.63105	0.00615	0.57222	0.17647	1	0.41888	0.76242	0.6788	-0.16386	-0.06621	0.62725	-0.30246	0.26695	0.26257	-0.10194	-0.17915	-0.28768
Ba	-0.2467	0.23705	0.28739	0.23835	0.22305	0.73357	0.41888	1	0.58106	0.46699	-0.15445	0.03065	0.46586	-0.19228	0.42563	0.52355	-0.16115	-0.27762	-0.20611
V	-0.50239	0.31017	0.30905	0.13538	0.55772	0.43485	0.76242	0.58106	1	0.70864	0.05563	0.18234	0.61472	-0.07089	0.46537	0.28591	-0.31796	-0.2067	-0.08572
Cu	-0.62185	0.08754	0.21312	-0.16336	0.63246	0.44075	0.6788	0.46699	0.70864	1	0.1194	0.3175	0.71745	0.04125	0.25738	0.05544	-0.18039	0.05409	0.05984
Ga	-0.46188	0.22848	-0.30645	-0.38516	0.47855	0.26086	-0.16386	-0.15445	0.05563	0.1194	1	0.61319	-0.02946	0.78105	-0.22536	-0.3679	-0.0526	0.51122	0.70805
Pb	-0.35255	0.47707	-0.32629	-0.12242	0.38467	0.36786	-0.06621	0.03065	0.18234	0.3175	0.61319	1	0.24618	0.75531	0.08725	-0.28837	-0.03395	0.42221	0.75822
Ni	-0.38894	0.47373	0.20608	0.06875	0.32709	0.27709	0.62725	0.46586	0.61472	0.71745	-0.02946	0.24618	1	-0.05561	0.35822	0.14694	-0.07806	-0.27687	-0.00152
Nb	-0.2898	0.31342	-0.44915	-0.22689	0.35131	0.25681	-0.30246	-0.19228	-0.07089	0.04125	0.78105	0.75531	-0.05561	1	-0.12826	-0.43395	0.10757	0.54829	0.94448
Rb	0.20161	0.34794	0.07669	0.74721	-0.11973	0.09959	0.26695	0.42563	0.46537	0.25738	-0.22536	0.08725	0.35822	-0.12826	1	0.53735	-0.15874	-0.44709	-0.08746
Sr	0.15891	0.24873	0.42456	0.58585	-0.26569	-0.01987	0.26257	0.52355	0.28591	0.05544	-0.3679	-0.28837	0.14694	-0.43395	0.53735	1	-0.30125	-0.50104	-0.43714
Y	-0.02628	-0.3568	-0.0175	-0.28635	0.1134	0.0431	-0.10194	-0.16115	-0.31796	-0.18039	-0.0526	-0.03395	-0.07806	0.10757	-0.15874	-0.30125	1	0.18744	0.1411
Zn	-0.4221	-0.1482	-0.08987	-0.50511	0.46622	0.20731	-0.17915	-0.27762	-0.2067	0.05409	0.51122	0.42221	-0.27687	0.54829	-0.44709	-0.50104	0.18744	1	0.50732
Zr	-0.27107	-0.08468	-0.45162	-0.21077	0.29739	0.19954	-0.28768	-0.20611	-0.08572	0.05984	0.70805	0.75822	-0.00152	0.94448	-0.08746	-0.43714	0.1411	0.50732	1

Table 5.1 Pearson's correlation matrix showing the association of major and trace elements at Kilombe

5.2.1.2 Principal component analysis

Principal component analysis aims to reduce the dimensionality of data so that the key elements can be expressed in a smaller number of new variables. In this study PC1, PC2, PC3 and PC4 account for approximately 76% of the total variation in the entire geochemical data set. The principal component scores determined by eigenvectors show that PC1 accounts for 30%, PC2 27%, PC3 12% and PC4 6% of original variance. The bulk of the variance is therefore accommodated by PC1 and 2 and equals 57%.

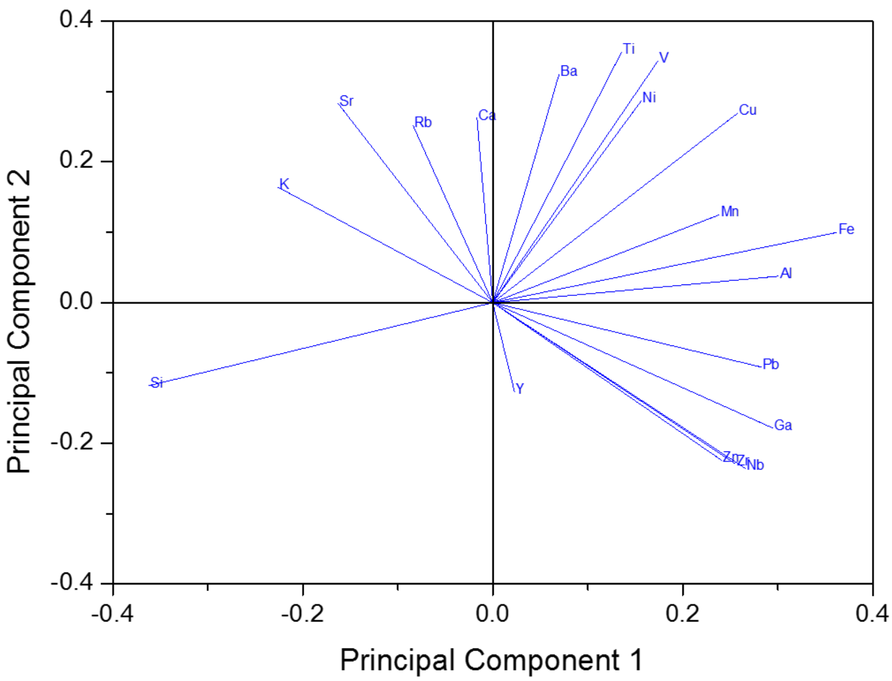

Figure 5.1 Principal component loading plot showing the distribution of major and trace elements for Kilombe across PC1 and PC2.

Figure 5.1 shows that when PC1 and 2 values are plotted for individual elements four broad element associations can be recognised. One of the most obvious controls on the bulk geochemistry is changes between Si or quartz, and most other elements. This is shown by the fact that Si has a negative PC1 score whilst all other elements have positive scores.

- Group 1 Si (Quartz)
- Group 2 K, Rb and Sr (Feldspars)
- Group 3 Al, Fe and Mn (Clay minerals/micas)
- Group 4 Zn, Zr, Nb, Pb and Ga (Heavy minerals, Zircon)

The remaining elements are more evenly distributed across both PC1 and PC2 and also show moderate correlations to one another in r values in Pearson's matrix.

5.3 Mineralogy

In sedimentary rocks Si is mainly concentrated in the detrital component produced during chemical weathering, the main sources of which include quartz and the feldspars. The abundance of Si in sediment samples therefore provides a broad indication of quartz which in turn is mostly inversely related to the amount of clay. Elements found to be in close association with Si can be assumed to be linked in to coarser grain sizes and often the detrital component. In this study K shows a close, but moderate, association with Si in Pearson's correlation matrix and PCA, as well as with Rb and Sr, this suggests that K is being controlled by detrital grains and specifically the K-feldspars. The strong association of K and Rb also suggests concentration in K-feldspars. K shows further but moderate correlation with Sr suggesting that Sr is also concentrated in the K-feldspars (the main carrier of Sr) and/or incorporation into the clay minerals along with Ba. The weak correlation observed between Ti and Al suggested that Ti is not concentrated in the phyllosilicates and is concentrated in other mafic minerals instead, perhaps clinopyroxene, this suggestion may be further supported by the strong correlation of Ca and Ti (r = 0.63). The positive correlation of Fe and Al suggests that Fe is controlled by the aluminous phases, in part the clay minerals and/or micas. The moderate correlation of Fe and Mn may be indicative of the co-precipitation of both elements in the sediments. In sedimentary rocks Ga is generally concentrated in the clay minerals and micas and usually shows a strong and positive correlation with Al regardless of depositional environment. Ga shows no correlation with Al statistically and closer affinity with Nb, Pb and Cu. Ga is therefore associated with the heavy minerals in this record.

5.4 Results stratigraphical variation

Figures 5.2 and 5.2 a show the variation in analysed measurements with stratigraphy. All elements analysed were compared with globally average values for intermediate rocks from Krauskopf (1982) and are deemed to be consistent with values for the local bedrock geology of trachytes and trachyphonolites. In terms of geochemical composition the dominant element in the Kilombe assemblage, as would be expected, is Si and therefore any variation in this element would significantly affect changes in concentration of other elements either by dilution or concentration and not being related to changes in source provenance. The sampling resolution allows a strong characterisation of elemental distributions based on stratigraphical variation, and there does appear to be a strong relationship between element concentration and changes in lithology.

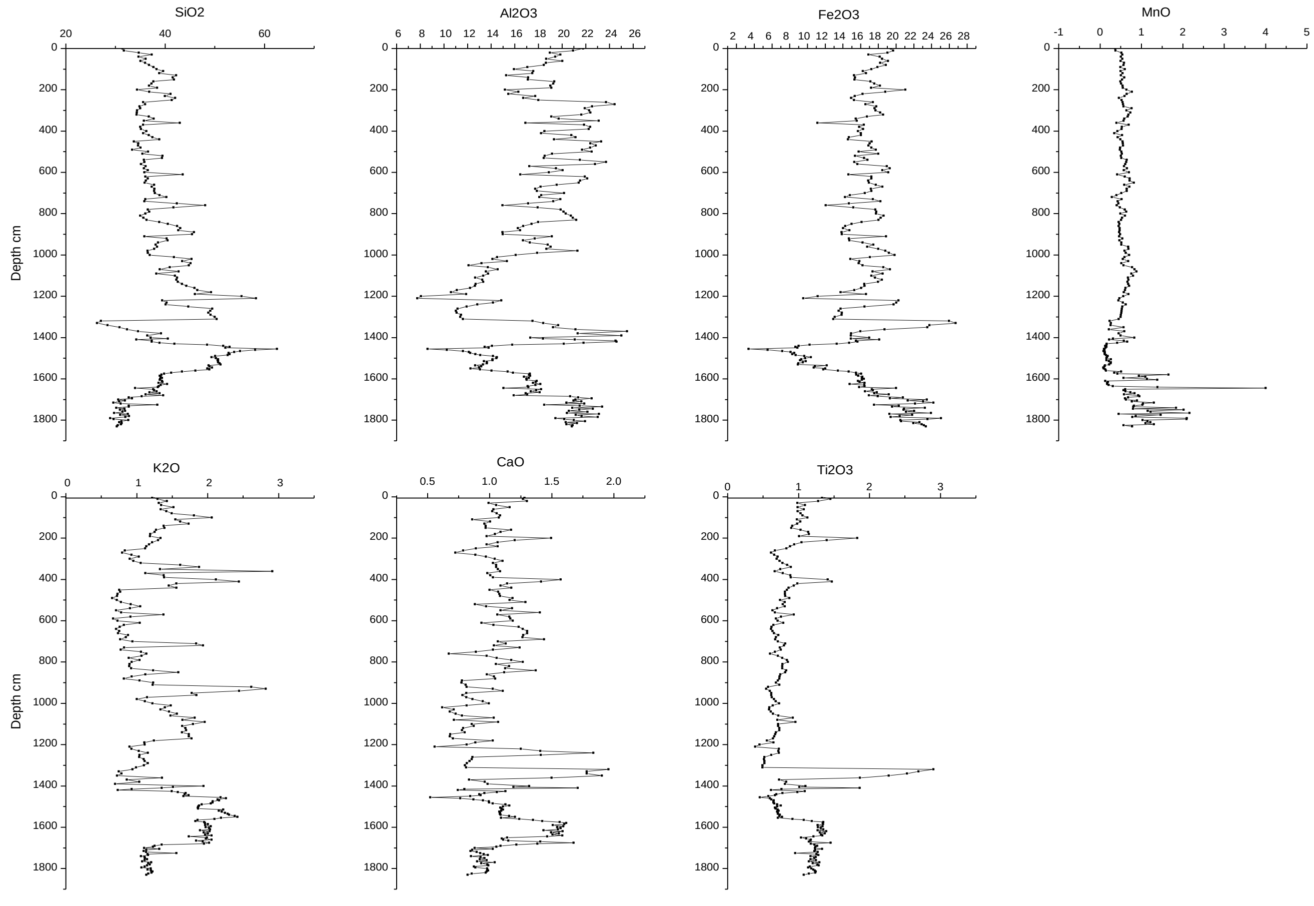

Figure 5.2 a Stratigraphical variation of major elements for the Kilombe sequence

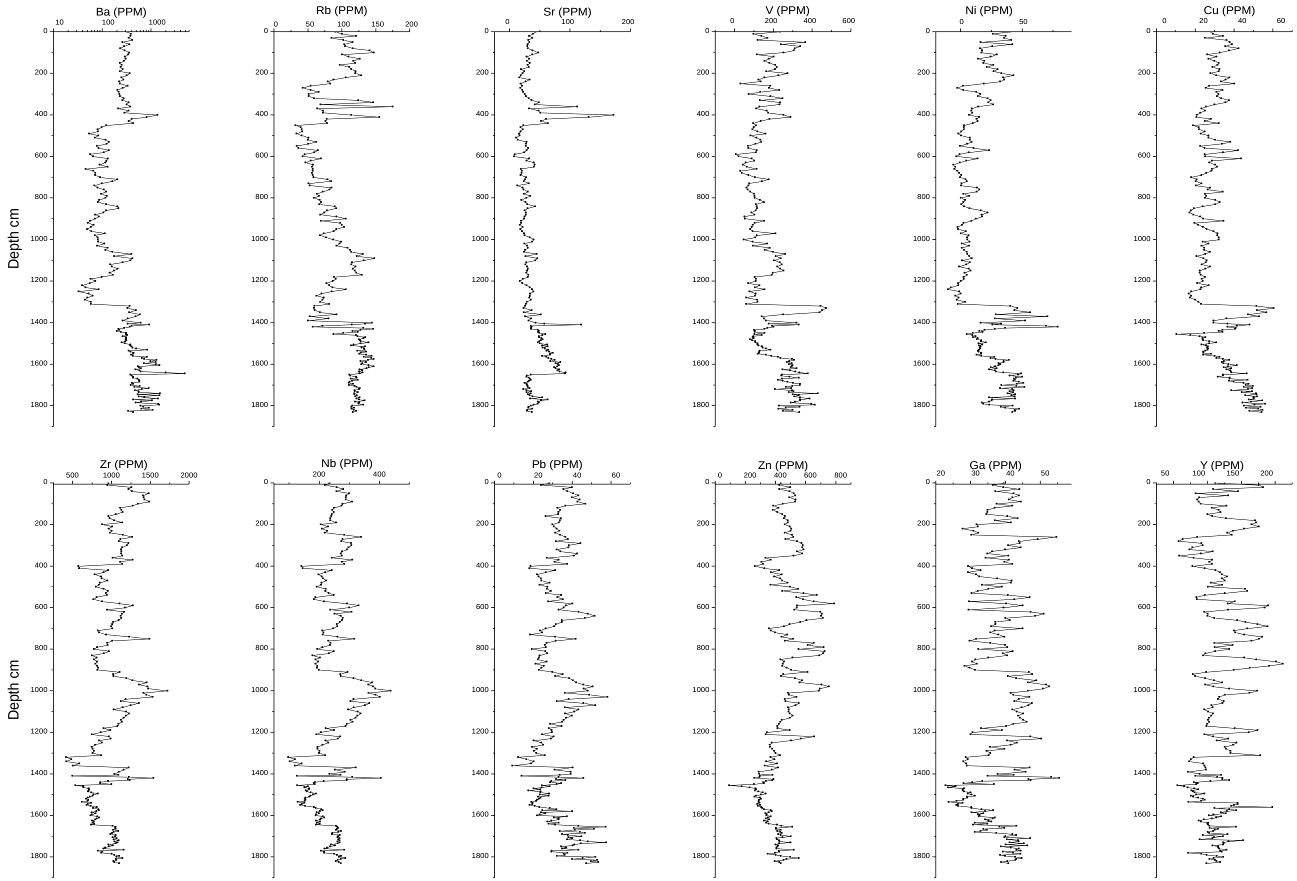

Figure 5.2 b Stratigraphical variation of trace elements for the Kilombe sequence

Lithological unit and sample numbers associated with each unit	Number of samples in each unit	SiO_2	Al_2O_3	CaO	K_2O	Fe_2O_3	MnO	Ti_2O_3
16 (127-144)	18	**37.1** (31.4 - 42.2)	**18.4** (15.9)	**1** (0.85-1.2)	**1.4** (1.1-2)	**17.6** (15.3-19.4)	**0.51** (0.37-0.58)	**1** (0.97-1.3)
15 (84-126)	43	**36.5** (34.42)	**20.3** (15.4	**1** (0.78 - 1.5)	**1.1** (0.7-2.9)	**16.7** (11-21.1)	**0.56** (0.34 -76)	**0.87** (0.68 - 0.98)
14 (70-83)	14	**37** (35-43)	**19.4** (18-22.5)	**1.1** (0.93-1.4)	**0.97** (0.93 - 1.4)	**16.7** (14.7-18.4)	**0.57** (0.28-0.81)	**0.69** (0.61-0.81)
13								
F (66-69)	4	**42** (36.5 -48)	**17.4** (14.9-19.8)	**0.89** (0.6-1)	**1** (0.88-1.3)	**14.8** (12-17.6)	**0.48** (0.4-0.6)	**0.68** (0.59-0.77)
E (62-65)	4	**35.8** (35-36.8)	**20.5** (20.1-20.9)	**1.1** (1-1.2)	**0.95** (0.89-1**)**	**18** (17.7-18.6)	**0.56** (0.49-0.63)	**0.80** (0.77-0.85**)**
D (57-61)	5	**40.2** (35 -42.4)	**17** (16.2 - 17.9)	**1.1** (0.9-1.3)	**1.2** (0.9-1.5)	**14.8** (14-16.1)	**0.46** (0.44-0.47)	**0.77** (0.72-0.83)
C (55-56)	2	**44** (42.6 -45**)**	**15.7** (14.9-16.4)	**0.9** (0.77-1)	**0.9** (0.81-1)	**14.2** (13.8-14.7)	**0.46**	**0.71** (0.70-0.72)
B (53-54)	2	**45.3**	**14.9**	**0.77**	**1.2**	**13.8**	**0.48**	**0.68**
A (50)	1	**40.3**	**17.6**	**0.8**	**2.6**	**14.6**	**0.53**	**0.57**
12								
E (45-49)	5	**38.6** (37-40.5)	**18** (16.7-19)	**0.9** (0.78 – 1)	**2** (1.4-2.8)	**16.6** (14.7-17.9)	**0.57** (0.51-0.68**)**	**0.59** **(**0.54-0.62)
D (39-44)	5	**39.3** (36-45)	**16.7** (14.1-21.2)	**0.84** (0.81-0.94)	**1.2** (1-1.4)	**17.9** (17-18.7)	**0.61** (0.55-0.7)	**0.65** (0.58-0.62)
C (36-38)	3	**44.4** (43-45)	**12.6** (12-31.1)	**0.7** (0.6-0.72)	**1.4** (1.3-1.5)	**16.5** (15.7-16.2)	**0.58** (0.51-0.68)	**0.61** (0.58-0.64)
B (33-35)	3	**40.8** (38.9-42.6)	**13.9** (13.5-14.5)	**0.8** (0.7-1)	**1.6** (1.4-1.8)	**18.4** (17.3-19.3)	**0.83** (0.7-0.88)	**0.7** (0.7-0.92)
A (27-32)	6)	**41.7** (38 -43)	**13.1** (12.6-13.7)	**0.8** (0.7-1)	**1.7** (1.6-1.9)	**17.6** (16.4-18.4)	**0.7** (0.6-0.8)	**0.75** (0.7-0.95)
11 a (21)	1	**55.383888**	**8.068165**	**0.8143344**	**1.1106412**	**11.15166**	**0.56386704**	**0.4504**
11 (10-26)	17	**47** (39.4-50.3)	**11.5** (10.6-14.8)	**0.95** (0.55-1.9)	**1.1** (0.8-1.7**)**	**15** (12-20.2)	**0.55** (0.49-0.7)	**0.57** (0.33-0.7)
10 a (5)	1	**32.344704**	**21.143505**	**1.4985432**	**1.3563796**	**18.700476**	**0.21537216**	**1.8**
10 (1-9)	8	**32.4** (27.1-	**20.5** (17.3-	**1.4** (0.83-1.95)	**1** (0.72-1.9)	**20** (14 - 25.9)	**0.43** (0.21-0.82)	**1.7** (0.7 –

		39)	25.4)					2.9)

Lithological unit and sample numbers associated with each unit	**Number of samples in each unit**	**SiO_2**	**Al_2O_3**	**CaO**	**K_2O**	**Fe_2O_3**	**MnO**	**Ti_2O_3**
9 (k50)	1	**40.5**	**18.3**	**1.1**	**1.5**	**14.9**	**0.31**	**1**
8 (k49)	1	**35.7**	**22.7**	**1.2**	**1.1**	**16.7**	**0.39**	**1.3**
7 (k41-k48)	7	**46.2** (37.3-52.1	**17.6** (13.4-24.6)	**0.93** (0.74-1.1)	**1.5** (0.73-1.6)	**11.4** (8.6-15.6**)**	**0.25** (0.12-0.65)	**0.76** (0.57-1)
6 (k40)	1	**60.3**	**9.4**	**0.6**	**2.2**	**4.4**	**0.1**	**0.52**
5 (k31-k40)	10	**52.9** (50.1-55.1)	**12.6** (11.6-14.1)	**0.99** (0.87-1.1)	**2** (1.9-2.1)	**7.9** (5.5-9.6)	**0.12** (0.08-0.18)	**0.64** (0.59-0.69)
4 (k24-k30)	7	**50.9** (49.3-53)	**13.8** (12.76-14.4)	**1.08** (0.99-1.1)	**1.9** (1.8-2)	**9.3** (8.3-10.3)	**0.16** (0.11-0.26)	**0.68** (0.64-0.75)
3 (k17-k23)	7	**48.2** (41.2-51.2)	**13.6** (12.2-15.8)	**1.1** (1-1.2)	**2.1** (1.8-2.4)	**11** (8.9-15.4)	**0.2** (0.08-0.5)	**0.8** (0.7-1.1)
2 (kl-59-k16)	19	**38.5** (33.9-40.3)	**17.3** (15-18.2)	**1.4** (1-1.6)	**1.97** (1.7-2)	**16.4** (14.7-20**)**	**0.85** (0.1-4)	**1.2** (1-1.3)
1 (kl1-kl57)	32	**32.2** (28.9-38.8)	**20.8** (15.9-23.3)	**0.099** (0.82-1.6**)**	**1.24** (1.06-2)	**21.2** (16.9-24.2**)**	**1** (0.5-2)	**1.2** (0.9-1.2)

Table 5.2 continued Major element data for each lithological unit for the Kilombe sedimentary sequence

Lithological unit and sample numbers associated with each unit	Number of samples in each unit	Ba (PPM)	V (PPM)	Cu (PPM)	Ga (PPM)	Pb (PPM)	Ni (PPM)	Nb (PPM)	Rb (PPM)	Sr (PPM)	Y (PPM)	Zn (PPM)	Zr (PPM)
16 (127-144)	18	309	212	32	39	**36**	**26**	263	111	34	116	460	1213
15 (84-126)	43	**253**	**144**	**29**	**37**	**31**	**13**	244	**72**	36	115	488	**998**
14 (70-83)	14	104	84	26	40	34	0.7	253	61	26	143	534	1060
13													
F (66-69)	4	**101**	**77**	**28**	**34**	**31**	**11**	**255**	**75**	**24**	**147**	**562**	**1098**
E (62-65)	4 (62-65)	**102**	**122**	**28**	**38**	**24**	**3.3**	**221**	**65**	**27**	**113**	**678**	**864**
D (57-61)	5 (57-61)	**153**	**107**	**21**	**33**	**21**	**9.9**	**190**	**80**	**30**	**166**	**508**	**787**
C (55-56)	2 (55-56)	**79**	**76**	**20**	**29**	**24**	**17**	**192**	**80**	**25**	**176**	**446**	**821**
B (53-54)	2 (53-54)	**64**	**103**	**29**	**39**	**26**	**10**	**246**	**87**	**21**	**118**	**559**	**962**
A (50)	1 (50)	51	103	19	47	35	2	269	97	19	79	451	1022
12													
E (45-49)	5 (45-49)	**69**	**113**	**26**	**46**	**39**	**0.34**	**332**	**91**	**20**	**101**	**561**	**1259**
D (39-44)	5 (39-44)	**85**	**106**	**29**	**46**	**47**	**5**	**390**	**85**	**31**	**140**	**621**	**1504**
C (36-38)	3 (36-38)	**108**	**143**	**24**	**44**	**42**	**3.6**	**339**	**104**	**28**	**119**	**489**	**1278**
B (33-35)	3 (33-35)	**245**	**224**	**24**	**46**	**44**	**5.9**	**344**	**122**	**31**	**112**	**523**	**1248**
A (27-32)	6 (27-32)	**262**	**228**	**25**	**43**	**38**	**5.2**	**317**	**123**	**32**	**102**	**478**	**1150**
11 a (21)	1 (21)	73	108.6	23.9	30.6	29.6	0.2	206.5	86.7	17	161.1	344	864.8
11 (10-26)	17 (10 -26)	**76**	**121**	**21**	**39**	**26**	**-0.33**	**237**	**89**	**29**	**128**	**429**	**904**
10 a (5)	1 (5)	595	251	47.3	28.9	9.2	28.8	119.6	92.1	51.8	95.9	328.6	501.5
10 (1-9)	8 (1-9)	416	300	45	35	**26**	**41**	194	80	35	89	359	800
9 (k50)	9	333	176	36.7	42.4	**33.6**	**32.9**	270.9	134.4	57.8	120.7	380.6	1088
8 (k49)	1	917	331	48.1	34.9	**13.9**	**25.9**	126.6	114.8	118.7	82.7	297.6	497
7 (k41-k48)	7	276	147	37	42	**34**	**37**	268	110	40	108	328	1125
6 (k40)	1	311	154.2	24	36	**32**	**10**	185.5	102	49.4	83.8	258	999
5 (k31-k40)	7	304	100	21	26	**23**	**11**	155	121	52	73	227	661
4 (k24-k30)	10	410	133	26	28	**23**	**16**	161	128	57	90	295	720
3 (k17-k23)	7	556	193	29	29	**23**	**22**	178	136	64	143	310	764
2 (kl-59-k16)	19	1202	296	37	34	**30**	**32**	203	132	79	109	353	781
1 (kl1-kl57)	32	7-4	302	36	40	**41**	**39**	225	119	35	112	435	1024

Table 5.2 (a) Trace element data for each lithological unit for the Kilombe sedimentary sequence

5.4.1 Lithological units

Unit 1 Yellowish red claystone

The concentration of major elements in this unit is characterised by low SiO_2, CaO, and K_2O, and by high Fe_2O_3, Al_2O_3, and MnO. The high Al_2O_3 and low SiO_2 values are typical of clay enriched sediments. Increased values of Fe_2O_3 and TiO_2 indicates the presence of heavy minerals and iron oxides. Higher values of MnO are also tied to the presence of iron oxides in this unit. Values of Rb and Sr are low whilst all other trace elements are high.

Unit 2 Brown claystone

This unit is characterised by a reduction in values of both Al_2O_3 and Fe_2O_3 than the previous unit and by an increase in SiO_2, CaO and K_2O both peak in this unit. Values again indicate the presence of iron oxides and increasing levels of SiO_2 would indicate an increase in the amount of quartz grains in the sediments. The trace elements of Rb, Sr and Y increase whilst all other trace elements decrease, suggesting increased contribution from the feldspars.

Unit 3 Pale yellow claystone

The units is defined by further peaks in SiO_2 and K_2O and reduction in values of $Al_2O_{3,}$ Fe_2O_3, MnO and CaO. All trace elements further decline however peaks in Rb and Sr are observed. The increase in both Si, K Rb and Sr indicates significant increase in the detrital component of both Quartz and Feldspars along with progressive loss of the iron-oxides and the heavy metals.

Unit 4 Grey claystone/diamictite

The geochemical properties are similar to unit 3. A further peak in SiO_2 is observed and a decline in $Al_2O_{3,}$ Fe_2O_3 and MnO. Rb and Sr remain constant whilst other trace elements further decline. In this unit the concentration of quartz increases whilst the clay minerals and iron oxides decline.

Unit 5 Pale brown palaeosol

The geochemical properties are similar to the previous 2 units. However, a further increase in values of SiO_2 and K_2O is observed whilst mean values of Al_2O_3, Fe_2O_3, and MnO further decline. Rb and Sr values increase from the previous unit whilst all other trace elements decline. This unit sees a further increase in quartz and the K-feldspars.

Unit 6 White tuff

The geochemical properties are similar to the previous 3 units. However, a further increase in values of SiO_2 and K_2O is observed whilst mean values of Al_2O_3, Fe_2O_3 and MnO decline. The trace elements of V and Ba also peak in this unit. The increase of both Ba and K may also indicate enrichments of K-feldspars along with Quartz and a further decline in the clay minerals and iron oxides.

Unit 7 Tuffaceous pale brown claystone

This unit is defined by a marked increase in in mean values of Al_2O_3, Fe_2O_3, CaO and MnO and by a marked decline in values of SiO_2 and K_2O. All trace elements increase other than Sr which declines. Quartz and the feldspars decline in this unit whist the clay minerals and iron-oxides increase. Zr and the elements associate with the heavy minerals also increase in this unit.

Unit 8 Beige tuff

The units is defined by low mean values of SiO_2 and K_2O. Al_2O_3, Fe_2O_3, CaO and MnO are high. Peaks in the trace elements of V and Sr are also observed. This units is characterised by a low concentration of quartz and feldspars and by a high concentration of clay minerals and iron oxides.

Unit 9 Three-banded tuff

The defining geochemical properties of this unit are an increase in SiO_2 and a reduction in Al_2O_3. The other major oxides are similar to the previous unit. The trace elements of Ni, Ga, Nb and Zr show peaks whilst Sr declines.

Unit 10 Dark brown tuffaceous clays

In this unit mean values of SiO_2 and K_2O are low whilst Al_2O_3, Fe_2O_3, CaO and MnO are high. A number of trace elements peak in this units including Ba, V, Ni and Cu. Rb declines accompanied by a small decline in in this unit. Elements associated with the heavy minerals Zr and Nb peak and the decline. Ti_2O increase to > 2 at the top of this unit similar to unit 10 A this may in fact be two lithological units the upper unit being representative of a non-local source.

Unit 10 A Orange clay band

This unit is defined by low mean values of SiO_2 and MnO and by high values of K_2O, Al_2O_3, Fe_2O_3 and CaO/ The trace elements of Zr and Nb decline in this unit as do Rb and Sr. Ba is shown to increase. Ti_2O increase to 1.8 which may indicate a different source rock for this unit.

Unit 11 Pale brown tuff

In this unit mean value of SiO_2 are high and all the other major oxides are low with some increase towards the top of the unit. The trace elements of Zr, Nb, Zn and Pb all show a gradual increase to much higher values in this unit. Rb and Ba also increase. Sr peaks at the base of the unit.

Unit 11 A White tuff

In this unit all the major oxides are low aside from SiO_2 which peaks to one of its highest values for the sequence. Y also peaks in this unit.

Unit 12 Brown clay series

12 A Light gray tuff

In this unit mean values of SiO_2, K_2O Fe_2O_3, and MnO are high whilst Al_2O_3 and CaO are lower. Trace elements of Rb, Sr and Ba also peak in this unit.

12 B Yellowish brown clayey tuff

In this unit mean values of SiO_2, K_2O Fe_2O_3, and MnO are high whilst Al_2O_3 and CaO are low. Rb, Sr and Ba are high.

12 C Brownish gray tuffaceous clay

In this unit mean values of SiO_2 are lower and K_2O is still. Major oxides of Al_2O_3, Fe_2O_3, and MnO are higher. Ba, Rb and Sr decline in this unit compared to the previous.

12 D Yellowish brown tuffaceous clay

This unit is defined by slightly lower values of SiO_2 and K_2O than the previous units which decline throughout the units accompanied by an increase in Al_2O_3, Fe_2O_3, CaO and MnO. Zr peaks and Rb and Sr decline.

12 E Yellow tuff

In this unit the defining properties are lower values of SiO, and an increase in K_2O and Al_2O_3. Fe_2O_3 and MnO decline slightly at the top of the unit. A slight increase in Rb is noted and Zr declines.

Unit 13 Orange clay series

13 A White tuff

This unit is defined by an increase in Al_2O_3 little change is observed in the other major elements and Rb also increases.

13 B Yellow clay

In this unit mean values of SiO_2 and K_2O decline whilst Al_2O_3, Fe_2O_3, CaO and MnO all increase. Rb declines along with Zr whilst Sr increased.

13 C White clayey tuff

In this unit SiO_2 increases, a slight declines is noted in Al_2O_3, and MnO is also low. Rb decline further whilst Sr increases.

13 D Yellow clay

Values of SiO_2, decline throughout this unit as Al_2O_3 and Fe_2O_3 increase. CaO also increases whilst K_2O is much more variable. Ba and Va both peak in this unit.

13 E White tuff

In this unit mean values of SiO_2, and K_2O reduce from the previous unit whilst Al_2O_3, Fe_2O_3, and MnO all peak. V increases, Rb and Sr are low.

13 F Brownish yellow clays

SiO_2 increases in this unit accompanied whilst Al_2O_3 and Fe_2O_3 and MnO all decline. Zr also increases in this unit.

Unit 14 Brown banded tuff

In this unit mean values of SiO_2 and CaO are low whilst $Al_2O_{3,}$ K_2O $Fe_2O_{3,}$ CaO and MnO are high. Little variation in the trace elements is observed.

Unit 15 Pink brown earthy tuff

SiO_2 is low throughout this unit, however, a marked increase is noted towards higher values at the top of this unit. $Al_2O_{3,}$ Fe_2O_3 and MnO are high but show some decline when SiO_2 declines at the top of the unit. Two large peaks in K_2O are noted in the centre of this unit. Ba and V peak whilst an increase in both Rb and Sr is also noted in the trace elements.

Unit 16 Orange brown earthy tuff

An increase in SiO_2 occurs at the base of this unit and then declines gradually to the top of the sequence. Al_2O_3 and Fe_2O_3 show the opposite trend. Some decline in values of MnO are observed at the top of the unit. The other major oxides are more variable. Rb declines throughout as Sr increases. Ba and V both peak

5.4.2 Major and trace element data summary

The influence of lithology is clearly shown at Kilombe as the primary control on major changes observed in the major and trace element data set both on the main site and at FHC. The use of multivariate statistics with major and trace element data can only provide a broad indication of the mineralogy of any sequence. However, some conclusions are possible. The main changes at Kilombe main site and FHC appear to be controlled by variability between the groups representing the detrital components, Quartz and Feldspars (groups 1 and 2) and the clays, iron oxides (group 3) and to a lesser degree the heavy mineral components (group 4). The most pronounced variations between these groups occur on the main site. Variation in concentration between detrital minerals and the clay minerals can often be used to reflect changing environmental conditions such as increasing aridity or, the sudden deposition of material of primary igneous origin. However on the main site, specifically units 2 to 6, an increase in quartz occurs accompanied by the progressive loss of the major oxides associated with the clay minerals and iron-oxides, along with a reduction in the concentration of the heavy metals, this may also indicate post-depositional processes such as dissolution. The following section will discuss the effect of dissolution and Chapter 7 will further examine implication environmental of the major and trace element data.

5.4.3 Burial diagenesis

The loss of iron-oxides through post-depositional diagenetic dissolution has been widely documented in both mineral magnetic and geochemical studies and in a range of environmental settings, marine and lacustrine (Bloemendal *et al.*, 1992; Haese *et al.*, 1998; Kostka & Nelson, 1995; Zhang *et al.*, 2001). The effects on loss/transformation of clay minerals is also widely known (Zhang *et al*., 2001). The major element Fe is universal in sedimentary environments and its reduction during burial diagenesis and role in the cycling of many other elements, especially the heavy metals is known to be significant (Burdige, 1993). In terms of the effects of diagenesis, the loss and speciation of forms of iron-oxides is linked to redox conditions and organic matter content and decomposition (Rowan *et al.*, 2009). However, changes in sedimentation rates have also been shown to play a significant role in the effects of diagenesis on iron-oxides (Liu *et al.*, 2004).

At Kilombe results show the progressive loss of Fe and Mn in conjunction with the heavy metals of Zn, Cu, Ni and Pb, across units 2-6, which may be indicative of post-depositional diagenetic dissolution. Zhang *et al.,* (2001) and Burdige (1993) have documented the close association of iron-oxide reduction and cycling of heavy metals in marine settings and a similar decline in Fe, Mn and heavy metals have been documented in close association with another. Zhang *et al.,* (2001) also suggest the close link between absorption of heavy metals by fine grained iron oxides, especially magnetite which are dissolved first during dissolution due to high surface to volume ratio.

An increase in major and trace element associated with detrital minerals, quartz and feldspars can often be an indication of increasing aridity when occurring in conjunction with a reduction in concentration of the clay minerals. The major and trace elements of Si, K, Rb and Sr associated with these minerals increase progressively to much higher values across units 2-6. However, in this case, the increase is most likely due to the loss of iron-oxides via burial diagenesis and dissolution rather than an increase in detrital minerals due to changing palaeoclimatic conditions. The effects of dissolution on the Kilombe sediments will be examined in more detail in Chapter 6 Environmental magnetism through particle size separation.

5.5 Evaluation of chemical weathering indices

5.5.1 Source rock

Chapter 4 provides a summary of the underlying geology for Kilombe which includes both mafic (basalts) and intermediate (trachyte and trachyphonolite). As the basalts are not known to penetrate in the immediate local area, the only possible source material at the Kilombe are trachytes and trachyphonolites. Details of the petrographic studies for the Kilombe trachytes and trachyphonolites summarised in Chapter 3 show these to be very similar geochemically.

5.5.2 Petrology and mineralogy of Kenya trachytes and trachyphonolites

Geological reports of Jones (1979) and Bishop (1978) suggest the source rock of the Kilombe sedimentary sequence to be the local trachytes and trachyphonolite lavas. The petrology of the Kenya type phonolites or trachyphonolites are characterised as having a trachyoid texture which is the result of the parallel alignment of groundmass alkali feldspar plates (Lippard, 1973). The only common phenocryst mineral is sanidine and most of the trachyphonolite lavas in the Kenya Rift are classed as aphyric. Alkali feldspars albite, anorthoclase, microcline, orthoclase and sanidine comprise 60-70% of the mode whereas Nepheline comprises less than 15% in all lavas, then Soda-amphiboles, aenigmatite, aegirine-augite, analcite. Alkali iron rich mafic minerals occur interstitally (Lippard, 1973). Pale green clinopyroxene and opaque ore are generally less than 10%.

The petrography of the trachytes show the earlier flows to be abundant in feldspar phenocryst sanidine whereas the later flows are abundant in anorthoclase (up to 35%). Alkali feldspar constitute the groundmass and are fluidal in texture with bimodal grain-size distribution. Ferroaugite phenocrysts vary in abundance and form less than 1% of the rock. Groundmass mafic minerals aenigmatite and katophorite comprise around 15-20%. Pyroxene constitutes around double the amount of amphibole and taken together both minerals form around 15-20% of the rock. Quartz can be present in both the groundmass and with feldspars but constitute up to 25% of alkali rhyolites.

5.5.3 Ti wt % values and source rock composition

Ti wt % values for the sedimentary sequence at Kilombe range between 0.49 and 2.9 with an average for the sequence of 0.93. The average values for Ti in intermediate alkaline rocks is around 1.2 for East Africa (Wedepohl, 1978). Data from geochemical and petrographic studies for Kilombe and the Central Rift show that Ti wt% values for trachytes, trachyphonolites and phonolites range from 0.39 to 1.2 (the higher values of 1.2 being representative of phonolitic nephelinites which generally only occur in western Kenya (Jones, 1979). Average values of Kenya type (trachyphonolites) are 0.65 and trachytes 0.88 (Lippard, 1973).

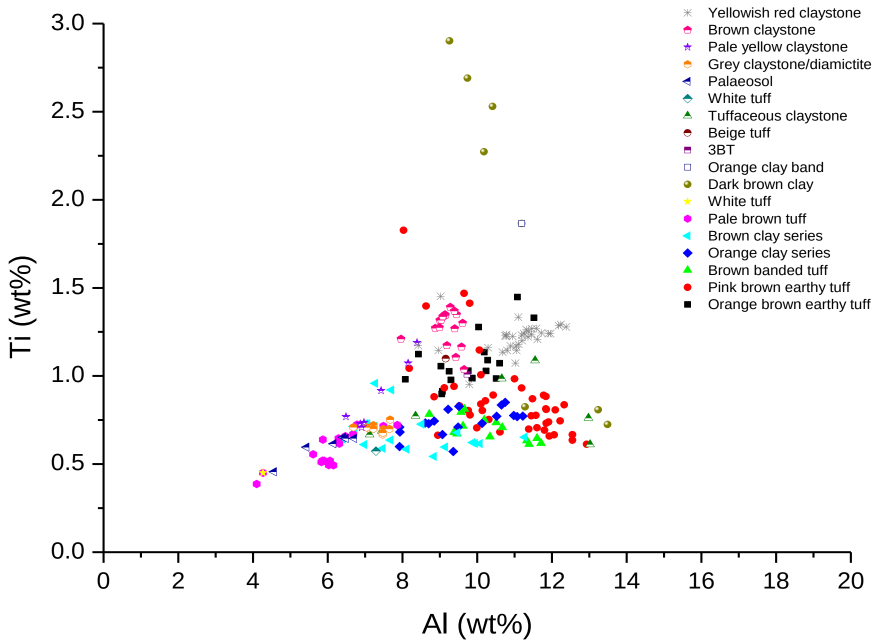

Figure 5.3 Bivariate plot of Ti versus Al

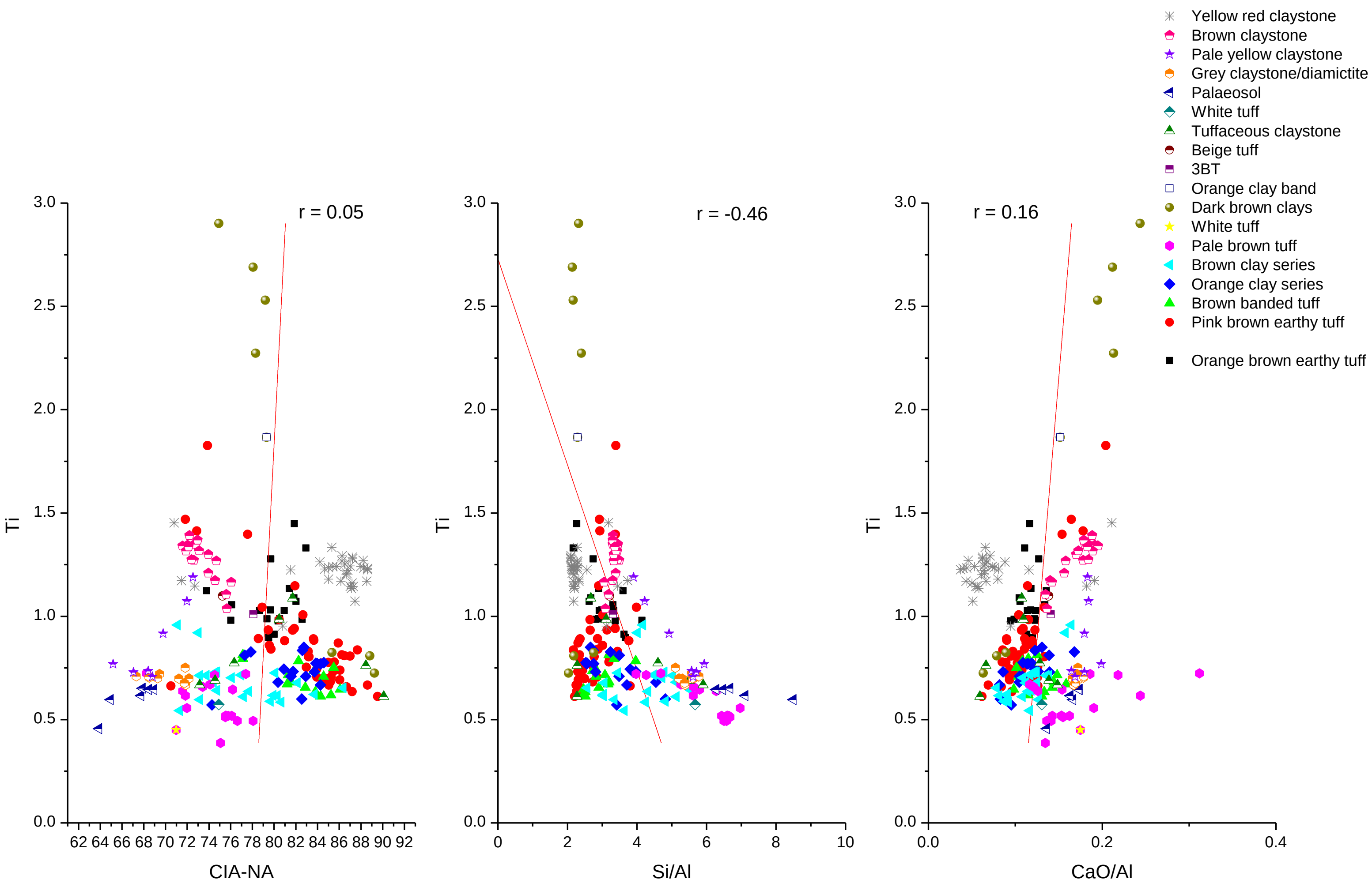

Figure 5.4 Bivariate plots of Ti versus chemical weathering indices

5.5.4 Ti wt % vs chemical weathering indices

Linear regression analysis of Ti wt % versus chemical weathering indices shows that there is only a weak to moderate correlation between Ti and the chemical weathering indices. This suggests that Ti does not increase with chemical weathering intensity. Results in Figure 5.4 show that all the chemical weathering indices aside from Si/Al have no statistical correlation with Ti. However, Si/Al does shows a negative and moderate correlation with Ti ($r = - 0.46$). As there is no known mechanism for increasing Ti there may be some influence of provenance on this index. As most of the Kilombe sediments fall well within the range of average Ti wt% values for intermediate alkaline rocks, this would not affect the use of Si/Al.

5.5.6 Bi-plot Ti versus Al and ratios of (Al/Ti and Ti/Al)

The bivariate plot shown in Figure 5.3 of Ti versus Al for the entire Kilombe sequence shows that in relation to source rock composition there are three distinct groups in the sample set with the distribution controlled by Ti values. Those with lower Ti values that fall within the range of both published values for the Kilombe trachytes and trachyphonolites (0.45 – 0.88) and those with high Ti above 0.9 (average 1.2). The higher Ti values of 1.2% at Kilombe occur mainly within three lithological units (yellow red and brown claystones and the orange brown earthy tuff) as shown in Figure 5.2, however these are well within the range of intermediate rocks. The exception to this are third group of samples occurring within the dark brown clays and orange clay band, which yield average Ti wt % values of 2.4 these values may indicate a more mafic source (Wedepohl, 1978).

The ratios of Ti/Al and Al/Ti are useful in determining source rock type whether mafic, felsic or intermediate. Values for the ratio of Ti/Al for the Kilombe sediments average 0.93 but fall within a wide range of 0.04 to 2.9. The higher group still fall well within the range of alkaline igneous intermediate rocks for East Africa. There is also one outlier group with average Ti (wt%) of 2.4 which occurs across four samples. Ti/Al ratio shows a decreasing trend within the record up-section. This most likely indicates that Al may have been lost by either dissolution or by removal of the more aluminous phases e.g. the clay minerals.

The Al/Ti ratios also fall within a narrow range with values of 5.9 to 12.7 (with two outlier peaks of 17 and 21 are noted at the top of the record) and the average values are 9.2. As values of the ratio are relatively uniform this suggests that the source rock has not changed significantly. Comparison to average Al/Ti values for central rift and East African intermediate rocks (9-17) demonstrates that these values are also well within the range for intermediate rocks. Both the ratio of Al/Ti and bivariate plot of Ti versus Al suggest intermediate rock for parent material.

5.5.7 Bi-plot Ti versus Zr & Ti/Zr ratio

Figure 5.5 the bivariate plot of Ti versus Zr also identifies three distinct groups of samples similar to those determined in Figure 5.3. Ti/Zr ratios average 10.5 at Kilombe, with a range of 5.5 to 15.6. Ti/Zr values of Central Rift intermediate rocks average 4 – 14 which again places the Kilombe sediments within the range of intermediate rocks for this area.

5.5.8 Summary

In summary all data presented above suggests that the source rock of the Kilombe soils and sediments is intermediate alkaline rock with one small outlier group with higher Ti wt % values which may have a different provenance, although it is not possible to assign source identity with these data. As an increase in Ti wt% values to 1.2, higher than those previously observed in local trachytes and trachyphonolites, occurs in three lithological units any possible effects of this change will now be examined statistically in the following sections.

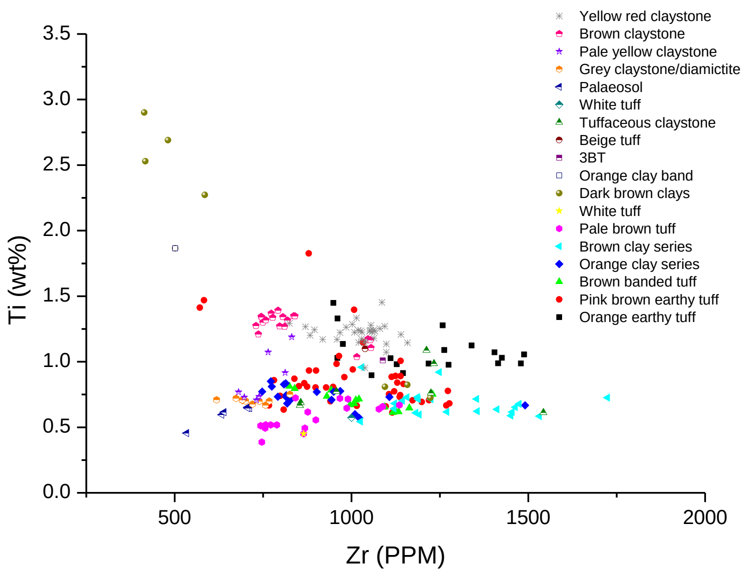

Figure 5.5 Bivariate plot of Ti versus Zr

5.6 Immobile element ratios and linear regression analysis

This section will examine statistically any influence of sorting signal and provenance on chemical weathering intensity. Figure 5.8 displays trends to depth of the immobile element ratios and chemical weathering indices used in this part of the study. None of the immobile element ratios indicative of changes in source population (Ti/Al and Zr/Ti) or sorting signal (Zr/Rb) exhibit similar curves or variability to those exhibited by the chemical weathering indices.

5.6.1 Linear regression – provenance

Figures 5.6 show the statistical correlation of Ti/Zr to chemical weathering indices. The bi-plots of Ti/Zr to CWI's show again a weak to non-existent statistical correlation in the following order Ti/Zr to CaO/Al, Si/Al and CIA (r=0.36, r=-0.2, and r=-0.12). In summary there is no real correlation statistically in terms of changes in provenance on this data set with chemical weathering intensity.

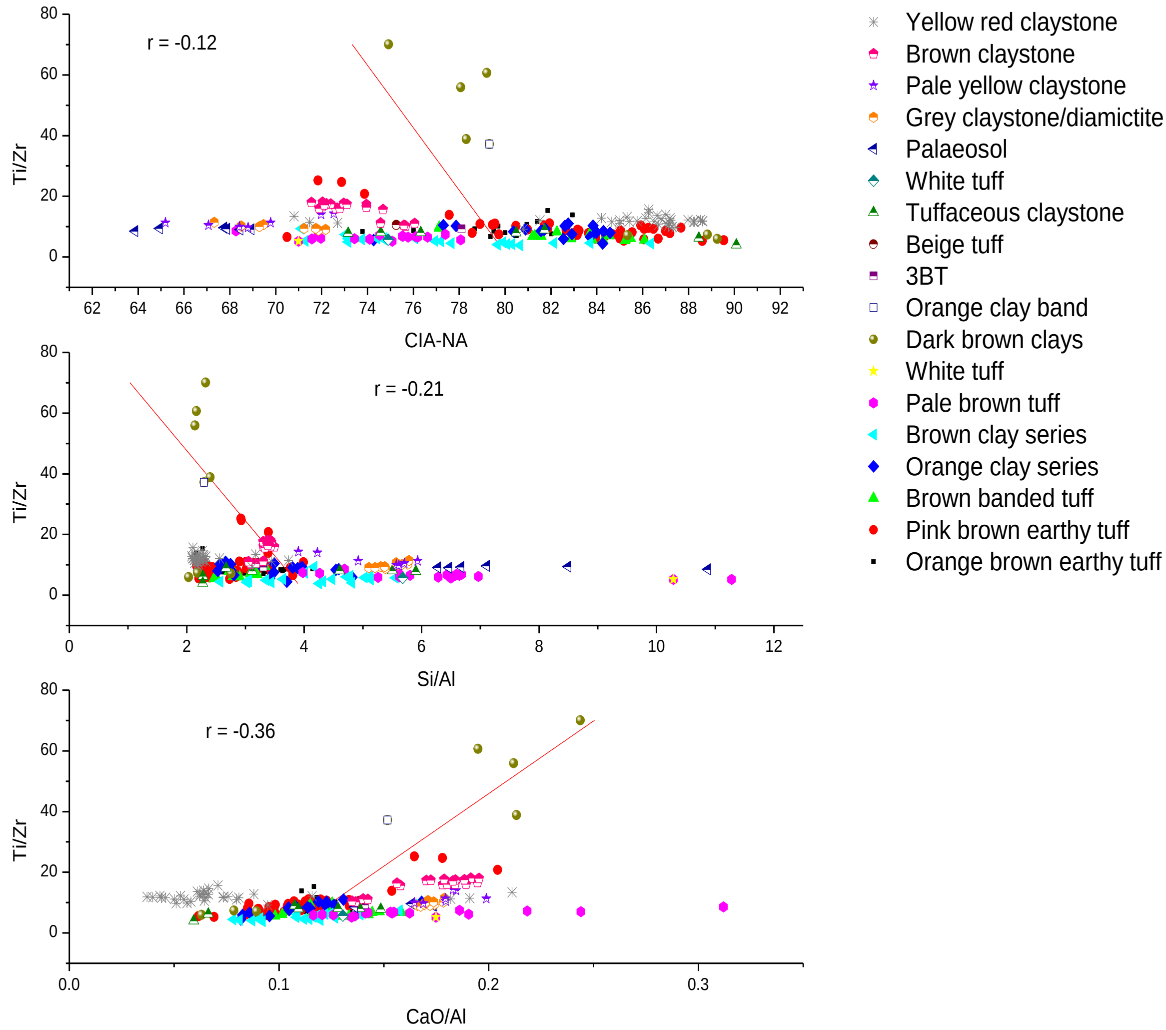

Figure 5.6 Linear regression analysis of Ti/Zr ratio to chemical weathering indices

5.6.2 Sorting signal (Zr/Rb ratio)

In terms of evaluating any possible effects of changes in sediment grain size on chemical weathering indices the following elements were selected as a ratio Zr and Rb based on literature review. The ratio of Zr/Rb has a range of 5 – 27 with an average of 11. From a depth of 1100 to 200 cm a trend towards increasingly higher values is observed which may indicate a substantial coarsening of the sediment over time from finer grained to coarser silt. Zr/Rb ratio remains relatively stable in the lower and top sections of the sequence which may suggest these parts of the record are not overtly influenced by changes in grain size or sorting signal. Figure 5.8 shows a comparison of Zr/Rb with chemical weathering indices. This ratio does not exhibit similar behaviour to the chemical weathering indices.

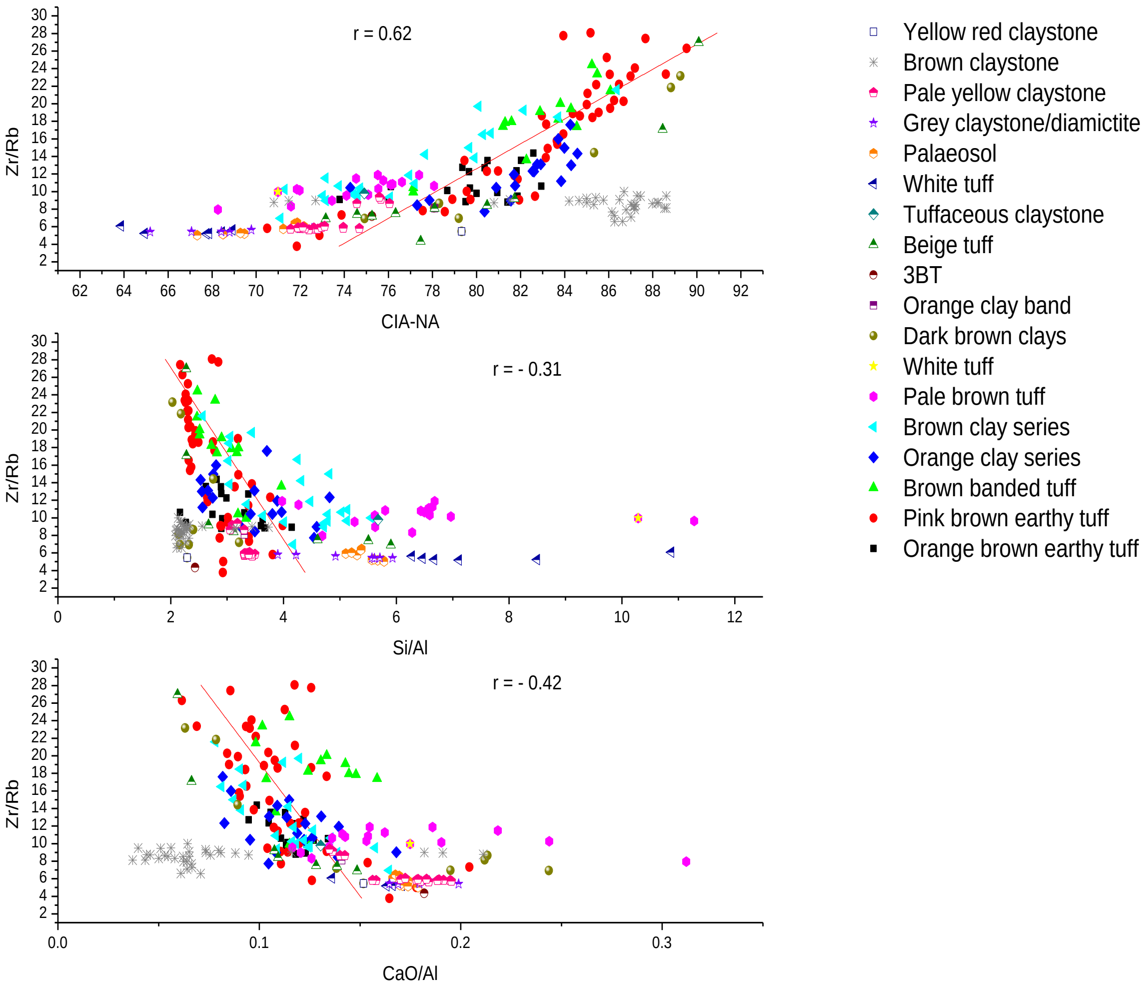

Figure 5.7 Linear regression analysis of Zr/Rb ratio to chemical weathering indices

5.6.3 Linear regression Zr/Rb

Figure 5.7 displays results of linear regression analysis of Zr/Rb to the chemical weathering indices used in this study. All the indices show a weak to moderate correlation. The highest correlation is between Zr/Rb and CIA being r = 0.62, Ruxton ratio and CaO/Al all show a weak and moderate correlation with Zr/Rb (r = - 0.31 and r = - 0.42). Although no strong correlations between Zr/Rb and the chemical weathering indices have been obtained, data above shows that a significant proportion of the record for CIA is being influenced by sorting signal.

5.7 Results - Chemical weathering indices

5.7.1 Linear regression analysis of chemical weathering indices

Figure 5.8 shows the results of linear regression analysis for all chemical weathering indices used in this study to CIA (selected as an index shown to be most widely used and globally applicable). The strongest correlations are for CIA to Ca/Al which is $R^2$0.65 and moderate for CIA to Si/Al $R^2$0.51. A weak correlation is obtained between Si/Al and Ca/Al being R^2= 0.2. The linear correlations with CIA suggest that all these indices are useful in inferring the history of chemical weathering intensity at Kilombe.

5.7.2 Chemical Index of Alteration

Figure 5.9 plots the chemical weathering indices used in this study to depth and includes the CIA index. This index increase with enhanced chemical weathering. After correction for CaO present in the silicate fraction of the rock the measured value then indicates the proportion of Al_2O_3 versus labile oxides. Due to the poor measurement of Na in this record this element was removed from the CIA equation following a similar approach as taken by Bloemendal *et al.,* (2003).

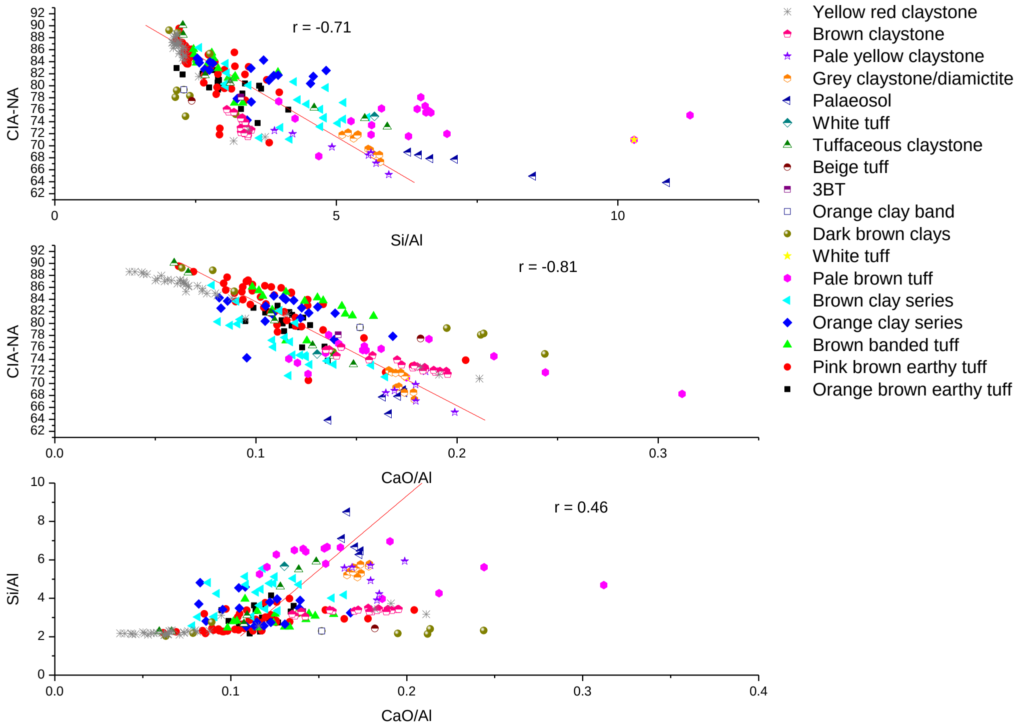

Figure 5.8 Linear regression analysis of chemical weathering indices

5.7.2 Chemical Index of Alteration cont..

$$CIA = (Al_2O_3 / (Al_2O_3 + CaO^* + K_2O)) \times 100$$

CIA values for the Upper Continental Crust, unaltered potassic feldspars and unweathered igneous rocks are around 50 whereas idealised muscovite yields a value of around 75. Illite ranges between 75 and 85 with Kaolinite and chlorite giving the highest values approaching 100 (Nesbitt & Young, 1982). Average values for Kenya type trachytes and trachyphonolites yield CIA values of 45 and 46 respectively and values for the sedimentary sequence range from 48 to 92 with an average of 72. The CIA shows an overall increase throughout the Kilombe sequence.

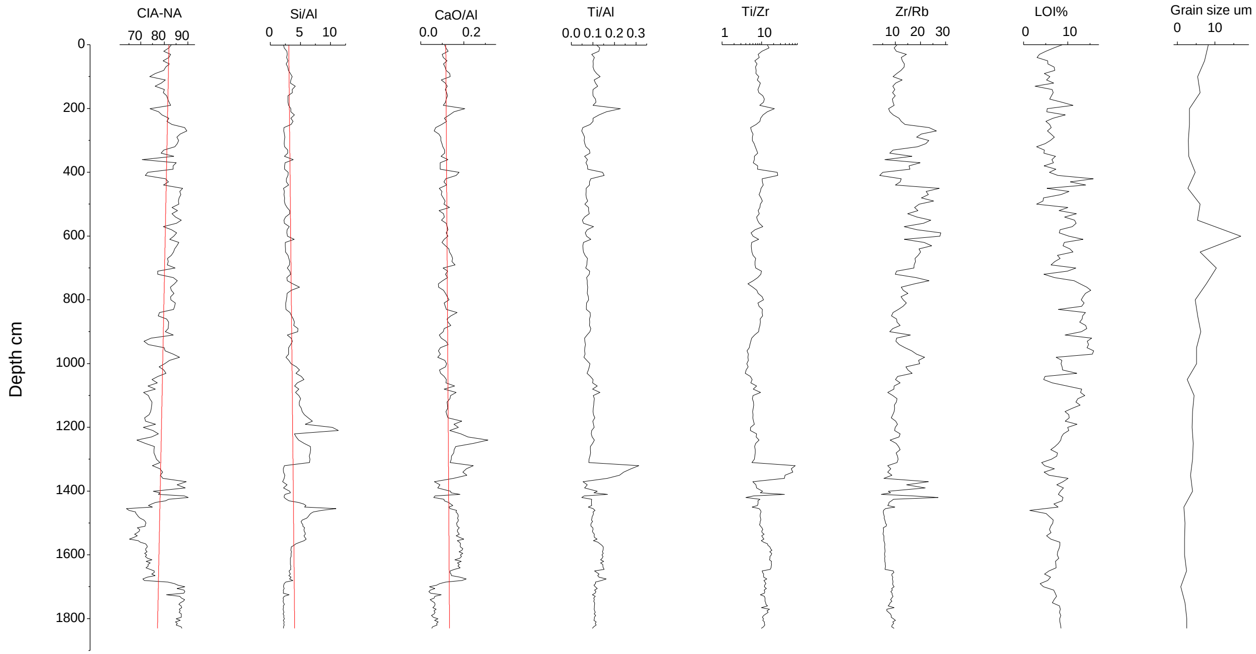

Figure 5.9 Chemical weathering indices, immobile element ratios, loss-on-ignition and mean grain size for the Kilombe sequence to depth

5.7.3 Ruxton Ratio

The Ruxton Ratio is negatively correlated with chemical weathering intensity. Optimum fresh values are > 10 and optimum weathered values are 0. Ruxton ratio values for the Kilombe trachyte's and trachyphonolites are 4 and 3.5. However values for the sedimentary sequence at Kilombe range from 2 to 10 with an average of 3.6. This ratio shows an overall decline throughout the sequence.

5.7.4 CaO/Al

CaO/Al has been shown to correlate well with chemical weathering intensity although Zhang *et al*., (2002) suggest this ratio is affected by sorting signal to some extent. Values for the trachyte and trachyphonolite lavas at Kilombe are 0.07 and 0.08 with values for the weathering profile ranging from 0.05 to 0.31 with an average of 0.12. This ratio declines with chemical weathering intensity and ratios at Kilombe show an overall decline up section.

4.7.5 Chemical weathering indices lithological units

In terms of response to changes in lithology CIA and Si/Al appear to be influenced by changes in lithology in the lower part of the sequence, specifically the units suggested to be effected by dissolution, but not at all at Farmhouse Cliff. CaO/Al transcends the boundaries of all the lithological units at Kilombe including the main site.

5.7.6 Bivariate plot CaO/Al_2O_3 versus K_2O/Al_2O_3

The bivariate plot, initially developed by Garrels & Mackenzie (1971) of Na_2O/Al_2O_3 versus K_2O/Al_2O_3 can be used to reveal the removal of Na versus K during the chemical weathering process in relation to either source rock composition or values for the Upper Continental Crust. This approach was adapted by substituting Na for Ca due to the poor measurement of

Na in this record. Chemical weathering processes can be characterised by an early stage which sees the removal of Na and Ca, an intermediate stage which sees the removal of K and an advanced stage which sees the removal of Si. Figure 5.10 shows the CaO/Al_2O_3 versus K_2O/Al_2O_3 diagram for the Kilombe samples. This plot shows that the Kilombe sediment samples all fit well along a weathering trend line when compared to the parent rock composition of the Kenya trachytes and trachyphonolites. The plot also shows that the most of the sediments are evidently depleted in both Ca and K when compared to parent rock values. Some samples in units affected by dissolution show little depletion of both Ca and K.

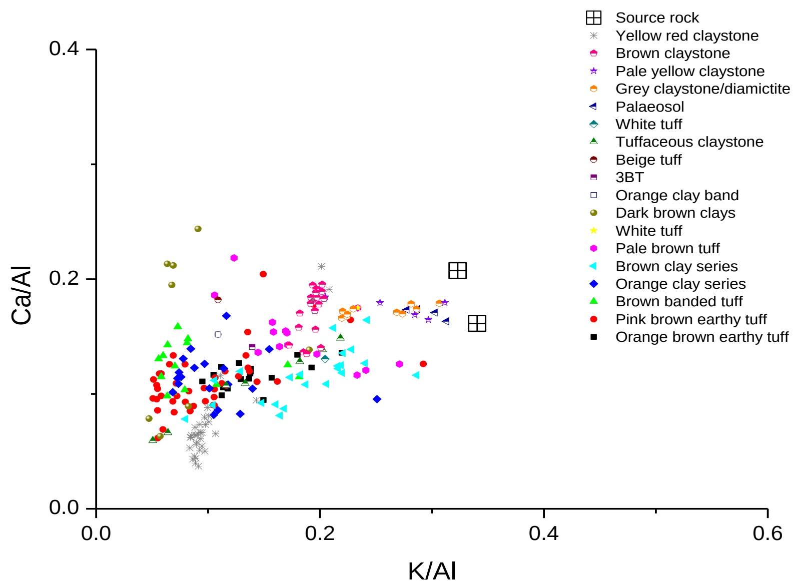

Figure 5.10 bivariate plot of Cao/ Al_2O_3 versus K_2O/Al_2O_3

5.7.7 Ternary diagram A-C-K

Figure 5.10 is the ternary plot (A-C-K) of the Kilombe soils and sediments compared to Kenya trachytes and trachyphonolites. This approach was adapted in terms of losing Na from the equation as in the CIA index from A-CN-K to become the A-C-K diagram. The data is convergent which would indicate that the source rock has not changed significantly during the Pleistocene. The data is also distributed along the weathering trend lines of source rock similar to the Ca_2O/Al_2O_3 versus K_2O/Al_2O_3 diagram. Overall the data exhibits two trends, one parallel to the A-C axis from the likely source rock material which would indicate an early Ca (mainly plagioclase) removal stage with little leaching of K (mainly potassium feldspar) which would correspond to an incipient stage of chemical weathering. The second trend documents a move away from the K axis which would indicate a more advanced stage of weathering of K removal.

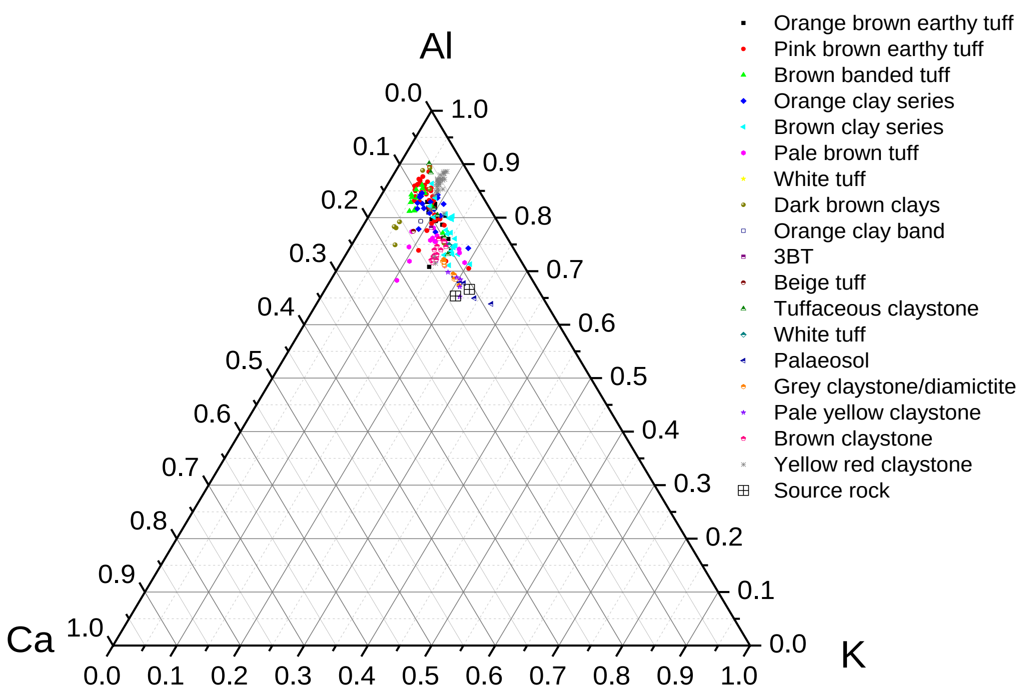

Figure 5.11 ternary A-C-K diagram

5.7.8 Summary

In summary the other chemical weathering indices used at Kilombe show moderate to strong correlations statistically with the CIA and all show a trend up section towards enhanced chemical weathering, which suggests they are all useful to infer chemical weathering intensity at this site. Although a moderate to strong statistical correlation is obtained through linear regression analysis it is apparent that the different chemical weathering indices display different patterns. In general the CIA exhibits a different trend to Si/Al and CaO/Al displaying a much larger amplitude of variability. Si/Al follows broadly the same pattern as Ca/Al at the bottom of the sequence however shows a steady decline up section rather than recording any amplitudes of variability from a depth of 10 metres up section. All the chemical weathering indices record changes in chemical weathering intensity at Kilombe from incipient through to moderate and intense suggesting they are useful to examine palaeoenvironmental change on derived sequences. These changes will be further discussed in Chapter 7.

One of the most prominent features observed in the geochemical data set at Kilombe is the general up-section trend noted in all indices towards enhanced chemical weathering. This may be suggestive of a long-term trend of increased chemical weathering intensity during the Pleistocene at this site. This view does not however account for other influences on the variability in this dataset, such as changes in provenance or sorting signal. In terms of provenance both the statistical correlation to immobile element ratios and bi-plots of Ti/Al and Ti/Zr are suggestive of two potential sources for parent rock. However, all the data bar one discrete unit falls well within the range of intermediate alkaline igneous rocks for Kenya which suggests that if the source population has changed it has not changed significantly enough to effect the application of chemical weathering indices at this site. This view is further supported by the fact that the ternary A-C-K diagram is convergent rather than scattered and the distinct weathering trend line from the Kenya trachytes and trachyphonolites on the bivariate plot of Ca_2O/Al_2O_3 versus K_2O/Al_2O_3. There is however a weak to moderate correlation between Zr/Rb (as a proxy for grain size) and the chemical weathering indices. As the correlation is weak to moderate rather than strong, it can therefore be considered that changes in chemical weathering intensity can be taken as exhibiting the main control on the observed variation in the geochemical data sets at Kilombe making this a reliable proxy for assessing environmental change.

5.8 Preliminary palaeoclimatic inference

The main controls exerted on chemical weathering intensity in terrestrial climate archives are changes in temperature and precipitation given similar parent material. The overall trend at Kilombe appears to be for increasing whole rock and/or post-depositional weathering intensity during the Quaternary with substantial variability observed in the record over a 500,000 year period. Examining the causes of these changes via changes in chemical weathering indices is complex for the following reasons. In terms of sedimentary rock sequences, geochemical analysis of bulk samples contains information on chemical weathering intensity from at least three main sources (once grain size and provenance have been accounted for) e.g. initial weathering from source rock, during transportation and at the final site of deposition. In general, the long-term increasing trend towards enhanced chemical weathering may possibly indicate a long-term increasing trend in warmer temperatures and/or increased precipitation in the basin. Since climate in the Central Rift Valley is mainly controlled by the East African monsoon systems this would be suggestive of an increasing trend in intensity of the monsoon systems. This explanation is unlikely for the following reason. Long-term trends of palaeoclimatic change observed in other East African lacustrine, marine and terrestrial archives generally indicate increasing aridification during the Quaternary rather than increasing precipitation. Therefore, the following explanation is suggested, the observed long-term trends towards enhanced chemical weathering may be the result of decreased erosion, transportation and deposition rates that have resulted in longer exposure times to chemical weathering processes. Although the long-term trends are most likely the result of long exposure times making a palaeoclimatic inference difficult the results of the chemical weathering indices will be more fully investigated in Chapter 7 including removal of sections that may have been affected by dissolution and consideration of variability that may be cause by extensive volcanic activity, to establish whether this proxy is able to provide a link between changes in chemical weathering intensity and changes in palaeoclimate at this site.

5.9 Conclusions

The following conclusions can be drawn from results presented in this chapter:

- The strongest influence on changes in the geochemical data set at Kilombe is chemical weathering intensity rather than source rock or sorting signal.
- Source rock is confirmed as intermediate with one outlier group indicating a more mafic source.
- The competing influence of changes in grain size/sorting signal and lithology may be affecting the chemical weathering indices to some degree (however, weak to moderate statistically).
- An increase towards enhanced chemical weathering up-section is noted as part of a long-term trend which may in turn be linked to changes in the East African Monsoon system and/or low sedimentation rates.
- Observed variation in the individual major and trace element data set are heavily influenced by changes in lithology at Kilombe and are not reliable proxies for

palaeoclimatic change. As a future direction these data will be investigated in the context of facies association and depositional environment.

- There is evidence for dissolution across units 2-6 leaving signal from the detrital component in the major and trace elements and indication of incipient chemical weathering from chemical weathering indices. This makes any palaeoclimatic inference problematic across these units and any influence on overall trends will be further examined in Chapter 7.
- The use of desktop XRF provides a rapid approach to estimate chemical weathering intensity at Kilombe.

Chapter Six Environmental magnetism results

6.1 Introduction

The literature review presented in Chapter three (Theory and methods) demonstrates that changes in the magnetic properties of bulk sediment/soil samples can often be influenced by a number of autogenic factors including changes in parent material, lithology, dissolution and sediment grain size as well as climate change. It is therefore necessary to firstly assess whether any changes in the magnetic properties of the Kilombe samples result from any of the above factors before examining a possible climatic response of the sediment samples to orbitally forced climate change. The major and trace element geochemistry results (Chapter 5) show that the parent material for the Kilombe soils and sediments has not changed significantly during the Pleistocene with all of the data (except for Samples 5-9 on Farmhouse cliff) falling within the range expected for intermediate alkaline rocks. The first part of this chapter examines statistically the main controls on the bulk magnetic susceptibility (MS) values using Pearson correlation matrix, principal component analysis (PCA) and linear regression analysis. The second part discusses the magnetic properties of each lithological unit and attempts to further establish whether the magnetic signal can be linked to changes in pedogenic intensity. The final section considers the origin of the fine grained ferrimagnetic component of the Kilombe samples and then selects any magnetic parameters possibly responding to climate for further discussion in Chapter 7.

6.2 Magnetic parameters selected

Based on the literature review there may be four possible sources of strongly magnetic particles contributing to the bulk susceptibility in the Kilombe soils and sediments: 1/

primary ferrimagnetic minerals derived from source rock of an igneous origin, 2/ secondary (neoformation) ferrimagnetic minerals produced during pedogenesis, 3/ secondary (neoformation) ferrimagnetic minerals produced during burning, 4/ bacterial magnetosomes.

In order to investigate the mineral magnetic properties and sources of strongly magnetic particles in the Kilombe soils and sediments the following magnetic parameters, described in Table 6.1, were selected based on literature review. The biplot of Oldfield (1994), and Oldfield & Crowther (2007) Fig 6.5 was selected to examine the sources of fine grained magnetite in the sequence and the plot of Dearing *et al*., (1997) shown in Fig 6.4 was selected to further examine the type and concentration of magnetic grain size.

6.3 Statistical analysis

A review of the use of multivariate statistics in palaeoenvironmental reconstruction is provided within Chapter 3, Theory and Methods.

6.3.1 Inter- relationships among the magnetic parameters

Correlations were determined for both magnetic parameters and interparametric ratios of the Kilombe sequence by producing a Pearson correlation matrix together with LOI values and the results are presented in Table 6.2. The relationship between magnetic parameters and inter-parametric ratios shows that the strongest correlation with MS is obtained for χ_{FD}, χ_{ARM}, SIRM and SOFT ($r = 0.89, 0.87, 0.81$ and 0.7, $p<0.01$). Moderate and weak, but statistically significant relationships with χ_{LF} were obtained for S-ratio, HIRM, $\chi_{FD}\%$ and LOI% ($r = -0.49, 0.31, 0.28$ and -0.24, $p<0.05$). Correlations with interparametric ratios were not statistically significant. SIRM is correlated with SOFT ($r = 0.95$, $p<0.01$).

Magnetic parameters & ratios	Units	Interpretation
Low frequency magnetic susceptibility (χlf)	10^{-8} m^3/kg	Sensitive to bulk ferrimagnetic mineral content & also superparamagnetic and coarse multi-domain grains
Frequency-dependent magnetic susceptibility (χfd)	10^{-8} m^3/kg	Indicates concentration of superparamagnetic ferrimagnetic grains (SP grains form pedogenically in soils/palaeosols) which can increase with increasing annual rainfall
Frequency-dependent magnetic susceptibility (χfd %)	%	Indicates the proportional contribution of SP grain to the bulk measurement
Anhysteretic remanent magnetisation (χarm)	10^{-8} m^3/kg	Sensitive to the concentration of ferrimagnetic grains in the single domain range which includes pedogenic grains as with χfd, the concentration of which can increase with increasing annual rainfall
SIRM	10^{-5} Am^2kg^{-1}	Sensitive to the concentration of remanence holding material (ferromagnetic)
HIRM	-	Sensitive to the concentration of low-coercivity minerals (hematite and goethite)
SOFT	-	Sensitive to the concentration of high-coercivity minerals (magnetite and maghemite)
S ratios (-100mt, -300mt)	-	Sensitive to the concentration of antiferromagnetic minerals and coarser ferromagnetic minerals
Xarm/χfd	-	Relative proportion of SD and SP ferrimagnetic grains
Xarm/SIRM	10^{-3}/Am	Sensitive to ferrimagnetic grain size in the SD range. Ratio is known to increase with intensity of pedogenesis
SIRM/χlf	-	Sensitive to changes in magnetic grain size and the presence of greigite

Table 6.1 The magnetic parameters and interparametric ratios used in this part of the study, their units and interpretation

	XLf 10-8m3kg-1	**Xfd 10-8m3kg-1**	**Xfd%**	**Xarm 10-8m3kg-1**	**SIRM 10-5Am2kg-1**	**HIRM**	**SOFT**	**S-ratio (-300)**	**S-ratio**	**Xarm/SIRM 10-3mA-1**	**Xarm/XLf**	**Xarm/Xfd**	**SIRM/Xlf**	**LOI%**
XLf 10-8m3kg-1	1	0.89046	0.28327	0.87914	0.81332	0.31265	0.77932	-0.49329	-0.56745	0.11818	0.16192	-0.17024	0.16807	-0.2406
Xfd 10-8m3kg-1	0.89046	1	0.46787	0.71337	0.59593	0.23705	0.56072	-0.47255	-0.57715	0.20713	0.04429	-0.3498	-0.0831	-0.1492
Xfd%	0.28327	0.46787	1	0.12346	0.02602	-0.02091	-8.94E-04	-0.53584	-0.62901	0.25213	-8.49E-02	-0.67119	-0.34382	0.29163
Xarm 10-8m3kg-1	0.87914	0.71337	0.12346	1	0.81838	0.32487	0.78347	-0.40223	-0.44775	0.32873	0.48861	0.16044	0.31505	-0.22871
SIRM 10-5Am2kg-1	0.81332	0.59593	0.02602	0.81838	1	0.39414	0.94401	-0.43437	-0.4548	-0.07353	0.26401	0.03185	0.6506	-0.18634
HIRM	0.31265	0.23705	-0.02091	0.32487	0.39414	1	0.32573	0.24958	-0.0989	0.02308	0.1977	0.08095	0.29647	-0.20785
SOFT	0.77932	0.56072	-8.94E-04	0.78347	0.94401	0.32573	1	-4.26E-01	-0.46992	-0.03372	0.26388	4.87E-02	0.59725	-0.17897
S-ratio (-300)	-0.49329	-0.47255	-0.53584	-0.40223	-0.43437	0.24958	-0.42622	1	0.81487	-0.12549	-0.13432	0.34826	-0.14787	-0.19293
S-ratio	-0.56745	-0.57715	-0.62901	-0.44775	-0.4548	-0.0989	-0.46992	0.81487	1	-0.24614	-0.20543	0.38423	-0.08888	-0.16353
Xarm/SIRM 10-3mA-1	0.11818	0.20713	0.25213	0.32873	-0.07353	0.02308	-0.03372	-0.12549	-0.24614	1	0.75976	0.38831	-0.18894	-0.12067
Xarm/XLf	0.16192	0.04429	-0.08489	0.48861	0.26401	0.1977	0.26388	-0.13432	-0.20543	0.75976	1	0.68727	0.41143	-0.2596
Xarm/Xfd	-0.17024	-0.3498	-0.67119	0.16044	0.03185	0.08095	0.04866	0.34826	0.38423	0.38831	0.68727	1	0.37494	-0.3557
SIRM/Xlf	0.16807	-0.0831	-0.34382	0.31505	0.6506	0.29647	0.59725	-0.14787	-0.08888	-0.18894	0.41143	0.37494	1	-0.19051
LOI%	-0.2406	-0.1492	0.29163	-0.22871	-0.18634	-0.20785	-0.17897	-0.19293	-0.16353	-0.12067	-0.2596	-0.3557	-0.19051	1

Table 6.2 Pearson’s correlation matrix showing the association of magnetic parameters and interparametric ratios

6.3.2 Principal component analysis

Principal component analysis was used to further examine the relationship between magnetic parameters and evaluate the degree to which changes in type, concentration and grain size of magnetic minerals were influencing changes in the magnetic data set. Extracted eigenvalues (>1) show that PC1 – 4 account for approximately 85 % of the total variance in the entire magnetics data set. PC1, PC2, PC3 and PC4 account for 38%, 22%, 14% and 8% of the total variance, respectively. The bulk of total variance is controlled by the first two principal components (60% of the total variance) which are summarised below.

In summary the results of PCA show that changes in the magnetic properties of the Kilombe data set appear to be mainly controlled by the following parameters and in the following order:

- **PC1** χ_{LF}, χ_{ARM}, SOFT, χ_{FD} and SIRM.
- **PC2** χ_{ARM}/χ_{FD}, χ_{ARM}/χ_{LF} and SIRM/χ_{LF}, χ_{FD}% has a negative correlation with other parameters on this principal component.

The PCA loading plot shown for PC1 and PC2 is shown in Figure 6.1. The plot shows that LOI% has a negative PC1 score while all of the other magnetic parameters and interparametric ratios have positive scores. The magnetic parameters appear to be quite evenly distributed across both principal components; however, interparametric ratios associated with magnetic grain size fall closer together while the concentration parameters are more evenly distributed.

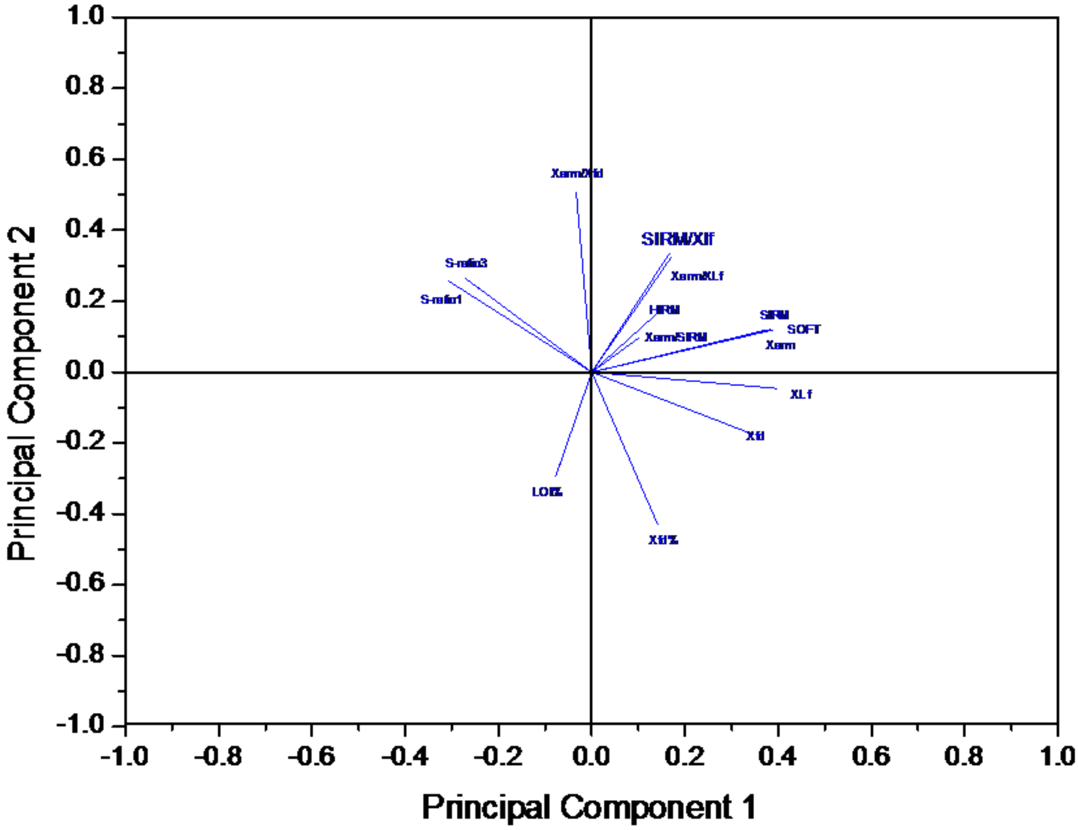

Figure 6.1 Principal component loading plot showing the distribution of magnetic parameters and interparametric ratios for Kilombe across PC1 and PC2

6.3.3 Linear plots

The linear plots of both χ_{FD} and $\chi_{FD}\%$ versus χ_{LF} (Fig. 6.2) suggest that changes in the concentration of SP grains contribute significantly to the overall trends in MS (r^2 = 0.80), confirming the results of the PCA and the Pearson correlation coefficient matrix, whereas variation in the proportion of SP grains do not affect changes in MS values to any significant degree (r^2 =0.16). Some samples deviate significantly from the regression line and this will be examined more closely within this chapter.

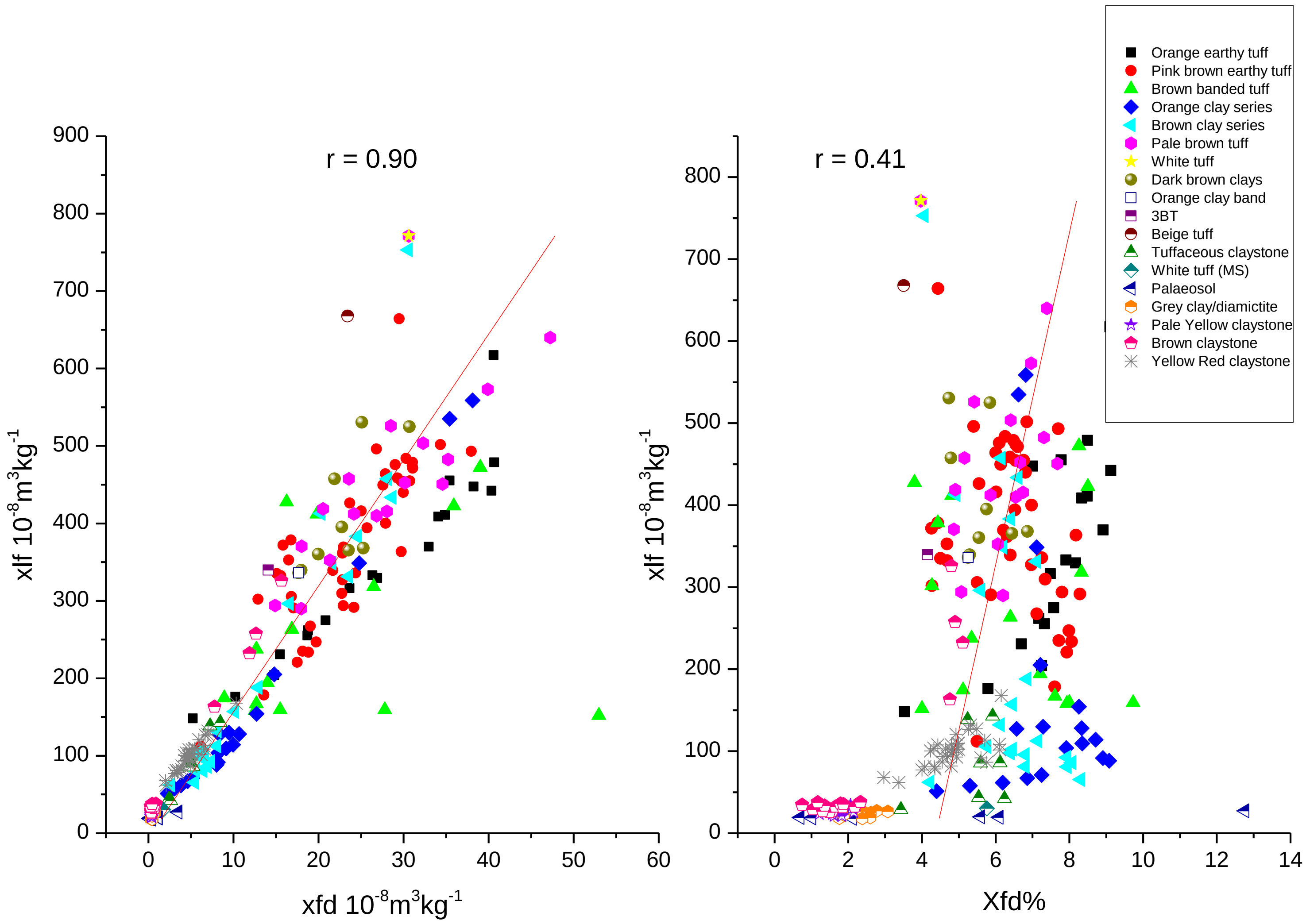

Figure 6.2 Linear regression analysis of χlf versus χfd and χfd%

6.3.4 Summary

MS or χ_{LF} values are generally representative of the bulk content of ferrimagnetic minerals (magnetite/maghemite); however, this parameter is also sensitive to SP and coarse MD grains. In general, the results of statistical analyses suggest that the main contribution to MS in this sequence is from parameters sensitive to both the concentration of magnetite/maghemite and the concentration of SD and SP ferrimagnetic grains. This further suggests that magnetic enhancement in the Kilombe soils and sediments may perhaps be attributed to the neoformation of ultrafine (SD and SP) pedogenic ferrimagnetic magnetite/maghemite. However, variation in the proportion of SP grains does not correlate statistically with variation in MS.

6.4 Results - magnetic properties and lithology

Figure 6.3 displays the mineral magnetic parameters and interparametric ratios for the Kilombe sedimentary sequence versus depth and lithology. The parameters display significant variation with depth in accordance with changes in lithology. However, there is some variability in some parameters within and between individual lithological units. Average values and ranges for each magnetic parameter for the entire Kilombe sequence and for each lithological unit are presented in Table 6.3 and the following sections describe the defining magnetic properties of each unit.

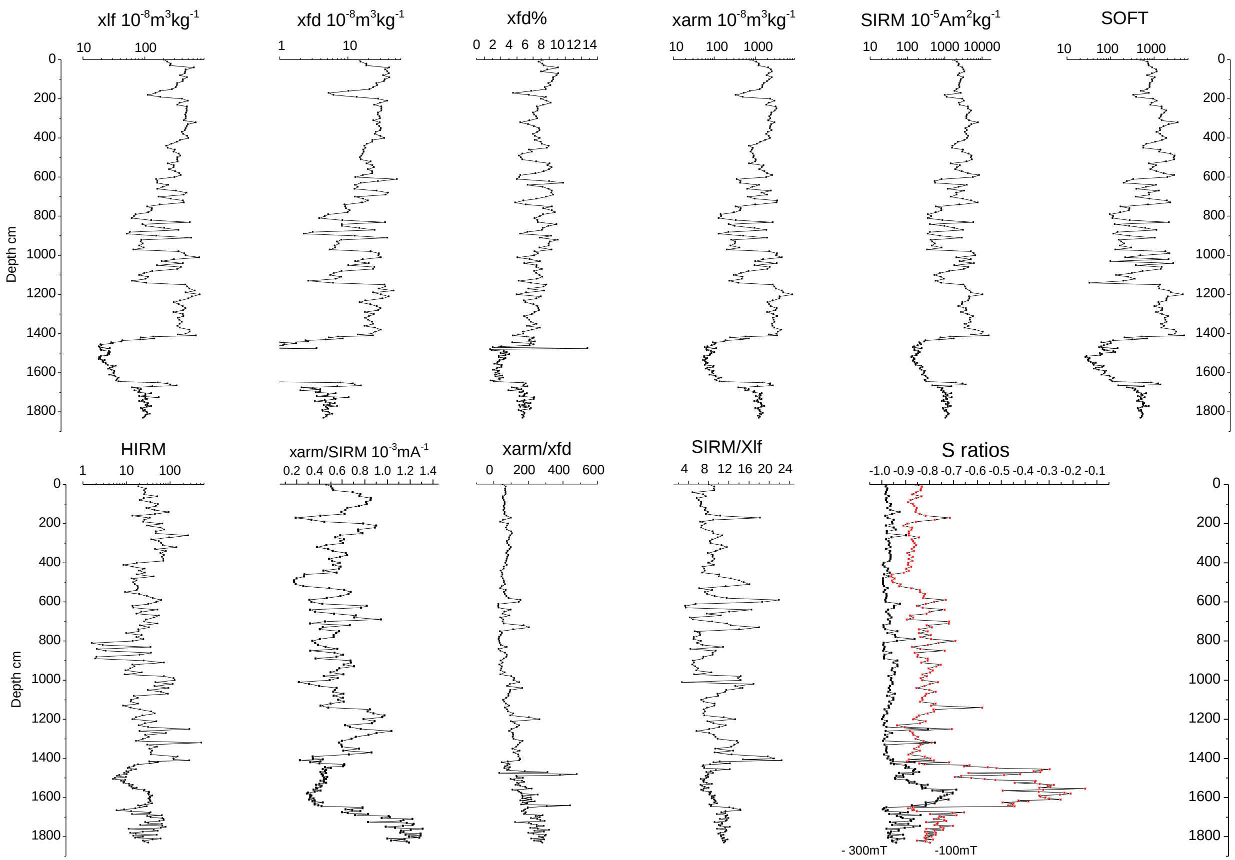

Figure 6.3 Mineral magnetic parameters and interparametric ratios to depth

Lithological unit and sample numbers associated with each unit	Number of samples in each unit	χlf	χfd	χfd%	χarm	SIRM	HIRM	SOFT
16 (127-144)	18	**342.3** (148.2-617.3)	**26.5** (5.2-40.5)	**7.5** (3.5-9.1)	**1615** (519-2540.4)	**2499.6** (1643.2 – 3344.4)	**35.2** (13.6-93.1)	**811.6** (485.9 – 1031.7)
15 (84-126)	43	**373.3** (220-664.1)	**23.2** (12.9 -37.9)	**6.3** (4- 8.2)	**351.6** (330 – 2558.3)	**3587.5** (824.1- 7727)	**47.4** (9.2 – 260.4)	**1495.4** (333 -2963.1)
14 (70-83)	14	**265.5** (151.9 – 472.4)	**22.2** (8.9-52.9)	**6.7** (3.7-9.2)	**1362.4** (351.6 -3497.5)	**2625** (633.7 – 7697.3)	**30.4** (13.7-56.2)	**854.5** (238.9 – 2352)
13	-	-	-	-	-	-	-	-
F (66-69)	4	**120.3** (109.4-129.9)	**9.8** (9.1-10.6)	**8.1** (7.2-8.7)	**375.6** (304-441.6)	**691** (576-806.7)	**17**	**219.2** (167.4-273)
E (62-65)	4	**81.7** (61.6-127.3)	**5.4** (3.8-8.6)	**6.7** (6.1-6.2)	**188.7** (128.4-335.9)	**502.3** (353-866)	**10.6**	**149.4** (96.3-276)
D (57-61)	5	**256** (91-535)	**18.2** (8.1-35.4)	**7.5** (6.6-8.9)	**1205** (225-2653)	**2417** (403.6-5825.1)	**19.6**	**872** (124.5-2207.7)
C (55-56)	2	**54** (51-57)	**2.6** (2.2-3)	**4.8** (4.3-5.3)	**175** (128-122)	**376.5** (349.4-403.7)	**1.9**	**130.8** (116.3-145)
B (53-54)	2	**356.5** (154.1-558.9)	**25.4** (12.7-38.1)	**7.5** (6.8-8.2)	**1226** (505-1947)	**1809.4** (749.4-2869.4)	**48.4**	**659.8** (273.8-1045.8)
A (50)	1	**88.3**	**8**	**9**	**258.1**	**419.5**	**13.8**	**155.2**
12	-	-	-	-	-	-	-	-
E (45-49)	5	**84** (65.3 -95)	**6.5** (5.4-7.3)	**7.8** (6.7 -8.3)	**300.4** (204.3-409.5)	**522.1** (334)	**13.7**	**194.5** (129-299)
D (39-44)	5	**457.8** (296-753)	**25.1** (16.1-28.6)	**5.7** (4-6.6)	**2965** (1553.6-4467.7)	**4927.5** (2042.6-6567)	**96.5**	**1358.2** (216.5-2240)
C (36-38)	3	**252.6** (157-412.6)	**14.4** (10.1-20.3)	**6** (4.9-6.8)	**1773.3** (966-3355.8)	**3459** (2042.6-6576)	**55.6**	**1084.2** (100.4 -2767.7)
B (33-35)	3	**282.2** (132-383.2)	**18.7** (8-24)	**6.5** (6.1-7.1)	**1640.3** (687.3-2254.9)	**2951.1** (1306-4313)	**55.4**	**1159** (550-1497.5)
A (27-32)	6	**93.5** (62-105.5)	**5.8** (2.6-8)	**6** (4.2-6.7)	**387.8** (232-487.1)	**730.6** (568.4 -939)	**13.8 (8-18.2)**	**215.5** (33.1-363.2)

Table 6.3 Average and ranges for magnetic parameters and interparametric ratios for each lithological unit for the Kilombe sequence

Lithological unit and sample numbers associated with each unit	Number of samples in each unit	χlf	χfd	χfd%	χarm	SIRM	HIRM	SOFT
11 a (21)	**1**	**77.1**	**30.6**	**3.9**	**8067.1**	**10215**	**13.6**	**4573.6**
11 (10-26)	17	**418.7** (294-639)	**27.8** (14.9 -47.2)	**6** (3.9-7.6)	**3399** (1956.4 -4800)	**4200** (2301.9-5700)	**44.6** (16.6 -80.4)	**1792** (1105.5-2091)
10 a (5)	**1**	**336.1**	**17.6**	**5.2**	**2644.6**	**4330.1**	**38.8**	**1688.5**
10 (1-9)	8	**408** (336.1-530)	**22.7** (17.6-30.6)	**5.6** (4.7-6.8)	**3084.8** (2549.7-4348.6)	**5791.6** (3407.8 -10476)	**113** (29.7-149.8)	**2132.2** (1434-3223.5)
9 (k50)	**1**	**339.7**	**14**	**4.15**	**2157.9**	**5035.5**	**121.9**	**2163.8**
8 (k49)	**1**	**667.7**	**23.4**	**3.5**	**3443.6**	**3443.6**	**275.2**	**4907.8**
7 (k41-k48)	7	**71.4** (28.7-142.8)	**4**	**5.4** (3.4-6.1)	**307.1** (92.4-708.7)	**671.2** (206.4-1751.2)	**24.4** (11.6-52.8)	**251.3** (61.7-704.3)
6 (k40)	**1**	**30.4**	**1.7**	**5.7**	**106.8**	**215.5**	**10.7**	**102**
5 (k31-k40)	7	**20.4** (18 -27.2)	**0.9** (0.1-3.4)	**4.1** (0.8 – 12)	**75.5** (63.7 -111.8)	**171.6** (152.1-241.4)	**9.9** (6.8-12.7)	**78.1** (54.8-145.2)
4 (k24-k30)	7	**24.2** (19.5-27)	**0.5** (0.1-0.8)	**2.2** (0.8 - 3)	**67.2** (53.3-100.5)	**177** (135.8-215)	**7.1** (4.9-9.3)	**75** (28.3-130.1)
3 (k17-k23)	7	**23.6** (18.3-33.9)	**0.44** (0.3-0.6)	**1.8** (1.5-2.6)	**67.2** (53.3-97.1)	**177.9** (128.7-256.4)	**17.9** (8.5-33.1)	**41.3** (26.5 -69.7)
2 (kl-59-k16)	19	**79.9** (25.5-325.9)	**3** (0.38-15.6)	**2.3** (1 -5.1)	**572.2** (61.5-2329.3)	**770.9** (212.8-3667.1)	**28.1** (5.9-39.1)	**496.6** (237.1-758.8)
1 (kl1-kl57)	32	**100.4** (61.9-131.8)	**4.9** (2-10.3)	**4.8** (2.9-6)	**1174.5** (387-1539.6)	**1094.2** (650.6-1499.7)	**39.1** (11.2-79.6)	**496.6** (237.1-758.8)

Table 6.3 *continued* Average and ranges for magnetic parameters and interparametric ratios for each lithological unit for the Kilombe sequence

Lithological unit and sample numbers associated with each unit	Number of samples in each unit	S ratio (300mt)	S ratio (100mt)	χarm/SIRM	χarm/χfd	SIRM/χlf
16 (127-144)	18	**-0.97** (-0.92 - -0.98)	**-0.84** (-0.71- - 0.88)	**0.63** (0.19-0.85)	**63.5** (51.2-72.7)	**8** (5.6-18.1)
15 (84-126)	43	**-0.97** (-0.89 - -0.99)	**-0.87** (-0.73 - -0.96)	**0.51** (0.17 – 0.88)	**73.9** (36.7- 154)	**9.7** (6.2 – 21.9)
14 (70-83)	14	**-0.96** (-0.92 - -0.99)	**-0.81** (-0.71 - -0.89)	**0.56** (0.31-0.94)	**76.2** (25.7-171.9)	**9.4** (3.3-17.9)
13	-	-	-	-	-	-
F (66-69)	4	**-0.94** (-0.93 - -0.97)	**-0.82** (-0.79 - -0.84)	**0.54** (0.52-0.57)	**38.3** (30.6-46.6)	**5.7** (5-6.2)
E (62-65)	4	**-0.94** (-0.86 - -0.99)	**-0.76** (-0.69 - -0.80)	**0.37** (0.33-0.4)	**33.4** (27.9-40.1)	**6** (5 -6.8)
D (57-61)	5	**-0.98** (-0.95 - -0.99)	**-0.83** (-0.73 - -0.87)	**0.49** (0.32-6)	**56.3** (27.5 -74.9)	**8.4** (4.4-10.8)
C (55-56)	2	**-0.98** (-0.98)	**-0.82** (-0.80- -0.85)	**0.45** (0.36-0.55)	**64.7** (57-72.5)	**15** (14.9-15.2)
B (53-54)	2	**-0.93** (-0.93- -(-0.94)	**-0.82** (-0.80 - - 0.83)	**0.67**	**45.3** (39.6-51)	**12** (10-14)
A (50)	1	**-0.93**	**-0.75**	**0.61**	**32.1**	**16.3**
12	-	-	-	-	-	-
E (45-49)	5	**-0.94** (-0.93- 0.95)	**-0.79** (-0.77 - -0.82)	**0.58** (0.49-7)	**45.8** (37.6-62.9)	**6** (5.3-8.5)
D (39-44)	5	**-0.96** (-0.95- -0.97)	**-0.80** (-0.79 - -0.83)	**0.41** (0.21-0.56)	**114.8** (93.7-146.2)	**12.4** (2 – 16)
C (36-38)	3	**-0.96** (-0.96)	**-0.82** (-0.82 - -0.85)	**0.49** (0.39-0.55)	**112** (77.3-165.2)	**13.1** (11.4 -14)
B (33-35)	3	**-0.96** (-0.94 - -0.97)	**-0.80** (-0.77 - - 0.81)	**0.55** (0.52-0.61)	**86.9** (84-91)	**10.7** (7.4-13.1)
A (27-32)	6	**-0.96** (-0.96- -0.97)	**-0.71** (-0.58- -0.79)	**0.52** (0.4-0.6)	**68.4** (54.2-88.7)	**12.8** (11.7-13.9)

Table 6.3 *continued* Average and ranges for magnetic parameters and interparametric ratios for each lithological unit for the Kilombe sequence

Lithological unit and sample numbers associated with each unit	Number of samples in each unit	S ratio (300mt)	S ratio (100mt)	χarm/SIRM	χarm/χfd	SIRM/χlf
11 a (21)	**1**	**-0.99**	**-0.86**	**0.78**	**263**	**10.9**
11 (10-26)	17	**-0.97** (-0.80 - -0.99)	**-0.84** (-0.70 - -0.93)	**0.82** (0.62-1)	**123.2** (77-263)	**9.4** (5-13)
10 a (5)	**1**	**-0.98**	**-0.84**	**0.61**	**149.7**	**11**
10 (1-9)	8	**-0.95** (-0.77 - -0.98)	**-0.83** (-0.79 - -0.88)	**0.59** (0.34-0.85)	**139.4** (108.3-166.4)	**8.2** (5.5 – 9.8)
9 (k50)	**1**	**-0.95**	**-0.88**	**4**	**153.2**	**14.8**
8 (k49)	**1**	**-0.96**	**-0.78**	**0.23**	**146.9**	**22.4**
7 (k41-k48)	7	**-0.89** (-0.86- -0.96)	**-0.7** (-0.55- -0.84)	**0.49**	**77**	**8.6** (6.7 – 12.2)
6 (k40)	**1**	**-0.90**	**-0.52**	**5**	**61.3**	**7.1**
5 (k31-k40)	7	**-0.89** (-0.84—0.93)	**-0.53** (-0.33- -0.69)	**0.43** (0.41-0.46)	**227** (32.1-480.1)	**7.7** (6.4 – 8.8)
4 (k24-k30)	7	**-0.86** (-0.80 - -0.89)	**-0.37** (-0.28 - - 0.54)	**0.44** (0.41-0.47)	**141.2** (97-168.8)	**7.2** (6.4-8.6)
3 (k17-k23)	7	**-0.77** (-0.70 - - 0.83)	**-0.21** (9-0.14 - -0. 49)	**0.37** (0.29-0.46)	**154.7** (126.1-219	**7.4** (6.5 – 8.4)
2 (kl-59-k16)	19	**-0.82** (-0.70 - -0.98)	**-0.49** (-0.21—0.89)	**0.44** (0.29-0.78)	**205** (161.1-441.6)	**9.9** (8.3 – 14.2)
1 (kl1-kl57)	32	**-0.92** (-0.83 – 0.97)	**-0.77** (-0.65 - -0.85)	**1** (0.6-1.29)	**246.1** (124-320.3)	**10.8** (9.1-11.9)

Table 6.3 *continued* Average and ranges for magnetic parameters and interparametric ratios for each lithological unit for the Kilombe sequence

Unit 1 Yellowish red claystone

This unit is characterised by low values of χ_{LF}, χ_{ARM}, χ_{FD}, SOFT and SIRM, and low to moderate values of χ_{FD}%. Values of HIRM increase systematically up section while all other parameters decline. χ_{ARM}/SIRM exhibits is highest values for the entire sequence in this unit. S-ratios (-300mT), are low and negative whilst higher mean values of S-ratio (-100mT) are observed.

- The mineralogy is dominated by a low concentration of ferrimagnetic minerals (magnetite/maghemite) in a variety of grain sizes, with the significant contribution of imperfect antiferromagnetic minerals in some intervals.
- Values of χ_{arm}/SIRM peak in this unit indicating the contribution of fine SD ferrimagnets whilst higher mean values of S-ratio (100mT) indicate a higher proportion of either viscous single domain or multi-domain ferrimagnets. The concentration and proportion of ultrafine SP grains are low.
- As HIRM increases other parameters associated with the concentration of SD and SP magnetite/maghemite decrease. This suggests that the contribution from imperfect antiferromagnetic minerals may be more representative of the detrital component rather than being of pedogenic origin.
- The mineralogy and grain size suggests that the unit is defined by a mixed magnetic assemblage of both detrital and perhaps pedogenic origin.

Units 2 – 6 (5 units, Brown claystone, Pale yellow claystone, Grey claystone/diamictite, Pale brown Palaeosol and White tuff)

A major change in the magnetic properties of units 2 – 6 is observed. Unusually low values of χ_{LF}, χ_{FD}, χ_{ARM} and SIRM are noted across all units, and mean values of S-ratio (100mT and 300mT) decrease to -0.4 and -0.82 respectively. The decrease noted in S ratio values occurs progressively up section. Little change is evident in χ_{ARM}/χ_{FD}. Values of HIRM increase relative to SOFT. Variability in mean values is noted for some parameters between these units, which are described below.

Unit 2 Brown claystone

- A larger peak in HIRM relative to other units and higher S ratio (300 mT) (-0.70).

Unit 4 Grey claystone (diamictite)

- A peak in χ_{LF} and increase to lower negative values of S-ratio (100mT).

Unit 5 Palaeosol

- Two peaks in χ_{FD}% (5.5, 6) at the top of this unit and very high and negative S ratio (100mT) values, (-0.29, -0.33).

Unit 6 White tuff (re-sedimented)

- Peak in χ_{FD}%.

Magnetic properties units (2-6)

The magnetic properties of units 2-6 are dominated by a mixture of ferri- and imperfect antiferromagnetic minerals with magnetic grain sizes in the range of both coarser MD and SD grains with little or no contribution from ultrafine ferrimagnetic grains. The brown claystone shows a dominance of imperfect antiferromagnetic minerals as indicated by higher negative S ratio (300mT) and HIRM values. The top of unit 6 (palaeosol) shows a distinct change to higher χ_{FD}% values suggesting the increased contribution of ultrafine ferrimagnetic grains with a mixture of detrital MD grains. These units document the highest contribution from imperfect antiferromagnetic minerals and coarse MD grains in the sequence, which strongly suggests a detrital origin. Another possible explanation for these values is dissolution via burial diagenesis and loss of the fine grained ferrimagnetic component. Section 6.6 will examine the magnetic properties of these units from fractioned samples in order to further explore these possibilities.

Unit 7 Tuffaceous pale brown claystone

This unit is defined by marked increases in χ_{LF}, SIRM and SOFT which occur gradually throughout the unit, compared to units 2-6. Indicators of a fine magnetic grain size, χ_{ARM}, χ_{FD}, χ_{FD}% and χ_{ARM}/SIRM, all increase throughout the unit. S-ratios (100mT & 300mT) both decrease to lower negative values.

- The mineralogy is dominated by a higher concentration of ferrimagnetic magnetite/maghemite relative to the previous units, with some contribution from imperfect antiferromagnetic minerals, in a variety of grain sizes. The concentration of ferrimagnetic minerals increases throughout the unit.
- The range of magnetic grain sizes includes SD, ultra-fine and with some contribution from MD ferrimagnets.

Unit 8 Beige Tuff

The values of χ_{LF} χ_{ARM}, SIRM and SOFT peak in this unit. Indicators of fine magnetic grain size χ_{FD}% and χ_{ARM}/SIRM are low.

- The magnetic properties are dominated by a high concentration of magnetite/maghemite with a low proportion of ultrafine SP grains.

Unit 9 Three-banded tuff

This unit is defined by peaks in χ_{LF}, SIRM and SOFT. Mean values of χ_{ARM} are high; however, the values of other indicators of fine magnetic grain size, χ_{FD} and χ_{ARM}/SIRM, are moderate and low respectively.

- The magnetic properties are dominated by a high concentration of magnetite/ maghemite in the SD range with a low to moderate contribution from SP grains.

Unit 10 Dark brown tuffaceous clays

This unit is characterised by high mean values of χ_{LF}, χ_{FD}, χ_{ARM}, SIRM and SOFT. Values of χ_{FD} % are moderate while values of χ_{ARM}/SIRM and SIRM/χ_{LF} are low. S ratio (300mT) is low and negative whilst S ratio (100mT) exhibits slightly higher mean values.

- The magnetic mineralogy is dominated by a high concentration of ferrimagnetic minerals (magnetite/maghemite) in a variety of grain sizes, with little contribution from imperfect antiferromagnetic minerals.
- The magnetic grain sizes suggest contribution from SP, coarse SD grain and higher proportion of either viscous single domain or multi-domain ferrimagnets as indicated by higher mean values of S-ratio (100mT). The concentration and proportion of ultrafine SP grains are high and moderate respectively.

Unit 10 (A) Orange clay band

This unit occur within unit 10 and the magnetic properties are similar to those outlined above. Peaks in χ_{ARM}, SIRM, SIRM/χ_{LF} are observed compared to unit 10, whilst lower mean values of χ_{FD}, χ_{FD}%, χ_{ARM}/SIRM and S ratio (100mT) occur.

- The magnetic properties are dominated by magnetite/maghemite with little contribution from imperfect antiferromagnetic minerals.
- A reduction in the concentration of fine and ultrafine ferrimagnetic minerals is observed with an increase in coarser grain sizes (SD and MD).

Unit 11 Pale brown tuff

This unit is defined by an increase in mean values of χ_{LF}, χ_{FD} and χ_{ARM} compared to unit 10, whilst mean values of SOFT decline. Values of SIRM/χ_{LF} are much lower than in the previous unit whilst mean values of χ_{ARM}/SIRM increase. One sample, from 1250 cm depth, exhibits higher negative values in both S ratio parameters and a significant peak in HIRM.

- The magnetic properties are dominated by a lower concentration of magnetite/maghemite with little contribution from imperfect antiferromagnetic minerals.
- An increase in the concentration of fine ferrimagnetic minerals is noted compared to the previous unit.
- The concentration of fine ferrimagnetic minerals increases throughout the unit.

Unit 11 (A) White tuff

This unit occurs within unit 11 at the depth of 1200 cm. The unit is characterised by peaks in χ_{LF}, χ_{ARM}, SIRM and SOFT. Peaks in χ_{ARM}/χ_{FD} and SIRM/χ_{LF} are also observed.

- The magnetic properties are dominated by a high concentration of ferrimagnetic minerals.
- The dominant grain size appears to be SD which increases relative to SP grains.

Lithounit 12 Brown clay series

The following unit has been divided into five subunits which represent very clayey weathered tuffs.

Sub-units 12 **a** and **e** are similar in terms of concentration based parameters, and are characterised by low values of χ_{LF}, χ_{ARM}, χ_{FD} and SOFT.

Sub units **b**, **c** and **d** are characterised by much higher values of χ_{LF}, χ_{ARM}, χ_{FD} and SOFT compared to **a** and **e**. Mean values of χ_{LF} and SOFT are also high in these units compared to the rest of the sequence. Indicators of magnetic grain size are similar in all units and S ratio (300mT) is low and negative

- The magnetic properties of subunits b, c and d suggest domination by a higher concentration of ferrimagnetic minerals than in a and e, and a higher concentration of SD magnetite.
- There is little contribution from imperfect antiferromagnetic minerals in any of these units.
- The concentration of ultrafine ferrimagnetic grains is also much higher in unit's b, c and d.

Lithounit 13 Orange clay series

Unit 13 is divided into 6 subunits which correspond to the deposition of volcanic tuffs and weathered clay products (units **a**, **c** and **e** represent white tuffs and units **b**, **d** and **f** represent interstitial orange clay deposits)

The magnetic properties of the white tuffs (**a, c** and **e)** are similar. Values of χ_{LF}, χ_{FD}, χ_{ARM} and SOFT are all low.

- The magnetic properties of subunits **a, c** and **e** are dominated by a low concentration of SD magnetite and a low concentration of SP grains of ferrimagnetic origin.
- Unit c has a very low concentration of SP grains and thus lower χ_{LF} values.

The magnetic properties of the orange units are more variable and are defined as: Unit **b** has high χ_{LF} values and high values for χ_{FD}, χ_{ARM} and χ_{ARM}/SIRM. SOFT values are low, and Unit **d** has high χ_{LF} values compared to other subunits, but lower values than in unit **b.** This reduction is explained by lower χ_{ARM}/SIRM values and slightly lower χ_{FD} values. Unit **f** has low χ_{LF} values and low χ_{FD}, χ_{ARM} and SOFT, and values of χ_{ARM}/SIRM are average compared to other subunits.

- The magnetic properties of subunits **b** and **d** are dominated by high concentration of SD magnetite and a high concentration of ultrafine ferrimagnetic grains. The concentration of these grains are lower in unit **d** than **b**.
- The magnetic properties of subunit **f** are dominated by a low concentration of SD magnetite and a low concentration of fine and ultrafine ferrimagnetic grains.

All units are dominated by magnetite/maghemite with a higher contribution from imperfect antiferromagnetic minerals in unit **a**.

Unit 14 Brown banded tuff

This unit exhibits significant variability in both concentration and grain-size dependent parameters and is defined by mean lower values of χ_{LF}, χ_{ARM}, SIRM and SOFT relative to other units on FHC. A large peak in SIRM/χ_{LF} is defined by two samples at the base of the unit. Indicators of fine magnetic grains (χ_{FD} and χ_{FD}%) are also low at the base of the unit but then increase to very high values throughout most of the unit. S ratio (100mT) values are variable with a wide range.

- The magnetic properties are dominated by ferrimagnetic minerals with an increase in imperfect antiferromagnetic minerals at the top of the unit.
- Magnetic grain sizes are variable including fine and ultrafine ferrimagnets; S ratio (100mT) values indicate some contribution from MD or VSD grains.
- The concentration and proportion of SP grains increase throughout this unit whilst fine SD ferrimagnetic grains decline.

Unit 15 Pink brown earthy tuff

Mean values of χ_{LF}, χ_{ARM}, and χ_{FD} increase gradually throughout this unit to much higher value at the top. Values of SOFT and S ratio (300mT) decline overall up section whilst HIRM also increases gradually throughout the unit. Two peaks in SIRM/χ_{LF} are observed at the base of the unit accompanied by peaks in HIRM and S ratio (100mT). Values of χ_{ARM}/χ_{FD} and χ_{ARM}/SIRM also increase throughout the unit.

- The magnetic properties are dominated by magnetite/maghemite, the concentration of which decreases throughout the unit.

- The concentration of imperfect antiferromagnetic minerals increases relative to ferrimagnetic minerals up section.
- Indicators of fine magnetic grain sizes also increase up section. However the proportional increase of SD ferrimagnets is greater than the increase in ultrafine SP grains.
- Coarser SD and MD grain sizes are present at the base of this unit, similar to unit 14.

Unit 16 Orange brown earthy tuff

Mean values of χ_{LF}, χ_{ARM} and SOFT decrease in this unit; however, these values are still high in relation to other units in the sequence. Highest mean values observed for χ_{FD}% occur in this unit. Most parameters exhibit a steadily increasing trend towards higher values in the centre of the unit and then a steady decline. A large peak at the base of this unit is noted in SIRM/χ_{LF}, S ratio (100mT) and HIRM.

- The concentration of ferrimagnetic minerals decreases from the previous unit. However the unit is still dominated by magnetite/maghemite ranging from SD to SP.
- A high concentration and proportion of ultrafine SP grains.
- The magnetic grain size is much coarser (SD and MD) at the base of this unit, similar to the base of unit 14 and 15.

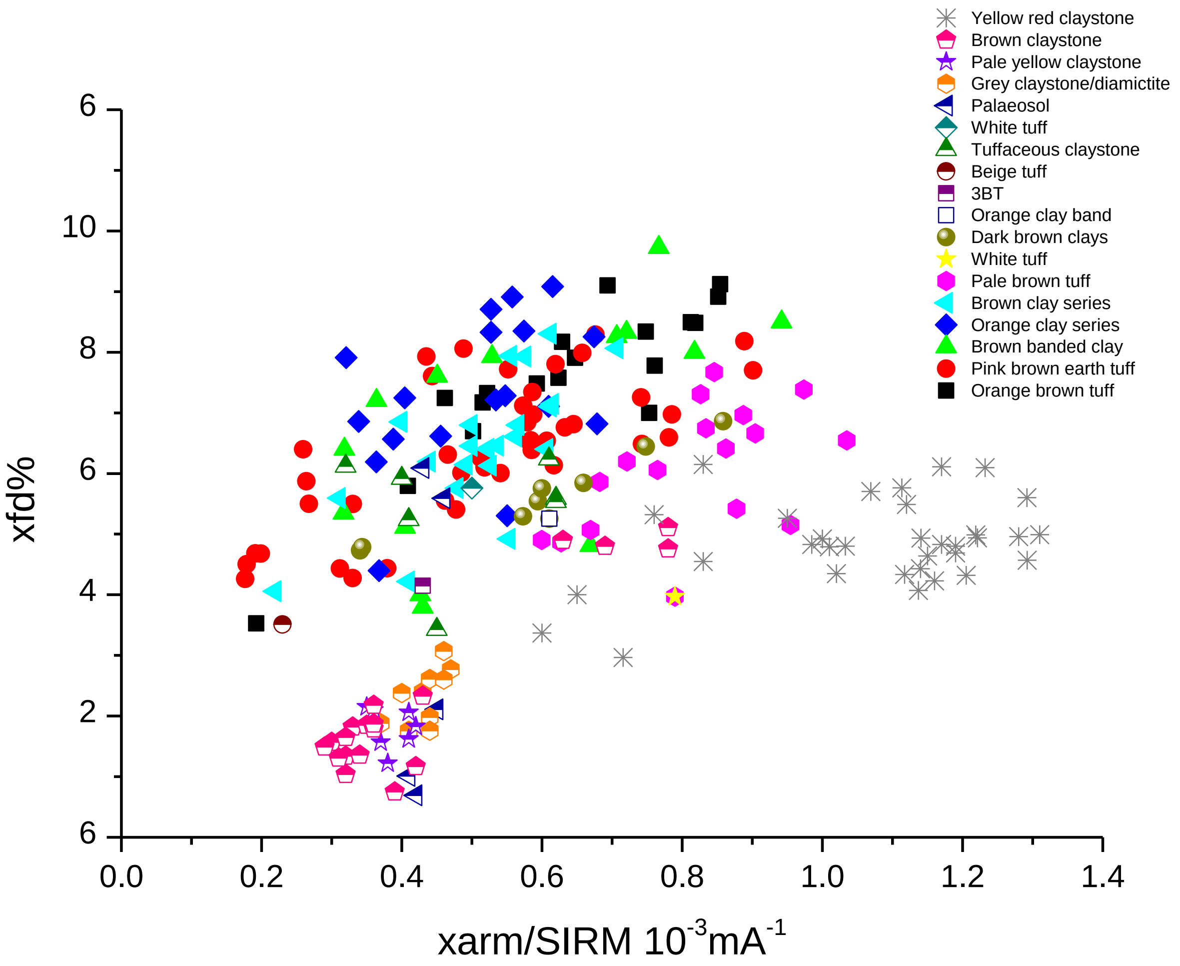

Figure 6.4 Plot of Dearing *et al*., (1997) showing χfd% versus χarm/SIRM for the Kilombe sequence

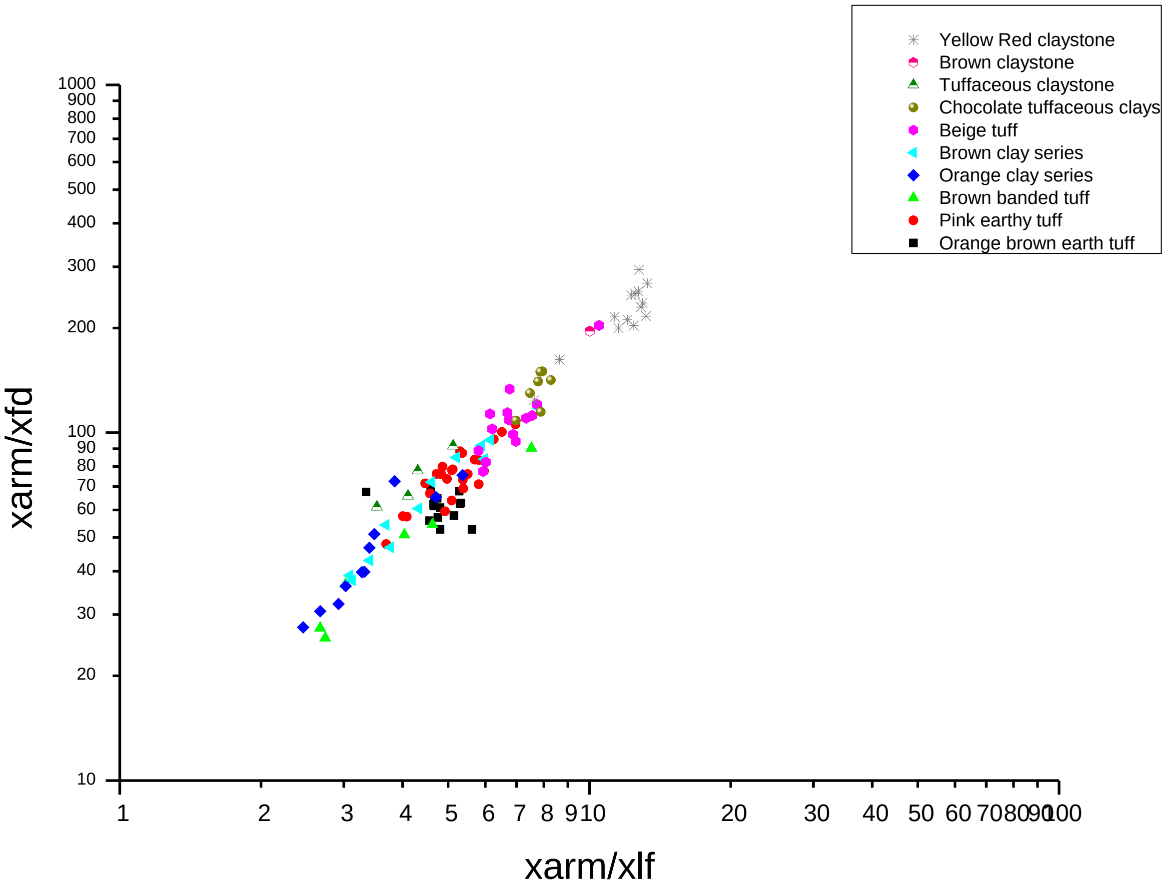

Figure 6.5 Biplot of Oldfield (1994) for the Kilombe soils and sediments

6.4.1 Plot of Dearing *et al*., (1997)

Estimations of magnetic concentration and grain size can also be examined by combining data of χ_{FD}% values with χ_{ARM}/SIRM (Dearing *et al.*, 1997), Fig 6.4, in a semi-quantitative mixing model. Values between 0 and 0.2 generally indicate MD + PSD grains whereas values between 0.2 and 0.8 indicate coarse SSD grains, and values above 0.8 indicate fine SSD grains. For the Kilombe samples this plot suggests that a range of grain sizes is present in the samples with the dominant grain size falling in the coarse SSD range. X_{FD}% displayed on this plot indicates that the percentage of SP grains in the sample is less than 50% with only a small percentage of the samples > 50%.

6.4.2 Summary of results

Results presented above for each lithological unit show that the magnetic mineralogy/grain sizes of the Kilombe sequence are dominated by ferrimagnetic minerals (magnetite/maghemite) in a variety of grain sizes, ranging from coarse to fine SD and ultra-fine and SP. Exceptions to this are units 2-6 which show a significant increase in imperfect antiferromagnetic minerals and coarse MD ferrimagnetic grains.

The following sections attempt to define the source of the fine grained ferrimagnetic component in the Kilombe samples.

6.5 Sources of fine grained ferrimagnetic magnetite/maghemite

Sources of magnetic minerals in sediments and soils can include bacterial magnetosomes, greigite, from anthropogenic processes and burning together with the secondary formation of magnetite/maghemite via pedogenic processes (Liu *et al*., 2012 Oldfield & Crowther, 2007). Anthropogenic processes can be excluded due to the age of the sequence. However, wildfire is an important part of the East African landscape and burning may in part contribute to the MS signal. Mullins (1977) demonstrates one mechanism contributing to the magnetic enhancement of soils/sediments is heating. Heating by both burning and pedogenesis causes magnetic enhancement and can produce a much stronger MS signal in soils/sediment sequences. Ultra-fine-grained magnetite and or maghemite are produced during heating and through oxidation via cooling. It is likely due to the age of the Kilombe sedimentary sequence that the sediments may include quantities of ultra-fine ferrimagnetic minerals due to burning via wildfire. A marine core record produced by Bird & Cali (1998) points to a low incidence of wildfire in sub-saharan African between 1 Ma and 400,000 Kya; however, this record may not be representative of local conditions. Ultrafine ferrimagnetic minerals have also been shown to occur as a result of volcanic activity (Worm & Jackson, 1998).

6.5.1 Examining the pedogenic origin of fine-grained ferrimagnetic minerals

The biplot χ_{ARM}/χ_{LF} versus χ_{ARM}/χ_{FD} of Oldfield (1994) and Oldfield & Crowther (2007) is used here to examine the source of fine-grained magnetite in the sediment/soil samples. This plot permits a comparison between pedogenic materials created through a range of processes, including burning and also weathering environments together with the Kilombe samples. Oldfield (1994; 2007; 2012) outlined criteria for the use of this method that enables the varying proportion of ferrimagnetic grains both above and below the SP/SD grain size range, and finer, to be assessed. According to Oldfield (1994; 2007), only samples which meet the following criteria should be selected:

- 1/ χ_{LF} values > 15 x 10^{-8} m^3/kg.
- 2/ χ_{FD}% values > 5 and χ_{ARM}/SIRM values > 0.5 x 10^{-3} 1/ma.

- 3/ HARD % values < 10.

The application of the three criteria therefore exclude samples that are strongly affected by diamagnetism; ensures that only samples with grain sizes in the SD and finer range are included; and excludes samples in which the contribution from high-coercivity anti-ferromagnetic minerals are is significant. In terms of the Kilombe samples 48 % passed the selection criteria and are included in the plot shown in Figure 6.5.

All of the sediment samples that meet the criteria plot well within the range of values, as defined by Oldfield (1994, 2012), shown to represent pedogenically-enhanced Asian and European soils and palaeosols. All of the samples plot well outside of the range of bacterial magnetite and therefore this source can be ruled out as a source of magnetic minerals in the samples. Therefore it can be suggested that, in those samples plotting within or just outside the envelope of values reported for magnetically-enhanced soils and palaeosols, the magnetic grain-size distribution of the fine ferrimagnetic component is similar to that produced by soils and palaeosols during weathering and pedogenesis. This provides a strong indication that some of the magnetic data (48%) from the Kilombe bulk sediment/soil samples may be the result of weathering and pedogenesis and may hold further climatic information.

6.5.2 Discussion

The results presented above clearly demonstrate the influence of lithology on the magnetic properties of the Kilombe samples. For the most part, the individual magnetic parameters and interparametric ratios exhibit distinct up-section variations in accordance with changes in lithology with some of the major changes in magnetic properties being especially evident at the boundaries between lithological units. However, most of the units also show evidence for the formation of secondary ultrafine ferrimagnetic materials produced as a result of pedogenesis. The plot of Oldfield (2007) allowed further distinction to be made regarding this component with results suggesting evidence for pedogenesis of varying degrees in most units at Kilombe FHC; only samples from unit 1, 2 and 7 passed the criteria from the main site.

6.5.3 Volcanic activity

The magnetic properties of the volcanic tuffs both primary and re-worked all yield a signal similar to that produced during pedogenesis and/or heating i.e. contribution to the signal from ultrafine ferrimagnetic minerals. On the main site the three tuffs do not meet the criteria for comparison to Asian and European soils and did not show evidence for overprinting in thin section. Samples from a number of tuffs from FHC do meet the criteria for the plot of Oldfield (1994), however it is likely that some and/or most these units have been subject to alteration occurring either during transportation or post-depositionally, as well as through heating via mechanical processes of eruption. It may be that some volcanic tuffs do exhibit similar magnetic properties to those produced during pedogenesis however, it is not possible to conclude this with the Kilombe data set at the present time.

6.5.4 Detrital signal or dissolution

Unusually low values of χ_{LF}, SIRM, χ_{ARM} and χ_{FD} are observed in samples from units 2 -6 at the Kilombe main site, together with an increase in HIRM and significant changes in both S ratio parameters. This suggests significant reduction of magnetite and perhaps dissolution via burial diagenesis. Values become progressively lower which suggest increasing alteration of these sediments up-section. This effect is confined to these specific units and is not observed in any other part of the record. This effect, however, could also be the result of environmental change and influx of detrital, non-weathered sediments.

Data presented in Figure 6.2, the biplot of χ_{LF} versus χ_{FD}% may also indicate diagenesis with samples from units 2-6 plotting away from the regression line suggesting removal of the fine grained component with the remaining signal suggestive of the paramagnetic component.

6.6 Particle size separation

The effects of dissolution on an environmental signal are known to be pronounced (Zhang *et al*., 2001; Bloemendal *et al*., 1992). However, if the conditions leading to burial diagenesis and dissolution can be determined this can often impart information on the specific environmental processes such as changes in redox conditions and/or sedimentation rates (Turner, 2010). The distribution of sediment grain sizes or particle sizes can be used to provide important information on sediment transportation processes and depositional environments (Ashley, 1978). Particle size analysis has been employed successfully across a range of proxy archives and environmental settings (Brown, 1985; Heward, 1978; Sun *et al.*, 2002). In comparison, the application of environmental magnetism in studies of sediment grain sizes are rare. The majority of previous studies have been mainly concerned with sediment source and provenance studies of Aeolian, river and coastal environments (Hao *et al.*, 2008; Maher *et al.*, 2009; Oldfield *et al.*, 1985; Lyons *et al.*, 2010, 2012).

6.6.1 Sample selection

This part of the study attempts to further quantify the potential effects of dissolution (as also demonstrated in Chapter 5, Geochemistry by the progressive loss of Fe, Mn and the heavy metal trace elements from units 2-6) on specific particle size fractions of bulk sediment samples at Kilombe using magnetic measurements. Eight samples were analysed over 7 particle size fractions. Two samples unaffected by dissolution, RC1 and BT8, were selected for comparison with the other six. Sample 7, tuffaceous claystone, comes from the base of a unit in which the magnetic properties are observed to change. Sample 5, which represents a palaeosol, also appears to have been affected by dissolution despite representing a period in which a break in sedimentation and a hiatal surface is recorded at this site. The 8 samples shown here represent three facies associations, claystone, reworked tuff and palaeosol.

6.6.2 Results

The results of particle size distribution and magnetic parameters for each sample are shown in Figures 6.6 a – i. The fine grained fractions are highlighted in black and the coarser fractions in grey. Samples known to be unaffected by dissolution are highlighted in blue for comparison. The weight percent per particle size fraction for each sample is shown in Figure 6.6 a.

6.6.3 Particle size distribution of the soils and sediments

The results of particle size separation are broadly comparable to results obtained from Coulter laser diffraction (see Chapter Four and appendix 4) although the latter method tends to underestimate the clay grade fraction in all samples (see also Hao *et al*., 2008) and the sand sized fraction in BC 2. The particle size distribution graphs of all samples exhibit peaks in the clay grade fractions, regardless of facies association. Particle size distributions are polymodal with the main contribution to the bulk sediments being the clay grade and fine silt fractions. The percentage contribution of the < 2 µm fraction is less in samples wt7 and bt8 (reworked tuffs), and sample bt8 exhibits a further peak in the fine silt fraction.

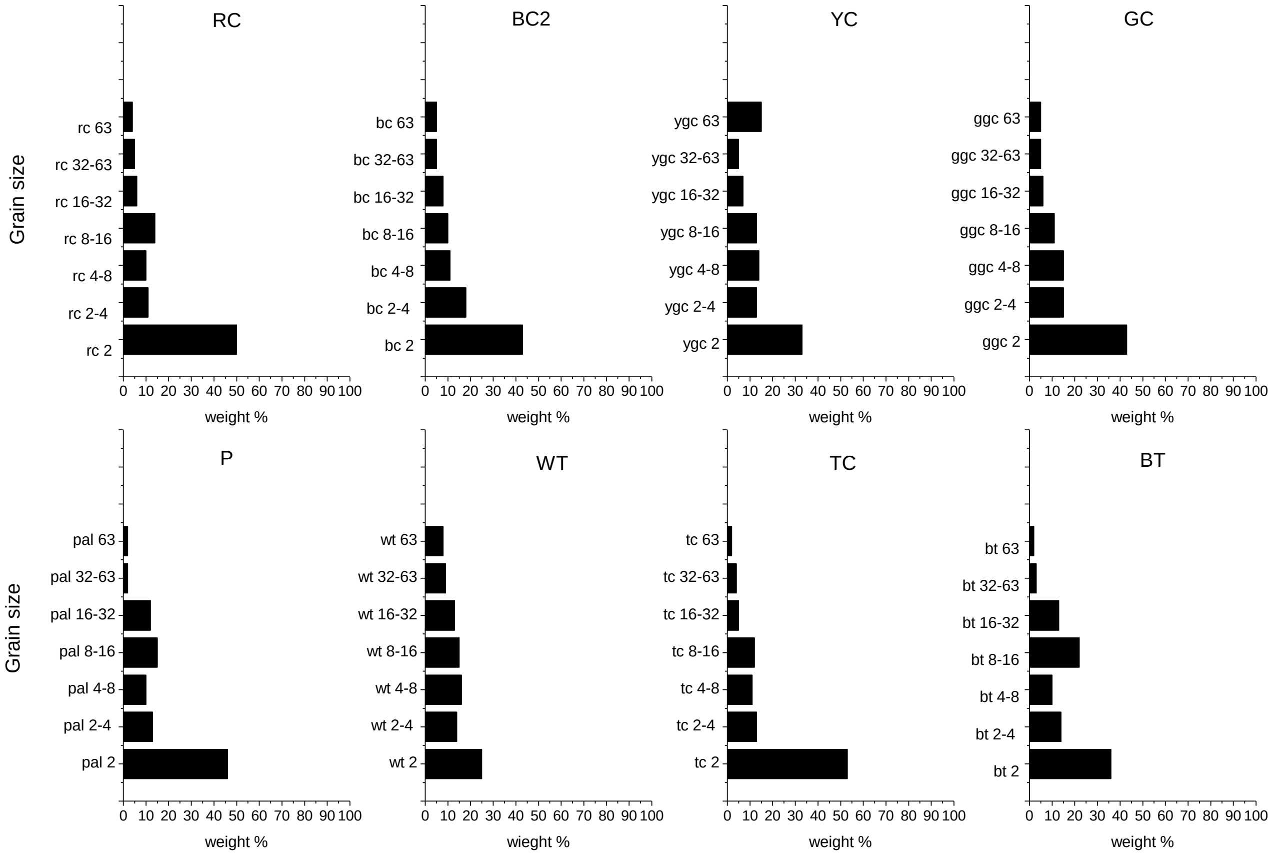

Figure 6.6 (a) X axis shows weight percent totals for each individual grain size per sample. Samples on the Y axis represent lithostratigraphic units 1- 8 (rc, red claystone, bc, brown claystone, ygc, yellow grey claystone, ggc, grey claystone, pal, palaeosol, wt, white tuff, tc, tuffaceous claystone, bt, beige tuff. Each particle size fraction for each lithostratigraphic unit is also displayed <2 µm. 2-4 µm, 4-8 µm, 8-16 µm, 16-32 µm, 32-63 µm and >63 µm

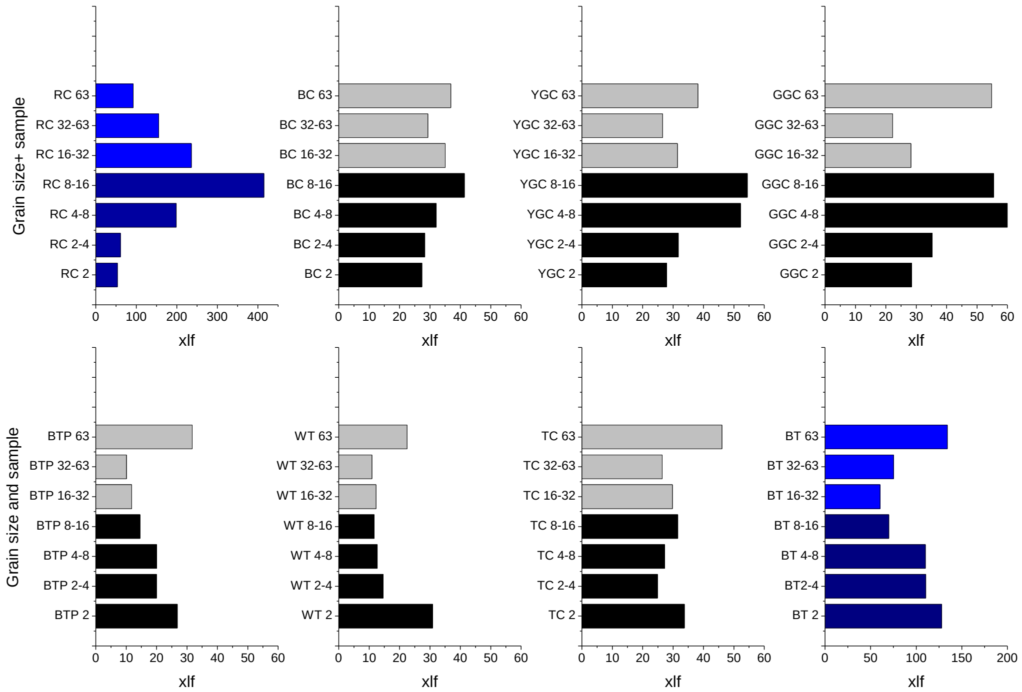

Figure 6.6 (b) X axis shows χlf measurements for each particle size fraction for the Kilombe samples Samples on the Y axis represent lithostratigraphic units 1- 8 (rc, red claystone, bc, brown claystone, ygc, yellow grey claystone, ggc, grey claystone, pal, palaeosol, wt, white tuff, tc, tuffaceous claystone, bt, beige tuff. Each particle size fraction for each lithostratigraphic unit is also displayed <2 µm. 2-4 µm, 4-8 µm, 8-16 µm, 16-32 µm, 32-63 µm and >63 µm

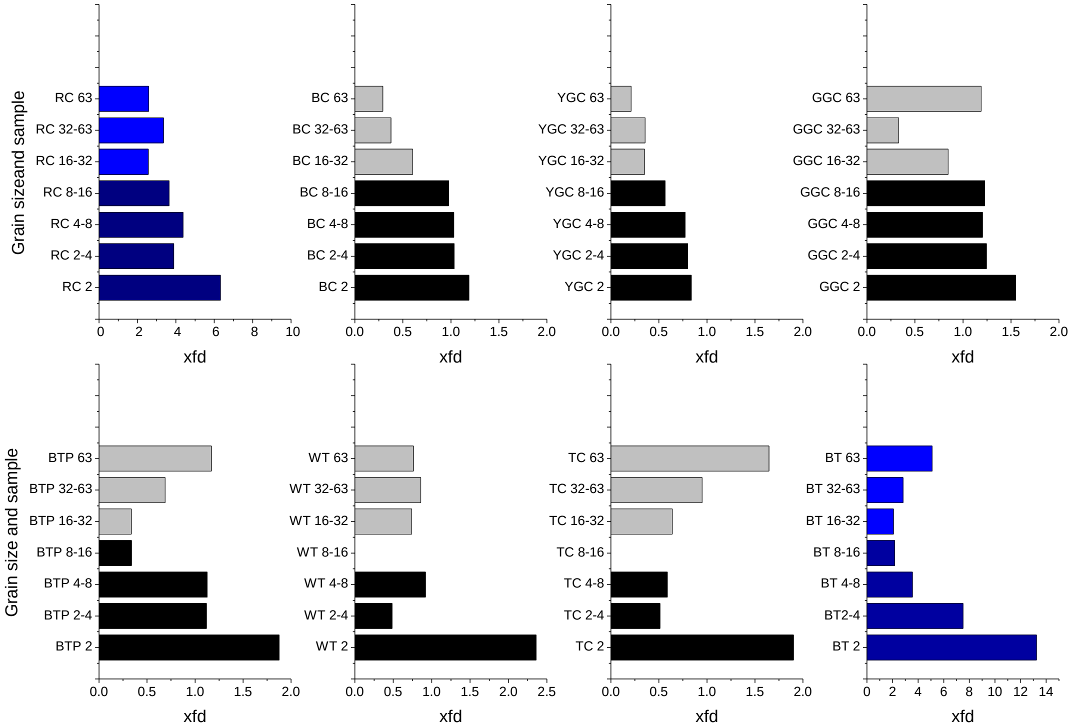

Figure 6.6 (c) X axis shows χfd measurements for each particle size fraction for the Kilombe samples Samples on the Y axis represent lithostratigraphic units 1- 8 (rc, red claystone, bc, brown claystone, ygc, yellow grey claystone, ggc, grey claystone, pal, palaeosol, wt, white tuff, tc, tuffaceous claystone, bt, beige tuff. Each particle size fraction for each lithostratigraphic unit is also displayed <2 µm. 2-4 µm, 4-8 µm, 8-16 µm, 16-32 µm, 32-63 µm and >63 µm

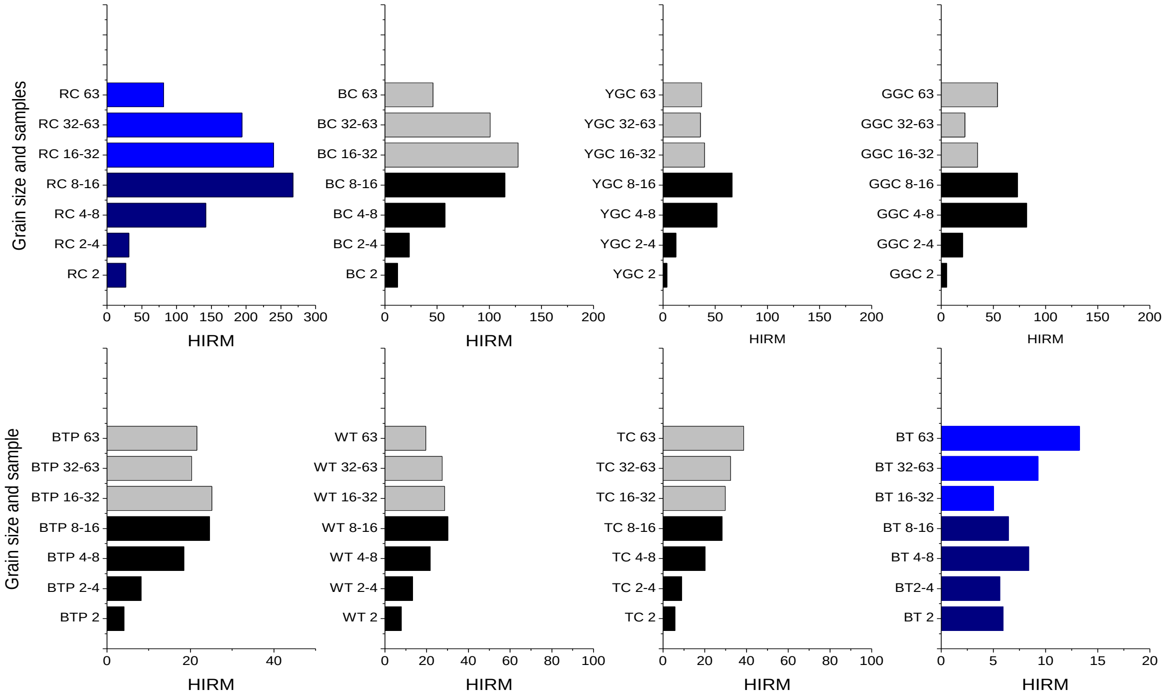

Figure 6.6 (d) X axis shows HIRM measurements for each particle size fraction for the Kilombe samples Samples on the Y axis represent lithostratigraphic units 1- 8 (rc, red claystone, bc, brown claystone, ygc, yellow grey claystone, ggc, grey claystone, pal, palaeosol, wt, white tuff, tc, tuffaceous claystone, bt, beige tuff. Each particle size fraction for each lithostratigraphic unit is also displayed <2 µm. 2-4 µm, 4-8 µm, 8-16 µm, 16-32 µm, 32-63 µm and >63 µm

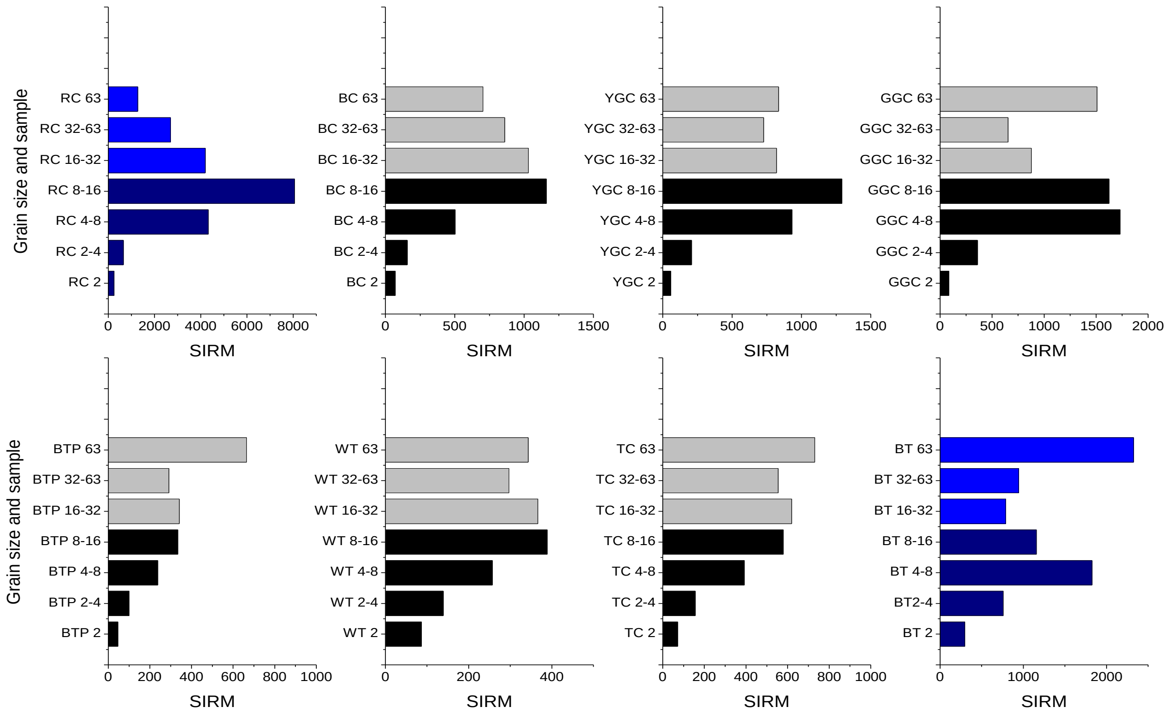

Figure 6.6 (e) X axis shows SIRM measurements for each particle size fraction for the Kilombe samples. Samples on the Y axis represent lithostratigraphic units 1- 8 (rc, red claystone, bc, brown claystone, ygc, yellow grey claystone, ggc, grey claystone, pal, palaeosol, wt, white tuff, tc, tuffaceous claystone, bt, beige tuff. Each particle size fraction for each lithostratigraphic unit is also displayed <2 µm. 2-4 µm, 4-8 µm, 8-16 µm, 16-32 µm, 32-63 µm and >63 µm

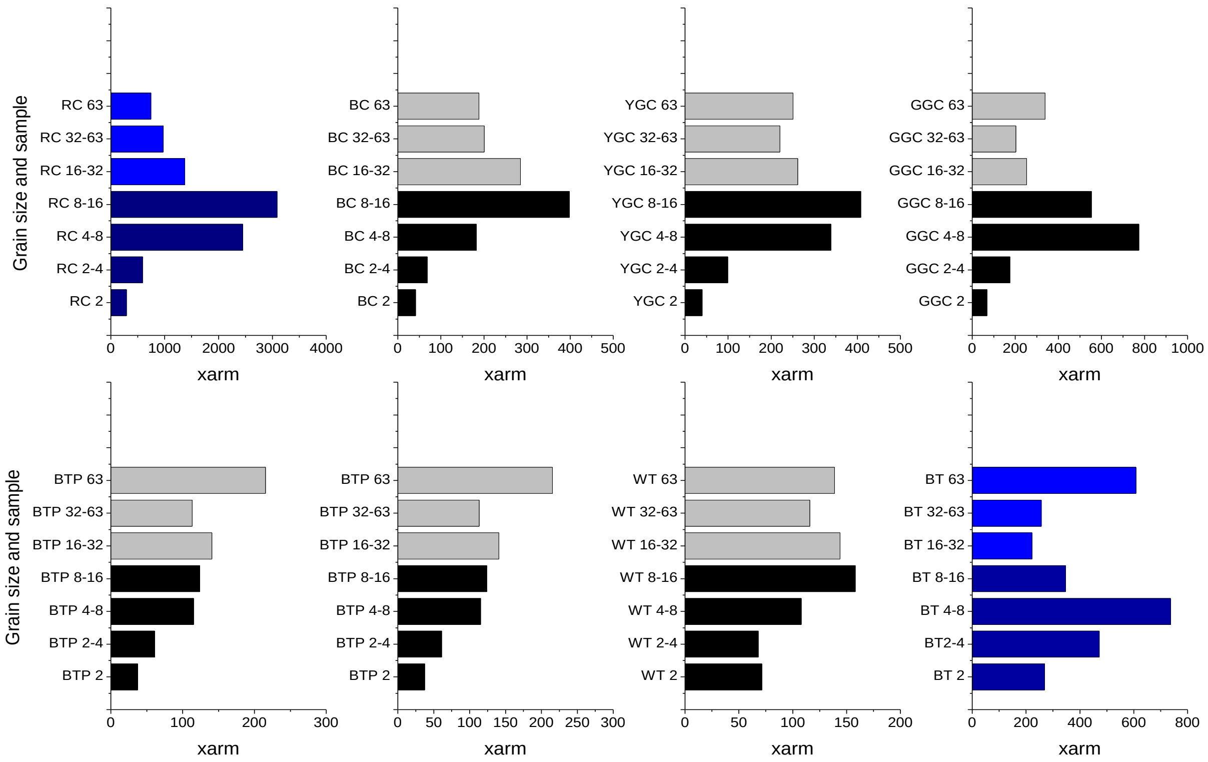

Figure 6.6 (f) X axis shows χarm measurements for each particle size fraction for the Kilombe samples. Samples on the Y axis represent lithostratigraphic units 1- 8 (rc, red claystone, bc, brown claystone, ygc, yellow grey claystone, ggc, grey claystone, pal, palaeosol, wt, white tuff, tc, tuffaceous claystone, bt, beige tuff. Each particle size fraction for each lithostratigraphic unit is also displayed <2 µm. 2-4 µm, 4-8 µm, 8-16 µm, 16-32 µm, 32-63 µm and >63 µm

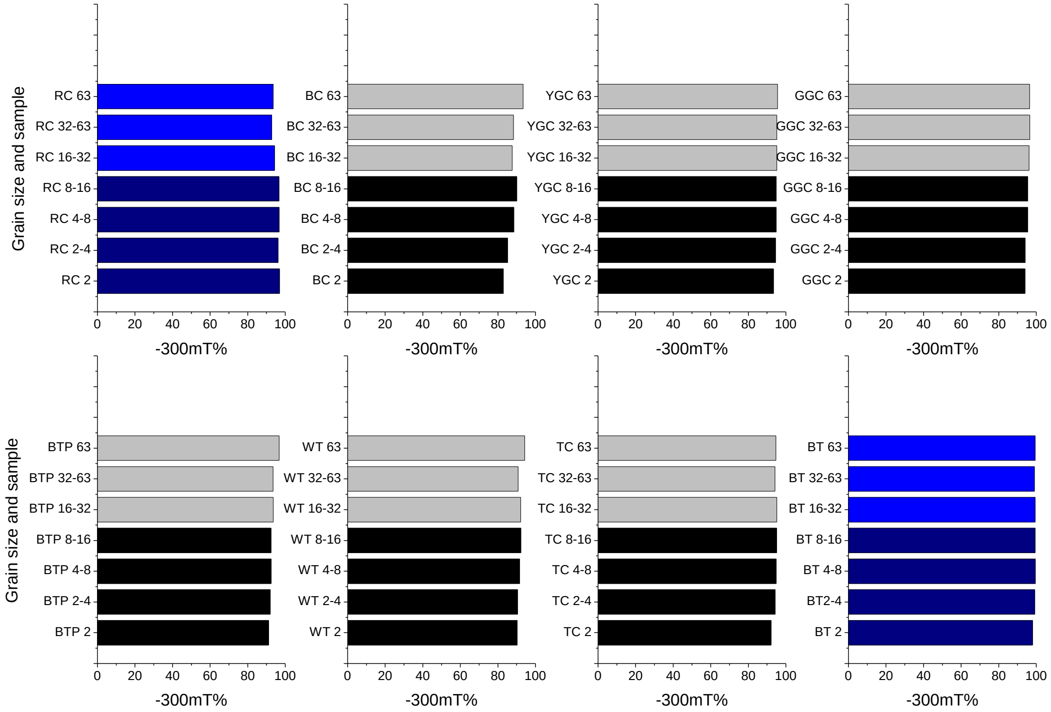

Figure 6.6 (g) X axis shows -300mT measurements for each particle size fraction for the Kilombe samples. Samples on the Y axis represent lithostratigraphic units 1- 8 (rc, red claystone, bc, brown claystone, ygc, yellow grey claystone, ggc, grey claystone, pal, palaeosol, wt, white tuff, tc, tuffaceous claystone, bt, beige tuff. Each particle size fraction for each lithostratigraphic unit is also displayed <2 µm. 2-4 µm, 4-8 µm, 8-16 µm, 16-32 µm, 32-63 µm and >63 µm

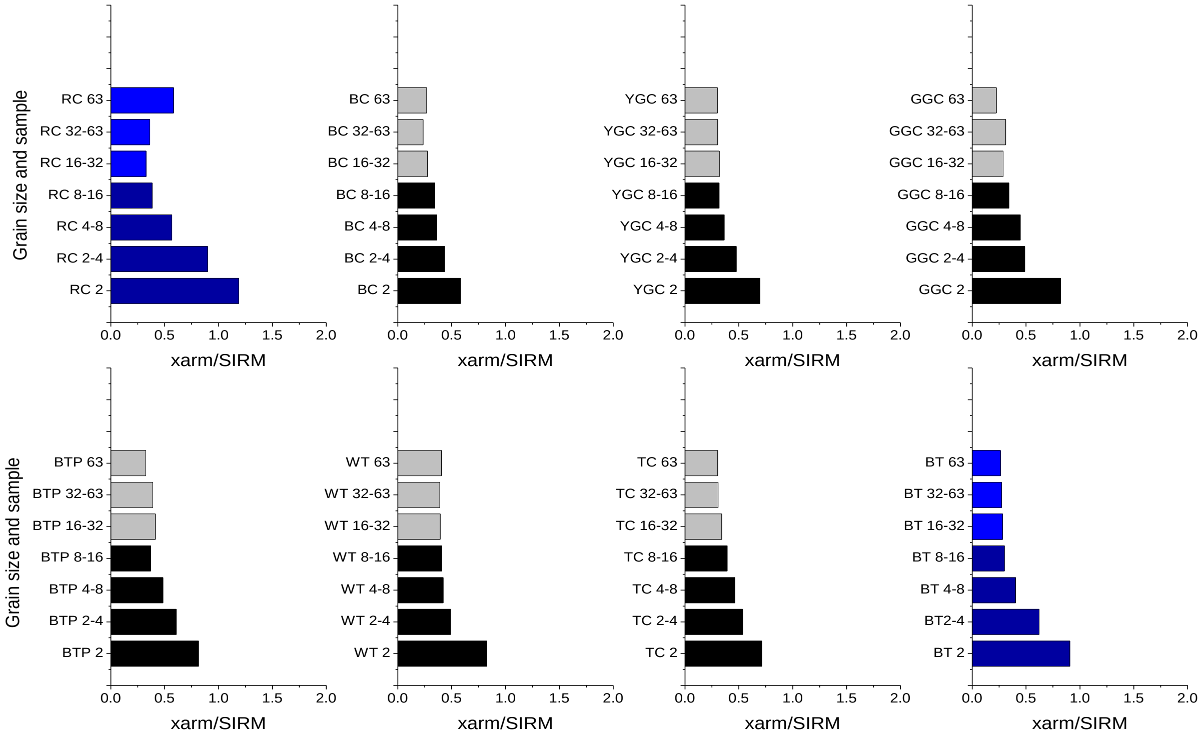

Figure 6.6 (h) X axis shows xarm/SIRM measurements for each particle size fraction for the Kilombe samples. Samples on the Y axis represent lithostratigraphic units 1- 8 (rc, red claystone, bc, brown claystone, ygc, yellow grey claystone, ggc, grey claystone, pal, palaeosol, wt, white tuff, tc, tuffaceous claystone, bt, beige tuff. Each particle size fraction for each lithostratigraphic unit is also displayed <2 µm. 2-4 µm, 4-8 µm, 8-16 µm, 16-32 µm, 32-63 µm and >63 µm

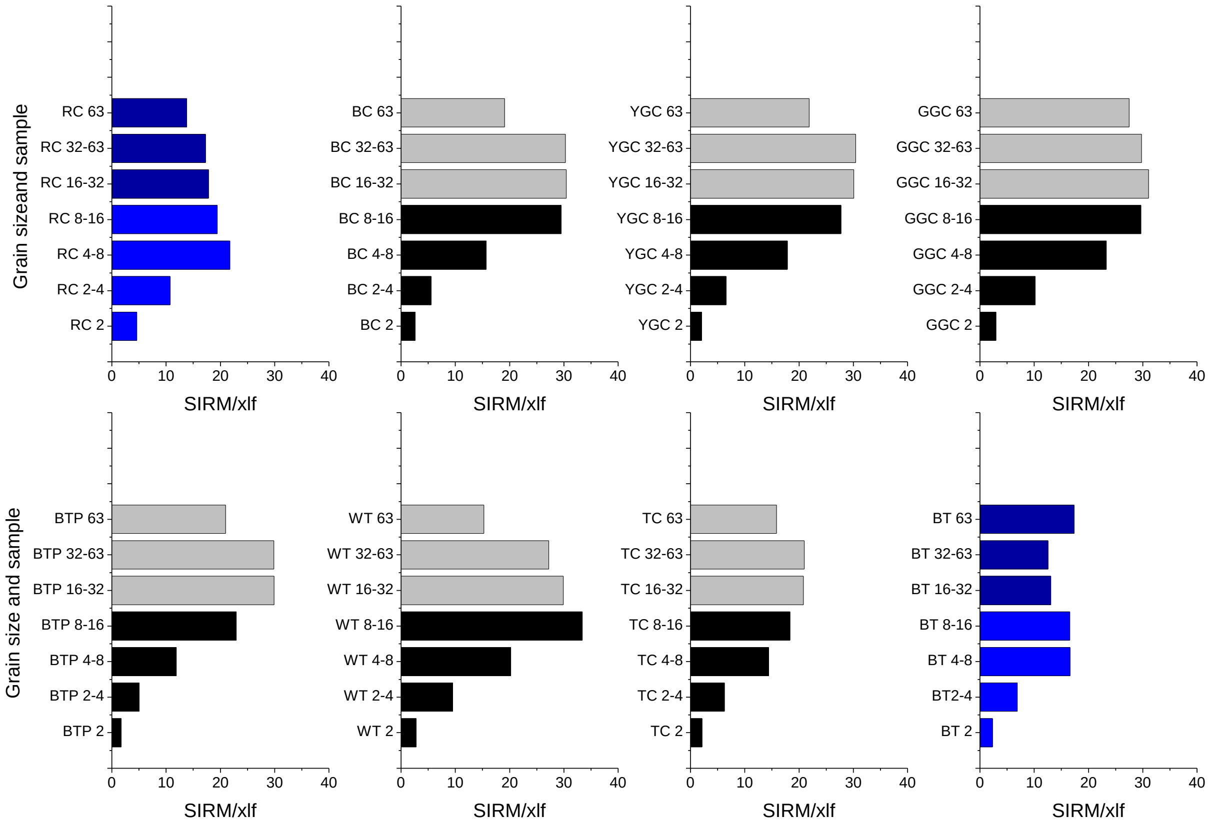

Figure 6.6 (i) X axis shows SIRM/χlf measurements for each particle size fraction for the Kilombe samples. Samples on the Y axis represent lithostratigraphic units 1- 8 (rc, red claystone, bc, brown claystone, ygc, yellow grey claystone, ggc, grey claystone, pal, palaeosol, wt, white tuff, tc, tuffaceous claystone, bt, beige tuff. Each particle size fraction for each lithostratigraphic unit is also displayed <2 µm. 2-4 µm, 4-8 µm, 8-16 µm, 16-32 µm, 32-63 µm and >63 µm

6.6.4 Particle-size specific mineral magnetic measurements

Figure 6.6 a – i, presents the results of the magnetic measurements for the seven particle size fractions, ranging from < 2 µm to > 63 µm (clay to coarse sand) for the sediment and soil samples at Kilombe. For each sample, the results are shown on a mass-specific basis and for a range of both concentration and grain size dependent parameters.

Figure 6.6 b shows that MS, or χ_{LF}, values are quite irregularly distributed across the samples. Four samples have peaks in the very fine silt and/or fine silt fractions (samples 1- 4) and four samples (5-8) have bimodal peaks in both the clay grade and sand fractions. MS values are much lower for each particle size fraction in the samples suggested to be affected by dissolution. The values of concentration dependent parameters HIRM, SIRM and χ_{ARM} are also quite irregularly distributed across the samples (Figure 6.6 d, e and f).

Figure 6.6 g shows that values for mineralogy-dependent parameter S ratio (IRM reverse % -300mT) are much lower in samples 2-7 and decrease towards the finer grain sizes with minimum values occurring the <2 µm and 2-4 µm) particle size fractions. Exceptions to this are samples RC1 and BT8.

Figures 6.6 c and h show that the indicators of fine magnetic grain size, χ_{FD} and χ_{ARM}/SIRM, decrease systematically with increasing grain size; however, some samples show a further increase in χ_{FD} across the >63 fraction. Values for χ_{FD} are much lower in the samples affected by dissolution.

Figure 6.6 i shows that values of SIRM/χ_{LF} are at their lowest across the < 2 and 2-4 µm fractions for all samples, and then increase as particle size increases (although peaks vary across the > 4-8 µm and above across all the samples). The two samples unaffected by dissolution have maximum SIRM/χ_{LF} values of < 22, while all the samples affected by dissolution, apart from wt7, exhibit maximum values > 30. In general the highest values occur in the coarser particle size fractions; however, three samples have SIRM/χ_{LF} values >30 in the fine silt fractions (BC2, GGC3 and WT7).

6.6.5 Magnetite reduction

Post-depositional changes to magnetic mineral assemblages can occur through dissolution, which is a diagenetic process characterised by the early loss of the finest magnetic fractions before loss of coarser grains (King & Channel, 1991). It has been generally assumed that the main process involved is the chemical reduction of magnetite, and this process has been clearly demonstrated in both marine and freshwater environments e.g. (Karlin, 1990; Snowball &Thompson, 1988). Robinson *et al.,* (2000) further suggested that due to their much larger surface area magnetite reduction generally affects fine grain sizes. An indication of magnetite reduction is shown to occur in all of the samples affected by dissolution at Kilombe. S-ratio values are not only much lower in these samples (although values would still indicate predominantly magnetite) but they decrease systematically as particle size decreases, demonstrating the greatest reduction in values across the clay grade and very fine silt fractions.

6.6.6 The loss of the fine grained ferrimagnetic component

A mineral magnetic assemblage consisting of a detrital component can often be an indicator of changing environmental conditions (Turner, 1997). However, if sediments have been shown to initially contain quantities of ultra-fine grained ferrimagnetic minerals and that these minerals are lost during the process of dissolution, then it cannot be considered that the remaining magnetic signal is of a detrital origin along with its associated environmental conditions. Numerous studies have shown that frequency-dependent magnetic susceptibility, χ_{FD} values, can be used to reflect the presence of magnetic grains close to the SP and SD boundary and, that this parameter can be used to indicate pedogenic processes via the formation of secondary fine-grained ferrimagnetic oxides (Hao *et al.*, 2008; Maher *et al.*, 2003). The Kilombe data clearly shows that χ_{FD} values are consistently higher in the < 2 µm fraction than any other particle size fractions across all samples. However, extremely low values of observed χ_{FD} <2 µm for all the samples affected by dissolution. This suggests that pedogenic material is largely absent from both the fine and coarse particle size fractions in all these particular samples. Values of χ_{ARM}/SIRM can also be used to indicate fine ferrimagnetic grain sizes in the SD range. At Kilombe although values are shown to decrease as grain size increases, similar to the trend observed in χ_{FD}, values are not significantly lower than those observed in the samples unaffected by dissolution. This may suggest that dissolution can be characterised by the primary loss of ultrafine SP materials prior to loss of fine grained ferrimagnets in the SD range. In addition, the HIRM values exhibit peaks in the coarser particle size fractions suggesting that the imperfect antiferromagnetic component is of detrital rather than pedogenic origin.

Figures 6.7 b and g shows results for χ_{FD} and χ_{ARM}/SIRM for all the samples. Although the overall trend in most samples is a decrease in values as particle size increases, a number of samples deviate from this pattern. Samples GGC4, BTP5, TC7 and BT8 all exhibit peaks in χ_{FD} values in the >63 µm fractions whilst samples RC1, BC2 and WT6 show an increase in χ_{ARM}/SIRM in the >63 µm fractions. Several explanations may account for this phenomenon. One explanation is the occurrence of undispersed aggregates in the coarser grades (Zheng *et al.*, 1991). However, this is unlikely as all samples were ultrasonically dispersed and then shaken for 24 hours in an automatic shaker. However, small amounts of fine-grained magnetic particles can adhere to coarser grades during separations. Lyons *et al.,* (2010) suggest that coatings on sand grains could include secondary magnetic minerals, either formed in situ or prior to transport and deposition. A third explanation is that fine grained magnetic particles have been shown to frequently occur as inclusions in larger particles derived from igneous materials (Hounslow & Maher, 1996).

6.6.7 Sediment accumulation rates

The ferrimagnetic iron sulphide greigite (Fe_3S_4) has been shown to be produced in the presence of organic matter and sulphates, as an intermediate product during the dissolution of magnetite (Snowball, 1993, Robert and Turner, 1993) and with pyrite occurring as the end product in reducing environments. It has also been argued that with a limited supply of organic matter then an intermediate composition, i.e. greigite, would be formed (Snowball and Thompson, 1988). The formation of greigite from detrital minerals, after burial under a redox front, leads to conditions in which magnetite is dissolved first and then hematite of detrital origin remains the dominant magnetic mineral (Demory *et al.*, 2005). This process has been shown to occur when sedimentation rates are low and when also the residence time of magnetite at the redox boundary is longer. However, when sedimentation rates are constant and burial is fast magnetite can either be preserved or transformed into greigite when conditions leading to sulphate reduction occur (Demory *et al.*, 2005).

Values of SIRM/χ_{LF} of around or greater than 30 can be used to indicate the presence of greigite in samples (Scoullos *et al.*, 2014). At Kilombe, values of SIRM/χ_{LF} > 30 occur only in samples affected by dissolution. Most of the peak values occur across the coarser particle size fractions, medium silt and above, suggesting that during dissolution greigite forms firstly from the detrital coarse grained component. Three samples GGC4, WT7 and BC2 have SIRM/χ_{LF} values of around 30 indicating a predominance of greigite in the fine silt (8-16 µm) particle size fraction. These values can be used to suggest the progressive formation of greigite occurring towards the finer fractions in these specific samples. LOI values are lower in the units affected by dissolution (Chapter 4, table 4.1); however, values are still around 4% - high enough to indicate the presence of organic matter in these units. At Kilombe it is likely that changes in sedimentation accumulation rates leading to rapid burial conditions have resulted in a reducing environment and subsequent loss of the fine-grained ferrimagnetic component and formation of greigite as an intermediate stage of dissolution across units 2-6.

6.6.8 Summary of the results of particle-size specific magnetic properties

Measuring the magnetic properties of particle size fractions produces much more detailed information on the contribution of the magnetic properties of the different particle size fractions to the magnetic signal of bulk sediment samples than can be obtained by bulk measurements alone. All of the indicators of fine magnetic grain size, χ_{FD} and χ_{ARM}/SIRM, exhibit a clear peak in the < 2 µm fraction, the clay grade, suggesting the dominance of ultrafine ferrimagnetic grains. However, values of χ_{FD} are much lower in samples affected by dissolution, suggesting the removal of this component. The effects of diagenetic dissolution on the magnetic properties of sediment/soil samples is a major biasing factor in terms of paleoclimate reconstruction, and the impact of particle size selective dissolution on the magnetic properties/characteristic of the Kilombe samples is clearly evident in terms of the reduction of magnetite, loss of the SP component and formation of greigite. However, the separation of samples into seven grain size fractions has enabled further information to be gained in terms of the potential effects changes in sediment accumulation rates on the magnetic signal at Kilombe.

6.7 Paleoclimate signal

The influence of changes in lithology, volcanic activity, and dissolution on the magnetic properties at Kilombe complicates interpretation of the data set in terms of reconstructing climatic changes. However, χ_{FD}% and χ_{ARM}/χ_{FD} are two parameters/ratios shown to transcend the boundaries of the individual lithological units in this record, suggesting that they may be potentially be useful for evaluating long-term climatic changes. As proxies for paleoclimate/palaeoenvironmental change, values of χ_{FD}% often provide an indication for the proportion of ultrafine ferrimagnetic grains (magnetite/maghemite) in a sample which lie at or near to the SP boundary and are known to form during chemical weathering and pedogenesis (Hao *et al.*, 2008). The interparametric ratio χ_{ARM}/χ_{FD} provides an indication in the concentration of fine ferrimagnetic grains in the SD range versus fine ferrimagnetic grains between the SD and SP range with variations in this ratio providing information in changes on the relative proportion of both (see table 6.1).

6.7.1 Results χ_{FD}% and χ_{ARM}/χ_{FD}

The results of both PCA and the Pearson's correlation matrix show that both χ_{FD}% and χ_{ARM}/χ_{FD} are strongly but negatively correlated with one another. In terms of their relationship with MS both parameters show a weak to non-existent correlation (χ_{FD}%, r= 0.28 and χ_{ARM}/χ_{FD}, r=-0.17). Figure 6.3 depicts trends in the magnetic data set to depth for the Kilombe sequence. It is evident that the variation of χ_{FD}% and χ_{ARM}/χ_{FD} are dissimilar to any of the other magnetic parameters or interparametric ratios suggesting a unique response in these parameters compared to the others.

6.7.1 Long-term trends in χ_{FD}% and χ_{ARM}/χ_{FD}

For the entire Kilombe sequence values of χ_{FD}% range between 0.69 and 12% with a mean of 5% (SD 2.9) whilst χ_{ARM}/χ_{FD} values range between 25 and 480 with a mean of 125 (SD 82). The strong but negative statistical correlation of both parameters suggest that both are linked to the pedogenic formation and increase of ultrafine SP magnetite/maghemite in this sequence. As the ratio of χ_{ARM}/χ_{FD} decreases, the relative proportion of SP ferrimagnetic grains increases relative to ferrimagnetic SD grains. However, as Figure 6.3 indicates, both parameters exhibit significantly different depth trends. The ratio of χ_{ARM}/χ_{FD} exhibits a gradual decline throughout the record with little variability noted up section. This ratio also appears to be unaffected by burial diagenesis in the units affected by dissolution on the main site. In terms of long-term trends χ_{FD} % shows a unique response to other parameters and appears almost cyclical. It exhibits a long-term trend towards increasing values up-section, with significant short-term variability. However, it must be considered that much of this variability may be related to lithological change. The cyclical character of χ_{FD}% is lost across units 2-7. Similar to the results of the chemical weathering indices the magnetic data shows a long-term trend towards increased values which may indicate a response to increased levels of precipitation and/or warmer temperatures.

6.7.2 Possible climatic significance of χ_{FD}% at Kilombe

The magnetic parameter of χ_{FD}% has been widely utilised to determine the proportion of SP material in a sample and to further determine the relationship between pedogenic intensity and rainfall/palaeorainfall (Balsam *et al.*, 2011). In soils and palaeosols values of χ_{FD}% that range between 5 and 8% can be used to indicate the presence of significant levels of SP magnetite and/or maghemite formed via pedogenic processes (Liu *et al.*, 2007). Also of particular relevance here are the following studies (Vidic *et al.*, 2004; Stinchcomb & Peppe, 2014) which clearly document the added influence of time and duration of weathering/residence times on the magnetic enhancement of soils and sediments. These papers and their implications for the Kilombe data set will be further discussed in chapter 7.

At Kilombe, average χ_{FD}% values of > 5%, and the biplot of (Oldfield, 1994), indicate significant quantities of ultrafine ferrimagnetic minerals formed by pedogenic processes. The climate at Kilombe is controlled by the East African monsoon systems and is characterised by seasonal wet-dry cycles which would be expected to result in enhanced pedogenesis. Modern mean annual rainfall is 917 mm which would favour the formation rather than reduction of SP magnetite/maghemite via pedogenic processes leading to magnetic enhancement (Balsam *et al.*, 2011). However, as most of the sediments at Kilombe are derived, any contribution to χfd% values may also include the signal from weathering at the source rock, during transportation and/or post-depositional. At Kilombe, similar to the trends observed in the geochemical record, the overall trend is for increasing values of χ_{FD}% throughout the record. As a proxy for rainfall and/or temperature, increased values of χ_{FD}% would generally relate to increased rainfall and/or temperatures. The upper part of the Kilombe sequence yields χ_{FD}% values of 7.5 which would indicate intense pedogenesis under increased rainfall. However, conclusions must be drawn similar to those outlined in the previous chapter that magnetic enhancement in this record may be the result of long exposure times and duration of chemical weathering intensity due to lower sedimentation rates. These trends will be further examined in Chapter 7.

6.8 Conclusions

The following conclusions can be made based on the changing magnetic properties of the Kilombe sediment/soil and volcanic samples:

- The main changes in the magnetic data set are controlled by changes in lithology.
- The magnetic mineralogy is predominantly magnetically “soft” magnetite and/or maghaemite, although magnetically “hard” minerals like hematite and/or goethite appear to contribute up to 50% towards the mineralogy and more in some units especially units 2 – 6. Iron sulphides, specifically greigite contribute to the signal in units 2-6 and some values of SIRM/χ_{LF} on FHC are close to 20 indicating coarse SD.
- A variety of magnetic grain sizes are present in most units/samples ranging from ultrafine ferrimagnetic grains to coarse MD of detrital origin.
- The proportion of pedogenic ultrafine magnetite increases as perhaps part of a long-term trend as evidenced by χ_{FD}% and χ_{ARM}/χ_{FD} values.
- Some of the volcanic samples also yield a signal similar to that produced by pedogenic processes and fall within the range of pedogenically-enhanced Asian and European soils. Some of the “pedogenic signal” in these sediments may represent a response to a variety of processes including duration of weathering, climate and volcanic activity i.e. fine grained ferrimagnetic component produced during eruptions.
- The results of particle-size separation shows that the fine grained ferrimagnetic component has been lost via burial diagenesis under conditions of increased/ rapid sediment accumulation rates in units 2-6 which shows that these sediments/soils are not of a detrital origin.

The use of the biplot of Oldfield (1994) permits further distinction of the units at Kilombe that have been subject to pedogenic processes. Most of the samples from FHC fall within or just outside the range of Asian and European soils, suggesting that most of the sequence has been subject to pedogenesis of varying degrees.

Chapter 7 A multi-proxy approach to examining palaeoenvironmental change at Kilombe

7.1 Introduction

Results presented in chapters 5 and 6 suggest that most of the observed variations present in the magnetic properties of the Kilombe soils and sediments can be attributed to changes in lithology. The magnetic data set does however provide stronger information on the neoformation of ultrafine ferrimagnetic minerals produced as a result of pedogenesis, with 48% of the Kilombe samples falling within or just outside the range attributed to European and Asian soils. The parameter χ_{FD}% and interparametric ratio of χ_{ARM}/χ_{FD} also appear to be responding to a longer-term trend suggesting that the intensity of pedogenesis is increasing throughout the record, although this increase can still not be seen as independent of lithology. Similar to the rock magnetic record it is also noted that changes in the concentration of individual major and trace elements are also being controlled primarily by changes in lithology. However, the chemical weathering indices also appear to hold further information on evaluating long-term trends of environmental change given the establishment of similar source rock, although influenced by sorting signal. The first part of this chapter will examine the limitations of context and techniques within this context. The second part will examine the suggested long-term trends of climate change within the context of other records including the East African aridification trend and then more local records. The third part will reconstruct the evolution of Quaternary environments at Kilombe using a multi-proxy approach including chronology, sediment accumulation rates, lithology, LOI%, some micromorphology and the magnetics and geochemical data. The final part of the chapter will then situate both the long-term trends of climate change and the more localised environmental record at Kilombe in the context of the wider Acheulean ca. 1 Ma.

7.2 Limitations of context and techniques

As the sedimentary record at Kilombe for the most part is derived and records extensive volcanic activity, the context for environmental reconstruction can be considered to be quite limited in terms of both the complexity of the sequence and the response of the techniques to a variety of environmental processes in bulk sediment samples. Organic proxies such as pollen and pedogenic carbonates are not preserved at Kilombe, necessitating the use of geological proxies. Phytoliths are also not preserved in any of the sediments at Kilombe main site but they are very well preserved and are abundant in sediments from FHC (Lem, 2014, pers comm), and will be further investigated as a future direction which will be discussed in Chapter 8

As discussed in previous chapters, the bulk sediment signal at Kilombe will contain information on weathering at source rock, during transportation and also post-depositional alteration i.e. in situ chemical weathering and pedogenesis. It is not possible to separate any of these factors when investigating chemical weathering intensity using chemical weathering indices on bulk samples. Although similar source rock for the Kilombe soils and sediments has been demonstrated validating use of chemical weathering indices for intermediate rocks, there is still most likely a strong influence of changes in lithology on the indices as well, although not overly apparent. Sorting signal has also been shown to influence the CIA index through comparison with Zr/Rb ratio.

In terms of the rock magnetic record, there are a number of complications. Where the deposition of primary airfall tuffs can be identified in the record (3BT and ashflow tuff, perhaps also lower FHC) these can cause underlying sediments to be re-heated via a process of low temperature oxidation and thus either re-magnetised or altered from their existing state therefore overprinting the initial magnetic signal (Geissman, 1988). In terms of derived sediments, as already discussed above, any signal may include pedogenic enhancement at source, during transport and post-depositional. Overprint can occur in both high and low-coercivity minerals. However, overprints are generally held in the ferrimagnetic minerals as these are both the easiest to remagnetise and, first to form during pedogenic activity occurring post-depositionally (Acton, 2007; Schmidt, 1993). It may be therefore, that the rock magnetic record at times can provide more information on localised conditions of pedogenic activity in terms of post-depositional alteration, both pedogenically and via heating and cooling of volcanic tuffs at Kilombe. This suggestion will be further considered during this chapter. To be considered also is that the signal is lost from both data sets through dissolution in the lower part of the record and across the main artefact horizon. A further complication is added in that both techniques are heavily influenced by exposure times to pedogenesis and chemical weathering intensity with rates of erosion and sediment accumulation providing a strong control on reduced or enhanced weathering. Any interpretation must therefore, take this and all other the above factors into account.

7.3 A multi-proxy approach

7.3.1 Soil forming factors of Jenny (1941)

The model of soil formation and transportation along with the new stratigraphic column and age models were discussed and presented in Chapter Four. It is now necessary to come back to these factors, and the age model, sedimentary log and model of relief/transportation which are presented together in Chapter Four. The implications of the new age determinations are now discussed below.

7.3.2 Examining the evolution of Quaternary environments at Kilombe

7.3.2.1 Geological evolution

The general geological evolution of the Kilombe area during the Quaternary has been provided by Jones (1979), Jennings (1971) and Bishop (1978). New age determinations via $^{40}Ar/^{39}Ar$ dating now provide further information in terms of two of the major eruptions from Kilombe. We now know that the trachyte and trachyphonolite lava flows were not contemporaneous with one another having been re-dated to 2.4 and 1.57 Ma respectively and, that the later date of 1.57 Ma now yielded for the trachyphonolite flow means that it is broadly contemporaneous with the 1.57 Ma eruption at the Kapthurin Formation (Deino & McBrearty, 2002). This now points to significant volcanic activity in this part of the Central Rift during this time frame.

The combined ages yielded through both palaeomagnetic and $^{40}Ar/^{39}Ar$ dating, as shown in Figure 4.8 a and b, allow further age constraint to be placed on the deposition of the first sediments at Kilombe, the basal yellowish red claystone, on the main site. It appears, that there is a substantial time gap of approximately 500,000 years between the eruption from Kilombe volcano and the deposition of the first recorded sediments. There are two possible explanations for this. Either there was a long period where no sedimentation occurred in this part of the basin, or that repeated phases of erosion have removed any sediments preceding the deposition of the basal claystones. In terms of the wider area around Kilombe extensive mapping has taken place geologically and since 2008 in terms of the new field research and no sediments or potential erosional surfaces have, as yet, been identified.

Periods of low or no sedimentation have been shown to occur as a result of extensive volcanic activity and faulting and it is suggested here that the repeated episodes of volcanic activity at 1.57 Ma may have resulted in a prolonged period at Kilombe where no sedimentation has taken place. This is however speculative and would need further investigation. A $^{40}Ar/^{39}Ar$ age of 1.03 Ma is now determined for the 3BT which has been previously suggested to represent an early eruption from proto Menengai. The ashflow tuff capping the sedimentary sequence is now determined to be 487 Ka which refines previous suggestions that by Jones (1975) that this represents an eruption from Menengai at 350,000 Ka. Further age determinations have been yielded by palaeomagnetic dating (Ashton, 2013; Davies, 2011) which allow significant refinements of the $^{40}Ar/^{39}Ar$ model, with three reversals recorded, Jaramillo, Santa Rosa and Brunhes-Matuyama. These new age determinations now enable the placement of the sedimentary sequence into a secure chronological framework within which to examine both the long-term trends of climate change within the sequence and the evolution of more localised environments at Kilombe main site and FHC.

7.4 Long-term trends of palaeoclimate change at Kilombe

One of the major features originally noted in both the rock magnetic record and record of chemical weathering intensity was what appeared to be an up-section trend towards an increase in both chemical weathering and pedogenic intensity during the Quaternary. The idea of an increase in chemical weathering intensity over time, suggested in Chapter 5, can no longer be supported at Kilombe. In Chapter 6, sections 6.6.4 – 6.6.8 post-depositional alteration has been shown to have effected samples by removal of the fine-grained ferrimagnetic component know to form during pedogenesis and by leaving a geochemical signature similar to unweathered detritus. This sudden and pronounced reduction in the major elements used in the chemical weathering indices in Chapter 5 had resulted in a biasing effect that appeared to show an increase in chemical weathering intensity. Figure 7.1 a shows that after removal of the units effected by post-depositional alteration the trend here is towards a reduction in chemical weathering intensity, with significant fluctuations, which are now evident in all three chemical weathering indices, although more pronounced in the CIA and CaO/Al. LOI % also shows an overall decline throughout the record, with substantial variability noted in the centre suggesting a decline in organic matter content of the sediments over time. Figure 7.1 b shows that in terms of the rock magnetic record, even after removal of units 2-6, there is still a strong trend towards increasing pedogenic intensity up-section. The differences observed here may reflect the differential response of both techniques to a variety of environmental processes including climate (temperature and/or rainfall), rates of erosion/time and pedogenic overprinting.

CIA values fall within a wide range for the Kilombe sequence, even after removal of the values for the affected units, and conditions in chemical weathering intensity are shown to range from incipient through to intense. CIA values for basal yellowish red claystone fall within a wide range (70 – 92) with an average of 82. Most of the values are however > 80 in this unit which would represent increased chemical weathering intensity under either conditions of increased precipitation and/or warmer temperatures or decreased rates of erosion and long exposure times. The upper part of the Kilombe sequence, also derived, corresponding to the pink and orange brown earthy tuffs yield much lower CIA values of 75 (range 59-82) with values decreasing up-section and representing moderate chemical weathering intensity.

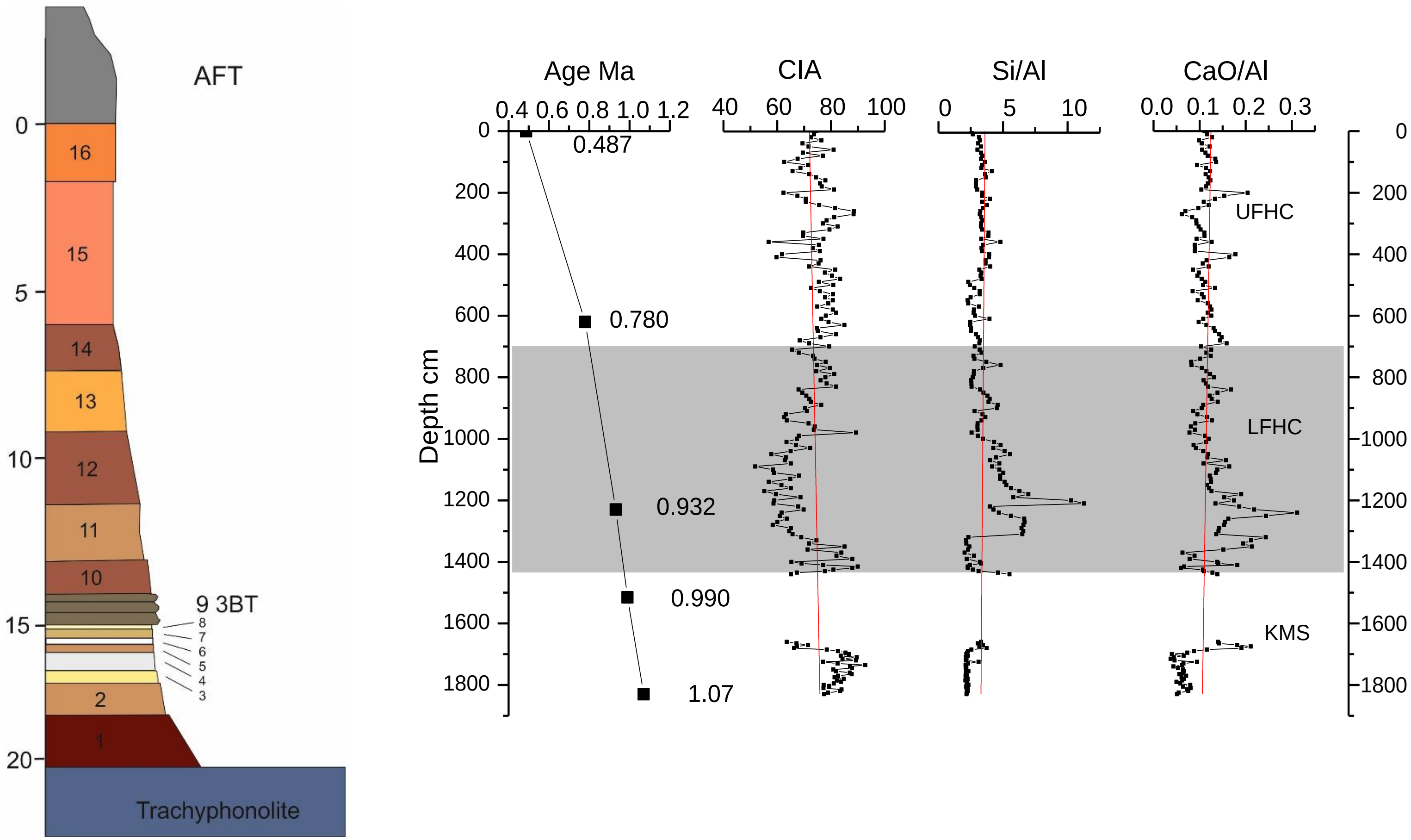

Figure 7.1 a Chemical weathering indices and age depth model for the Kilombe sedimentary sequence. The sequence is divided into three sections Kilombe Main Site (KMS), and Farmhouse Cliff, upper and lower (LFHC, UPFHC).

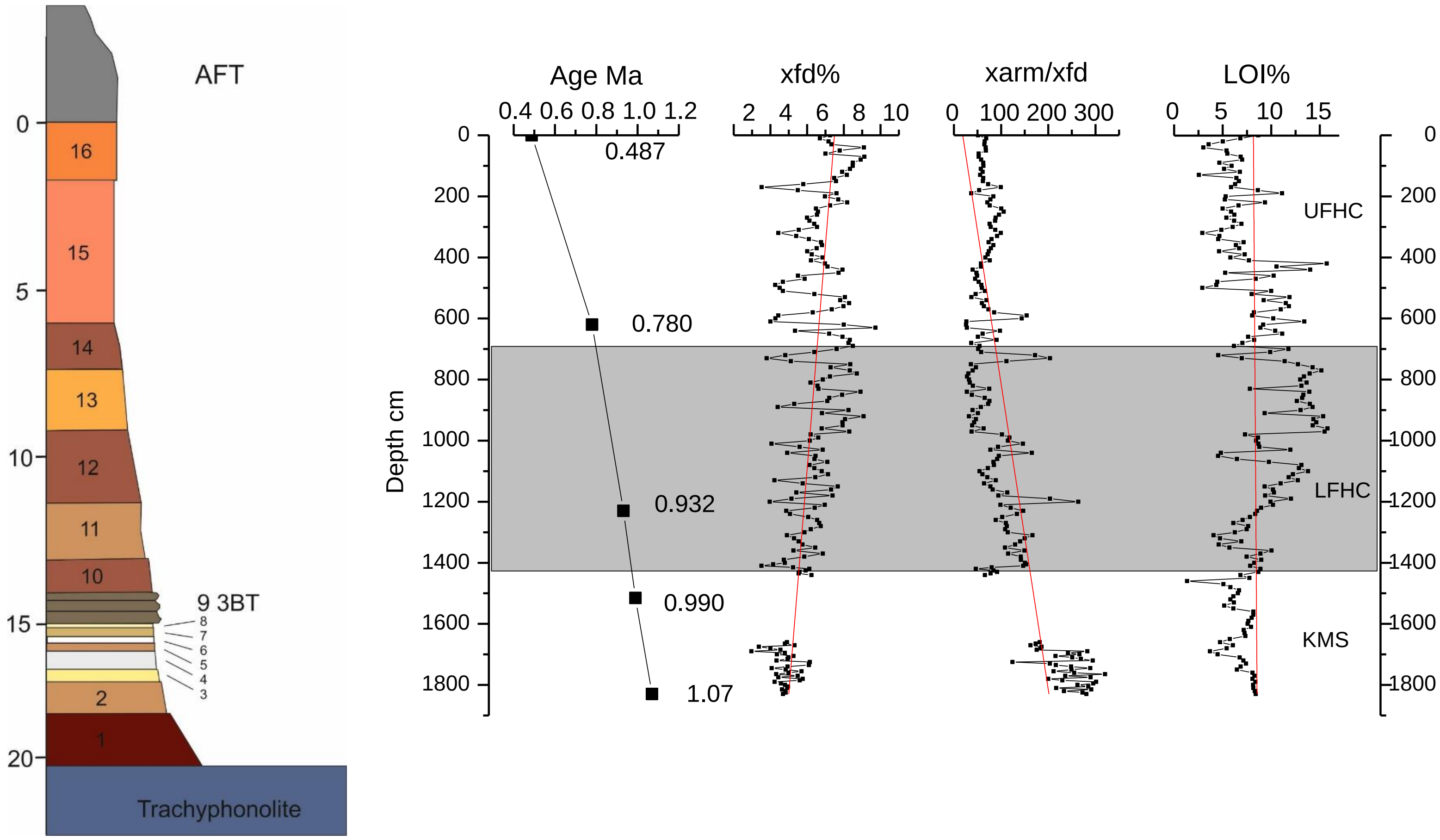

Figure 7.1 a Loss-on-ignition, $\chi_{FD\%}$ and χ_{FD}/χ_{ARM} and age depth model for the Kilombe sedimentary sequence. The sequence is divided into three sections Kilombe Main Site (KMS), and Farmhouse Cliff, upper and lower (LFHC, UPFHC).

In terms of the lower and upper sections of the Kilombe sequence χ_{FD}% and χ_{ARM}/χ_{FD} show almost the opposite trend. Values of χ_{FD}% in particular are low and also show quite a narrow range in the yellowish red claystone (4.8 and 2.9-6%). In the upper two units of FHC χ_{FD}% values average 7.3 (range 6-9). Values also increase up section in the upper sediments. An increase in magnetic enhancement through pedogenesis would generally indicate increased rainfall and/or warmer temperatures, a similar response to chemical weathering indices. However, both parameters clearly show a unique response in this record in the lower and upper sections when compared to the geochemical record. The observed differences in these trends will now be examined in the context of external climate records and sediment accumulation rates at Kilombe from the age depth model.

7.4.1 Palaeoclimate studies East African Rift System

On a regional scale, marine core records from the northwest Indian Ocean document a trend towards increasing aridity over the last 5 million years with substantial climate variability superimposed upon this trend (deMenocal, 2004; Feakins *et al.*, 2005). A general trend towards an increase in open grassland environments and reduction in forest is documented with variability noted on a more regional basis for East Africa (Trauth *et al.*, 2009; Feakins *et al.*, 2013). In terms of terrestrial and more localised records for the Rift Valley previous studies have utilised changes in fluctuations of lake-levels from a number of basins to infer past climate change with several deep lake phases noted across the East African Rift system at 2.7-2.5, 1.9-1.7 and 1.1-0.9 Ma (Bonnefille, 1995; Trauth *et al.*, 2005). The latter deep lake phase, which is also manifested at a more local level in the diatomite record of Elementeita, being coeval with the lower part of the Kilombe sequence which is 60 km to the NW. The deep-lake phase noted across the EARS and more locally at Elementeita is argued to the result of high sustained moisture phase in the Rift resulting in much wetter but highly variable phase occurring over a 200,000 year period (Trauth *et al.*, 2005; Potts, 2013). Increased levels of precipitation would favour chemical weathering intensity in the lower part of the sequence whilst decreased levels of precipitation would reduce chemical weathering intensity. However, variation between high/low moisture levels are also observed locally. The lake record at Olorgesaille however, shows a mix of high-stand and low-stand conditions between 1.1 – 0.9 (members 1 – 5) whilst Elementeita records a period of lake regression followed by a deep-lake phase (Trauth *et al.*, 2005; Owen *et al.*, 2008).

7.4.2 Sediment accumulation rates

Rates of sediment accumulation for the various deposits at Kilombe are difficult to assess and there are probably long periods of time where there is little active deposition as well as more erosional phases. Extensive evidence of soil formation to varying degrees indicates long periods of subaerial exposure when soils are forming on claystones and overprinting both primary and re-worked volcanic deposits. There is no evidence at Kilombe for any major erosional surfaces. The recognition of pedogenically altered horizons via the neoformation of ultrafine ferrimagnetic minerals can be used to provide evidence of both changes in accumulation rates and potentially the environmental conditions at the time of periods of subaerial exposure.

A very broad indication of sediment accumulation rates is provided by the age-depth model and these are shown to be highly variable at Kilombe both on the main site and FHC. The age model in Figure 4.8, whilst only being able to indicate sedimentation rates in a very broad sense, due to the number of ages available, associated error margins and the fact that sediment accumulation could have changed significantly at times and not being apparent in the age-model, shows that sediment accumulation rates were rapid, 3.93 cm/Ka, coeval with the deposition of the yellowish red claystone, whilst sediment accumulation rates are much lower, 2.1 cm/Ka, coeval with the deposition of the pink and orange brown earthy tuffs. Under a model of weathering duration an increase in sedimentation rates would be expected as a result of increased erosion due to changes in precipitation levels. In this case it most likely that increases in precipitation between 1.1-0.9 have at times resulted in increases erosion and accumulation rates at Kilombe main site and the lower part of FHC.

If sediment accumulation rates and duration of weathering were influencing changes in chemical weathering intensity then under a model of rapid accumulation a reduction rather than an increase would be expected for the basal claystones and an increase rather than reduction would be expected for the pink and orange brown earthy tuffs.

7.4.3 Pedogenesis and rates of sediment accumulation

Rates of sediment accumulation may also influence rates of post depositional weathering and pedogenic intensity in terms of duration times. As sediment accumulation rates are suggested to be rapid during the deposition of the basal yellowish red claystone this would potentially reduce the time for post-depositional alteration in terms of pedogenic overprinting and soil formation. The response observed in the rock magnetic data set clearly shows that pedogenic intensity was weak during the deposition of this unit, although the unit is altered to varying degrees. Further support comes from the micromorphology which also suggests evidence for weak pedogenesis in this unit. Sediment accumulation rates are significantly lower in the upper sections of the sequence coeval with the deposition of the pink and orange brown earthy tuffs, and the magnetic proxies for pedogenic intensity are shown to increase substantially within these units with most of the samples being comparative with values for Asian and European soils. As pedogenic overprinting generally effects the low coercivity minerals first, it is suggested here that the differences observed between the rock magnetic and geochemical records, for these parts of the record, are partly reflecting a stronger response to pedogenic overprinting, with magnetic enhancement and reduction controlled by duration of weathering, whilst the geochemical record is more strongly responding to precipitation and/or temperature, although rates of erosion may also still be a determining factor and will be discussed later on in this chapter.

The strongest correlation between external climate records in terms of precipitation, both locally and more regionally, and proxies at Kilombe appears to be with the chemical weathering indices rather than the rock magnetic record which may be used to suggest that at Kilombe a signal of palaeoclimate change is preserved within this sequence and is stronger in proxies for chemical weathering intensity. However, rates of erosion are also shown to either promote or inhibit chemical weathering intensity and cannot be ruled out as a causal factor here.

7.5 Environmental settings at Kilombe

7.5.1 Depositional environments

There are a number of depositional environments recorded at Kilombe both on the main site and FHC which are described in detail in Chapter Four and consist of colluvial sedimentary rocks, tuffs both primary airfall and re-worked, paleosols and tuffaceous clays/clayey tuffs. We have now been able to demonstrate that many of the units have been variously altered by pedogenesis, chemical weathering intensity and low temperature oxidation of volcanic tuffs. One of the most striking features at Kilombe is the number of changes in depositional environment/lithology that occur in some parts of the record over a relatively short period. This is especially apparent at Kilombe main site where 9 lithologic units representing four facies associations have now been identified within a 4 metre section, and in the lower part of FHC were 4 lithologic units are recorded, two of which have been subdivided into 5 and 6 subunits. A further notable feature is the range in values apparent per lithological unit in both the major and trace element and rock magnetic data, especially units 12 and 13, some of which would indicate detrital sediments of primary igneous origin and others, values of intensely weathered soils/sediments.

7.5.2 Kilombe Main site

We now know that the basal yellowish red claystone could not be older than 1.07 Ma, although it could be substantially younger, and the rest of the units are younger than 970,000 Ka on the main site suggesting rapid sediment accumulation rates on this part of the site. This is most likely linked to increased rates of erosion under much wetter conditions as suggested by CIA values of > 80 at Kilombe and by the higher levels of precipitation across the Rift Valley (Trauth *et al.*, 2005). The magnetic data may also suggest deposition under much wetter conditions with little time for soil formation post-depositionally due to more rapid accumulation rates. The rock magnetic record shows a mix of magnetic minerals of both detrital and pedogenic origin with only 30% of the samples in this unit meeting the criteria for comparison with Asian and European soils on the biplot of Oldfield (1994) and these are located throughout this unit suggesting at times increases in levels of pedogenic intensity in this unit. Most of the fossil fauna occurs around the contact points between this unit and the next unit, the brown claystone, and both the occurrence and preservation of the faunal remains can be explained by the occasional development of land surfaces and rapid sediment accumulation rates.

The suggestion of rapid sediment accumulation rates across Kilombe main site is further supported by the changing magnetic and geochemical properties of the soils and sediments across units 2 – 6. Values in all three chemical weathering indices would indicate incipient chemical weathering i.e. non-weathered detritus. An increase in elements associated with quartz and the feldspars is noted across these units also indicating an increase in detrital minerals. This increase is accompanied by the progressive loss of Fe and Mn and the heavy metals along with unusually low values of χ_{LF}, χ_{FD}, χ_{ARM} and SIRM suggesting a reduction in concentration of ultrafine ferrimagnetic minerals and an increase in the detrital component as indicated by mean S-ratio values. The results of particle size separation demonstrate that the fine grained ferrimagnetic component has been removed from the finer particle sizes and that the iron sulphide greigite has formed in each of these units suggestive of an intermediate stage of dissolution under rapid burial conditions. Bishop (1978) and Gowlett (pers comm) had originally suggested that units on the main site, which now correspond to the yellow grey claystone and the gray claystone/diamictite, were gleyed as an explanation to the distinct change in colour from brown to grey. We now know that this is due to burial diagenesis which is known to have a similar effect on the colour of soils and sediments and also on some of the magnetic properties i.e. loss of the signal. The main artefact horizon occurs at the top of the yellow grey claystone and Gowlett (1978) noted that at AH, 48% of the bifaces came from a 5 cm interval with a further 81% of the artefacts shown to occur within a 15 cm interval in this unit. Extensive research has been conducted on these bifaces from AH as representing variability in tradition from single hominin occupation unit. Further support for this interpretation now comes from the demonstration of rapid accumulation rates especially evident in the yellow claystone unit. Further to that, it is likely that the artefacts were preserved by the deposition of the grey claystone/diamictite i.e. landslide rather than an influx of pumice tuff as originally suggested by Bishop (1978). Diamictites are very difficult to identify in the field as many display features similar to palaeosols or even lacustrine. The diamictite in this case was identified via micromorphology in thin section (Stanistreet, 2014 pers comm). A period of rapid sedimentation rates due to increased erosion under much wetter conditions may have resulted in a period of landscape de-stabilisation resulting in a landslide.

A break in deposition/sedimentation is then recorded on the main site with the development of a hiatal surface and palaeosol indicating subaerial conditions, this deposit which has also been altered and some of signal lost provides little information on environmental conditions at the time other than a break in sedimentation. A period of extensive volcanic activity is now recorded at the site with the deposition of two reworked tuffs which may represent the more acidic phase of an eruption which culminated in the deposition of a primary airfall tuff, the 3BT, which as noted by Gowlett *et al*., (2015) would have been a landscape altering event. Unit 7 on the main site, which was deposited between the two reworked tuffs is now identified as a tuffaceous claystone, rather than a palaeosol. This claystone does shows strong evidence for pedogenic overprinting at the top of the unit with samples well within the range of European and Asian soils. However, as this unit underlies the 3BT alteration via heating and cooling under volcanic activity of this sedimentary unit must be considered. The tuffaceous claystone yields CIA values of 78 which increase to > 80 suggesting intense chemical weathering under either increased levels of precipitation or decreased rates of erosion.

7.5.3 Farmhouse Cliff

The environmental record at FHC will be examined in the context of the lower and upper sections marked on Figure 7.1 All these units are referred to in the lower Menengai Tuffs of Jones (1975), and Bishop (1978) and as on Kilombe main site are all within the range of Central Rift intermediate rocks, trachytes and trachyphonolites, aside from one unit which will be discussed further in this section. The lower section of FHC comprises a number of sedimentary units (10 – 13) which correspond to Bishop's (1978) orange brown pumiceous tuffs interbedded with finer-grained clayey weathered tuffs, and records a period of extensive volcanic activity and changes in weathering environments some of which may have been rapid.

The lower part of FHC appears to have been deposited and weathered between 0.97 and 0.799 Ka and comprises reworked, and perhaps some primary, weathered ashfall tuffs and tuffaceous clays along with less weathered primary material subject to subaerial exposure and pedogenic processes of varying degrees. This part of the sequence would be broadly comparable to Members 5 – 9 at Olorgesailie Formation.

The lowest units 10 and 10 A were originally recorded as one unit, in the field, with an orange clay band (see Chapter Four, Table 4.1). However, the geochemical properties of both the orange clay band and the upper 40 cm of this unit are significantly different to the lower section. Average TiO_2 of 2.4 and higher Fe_2O_3 and lower SiO_2 would generally indicate a more mafic source origin than intermediate. It is suggested here that, that this unit needs to be examined using micromorphology and there may be a non-local source for part of it.

The magnetic properties do not change significantly but any environmental interpretation would be unsound for this unit.

The deposition of unit 11 corresponds to a period of lake regression at Elmenteita and the end of a deep-lake phase across the Rift Valley. Chemical weathering intensity can be described as incipient and would generally indicate low levels of precipitation and or/lower temperatures or, decreased rates of erosion, and values decline throughout this unit. The rock magnetic record suggests that this unit is altered pedogenically with χ_{FD}% values ranging between 5.6 and 7.6 with an average of 6.3. Although sedimentation rates are argued to be rapid, they may have been lower in this particular unit with more time for pedogenesis to take place.

The environmental record for units 12 and 13 is extremely complex. These units show varied degrees of chemical weathering and pedogenic activity with some of the finer-grained tuffs weathering, perhaps rapidly, into tuffaceous clay deposits and some of the tuffs, even the fine-grained material showing no evidence of weathering at all. These units yield the largest ranges in values in both the magnetic and geochemical data sets with some of these large scale changes occurring across 10 cm sampling intervals. Across both units chemical weathering intensity is shown to increase up - section from values representing an incipient stage of weathering to those approaching intense. Intensity of pedogenesis also increases across these units as shown by an increase in χ_{FD}% which is accompanied by an increase in LOI%. However, substantial variability is recorded in both LOI% and χ_{FD}% values across these units.

The lowest part of the brown clay series (light gray tuff) shows little evidence for either chemical weathering or pedogenic activity, CIA values are also low and most of the samples do not meet the criteria for comparison against Asian/European soils suggesting a more detrital origin. Major and trace element data indicate higher levels of quartz and feldspars in this unit which indicates detrital material although the magnetic data do indicate neoformation of ultrafine ferrimagnetic minerals which could be either pedogenic or of volcanic origin. The fact that most samples do not meet the criteria of Oldfield (1994) may suggest the latter suggestion is correct. The units following deposition of this tuff (the yellowish brown tuff) still contain material of detrital origin (quartz and feldspars). However, subsequent units do appear to have undergone some pedogenic alteration. The concentration of ultrafine ferrimagnetic minerals does increases from the previous unit and the samples fall within the range of Asian and European soils. The next three subunits again show pedogenic alteration of varying degrees the uppermost subunit the yellow tuff is the most extensively altered with all samples being comparable to Asian and European soils and the highest LOI% within this unit and also high for the sequence in general. Measures of chemical weathering intensity indicate moderate chemical weathering. The distinct banding effect and changes in colour appears to be the result of changes in levels of pedogenic activity in this unit. Time i.e. exposure times may also be a factor here but this is difficult to demonstrate due to extensive volcanic activity.

A distinct change, both in colour and potentially weathering environments, is noted in the next unit (13), the orange clay series. This series records the deposition of three “white” tuffs with interstitial “orange” tuffaceous clayey deposits between them. The magnetic and geochemical properties of the lowest two white tuffs are very similar to the unweathered tuffs on Kilombe main site. However, all the samples were included for comparison with Asian and European soils and overlap. It must be noted that the “white” tuffs fall to the lower end of the plot just outside the envelope associated with burning. The CIA index yields values of 74 which would indicate moderate chemical weathering. The major and trace data shows a decline in elements associated with detrital minerals throughout this unit with the upper four subunits reflecting an increase in elements associated with the clay minerals. Pedogenic activity also is shown to increase in the upper subunits. LOI % values (av. 13) are high throughout. The upper unit (F) shows an increase in elements associated with detrital minerals and a reduction in concentration of Al_2O_3. In this unit there is generally a good correlation between chemical weathering intensity and pedogenic activity.

The upper part of FHC, Figure 7 extends from 780,000 to 487,000 Ka and has a duration of approximately 300,000 years. As discussed in Chapter Four, redoxmorphic features become more prominent in the upper six metres of FHC suggesting an increase in post-depositional weathering. Bishop (1978) also noted that the tuffs became much more “earthy” towards the top of FHC indicating long periods of subaerial exposure. Sediment accumulation rates are at their lowest for the entire sequence here.

The lowest unit of this section unit 14, yields average CIA values of 74 but shows a slight trend towards higher values throughout the unit indicating an increase in chemical weathering intensity or decreased rates of sedimentation. Mean values of the major oxides associated with detrital minerals are low whilst Al_2O_3, Fe_2O_3 and MnO are high suggesting an increase in the clay minerals and iron oxides. Only samples from the upper 60 cm of this unit fall within the range for Asian and European soils with some falling to the lower end of the envelope. LOI % values also increase throughout this unit.

The finer grained tuffs, along with the effects of varied degrees of pedogenic activity, which have been shown to create the distinct banding effect in the previous units become fewer and thinner within units 14, 15 and 16. This suggests a reduction in volcanic activity in the area and a return to sedimentation on the site.

In unit 15 CIA values are 76 and show an overall decline throughout the unit. LOI values are also much higher at the base of this unit (9.5%) and decline to average values of 6% throughout this unit. Sixty percent of the samples meet the criteria for the bi-plot of Oldfield (1994) and of those all fall well within the range of soils providing strong evidence for pedogenic activity throughout this unit. Values for χ_{FD}% show a very weak trend to lower values throughout this unit but are still high indicating strong pedogenesis. In general, there is a good correlation between chemical weathering intensity and pedogenic activity in this unit.

Unit 16 CIA values are 72 but show an increase to higher values are the top of this unit. LOI% values are quite variable (2 – 8.6, average 5.6) but also show some increase in the 40 cm. Most of the samples bar the lowest 20 cm all pass the criteria for the biplot and fall within the range of Asian and European soils again, as with the previous unit) showing evidence for strong pedogenic activity. At the top of sequence χ_{FD}% decline yielding the opposite trend to that in CIA and LOI%. An overall decline in SiO_2 occurs throughout this unit whilst Al_2O_3, Fe_2O_3 and MnO increase demonstrating an increase in concentration of clay minerals and the iron oxides. This unit underlies the ashflow tuff and therefore the top of this unit may have been subject to alteration similar to units 7, tuffaceous claystone.

7.5.4 Summary

The record of changing palaeoenvironments in the Kilombe sedimentary sequence is complex and highly variable and both the changing magnetic properties and geochemical evolution over time have been shown to partly reflect climate change over the longer-term and at Kilombe main site. However, a multi-proxy approach also documents the major influence of changes in lithology and depositional environment along with the added influence and complication on interpretation of this record of extensive volcanic activity. Rates of sediment accumulation have been shown to directly influence magnetic enhancement and reduction throughout this record driven by the factor of time, and more specifically exposure times to weathering in relation to pedogenic activity in this record. This effect appears to be less pronounced in the record of chemical weathering intensity. Dissolution via burial diagenesis strongly effects the record and both proxies at Kilombe main site, however particle size analysis has allowed further information to be gleaned on the environmental processes which have resulted in the dissolution.

Active volcanism or tectonism has been shown to alter weathering regimes through modification of palaeorelief in source areas and even generation of new relief and palaeohydrological regime (Campo *et al.*, 2010). In addition, volcanic events have also been shown to give rise to clay mineral assemblages that differ substantially to those that would have been produced if only climatic factors were at play (Pellenard *et al.*, 2003; Jeans, 2006). Environmental studies from volcanically active regions have also shown that ashfall tuffs can sometimes rapidly weather into clays even in as little time as two to three years, regardless of weathering environments. To be considered also is that highly labile volcaniclastic material can be supplied to sedimentary sequences by volcanic events, and this material has been shown to transform into smectite during early diageneis (Cuadros *et al.*, 1999). The CIA index and accompanying ternary plot allows identification of smectite however it cannot be considered that values representative of smectite following tuff deposition are climatically determined. These factors can all lead to erroneous conclusions regarding climatic influence unless the importance of all have been constrained. Due to extensive volcanic activity, and the limitations of both proxies to constrain any of the above factors it is not reliable to provide any interpretation climatically of units from lower FHC.

At times in the record, specifically in the basal claystone and upper FHC, notable differences are observed in the response of the rock magnetic and geochemical data sets argued here to represent a differential response to weathering duration which highlights the importance of a multi-proxy approach when investigating past climate change. To be considered also are the limitations of both proxies on derived sequences and the added complication of extensive volcanic activity which is shown to produce both ultrafine ferrimagnetic mineral assemblages and clay mineral assemblages that can differ substantially to those produced climatically. Magnetic susceptibility has been established as a worldwide proxy for palaeorainfall estimates with a number of statistical approaches taken to produce quantitative estimates of rainfall (Balsam *et al.*, 2011). However, there are a number of instances when the relationship between MS and rainfall has been questioned in specific environmental contexts (Bloemendal & Liu, 2005; Lyons *et al.*, 2012). Given the influence of weathering duration on the magnetics data set at Kilombe it would not be reliable to produce rainfall estimates using these data or approaches as any results would be misleading. However, statistical approaches using magnetic susceptibility in producing palaeorainfall estimates remain a completely unexplored methodology for East African palaeosols and represents a strong future direction for research into precipitation levels on hominin sites.

The next section will situate the environmental record at Kilombe, long-term trends and Kilombe main site, within the context of other East African records and within the context of the environmental records from other East African Acheulean ca. 1 million years ago.

7.6 Discussion

7.6.1 Introduction

The combined application of palaeomagnetic and $^{40}Ar/^{39}Ar$ dating has produced a strong chronology for the occurrence of the Acheulean, fossil fauna and the palaeoenvironmental record at Kilombe which now enables the placement of this record both archaeologically and environmentally within the context of other contemporaneous records. The sedimentary record during the Quaternary at Kilombe covers the end of the early and middle Pleistocene 1.07 Ma to 487 ka and the environmental history here has been shown to reflect the complex interplay between volcanic activity, changes in erosion/sediment accumulation rates and palaeoclimate change.

7.6.2 East African aridification trend

A long-term trend towards increasing aridity is observed in the record of chemical weathering intensity at Kilombe similar to the East African aridification trend under conditions of global cooling. The main controls exerted on chemical weathering intensity, climatically, are temperature and rainfall given the establishment of similar parent material. After removal of units on Kilombe main site, demonstrated to have been affected burial diagenesis, the trend in the geochemical record is for decreasing whole rock and/or post depositional weathering during the Quaternary with substantial variability in chemical weathering intensity superimposed upon this trend. There are two possible explanations in terms of examining a long-term trend towards reduced chemical weathering intensity. The first is that increased rates of erosion and sediment accumulation rates have led to shorter exposure times to chemical weathering intensity over time and the second is that a decrease in temperature and/or rainfall have resulted in reduced chemical weathering intensity due to a long-term trend in climatic conditions. At Kilombe, although rates of sediment accumulation have been shown to affect changes in the rock magnetic record to varying degrees there seems to be a less pronounced effect on the record of chemical weathering intensity at least in the lower part of the main site and the upper part of FHC. CIA values at Kilombe have been shown to reflect similar conditions in terms of precipitation levels from other East African records from the Central Rift Valley suggesting that the response here may be climatic rather than in response to rates of erosion. Further support for this interpretation comes from the differential response of the rock magnetic record, which at times in this record has been shown to reflect a much stronger response to post-depositional weathering and pedogenic activity driven ultimately by increases/decreases in sediment accumulation rates.

The suggested climatic response here of a long-term trend towards reduced chemical weathering intensity at Kilombe during the Quaternary would be compatible with general trends in East Africa during the Plio-Pleistocene towards aridification. Climatic causes of the East African aridification trend have been attributed to a number of factors. The first is that moisture transport was lowered across East Africa, and specifically the central Rift Valley, due to a reduction in the southeasterly monsoon system after intensification in Walker circulation around 1.7 Ma (deMenocal, 2004; Levin *et al.*, 2011). The second is that regional long-term trends in aridification are as a result of changes in zonal circulation due to tectonic uplift (Sepulchre *et al.*, 2006; Prommel *et al.*, 2013). These studies suggest that as uplift increases, regional rainfall decreases due to wind patterns becoming less zonal. Maslin *et al*., (2012) have also argued using data from carbon isotope records from soil carbonates, that the aridification trend is more of a gradual progression towards variable climates with intense arid periods rather than a progression towards aridification. A third explanation in the context of the Kilombe record is that variation in CIA values here may have been influenced by local erosion and sedimentation rates. Although, the record of chemical weathering intensity at Kilombe most likely reflects the complex interplay between sedimentation, volcanism and climate, it is more likely that the long-term trend of palaeoclimatic change reflected in the geochemical record during a 500,000 year period of the Quaternary at Kilombe represents a trend towards aridification and thus climate change.

7.6.3 Mid Pleistocene Revolution and climatic variability 1.1 – 0.7 Ma

Key events in hominin evolution have been argued to have occurred during periodic humid phases driven by precessional forcing at times of global climate change such as the Mid Pleistocene Revolution (Trauth *et al.*, 2005). One of the key time frames noted here in terms of examining selective pressures is the 1.1 – 0.9 Ma which is concordant with both the Mid Pleistocene Revolution and an extensive deep-lake phase across the East African Rift Valley (Trauth *et al.*, 2005). This deep-lake phase noted by Trauth and colleagues has been shown to occur during a time of large scale climatic variability driven by orbital precession, and a number of other studies including analysis of terrigenous dust records present a refinement to the duration of this period in East Africa 1 – 0.7 Ma and 1.1 – 0.7 Ma (Trauth *et al.,* 2009; Donges *et al.*, 2011). The lower part of the sedimentary sequence at Kilombe and particularly Kilombe main site are coeval with this phase of climatic variability and more specifically the deep-lake phase. The local manifestation at Kilombe main site can be seen through an increase in precipitation and/or warmer temperatures, resulting in increased erosion and more rapid sedimentation rates which may have then resulted in a period of landscape destabilisation and deposition of mudslide or diamictite. This is a very local impact, however one which may have impacted significantly upon local populations at this site. The record of environmental change at Kilombe also shows substantial variability across this time frame although due to complexities and substantial episodes of volcanism in the centre of the record it would be unreliable to interpret changes on shorter timescales at Kilombe as purely climatic. What is notable is the wide range of values in chemical weathering indices and magnetic parameters that at times appear to capture deposition of volcanic tuffs and subsequent weathering processes.

7.6.4 Identifying selective pressures from local sequences

The importance of the production of more localised records of climate change has been recently recognised by Potts (2013), and the production of local records of palaeoenvironmental change from within archaeological sites potentially enables the assessment of whether selective pressures, in terms of global and regional patterns of climate change, can be examined at a localised level, and therefore linked directly to archaeological and/or biological changes. In the central Rift Valley, Kenya, two records using geological proxies for chemical weathering intensity specifically the CIA index, from Kilombe and Olorgesaille, now document a long-term trend towards increasing aridity during the Quaternary with substantial variability noted upon these trends at both localities (Owen *et al.,* 2014). Due to the problems of establishing chronological controls, local variability in sedimentation rates and influence of volcanism/tectonism at both sites, it is not possible to directly or accurately compare both records of chemical weathering intensity on shorter timescales, although there may be times in both records where similar trends through time are apparent in chemical weathering intensity.

Potts (1999; 2013) notes that there are no major evolutionary events in the East African record of human evolution during the period 1.1 – 0.9 Ma, although the last appearance of *Paranthropus* and dispersal of the Acheulean out of Africa both may occur at the outset of this period. At Olorgesaille, a change in landscape use by hominin populations was noted in this period (Potts, 1999). At Kilombe, the major occupation surface also occurs during this period and despite persistent episodes of environmental change, both climatic and landscape altering, evidence of hominin populations occurs throughout the lower part of the sequence and also now at FHC. This points to the attractiveness of this locality for local populations despite the continued eruptions from Kilombe and Menengai volcanoes and landscape altering events such as the deposition of the 3BT and diamictite on the main site. The attractiveness of this locality for hominin populations is most likely explained by the abundance of raw material for manufacture of stone tools and number of channels and perhaps localised ponding that would have attracted both animals and humans, in terms of water availability, in absence of a large lake environment as seen at sites such as Olorgesaille, Kariandusi and Olduvai Gorge.

Whether the long-term trend of aridification or aspects of the much localised impact of wider climatic variability under orbital precession 1.1 – 0.9 Ma identified within the Kilombe sedimentary sequence can be taken as creating selective pressures for local populations here is difficult to assess. The local manifestation of wider trends in palaeoclimate change can vary significantly depending both the depositional environment and under very localised topographic features and can therefore be manifested in different ways environmentally and thus archaeologically. This further highlights the importance of the production of local records of environmental change in terms of examining impact upon local populations and examining variation between sites in the archaeological response to the local manifestation of wider climate change.

7.6.5.1 Directional change and variability selection

A number of environmental drivers of human evolution during the Plio-Pleistocene has been suggested including aridity, moisture levels and climatic variability (Vrba, 1995; Reed, 1997; deMenocal, 2004; Kingston, 2007; Trauth *et al.*, 2005; Potts 2012; Grove; 2012). It is suggested here that the aridification trend is also a major factor of evolutionary change to be considered along with climatic variability during the Plio-Pleistocene in East Africa. Long-term trends emphasising directional change are evident in local sequences such as Kilombe and Olorgesaille and wider including the Nihewan Basin, China and the Buffalo flowstone record, South Africa (Ao *et al*., 2010; Hopley *et al*., 2007; Owen *et al*., 2014), therefore theories emphasising directional change should therefore not be discounted as a causal factor. However, theories emphasising variability selection and plasticity are concordant with episodes of major climatic variability, both high and low, and major events in human evolution especially in an East African context. At Kilombe there is evidence, locally, for significant environmental change and variability occurring over a 500,000 year period with more heightened variability noted in this record between 1.07 Ma and 780 Ka than between 700 and 500 Ka. However, some of the higher amplitude variability within this record correspond to a period in which extensive volcanic activity was occurring making a purely climatic inference very difficult for these parts of the record. Further complication is added as some enhancement/reduction in both the rock magnetic and geochemical properties in parts of this record is more likely due to duration of weathering rather than climatic. This, however, highlights the limitations of some of the more localised records, and proxies for chemical weathering intensity and the technique of environmental magnetism, when examining palaeoclimatic change, especially in volcanically and tectonically active regions such as the East African Rift Valley. Final conclusions and future directions are presented in Chapter 8.

Chapter 8 Conclusions and future directions

8.1 Conclusion

The major aims of this thesis were to provide a local record of palaeoenvironmental change for the Acheulean occurrences at Kilombe 1.07 – 0.487 Ma, and to investigate whether any impact of global and regional climate change could be examined at a more localised level and on different timescales.

Previous palaeoenvironmental work was limited at Kilombe (Bishop, 1978) and environments surrounding the main artefact horizon were not understood climatically. The production of an environmental record from Kilombe now enables the placement of the Acheulean tradition at this site within a much stronger environmental context which can then be compared to environmental settings from a number of other Acheulean sites that are broadly contemporaneous with Kilombe including Olduvai Bed IV, and more locally the sites of Kariandusi and the Olorgesaille formation.

Based on the results of geochemistry a similar source rock, alkaline intermediate rock, was established for the entire Kilombe sequence, with the exception of one discrete section suggestive of a non-local, mafic, source. The establishment of an intermediate source rock confirms Bishops (1978) earlier interpretation that the sedimentary sequence was derived from local trachytes and trachyphonolites. Some refinements to the original stratigraphic column have however also been made through this PhD thesis based on new field descriptions and supplemented by some thin section laboratory work.

The present investigation on the Kilombe sedimentary sequence provides direct evidence for a long-term trend towards a decrease in chemical weathering intensity and therefore an increase in aridification/cooling during this part of the Quaternary (1.07 Ma – 487 Ka). This trend is consistent with the East African aridification trend and trends observed in other East African records of climate change. The influence of duration of weathering on chemical weathering intensity has been well documented. However, if the weathering duration model was the only determining factor at play then a reduction in chemical weathering intensity in the basal claystone and an enhancement in upper FHC sediments would be expected due to higher/lower sedimentation rates. Therefore, the decrease in chemical weathering intensity at Kilombe cannot be explained by the effects of weathering duration time.

The most important conclusions to be drawn from these data are therefore in the establishment of a long-term trend towards reduced chemical weathering intensity over time with an important note on the amount of variability in chemical weathering intensity superimposed upon this trend. However, due to the complexities of this sequence (volcanic activity and dissolution) it is not possible to examine climate change on shorter timescales with any degree of integrity. The principal conclusions can be summarised as follows:

- The main Acheulean occurrence has now been placed in an environmental context corresponding to increased precipitation levels with local impact in the form environmentally of increased rates of erosion, which, may also have resulted in a period of landscape de-stabilisation which may have impacted upon local hominin populations.

- The combined application of major and trace element geochemistry and environmental magnetism has provided further information on both chemical weathering intensity and also the occurrence of pedogenic activity within the sequence with at times a differential response observed in both techniques relating to the factors of both climate and time. A multi-proxy approach here has allowed a stronger climatic inference to be established for the geochemical data set.
- The establishment of magnetic enhancement as a response to duration of weathering at Kilombe serves a cautionary note in the application of this technique on sequences were substantial time for weathering occurs.
- The importance of long-term trends of environmental change need to be re-recognised and considered in tandem with theories emphasising the role of climatic variability as both are evident in local records of environmental change from a number hominin sites and may therefore be influencing evolutionary traits in different ways within the hominin lineage.

Kilombe is an important site both archaeologically and now environmentally due to the fact that it is one of few, continuous records in an East African context and, due to the fact that it preserves a recurring or even continuous human presence. New age determinations have enabled the placement of this new record of environmental change at Kilombe to be examined in a more regional context both environmentally and archaeologically. The results of a multi-proxy approach here offer interesting information on the understanding of the evolution of Quaternary environments over a 500,000 year period. However also highlight both the complexities and limitations of examining palaeoenvironmental change from derived sequences in a volcanically and tectonically active area such as the East African Rift System and on a more localised level.

8.2 Future directions

There are a number of future directions to come from this thesis relating to both the record of environmental change at Kilombe and the wider application of techniques used here in reconstructing environmental change.

1/ at lower Farmhouse cliff it has been suggested here, that due to extensive volcanic activity it is not possible to establish a climatic response within the geochemical and magnetic data set. The identification and analysis of the clay mineral assemblages within LFHC and at Kilombe generally could represent an important future direction. Campo *et al.*, (2010) have demonstrated that smectite can form from volcanic ash regardless of weathering environment. These authors have already established an approach applying X-ray diffraction (XRD) and scanning electron microscopy (SEM) along with detailed facies analysis that enables the identification of volcanically rather than climatically derived smectite and allows a much stronger approach in analysing clay mineral assemblages that have formed via more than one environmental process in volcanically active regions.

2/ the production of a record of C3 and C4 vegetation through phytolith analysis would provide the strongest future direction for the FHC sediments at Kilombe. Preparation is under way and with analysis and results to follow later this year (Lem, 2015; pers comm). The phytolith data from FHC would provide further evidence in either confirming or refuting suggestions here of a long-term trend toward aridification which would be marked by a decrease and increase in C3 and C4 taxa respectively in the phytolith assemblage. These data will also provide an important record of palaeovegetation changes locally at Kilombe and the Central Rift Valley.

3/ Statistical models for the use of magnetic properties of soils and palaeosols as proxies for palaeorainfall estimates are well established (Balsam *et al.*, 2011; Maher & Possolo, 2013), and this technique may therefore provide an important direction in the quantitative reconstruction of past climatic conditions in East Africa due to the abundance of palaeosols preserved at East African hominin sites. The application of environmental magnetism in terms of producing palaeorainfall estimates for early hominin sites in East Africa remains completely unexplored. A rapid, inexpensive and non-destructive approach can be developed which would enable the production of palaeorainfall estimates at much higher resolution from palaeosols than is currently available from studies of oxygen isotopes in East Africa. Further to that the application of geological proxies to bulk soil samples does not rely on preservation of carbonates so would provide data for palaeosols in which carbonates have not preserved.

BIBLIOGRAPHY

Ao, H. Deng, C. Dekkers, M.J. Sun, Y. Liu, Q. Zhu, R. (2010). Pleistocene environmental evolution in the Nihewan Basin and implication for early colonization of North China *Quaternary International* **223-224,** 472-478

Acton, G. Yin, Q.Z. Verosub, K.L. Jovane, L. Roth, A. Jacobsen, B. Ebel, D.S. (2007). Micromagnetic coercivity distributions and interactions in chondrules with implications for paleointensities of the early solar system *Journal of Geophysical Research* **112** B3

Antón, S.C. Aiello, L.C. Potts, R. (2014). Evolution of Early *Homo*: An integrated biological perspective. Science **345,** 6192

Aronson, J.L. Hailemichael, M. Savin, S.M. (2008). Hominid environments at Hadar from palaeosol studies in a framework of Ethiopian climate change. *Journal of Human Evolution* **55**, 532-550

Ashley, G.M. (1978). Interpretation of polymodal sediments. *Journal of Geology* **86,** 411-421

Ashley G.M. Driese S.G. (2000). Paleopedology and paleohydrology of a volcaniclastic paleosol interval: implications for early Pleistocene stratigraphy and paleoclimate record, Olduvai Gorge, Tanzania. *Journal of Sedimentary Research* **70,** 1065–1080

Ashley G.M. (2007). Orbital rhythms, monsoons, and playa lake response, Olduvai Basin, equatorial East Africa (ca. 1.85 – 1.74 Ma). *Geology* **35**, 1091-10.94

Ashley G.M. Tactikos, J.C. Owen, R.B. (2009). Hominin use of springs and wetlands: Paleoclimate and archaeological records from Olduvai Gorge (1.79-1.74 Ma). *Palaeogeography, Palaeoclimatology, Palaeoecology* **272**, 1-16

Baker, B.H. Williams, L.A.J. Miller, J.A. Fitch, F.J. (Sequence and geochronology of the Kenya Rift volcanics. *Tectonophysics* **11,** 191-215

Barron, V. Torrent, J. De Grave, E. (2003). Hydromaghemite, an intermediate in the hydrothermal transformation of 2-line ferrihydrite into hematite. *American Mineralogist* **88,** 1679-1688

Barboni, D. Ashley, G.M. Dominguez-Rodrigo, M. Bunn, H.T. Mabulla, A.Z.P. Baquedano, E. (2010). Phytoliths infer locally dense and heterogeneous palaeovegetation at FLK North and surrounding localities during Bed I time, Olduvai Gorge, Tanzania. *Quaternary Research* **74**, 344-354

Balsam, W.L. Ellwood, B.N. Junfeng, Ji. Williams, E.R. Long, X. El Hassani, A. (2011). Magnetic susceptibility as a proxy for rainfall: Worldwide data from tropical and temperate climate. *Quaternary Science Reviews* **30,** 2732-2744

Behrensmeyer, A.K. Todd, N.E. Potts, R. McBrinn, G.E. (1997). Late Pliocene faunal turnover in the Turkana Basin, Kenya and Ethiopia. *Science* **278** 1589-1594

Behrensmeyer, A.K. Potts, R. Deino, A. Ditchfield, P. (2002). Olorgesaille, Kenya: a million years in the life of a rift basin. In Renaut, R.W. Ashley, G.M. (Eds) Sedimentation in Continental Rifts. SEPM Special Publication **73** 97-106

Bishop, W. W. (1978). Geological framework of the Kilombe Acheulian Site, Kenya, in (W. W. Bishop (ed.) Geological Background to Fossil Man. Edinburgh: Scottish Academic Press, pp329-336.

Bloemendal, J. King, J.W. Hall, F.R. Doh, S.J. (1992) Rock magnetism of late Neogene and Pleistocene deep sea sediments relationship to sediment source, diagenetic processes, and sediment lithology. *Journal of Geophysical Research* **97,** 4361-4375.

Bloemendal, J. Ehrmann, W. Hambrey, M.J. McKelvey, B.C. Matthews, R. Whitehead, J.M. (2003). Geochemical and rock magnetic records from sediments of the Cenozoic Pagodroma Group, Prince Charles Mountains, East Antarctica: implications for provenance and weathering. *Antarctic Science* **15,** 365-378

Bloemendal, J. Liu, X. (2005). Rock magnetism and geochemistry of two Plio-Pleistocene Chinese loess-palaeosol sequences – implications for quantitative palaeoprecipitation reconstruction. *Palaeogeography, Palaeoclimatology, Palaeoecology* **226,** 149-166

Blott, S.J. Pye, K. (2001) GRADISTAT: a grain size distribution and statistics package for the analysis of unconsolidated sediments. *Earth Surface Processes and Landforms* **26,** 1237-1248.

Blundell, A. Dearing, J.A. Boyle, J.F. Hannam, J.A. (2009). Controlling factors for the spatial variability of soil magnetic susceptibility across England and Wales. *Earth Science Reviews* **95,** 158-188

Bobe, R. Behrensmeyer, A.K. Chapman, R. (2002). Faunal change, environmental variability and late Pliocene hominin evolution. Journal of Human Evolution **42**, 475– 497.

Bobe, R. Behrensmeyer, A.K. (2004). The expansion of grassland ecosystems in Africa in relation to mammalian evolution and the origin of the genus *Homo. Palaeogeography, Palaeoclimatology, Palaeoecology* **207,** 399-420

Bonnefille, R. (1995). A reassessment of the Plio-Pleistocene pollen record of East Africa In Vrba, E.S., Denton, G.H., Partridge, T.C., Burkle, L.H. (Eds), Palaeoclimate and Evolution with an emphasis on Human Origins. Yale University Press, New Haven, Connecticut, pp. 299-310

Bonnefille, R. (2010). Cenozoic vegetation, climate changes and hominid evolution in tropical Africa. *Global and Planetary Change* **72,** 390-411

Brain, C. K. (1981). The evolution of man in Africa: Was it a consequence of Cenozoic cooling? *Geological Society of South Africa Transactions* **17,** 1–19.

Brotzu, P. Morbidelli, L. Nicoletti, M. Piccirillo, E.M. Traversa, G. (1984). Miocene to Quaternary volcanism in Eastern Kenya: sequence and geochronology. *Tectonophysics* **101,** 75-86

Brown, F.H. Feibel C.S. (1991). Stratigraphy, depositional environments and palaeogeography of the Koobi Fora Formation. In: Harris, J.M. (Ed.), Koobi Fora Research Project vol 3 Oxford University Press, New York, pp 1-30

Brown, A.G. (1985). Traditional and multivariate techniques in the interpretation of floodplain sediment grain size variations. *Earth surface processes and landforms* **10,** 281-291

Burdige, D.J. (1993). The biogeochemistry of manganese and iron reduction in marine sediments. *Earth Science Review* **35,** 249-284.

Butzer, K. (1977). Environment, culture and human evolution. *American Scientist* **65,** 572–584.

Campisano, C.J. Feibel, C.S. (2007). Connecting local environmental sequences to global climate patterns: evidence from the hominin-bearing Hadar Formation, Ethiopia. *Journal of Human Evolution* **53,** 515-527

Do Campo, M. del Papa, C. Neito, F. Hongn, F. Petrinovic, I. (2010). Integrated analysis for constraining palaeoclimatic and volcanic influences on clay-minerals assemblages in orogenic basins (Palaeogene Andean foreland, Northwestern Argentina). *Sedimentary Geology* **228,** 98-112

Cerling, T.E. (1992). The development of grasslands and savannas in East Africa during the Neogene. *Palaeogeography, Palaeoclimatology, Palaeoecology* **97,** 241-247

Chen, H. L. Yang, S. F. Wang, Q. H. Luo, J. C. Jia, C. Z. Wei, G. Q. (2006). Sedimentary response to the early-mid Permian basaltic magmatism in the tarim plate. *Geology in China,* **33**, 545–55

Colman, S.M. (1982) Chemical weathering of basalts and andesites: evidence from weathering rinds *US Geological Survey* **1246:51**

Cuadros, J. Caballero, E. Huertas, J. Jiménez de Cisneros, C. Huertas, F. Linares, J. (1999). Experimental alteration of volcanic tuff: smectite formation and effect on ^{18}O isotope composition. *Clays and Clays Minerals* **47,** 769-776.

Dalan, R.A. Banerjee, S.K. (1996). Soil magnetism: an approach for examining archaeological landscapes. *Geophysical Research Letters* **23,** 185-188

Darwin, C. R. (1874). *The descent of man, and selection in relation to sex*. London: John Murray.

Dearing, J.A. Hay, K. Dann, R.J.L. Hay, K. Lees, J.A. Loveland, P.J. Maher, B.A. O'Grady, K. (1996). Frequency-dependent susceptibility measurements of environmental samples. *Geophysical Journal International* **124,** 228-240

Dearing, J.A. Bird, P.M. Dann, R.J.L. Benjamin, S.F. (1997). Secondary ferrimagnetic minerals in Welsh soils: a comparison of mineral magnetic detection methods and implications for mineral formation. *Geophysical Journal International* **130,** 727-736

Dearing, J.A. Hannam, J.A. Huddleston, A.S. Wellington, E.M.H. (2001). Magnetic, geochemical and DNA properties of highly magnetic soils in England. *Geophysical Journal International* **144**, 183-196

Deino, A. Kingston, J.D. Glen, J.M. Edgar, R.K. Hill, A. (2006). Precessional forcing of lacustrine sedimentation in the late Cenozoic Chemeron Basin, Central Kenya Rift. *Earth and Planetary Science Letters* **247** 41-60

Demory, F. Oberhansli, H. Nowaczyk, N.R. Gottschalk, M. Wirth, R. Naumann, R. (2005). Detrital input and early diagenesis in sediments from Lake Baikal revealed by rock magnetism. *Global and Planetary Change* **46,** 145-166

Dixon, J.L. Hartshorn, A.S. Heimsath, A.M. DiBiase, R.A. Whippler, K.X. (2012). Chemical weathering response to tectonic forcing: A soils perspective from the San Gabriel Mountains, California. *Earth and Planetary Science Letters* **323-324,** 40-49

Donges, J.F Donner R.V. Trauth, M.H. Marwan, N. Schellnhuber, H.J. Kurths, J. (2011). Nonlinear detection of palaeoclimate-variability transitions possible related to human evolution. *Proceedings of the National Academy of Sciences* USA **108** 20423-20428

deMenocal, P.B., (2004). African climate change and faunal evolution during the Pliocene-Pleistocene. *Earth and Planetary Science Letters* **220** 3-24

deMenocal, P.B. Bloemendal, J. (1995). Plio-Pleistocene climatic variability in sub-tropical Africa and the palaeoenvironment of hominid evolution. In Vrba, E.S. Denton, G.H. Partridge, T.C. Burkle, L.H. (Eds), Palaeoclimate and Evolution with an emphasis on Human Origins. Yale University Press, New Haven, Connecticut, pp. 262-288

Dosseto, A. Vigier, N. (2010). Changes in chemical weathering intensity in the Himalayas over the past 30 kyr. *American Geophysical Union*, Fall Meeting 2010, abstract #EP23C-02

Dunlop, D.J., Ozdemir, O. (1997). Rock Magnetism. Cambridge: University Press.

Duzgoren-Aydin, N.S. Aydin, A. Malpas, J. (2002). Re-assessment of chemical weathering indices: case study on pyroclastic rocks of Hong Kong *Engineering Geology* **63** 99-119

Dypvik, H. Harris, N.B. (2001) Geochemical facies analysis of fine grained siliclastics using Th/U, Zr/Rb, and (Zr+Rb)/Sr ratios. *Chemical Geology* **181,** 131-146

Evernden, J.G. Curtis, G.H. (1965). The potassium-argon dating of late Cenozoic rocks in East Africa and Italy. *Current Anthropology* **6**, 177-189

Emiliani, C. (1966). Palaeotemperature analysis of Carribean cores P6304-8 and P6304-9 and a generalised temperature curve for the past 425,000 years *Journal of Geology* **74,** 109-126

Ernst, W.G. (2000). Earth Systems Processes and Issues. Cambridge, University Press

Evans, M.E. Heller, F. (2003). Environmental Magnetism Principles and Applications of Enviromagnetics

Faith, J.T. Behrensmeyer, A.K. (2013). Climate change and faunal turnover: testing the mechanics of the turnover-pulse hypothesis with South Africa fossil data. *Palaeobiology* **39,** 609-627

Feakins, S.J. deMenocal, P.B. Eglinton, T.I. (2005). Biomarker records of late Neogene changes in northeast African vegetation. *Geology* **33,** 977-980

Feakins, S.J. Levin, N.E. Liddy, H.M. Sieracki, A. Eglinton, T.I. Bonnefille, R. (2013). Northeast African vegetation change over 12 million years. *Geology* **41,** 295-298

Feibel, C. S. Harris, J. M. Brown, F. H. (1991). Neogene paleoenvironments of the Turkana Basin. In Harris, J. M. (ed) Koobi Fora research project, Volume 3. Stratigraphy, artiodactyls and paleoenvironments: Oxford, UK, Clarendon Press, pp. 321–370.

Fedo, C.M. Nesbitt, H.W. Young, G.M. (1995) Unravelling the effects of potassium metasomatism in sedimentary rocks and paleosols, with implications for paleoweathering conditions and provenance *Geology* **23** 921-924

Ferrier, K.L. Kirchner, J.K. Finkel, R.C. (2011). Estimating millennial-scale rates of dust incorporation into eroding hillslope regolith using cosmogenic nuclides and immobile weathering tracers. *Journal of Geophysical Research Earth Surface* **116** F03022

Folk, R.L. (1965) Petrology of Sedimentary Rocks, Hemphill

Galan, E. Fernandez-Caliani, J.C. Gonzalez, I. Aparicio, P. Romero, A. (2008). Influence of geological setting on geochemical baselines of trace elements in soils. Application to soils of South-West Spain. *Journal of Geochemical Exploration* **98,** 89-106

Garrels, R. Mackenzie, E.T (1971) Evolution of sedimentary rocks Norton New York

Garzanti, E. Ando, S. France-Lanord, C. Censi, P. Vignola, P. Galy, V. Lupker, M. (2010) Mineralogical and chemical variability of fluvial sediments *Earth and Planetary Science Letters* **302:**107-120

Geissman, J.W. (1988). Paleomagnetism and Rock Magnetism of Quaternary Volcanic Rocks and Late Paleozoic Strata, VC-1 Core Hole, Valles Caldera, New Mexico, With Emphasis on Remagnetization of Late Paleozoic Strata. *Journal of Geophysical Research* **93,** 6001-6025

Gowlett, J. A. J. (1978). Kilombe - an Acheulian site complex in Kenya. In W. W. Bishop (ed.) Geological Background to Fossil Man. Edinburgh: Scottish Academic Press, 337-360.

Gowlett, J. A. J. (1988). A case of Developed Oldowan in the Acheulean? *World Archaeology* 20(1), 13-26.

Gowlett, J. A. J. and Crompton, R. H. (1994). Kariandusi: Acheulean morphology and the question of allometry. *The African Archaeological Review* **12**, 3-42

Gowlett, J.A.J. Brink, J.S. Herries, A.I.R. Hoare, S. Onjala, I. Rucina, S.M. (2015). At the heart of the African Acheulean: The Physical, social and cognitive landscapes of Kilombe. In, Settlement, Society and Cognition in Human Evolution Landscapes in Mind, Eds Coward, F., Hosfield, R., Pope, M., Wenban-Smith, F. Cambridge University Press, Cambridge, UK

Gregory, J.W. (1921). Rift Valleys and Geology of East Africa. Seeley Service. London.

Grove, M. (2011). Change and variability in Plio-Pleistocene climates: modelling the hominin response. *Journal of Archaeological Science.* **38** 3038-3047

Grove, M. (2012). Orbital dynamics, environmental heterogeneity, and the evolution of the human brain. *Intelligence* **40,** 404-418.

Grove, M. (2014). Evolution and dispersal under climatic instability: a simple evolutionary algorithm *Adaptive Behaviour* **22** 235-254

Haese R.R. Petermann, H. Dittert, L. Schulz, H.D. (1998). The early diagenesis of iron in pelagic sediments: a multidisciplinary approach. *Earth Planetary Science Letters* **157,** 233-248.

Hao, Q. Oldfield, F. Bloemendal, J. Guo, Z. (2008). Particle size separation and evidence for pedogenesis in samples from the Chinese Loess Plateau spanning the past 22m.y. *The Geological Society of America* **36,** 727-730

Harnois, L (1988). The C.I.W. index: a new chemical index of weathering *Sedimentary Geology* **55:319-322**

Harnois, L., Moore, J.M (1988). Geochemistry and origin of the ore chimmey formation, a transported paleoregolith in the Greenville Province of Southeastern Ontario, Canada *Chemical Geology* **69** 267-289

Hayashi, K., Fujisawa, H., Holland, H.D., Ohmotoe, H. (1997). Geochemistry of 1.9 Ga sedimentary rocks from northeastern Labrador, Canada. *Geochim. Cosmochim. Acta* **61,** 4115-4137

Hays, J.D. Imbrie, J. Shackleton, N.J. (1976). Variations in the Earth's orbit: pacemaker of the Ice Ages. *Science* **194** 1121

Herries, A.I.R. Latham, A.G. (2003). *The formation and sedimentary infilling of the caves of the Cave of Hearths and Historic Cave Complex, Makapansgat, South Africa. Geoarchaeology,* **19** 323-342

Heward, A.P. (1978). Alluvial fan and lacustrine sediments from the Stephanian A and B (La Magdalena, Cinera-Matallana and Sabero) coalfields, northern Spain. *Sedimentology* **25,** 451-488

Hill, T. Lewicki, P. (2006). Statistics: methods and applications: a comprehensive reference for science, industry, and data mining. StatSoft, Inc., Tulsa

Hopley, P. Marshall, J.D. Weedon, G.P. Latham, A.G. Herries, A.I.R. Kuykendall, K.L. (2007). Orbital forcing and the spread of C_4 grasses in the late Neogene: stable isotope evidence from South African speleothem. *Journal of Human Evolution* **53,** 620-634

Hopley, P. Maslin, M.A. (2010). Climate-averaging of terrestrial faunas – an example from the Plio-Pleistocene of South Africa. *Palaeobiology* **36,** 32-50

Hounslow, M.W. Maher, B.A. (1996). Quantitative extraction and analysis of carriers of magnetization in sediments. *Geophysical Journal International* **124,** 57-74

Jeans, C.V. (2006). Clay mineralogy of the Jurassic strata of the British Isles. *Clay Minerals* **41,** 187–307.

Jennings, D. J. (1971). Geology of the Kapsabet-Plateau area. *Report Geological Survey, Kenya* **63**

Jennings, D. J. (1971). Geology of the Molo area. Ministry of Natural Resources: Geological Survey of Kenya, Report No. 86.

Jenny, H. (1941). Factors in soil formation – A system of Quantitative Pedology. McGraw-Hill, New York.

Jones, W. B. (1975). The geology of the Londiani area of the Kenya Rift Valley. London: UCL: Unpublished PhD Thesis.

Jones, W. B. (1979). Syenite boulders associated with Kenyan trachyte volcanoes. *Lithos* **12,** 89-97

Jones, W. B. (1981). Chemical effects of deuteric alteration in some Kenyan trachyte lavas. *Mineralogical Magazine* **44,** 279-85

Jones, W. B. and Lippard, S. J. (1979). New age determinations and geology of the Kenya Rift-Kavirondo Rift junction, West Kenya. *Journal of the Geological Society,* London **136,** 693-704.

Joordens, J.C.A. Vonhof, H.B. Feibel, C.S. Lourens, L.J. Dupont-Nivet, G. van der Lubbe, J.H.J.L, Sier M.J. Davies, G.R. Kroon, D. (2011). Astronomically-tuned climate framework for hominins in the Turkana Basin. *Earth and Planetary Science Letters* **307**, 1-8

Karlin, R. (1990). Magnetite diagenesis in marine sediments from the Oregon continental margin. *Journal of geophysical research* **95,** 4405-4419.

King, B.C. Chapman, G.R., Robson, D.A., McConnell, R.B. (1972). Volcanism of the Kenya Rift Valley. *Philosophical Transactions of the Royal Society* **271,** 185-208

King, J.W. and Channel, J.E.T. (1991). Sedimentary magnetism, environmental magnetism, and magnetostratigraphy: *Reviews of Geophysics, Supplement,* 358-370.

Kingston, J.D. (1999). Environmental determinants in early hominid evolution: Issues and evidence from the Tugen Hills, Kenya. In P. Andrews & P. Banham (eds.) Late Cenozoic Environments and Hominid Evolution: a tribute to Bill Bishop. Geological Society. London, 69-84.

Kingston, J.D. (2007). Shifting adaptive landscapes: progress and challenges in reconstructing early hominid environments. *Yearbook of Physical Anthropology* **50** 20-58

Kingston, J.D. Deino, A.L. Edgar, R.K. Hill, A. (2007). Astronomically forced climate change in the Kenyan Rift Valley 2.7 -2.55 Ma: implications for the evolution of early hominin ecosystems. *Journal of Human Evolution* **53** 487-503

Kostka J.E. Nealson K.H. (1995) Dissolution and reduction of magnetite by bacteria. *Environmental Science Technology* **29,** 2535-2540.

Krauskopf, K.B. (1982). Introduction to geochemistry. Second edition: Singapore: McGraw-Hill International Editions

Kukla, G. Heller, F. Ming, L.X. Chun, X.T. Sheng, L.T. Sheng, Z. (1988). Pleistocene climates in China dated by magnetic susceptibility. *Geology* **16,**811-814

Leakey, M.G. Harris, J.M. (2003). *Lothagam: The Dawn of Humanity in Eastern Africa*. Columbia University Press, New York.

Lee-Thorp, J. Sponhemier, M. Luyt, J. (2007). Tracking changing environments using stable carbon stable isotopes in fossil tooth enamel: an example from the South African hominin sites. Journal of Human Evolution 53 595-601

Lepre, C.J. Quinn, R.L. Joordens, J.C.A. Swisher III, C.C. Feibel, C.S. (2007). Plio-Pleistocene facies environments from the KBS Member, Koobi Fora Formation: implications for climate controls on the development of lake-margin habitats in the northeast Turkana Basin (northwest Kenya). *Journal of Human Evolution* **53** 504-514

Leroy, S.A.G. Arpe, K. Mikolajewicz, U. (2011). Vegetation context and climatic limits of the Early Pleistocene hominin dispersal in Europe. *Quaternary Science Reviews* **30** 1448-1463

Levin, N.E. Brown, F.H. Behrensmeyer, A.K. Bobe, R. Cerling, T.E. (2011). Palaeosol carbonates from the Omo Group: isotopic records of local and regional environmental change in East Africa. *Palaeogeography, Palaeoclimatology, Palaeoecology* **307,** 75-89

Lisiecki, L.E. Raymo, M.E. (2005). A Pliocene-Pleistocene stack of 57 globally distributed benthic delta 0-18 records, *Palaeooceanography* **20** 1-17

Liu, J. Zhu, R.X. Roberts, A.P. Li, S.Q., Chang, J.H. (2004). High-resolution analysis of early diagenetic effects on magnetic minerals in post-middle-Holocene continental shelf sediments from the Korea Strait. *Journal of Geophysical Research* 109 (B03103).

Liu, Q.S. Roberts, A.P. Larrasoaña, J.C. Banerjee, S.K. Guyodo, Y., Tauxe, L. Oldfield. F. (2012). Environmental Magnetism: Principles and Applications, *REVIEW OF GEOPHYSICS*, RG4002

Lyons, R. Oldfield. F. Williams, E. (2010). Mineral magnetic properties of surface soils and sands across four North African transects and links to climatic gradients. *Geochemistry, Geophysics, Geosystems* **11**, Q08023

Lyons, R. Oldfield. F. Williams, E. (2012). The possible role of magnetic measurements in the discrimination of Sahara/Sahel dust sources. *Earth Surface Processes and Landforms* **37,** 594-606

Maher, B.A. (1998). Magnetic properties of modern soils and Quaternary loessic paleosols: paleoclimatic implications. *Palaeogeography, Palaeoclimatology Palaeoecology* **137,** 25-54

Maher, B.A. Thompson, R. (1991). Mineral magnetic record of the Chinese loess and palaeosols. *Geology* **19,** 3-6

Maher, B.A. Thompson, R. (1995). Paleorainfal reconstructions from pedogenic magnetic variations in the Chinese loess and paleosols. *Quaternary Research* **44,** 383-391

Maher, B.A. Alexseev, A. Alekseeva, T. (2003). Magnetic mineralogy of soils across the Russian Steppe: climatic dependence of pedogenic magnetite formation. *Palaeogeography, Palaeoclimatology Palaeoecology* **201,** 321-341

Maher, B.A. Watkins. S.J. Brunskill. G. Alexander J. Fielding, C. (2009). Sediment provenance in a tropical fluvial and marine context by magnetic fingerprinting. *Sedimentology* **56**, 841–861.

Maher, B.A. Possolo, A. (2013). Statistical models for use of palaeosol magnetic properties as proxies of palaeorainfall. *Global and Planetary Change* **111,** 280-287

Maslin, M.A. Christensen, B. (2007). Tectonics, orbital forcing, global climate change and human evolution in Africa. *Journal of Human Evolution* **53** 443-464

Maslin, M.A.,Trauth, M.H., (2009). Plio-Pleistocene pulsed climate variability and its influence on early human evolution. In: Grine, F.E., Leakey, R.E., Fleagle, J.G. (Eds.) The First Humans: Origins of the Genus *Homo.* Springer, New York, pp 151-158

Maslin, M.A, Pancost, R.D. Wilson. K.E. Lewis, J. Trauth, M.H. (2012). Three and half million year history of moisture availability of South West Africa: Evidence from ODP site 1085 biomarker records. *Palaeogeography, Palaeoclimatology Palaeoecology* **317-318,** 41-47

Maslin M.A. Brierley C. Milner A. Shultz S. Trauth M. Wilson K. (2014) East African climate pulses and early human evolution*. Quaternary Science Reviews.* **101,** 1–17

Maynard, J. B. (1992). Chemistry of modern soils as a guide to interpreting Precambrian paleosols. *Journal of Geology* **100,** 279–289.

McCall, G. J. H. (1964). Kilombe caldera, Kenya. *Proceedings of the Geologists' Association* **75,** 563-572.

Mclennan, S.M (1993) Weathering and global denundation *Journal of Geology* **101** 295-303

Mullins, C.E. (1977). Magnetic susceptibility of the soils and its significance in soil science: a review. Journal of Soil Science 28, 223-246

Nesbitt, H.W. Young, G.M. (1982). Early proterozoic climates and plate motions inferred from major element chemistry of lutites *Nature:* **279** 715-717

Nicholson S.E. (1996). A Review of Climate Dynamics and Climate Variability in Eastern Africa. The Limnology, Climatology and Paleoclimatology of the Eastern Africa Lakes. Gordon and Breach: New York.

Nicholson S.E. Selato, J.C. (2000). The influence of La Nina on African rainfall. *International Journal of Climatology* **20,** 1761-1776

Oldfield, F. Maher, B.A. Donoghue, J. Pierce, J. (1985). Particle-size related mineral magnetic source-sediment linkages in the Rhode River Catchment Maryland, U.S.A. *Journal of Geology* **142,** 1035-1046,

Oldfield, F. Crowther, J. (2007). Establishing fire incidence in temperate soils using magnetic measurements. *Palaeogeography, Palaeoclimatology Palaeoecology* **249,** 362-369

Owen, R.B. Potts, R. Behrensmeyer, A.K. Ditchfield, P. (2008). Diatomaceous sediments and environmental change in the Pleistocene Olorgesaille Formation, southern Kenya Rift Valley. *Palaeogeography, Paleoclimatology, Palaeoecology* **269,** 17-37

Owen, R.B. Renaut, R.W. Potts, R. Behrensmeyer, A.K. (2011). Geochemical trends through time and lateral variability of diatom floras in the Pleistocene Olorgesaille Formation, southern Kenya, Rift Valley. *Quaternary Research* **76,** 167-179

Owen, R.B. Renaut, R.W. Behrensmeyer, A.K. Potts, R. (2014) Quaternary geochemical stratigraphy of the Kedong- Olorgesaille section of the southern Kenya Rift valley *Palaeogeography, Palaeoclimatology, Palaeoecology* **396,** 194-212

Parker, A. (1970). An index of weathering for silicate rocks *Geological Magazine* **10,** 501-504

Pellenard, P. Deconinck, J. F. Huff, W. D. Thierry, J. Marchand, D. Fortwengler D. Trouiller, A. (2003). Characterization and correlation of Upper Jurassic (Oxfordian) bentonite deposits in the Paris Basin and the Subalpine Basin, France. *Sedimentology* **50,** 1035–1060.

Plummer, T. W. Bishop, L. Ditchfield, P. Hicks, J. (1999). Research on late Pliocene Oldowan sites at Kanjera South, Kenya. *Journal of Human Evolution* **36,** 151-170.

Plummer, T.W. (2004) Flaked stones and old bones: biological and cultural evolution at the dawn of technology. *Yearbook of Physical Anthropology* **47**, 118–164

Potts, R. (1996). Evolution and climate variability. *Science* **273,** 922-923

Potts, R. (1998). Variability selection in hominid evolution. *Evolutionary Anthropology* **7,** 81-96

Potts, R. (2013). Hominin evolution in settings of strong environmental variability. *Quaternary Science Reviews* **73,** 1-13

Prömmel, K. Cubasch, U. Kaspar, F. (2013). A regional climate model study of the impact of tectonic and orbital forcing on African precipitation and vegetation. *Palaeogeography, Palaeoclimatology, Palaeoecology*, **369,** 154-162

Price, J.R. Velbel, M.A. (2003). Chemical weathering indices applied to weathering profiles developed on heterogeneous felsic metamorphic parent rocks *Chemical Geology* **202,** 397-416

Reed, K.E. (1997). Early hominid evolution and ecological change through the Africa Plio-Pleistocene. *Journal of Human Evolution* **32,** 289-322

Retallack, G. J. (2001). Soils of the past: an introduction to paleopedology. Oxford, UK: Blackwell.

Ridolfi, F. Renzulli, A. Macdonald, R. Upton, B.G.J. (2006). Peralkaline syenite autoliths from Kilombe volcano, Kenya Rift Valley: Evidence for subvolcanic interaction with carbonatitic fluids. *Lithos* **91,** 373-392

Roberts, A. P. Turner, G. M. (1993) Diagenetic formation of ferrimagnetic iron sulphide minerals in rapidly deposited marine sediments, South Island, New Zealand. *Earth and planetary science letters* **115,** 257-273

Robinson, S. G. Jahota, J.T.S. Oldfield, F. (2000). Early diagenesis in North Atlantic abyssal plain sediments characterized by rock-magnetic and geochemical indices, *Marine Geology* **163,** 77– 107.

Rowan, C.J. Roberts, A.P. Broadbent, T. (2009). Reductive diagenesis, magnetite dissolution, greigite growth and palaeomagnetic smoothing in marine sediments: A new view. *Earth and Planetary Science Letter* **277,** 223-235

Rudnick, R.L. Tomascak, P.B. Njo, H.N. Gardner, L.R. (2004). Extreme lithium isotopic fractionation during continental weathering revealed in saprolites from South Carolina. *Chemical Geology* **212,** 45-57

Ruxton, B.P. (1968). Measures of the degree of chemical weathering of rocks *Journal of Geology* **76,** 518-527

Scheffler, K. Buehmann, D. Schwark, L. (2006) Analysis of late Palaeozoic glacial to postglacial sedimentary successions in South Africa by geochemical proxies- Response to climate evolution and sedimentary environment: *Palaeogeography, Palaeoclimatology, Palaeoecology*, **240,** 184-203.

Scoullos, M. Botsou, F. Zeri, C. (2014). Linking Environmental Magnetism to Geochemical Studies and Management of Trace Metals. Examples from Fluvial, Estuarine and Marine Systems. *Minerals* **4**, 716-745

Schmidt, P.W. (1993). Palaeomagnetic cleaning strategies. *Physics of the Earth and Planetary Interiors* **76,** 169-178

Sepulchre, P. Ramstein, G. Fluteau, F. Schuster, M. (2006). Tectonic uplift and Eastern Africa ardification. *Science* **313** 1419-1423

Shao, J. Yang, S. Li, Chao. (2012). Chemical indices (CIA and WIP) as proxies for integrated chemical weathering in China: Inferences from analysis of fluvial sediments *Sedimentary Geology* **265-266** 110-120

Shackleton, N. (1967). Oxygen isotope analysis and Pleistocene temperature re-assessed *Nature* **215**, 15017

Singer, M.J. Fine, P. Verosub, K.L. Chadwick, O.A. (1992). Time dependence of magnetic susceptibility of soil chronosequences on the California coast. *Quaternary Research* **37,** 322-332

Singer, M.J. Verosub, K.L. Fine, P. TenPas, J. (1996). A conceptual model for the enhancement of magnetic susceptibility in soils. *Quaternary International* **34-36,** 2443-2458

Snowball, I.F. Thompson, R. (1988). The occurrence of greigite in Freshwater sediments from Loch Lomond, *Journal of Quaternary Science* **3,** 121-125,

Snowball, I. F. (1993). Geochemical control of magnetite dissolution in subarctic lake sediments and the implications for environmental magnetism. *Journal of Quaternary science* **8,** 339-346.

Song, Y.J. Hao, G. Ge, J. Zhao, D. Zhang, Y. Li, Q. Zuo, X. Lu, Y. Wang, P. (2014). Quantitative relationships between magnetic enhancement of modern soils and climatic variables over the Chinese Loess Plateau. *Quaternary International* **334-335,** 119-131

Spiegel, C. Kohn, B.P. Belton, D.X. and Gleadow, A.J.W. (2007). Morphotectonic evolution of the central Kenya rift flanks: Implications for late Cenozoic environmental change in East Africa: *Geology* **35**, 427–430,

Stanistreet, I.G. (2012). Fine resolution of early hominin time, Beds I and II, Olduvai Gorge, Tanzania. *Journal of Human Evolution* **63,** 300-308

Strecker, M.R. Blisniuk, P.M. Eisbacher, G.H. (1990). Rotation of extension direction in the central Kenya Rift. *Geology* **18,** 299–302.

Stinchcomb, G.E. Peppe, D.J. (2014). The influence of time on the magnetic properties of late Quaternary periglacial and alluvial surface and buried soils along the Delaware River, USA. *Frontiers in Earth Sciences* **2,** 1-14

Sun, J.M. Liu, T.S. (2000). Multiple origins and interpretations of the magnetic susceptibility signal in Chinese wind-blown sediments. *Earth and Planetary Science Letters*, **180,** 287-296.

Sun, D. Bloemendal, J. Rea, D.K. Vandenberghe, J. Jiang, F. An, Z. Su, R. (2002). Grain-size distribution function of polymodal sediments in hydraulic and aeolian environments, and numerical partitioning of the sedimentary components. *Sedimentary Geology* **152,** 263-277

Thompson, R., Oldfield, F. (1986). Environmental Magnetism. Allen and Unwin, London, UK

Thompson, T. Bloemendal, J. Dearing, J.A. Oldfield, F. Rummery, T.A. Stober, J.C. (1980). Environmental applications of magnetic measurements. *Science* **207,** 481-486

Torrent, J., Liu, Q., Bloemendal, J. (2007). Magnetic enhancement and iron oxides in the upper Luochuan loess-paleosol sequence, Chinese Loess Plateau. *Soil Sci Soc Am J* **71,** 1570-1578

Trauth, M.H. Maslin, M.A. Deino, A.L. Strecker, M.R. (2005). Late Cenozoic moisture history of East Africa. *Science* **309** 2051-2053

Trauth, M.H. Maslin, M.A. Deino, A.L., Strecker, M.R. Bergner, A.G.N. Duhnforth, M. (2007). High- and low- latitude forcing of Plio-Pleistocene East African climate and human evolution. *Journal of Human Evolution* **53** 475-486

Trauth, M.H. Larrasoana, J.C. Mudelsee, M. (2009). Trends rhythms and events in Plio-Pleistocene African climate. *Quaternary Science Reviews* **28** 399-411

Trauth, M.H. Maslin, M.A. Deino, A.L. Junginger, A. Lesoloyiae, M. Odad, E.O. Olago, D.O. Olaka, L.A. Strecker, M.R. Tiedemann, R. (2010). Human evolution in a variable environment: the amplifier lakes of Eastern Africa. *Quaternary Science Reviews* **29** 2981-2988

Turner, G.M. (1997). Environmental magnetism and magnetic correlation of high resolution lake sediment records from Northern Hawke's Bay, New Zealand. *New Zealand Journal of Geology and Geophysics* **40,** 287-298

Vidic, N.J. Singer, M.J. Verosub, K.L. (2004). Duration dependence of magnetic susceptibility enhancement in the Chinese Loess-palaeosol of the past 620 ky. *Palaeogeography, Paleoclimatology, Palaeoecology* **211,** 271-288

Vrba, E.S. (1992). Mammals as a key to evolutionary theory. *Journal of Mammalogy* **73** 1-28

Vrba, E.S. (1995). The fossil record of African Antelopes (mammalian, Bovidae) in relation to human evolution and palaeoclimate. In: Vrba, E.S. Denton, G.H. Partridge, T.C. Burkle, L.H. (Eds), Palaeoclimate and Evolution with an emphasis on Human Origins. Yale University Press, New Haven, Connecticut.

Walden, J. Oldfield, F. Smith, J.P. (Eds) 1999. Environmental Magnetism: A Practical Guide, In: Technical guide, Vol 6, Quaternary Research Association, London

Wilford, J. (2012). A weathering intensity index for the Australian continent using airborne gamma-ray spectrometry and digital terrain analysis. *Geoderma* **183-184,** 124-142

Wintsch R.P. Kvale C.M. (1994). Differential mobility of elements in burial diagenesis of siliciclastic rocks. *Journal of Sedimentary Research* **A64**, 349-361.

Woodruff, L. G. Cannon, W.F. Eberl, D.D. Smith, D.B. Kilburn, J.E. Horton, J.D. Garrett, R.G. Klassen, R.A. (2009). Continental-scale patterns in soil geochemistry and mineralogy: Results from two transects across the United States and Canada. *Applied Geochemistry* **24,** 1369-1381

Wynn, J.G. (2004). Influence of Plio-Pleistocene aridification on human evolution: evidence from palaeosols of the Turkana Basin, Kenya. *American Journal of Physical Anthropology* **123,** 106-118

Xiong, S. Ding, Z. Zhu, Y. Zhou, R. Lu, H. (2010). A 6 Ma chemical weathering history, the grain size dependence of chemical weathering intensity, and its implications for provenance change of the Chinese loess-red clay deposit *Quaternary Science Reviews* **xxx:1-12**

Young, G.M. Nesbitt, H.W. (1998). Processes controlling the distribution of Ti and Al in weathering profiles, siliclastic sediments and sedimentary rocks. *Journal of Sedimentary Petrology* **68,** 448-455

Zabel, M. Schneider, R.R. Wagner, T. Adegbie, A.T. de Vries, U. Kolonic, S. (2001). Late Quaternary Climate Changes in Central Africa as Inferred from Terrigenous Input to the Niger Fan. *Quaternary Research*, **56,** 207-217.

Zhang, W. Yu, L., Hutchinson, S.M. (2001), Diagenesis of magnetic minerals in the intertidal sediments of the Yangtze Estuary, China, and its environmental significance. *The Science of the Total Environment* **266,** 169-175

Zhang, C.S. Wang, L.J. Li, G.S. Dong, S.S. Yang, J.R. Wang, X.L. (2002) Grain size effect on multi-element concentrations in sediments from the intertidal flats of Bohai Bay, China *Applied Geochemistry* **17** 59-68

Zheng, H. Oldfield, F. Yu, L. Shaw, J. An, Z. (1991). The magnetic properties of particle-sized samples from the Luo Chuan loess section: Evidence for pedogenesis. *Physics of the Earth and Planetary Interiors* **68, 250-258**

Zhou, L.P. Oldfield, F. Wintle, A.G. Robinson, S.G. Wang, J.T. (1990). Partly pedogenic origin of magnetic variations in Chinese loess. *Nature* **346,** 353-362

Appendix 1 Environmental magnetism

Depth cm	Sample	XLf 10-8m3kg-1	Xfd 10-8m3kg-1	Xfd%	Xarm 10-8m3kg-1	SIRM 10-5Am2kg-1	HIRM
0	144	204.36311	14.80562448	7.244763736	758.6064628	1643.219603	18.04652605
10	143	230.7983605	15.4593246	6.698195155	1060.98002	2113.704892	18.65944935
20	142	261.9535519	18.78415301	7.170795306	1226.094915	2378.183462	28.31424783
30	141	255.1765901	18.69432724	7.326035367	1211.168359	2321.69128	25.45241444
40	140	617.3555418	40.59322	9.1	2065.628885	2978.040716	26.92843924
50	139	455.3926271	35.42551734	7.779115257	2405.184068	3161.500617	25.27682609
60	138	447.6327945	38.24511	7	2518.346641	3344.431871	51.01616628
70	137	442.249523	40.34622365	9.122954701	2127.486167	2490.643585	25.08865001
80	136	369.8412698	32.97563157	8.916157892	1904.696184	2236.489604	20.2629108
90	135	478.8881386	40.67071798	8.492738638	2540.401196	3126.740041	35.48075625
100	134	410.960183	34.86906596	8.484779646	2188.448896	2672.996779	52.69149979
110	133	408.7982833	34.09632809	8.340624089	1945.852294	2600.782546	47.64377682
120	132	333.171521	26.34843581	7.908369759	1603.416963	2477.446602	29.01213592
130	131	329.461585	26.92075015	8.171134778	1503.334732	2391.036298	43.98366606
140	130	316.2443363	23.6616882	7.48209074	1473.842193	2486.001007	93.14985736
150	129	274.8836958	20.82657146	7.576503001	1282.320806	2056.062967	45.29779292
160	128	176.2751881	10.21248559	5.793490111	742.9283214	1817.850437	13.66908252
170	127	148.2242308	5.226878481	3.526331999	519.0231492	2696.669406	34.4604218
180	126	112.0978352	6.159550293	5.494798613	330.4191391	1000.743811	25.54781127
190	125	178.4434204	13.56886841	7.604017217	498.0393519	1123.034477	24.29117597
200	124	400.0494805	27.90147892	6.974506975	2329.037568	2965.083292	67.05591291
210	123	493.0987452	37.9705401	7.700392764	2943.763416	3266.454992	29.45826514
220	122	363.4754284	29.74082991	8.182349503	2113.563142	2378.318935	60.94108483
230	121	335.9450671	24.37041649	7.254286156	1851.819548	2497.753217	73.45994188
240	120	478.8611926	31.0536238	6.48489046	3120.229078	4201.308127	46.62913699
250	119	471.233068	31.07107946	6.593569418	3282.61937	4201.308127	46.62913699
260	118	474.1821615	31.03066125	6.544038087	2968.225873	5080.176087	260.4549932
270	117	464.0394089	27.85987958	6.003774475	2461.890734	4550.998358	95.15051998
280	116	449.5700556	27.5838813	6.135613561	2410.528871	3906.70612	37.23115832
290	115	458.5782256	29.28711367	6.386503335	2219.89611	3791.5917	55.41501739
300	114	454.6198456	29.72569111	6.538581938	2317.324964	3817.056249	63.06489487
310	113	426.3746169	23.6704525	5.551562302	2079.221146	4502.422931	68.36668469
320	112	664.3372703	29.47834646	4.437256161	2932.207791	7727.468504	141.3090551
330	111	495.9467384	26.80327021	5.404465466	2449.900855	5131.421919	45.42533375
340	110	475.8369083	29.02137645	6.09901753	2315.855485	4469.773402	80.46914531
350	109	454.77525	30.73597831	6.758498469	2263.722724	3577.35905	59.81591384
360	108	439.9376261	29.97615116	6.813727534	2506.515793	3884.500826	72.88552559
370	107	394.1040668	25.71479311	6.524873828	2016.031141	3463.714438	65.38252531
380	106	416.1460836	25.02002243	6.012317167	1850.05397	3813.829889	70.35896204
390	105	483.8466722	30.28501209	6.259216779	2164.452301	4223.824474	69.9405399
400	104	501.6164613	34.32603073	6.843082989	2295.113174	3962.603834	17.49201278
410	103	369.4071216	22.94798457	6.212112118	1748.134714	3353.621125	8.576559798
420	102	327.2601696	22.81604268	6.971836111	1311.653653	2231.896256	14.10831666
430	101	267.3584257	19.03411532	7.11932503	1092.089735	1905.257798	26.33539572
440	100	220.6282295	17.49614722	7.930148947	695.5268592	1598.615719	19.30038075

450	99	234.9979449	18.13604603	7.717533887	867.8182063	1572.97575	26.48325113
460	98	305.6670383	16.81531029	5.501185338	827.0306381	3089.481605	17.22073579
470	97	290.645838	17.06375965	5.870980215	770.1602246	2917.552259	42.25162958
480	96	352.7698458	16.50485437	4.678646592	871.6338689	4376.355226	13.03255283
490	95	371.7843137	15.84313725	4.261378619	921.6693763	5221.341176	16.89529412
500	94	335.224479	15.09134234	4.501861672	897.1296115	5016.295246	14.29252241
510	93	332.4282114	15.56454762	4.682077839	1024.676947	5357.944841	15.56064317
520	92	339.1207979	21.69273078	6.396756233	1002.737799	3867.037311	18.14493289
530	91	233.6410256	18.83076923	8.059701493	700.7539235	1435.876923	18.28123077
540	90	293.8404964	22.92576419	7.80211185	1583.824085	2557.367272	17.16099747
550	89	291.5784521	24.17078335	8.289632916	1436.226947	2123.807339	9.271936015
560	88	246.9223485	19.72064394	7.986577181	1257.647256	1912.987216	19.55539773
570	87	309.6573209	22.74143302	7.344064386	1665.889863	2841.648865	29.75033378
580	86	361.5675286	22.82087208	6.311648661	1948.357889	4182.360209	40.3642848
590	85	378.4871471	16.77201854	4.431331069	2588.378047	8301.276865	62.98482933
600	84	301.9314794	12.90375271	4.273735461	1856.864871	5626.060272	48.48523827
610	83	151.9196367	52.95628641	4	351.6960404	824.559378	31.58105133
620	82	159.3356092	27.79236695	8	436.4330845	533.7312237	13.79313288
630	81	159.1532732	15.48412387	9.729064039	425.2779315	554.6946296	14.43041944
640	80	237.6205186	12.70710475	5.347646248	1243.159422	3921.189273	51.57469812
650	79	194.3438284	14.00111452	7.204301075	853.7062227	2344.94706	22.08832544
660	78	158.095364	12.53745814	7.930313589	638.088147	1206.610788	16.98248281
670	77	318.2229034	26.5071131	8.329731399	2394.82309	3323.699599	56.28566376
680	76	472.447842	39.01895206	8.258890949	1430.466355	2023.973961	41.98399427
690	75	422.6000934	35.91899121	8.499522781	1957.025927	2078.176029	27.96586422
700	74	167.0456572	12.70733012	7.60709996	655.2661986	1454.594703	25.50963082
710	73	263.2785117	16.85090321	6.400409626	976.3689369	3068.364788	51.62038285
720	72	411.8723969	19.81784063	4.811645738	3407.5913	5093.649595	20.33914596
730	71	427.6755098	16.2425555	3.797868974	3309.038084	7697.365999	32.80454792
740	70	174.5744959	8.929039015	5.114744263	995.1450102	2458.69128	18.6410055
750	69	109.4223485	9.138257576	8.351363046	331.2196637	576.7913352	18.8634233
760	68	129.9061544	9.462332141	7.283975254	441.6934181	806.7035309	9.894929227
770	67	127.9883519	10.66178197	8.330275229	424.773402	805.7690573	22.35895449
780	66	114.1200131	9.938730649	8.709016393	304.8046815	578.0098218	16.90423741
790	65	70.9668353	5.143338954	7.247524752	143.6831925	355.4112985	24.43389545
800	64	67.06790123	4.598765432	6.85687989	146.9763866	434.3198148	13.88333333
810	63	61.62690737	3.814743176	6.190061029	128.4674501	353.3122179	1.612508059
820	62	127.3455776	8.361953113	6.566347469	335.9966549	866.3544871	2.864790205
830	61	535.0583343	35.40487467	6.61701209	2653.463111	5825.157676	35.85479958
840	60	91.6296766	8.164235891	8.910034602	225.0906562	403.6423589	2.092343056
850	59	103.8632686	8.217030744	7.911392405	314.1130409	979.370449	3.322132888
860	58	205.0939041	14.79383066	7.213198619	965.8302925	1807.636135	36.77683349
870	57	348.6303992	24.78159479	7.108271352	1870.960735	3069.751488	19.97337371
880	56	57.76381252	3.063629222	5.303717135	222.2078578	403.7475255	2.043126473
890	55	51.22701012	2.252610378	4.397309881	128.4334297	349.4431547	1.909763078
900	54	154.1281346	12.72598517	8.256756757	505.2055139	749.4117721	24.77074481
910	53	558.9145393	38.10919751	6.818430158	1947.090405	2869.412483	72.17112495
920	50	88.362736	8.024936994	9.081811359	258.1722447	419.5925189	13.81900783
930	49	85.89577017	6.92940667	8.067226891	324.1731974	458.8185362	15.29074635
940	48	92.33351987	7.321395262	7.929292929	314.3640348	546.6561276	12.25440683

950	47	80.92072871	6.425406204	7.940371159	249.8040424	450.0453471	9.499113737
960	46	95.75576097	6.509569067	6.798096533	409.583067	820.9566463	22.59835959
970	45	65.39029385	5.42934705	8.302986162	204.3761097	334.1518788	9.142591799
980	44	348.7731399	21.60383716	6.194237654	2203.840884	5019.400642	72.86003092
990	43	433.6564044	28.65830483	6.608527981	3376.049289	6004.964652	121.222919
1000	42	457.4273198	28.11628833	6.146613268	3226.845098	6567.013142	127.8375149
1010	40	753.0443655	30.55884676	4.05804069	4467.705332	2042.602686	46.14830174
1020	39	296.3143565	16.57930026	5.595172792	1553.629417	5003.869316	114.6098988
1030	38	188.1277868	12.88647165	6.849850241	997.2676849	2502.778186	44.16948405
1040	37	412.6874597	20.30238906	4.919555605	3355.807467	6071.692888	91.60272334
1050	36	157.0300475	10.1385264	6.456424462	966.6301039	1802.679181	31.10319213
1060	35	383.2789132	24.54952231	6.40513252	2254.998538	4313.432096	62.06494135
1070	34	331.424817	23.543583	7.103747758	1978.73637	3233.449409	89.75032852
1080	33	132.0146849	8.091706001	6.129398411	687.346318	1306.602607	14.6797033
1090	32	97.69839367	6.253496364	6.400817996	450.8100018	743.0275713	18.22464637
1100	31	81.09634852	5.513376717	6.798551128	299.1344671	529.0939534	12.85208785
1110	30	112.5769569	8.043828789	7.145182292	487.1122046	792.1911829	12.55738786
1120	29	102.1872717	6.596192686	6.455004205	468.5863247	939.4789223	18.50837953
1130	28	62.20458783	2.623476866	4.217497386	232.7838621	568.4862755	8.323077924
1140	27	105.5283044	6.076273808	5.757956449	388.4351161	811.3419064	12.67274294
1150	26	450.737302	34.58947752	7.67397714	2677.118525	3164.834517	20.5412343
1160	25	482.4984912	35.25447596	7.30664999	2903.780368	3514.090223	37.20956548
1170	24	525.9140475	28.50117597	5.419360085	3229.781041	3680.896729	44.57601026
1180	23	639.9322823	47.26131274	7.385361552	4462.141147	4583.302296	23.36313618
1190	22	457.4894401	23.5748583	5.153093434	4800.237242	5029.401061	16.53200477
1200	21	771.1644685	30.60534325	3.968718024	8067.102506	10215.59351	13.69969564
1210	20	573.0596218	39.91308326	6.964909363	3944.913267	4446.310613	48.54300091
1220	19	503.6259199	32.29222761	6.411947108	3894.95945	4516.855143	26.50188476
1230	18	370.5388383	18.01959412	4.863078376	2651.073187	4225.383718	19.13226032
1240	17	294.0935193	14.9029259	5.067410507	1988.89237	2971.259229	31.23923298
1250	16	352.4466943	21.35296825	6.058495822	2189.271253	2862.014726	277.3515877
1260	15	409.8844067	26.834159	6.54676259	2382.026907	2301.972163	20.01651333
1270	14	452.3253726	30.13706829	6.662696837	3318.450756	3670.21907	80.48662237
1280	13	415.4899444	28.02738554	6.745623069	3140.732316	3766.69448	27.07225381
1290	12	289.9432979	17.97484385	6.199434159	1956.465472	2712.537777	32.49417149
1300	11	412.2047954	24.15720209	5.860485458	2758.228677	4042.167658	23.94104922
1310	10	418.7848436	20.53607988	4.903730445	3418.157356	5700.185203	16.66824152
1320	9	339.4071914	17.96343537	5.292591267	2695.57289	4705.297012	522.7819789
1330	8	360.2540242	19.96604303	5.542212353	2801.613366	4714.770301	29.7962582
1340	7	395.2933266	22.7433182	5.753529512	2954.34814	4924.274332	50.5128593
1350	6	365.3259267	23.54010218	6.443589262	2549.765337	3407.874704	33.78664746
1360	5	336.1314325	17.66397799	5.255080686	2644.630251	4330.18852	38.86888014
1370	4	368.090253	25.25973511	6.862375438	2901.770929	3379.916726	36.23602189
1380	3	524.9176277	30.68369028	5.84542958	4348.6882	6593.5729	36.43842669
1390	2	530.6391654	25.10293001	4.730696798	3569.512932	10476.36407	149.8453052
1400	1	457.5010964	21.88733405	4.784105268	3297.438935	9592.759239	119.468963
1405	K50	339.7	14.09	4.15	2157.92	5035.57	121.9785257
1410	K48	667.75	23.43	3.51	3443.61	14995.2	275.208931
1415	K47	138.38	7.25	5.24	581.67	1410.47	33.26388889
1420	K46	85.85	5.25	6.12	243.2	769.54	52.81036217

1425	K45	142.82	8.45	5.92	708.71	1751.24	34.1260889
1430	K44	85.47	4.78	5.59	438.21	710.63	18.3464449
1435	K43	43.56	2.41	5.54	187.73	304.56	15.27444706
1440	K42	41.98	2.62	6.24	172.45	285.01	14.6235582
1445	K41	28.77	0.99	3.43	92.4	206.42	11.68349723
1450	K40	30.34	1.75	5.76	106.98	215.56	10.74413111
1455	K39	19.27	1.17	6.09	100.7	235.48	16.5055389
1460	K38	19.96	1.12	5.59	86.27	188.79	12.74126559
1465	K37	18.06	0.38	2.11	68.48	152.38	10.04127192
1470	K36	18.69	0.19	1.01	58.66	141.35	11.12207806
1475	K35	27.23	3.48	12.76	111.82	241.47	8.866100964
1480	K34	19.19	0.13	0.69	63.76	152.1	10.05422167
1485	K33	19.68	0.17	0.87	65.43	153.56	6.808536836
1490	K32	26.51	0.64	2.4	83.62	196.7	6.061895674
1495	K31	27.27	0.75	2.77	100.56	215.19	9.789675553
1500	K30	25.49	0.5	1.98	85.25	192.43	5.443689929
1505	K29	26.57	0.81	3.07	79.05	170.91	4.934741986
1510	K28	24.93	0.65	2.61	77.77	178.66	9.39368409
1515	K27	19.58	0.34	1.76	56.33	135.81	7.554827052
1520	K26	18.36	0.32	1.76	56.36	128.71	8.840245525
1525	K25	19.17	0.5	2.6	67	146.37	8.523260777
1530	K24	18.03	0.43	2.38	61.74	156.17	11.50241416
1535	K23	22.48	0.42	1.88	53.38	143.93	13.89646415
1540	K22	20.75	0.38	1.83	58.32	139.68	11.63008735
1545	K21	21.24	0.34	1.62	62.5	154.21	13.03762086
1550	K20	23.31	0.37	1.57	68.67	186.49	17.10737402
1555	K19	23.42	0.29	1.22	62.5	164.27	13.95633562
1560	K18	25.37	0.55	2.15	58.8	166.3	25.96143356
1565	K17	33.98	0.7	2.06	97.14	235.67	25.04911543
1570	K16	30.29	0.64	2.1	93.44	256.48	32.86255924
1575	K15	27.32	0.43	1.57	66.97	222.7	33.10893568
1580	K14	25.56	0.38	1.49	61.53	212.81	31.50906375
1585	K13	29.08	0.3	1.04	76.77	237.65	32.50629235
1590	K12	32.27	0.59	1.82	96.77	297.44	39.10696342
1595	K11	32.3	0.53	1.65	88.89	280.01	34.39688015
1600	K10	31.19	0.42	1.34	89.25	280.65	34.93743058
1605	K9	31.48	0.58	1.85	95.81	270.79	32.04852142
1610	K8	26.73	0.35	1.31	76.49	243.86	34.07087518
1615	K7	32.29	0.7	2.18	107.62	300.18	34.9361225
1620	K6	33.48	0.46	1.36	108.33	314.45	35.86089637
1625	K5	37.91	0.88	2.33	147.92	344.77	31.84758631
1630	K4	36.25	0.65	1.79	125.06	351.26	39.00845499
1635	K3	35.46	0.66	1.87	104.82	289.87	26.99549948
1640	K2	34.54	0.26	0.75	113.84	293.67	18.51647829
1645	K1	37.74	0.44	1.17	135.25	319.57	29.28499835
1650	KL63	163.21	7.78	4.76	1530.925429	1974.54	20.10566616
1655	KL61	232.39	11.88	5.11	2329.302516	3002.84	15.96812345
1660	KL59	257.67	12.64	4.9	2300.716712	3667.15	8.851123037
1665	KL57	325.99	15.64	4.8	2711.992535	466.77	5.943276307
1670	KL53	131.81	7.01	5.32	1138.395366	1499.74	12.72732613

1675	KL51	61.91	2.09	3.37	387.4905091	650.66	35.82359186
1680	KL49	77.04	3.08	4	564.5456661	872.05	33.79079458
1685	KL47	86.66	3.94	4.55	692.261904	834.75	13.36200354
1690	KL46	67.85176825	2.01279158	2.966454128	569.4259957	795.5141084	64.88702032
1695	KL45	81.95	3.92	4.79	949.0501587	938.46	30.03829564
1700	KL43	78.32	3.41	4.35	906.6594796	888.99	36.04500489
1705	KL41	126.69	6.66	5.26	1434.692982	1509.62	66.44428673
1710	KL40	102.6431537	5.117770379	4.98598318	1284.660136	1053.94278	70.50468615
1715	KL39	102.3481079	5.050505054	4.934634509	1359.163382	1191.543419	72.00299638
1720	KL37	81.0326348	3.511106176	4.332953241	1033.489741	925.0083158	57.35929704
1725	KL35	167.81	10.32	6.15	1280.069712	1540.01	26.89943527
1730	KL33	101.51	6.21	6.11	1261.336478	1082.65	31.81679909
1735	KL31	108.5387233	6.617166825	6.096595411	1431.25652	1161.494277	64.94637517
1740	KL30	92.88726578	4.586757102	4.937982686	1140.126418	933.6362332	20.85007174
1745	KL29	80.86372847	3.292806484	4.072043853	951.4331727	836.7949595	66.89368034
1750	KL28	98.30426857	4.74667217	4.828551434	1182.189583	1200.310597	79.6501909
1755	KL27	113.3772148	6.465875436	5.702976076	1365.738386	1277.628403	61.73282138
1760	KL26	109.76	5.47	4.99	1396.082316	1063.13	11.29490479
1765	KL25	103.4574976	4.46991404	4.320531758	1431.820708	1188.03553	42.28326648
1770	KL23	127.29	6.99	5.49	1650.363737	1469.4	52.3220526
1775	KL20	107.72	4.77	4.43	1382.950671	1212.1	23.93147032
1780	KL17	86.54244306	4.986197381	5.761563002	997.7406442	896.092236	12.26614907
1785	KL16	91.82905983	5.145299138	5.60312732	1182.350599	915.1695385	16.39712821
1790	KL15	100.24	4.24	4.23	1279.554202	1100.23	49.72234111
1795	KL13	93.74544128	4.285193282	4.57109511	1265.008164	979.0038293	14.47592998
1800	KL11	107.54	5.17	4.8	1352.39875	1133.43	23.85253756
1805	KL9	108.9829964	5.405838884	4.960258995	1539.671408	1202.795958	15.78296439
1810	KL7	120.72	5.94	4.92	1287.754723	1293.97	61.08258929
1815	KL5	102.82	4.77	4.64	1390.353992	1206.92	39.80518113
1820	KL4	102.275704	4.911591385	4.802305134	1145.440735	1109.061886	24.06286837
1825	KL3	98.6	4.76	4.83	1298.479859	1114.31	25.88132483
1830	KL1	93.29	4.38	4.69	1229.505282	1032.29	31.62471216

Depth cm	Sample	SOFT	S-ratio (-300)	S-ratio	Xarm/SIRM 10-3mA-1	Xarm/XLf	Xarm/Xfd
0	144	485.9669355	-0.978035162	-0.857831453	0.461658601	3.712051861	51.23772143
10	143	709.0956963	-0.982344319	-0.832678881	0.501952768	4.596999814	68.63042518
20	142	735.5981196	-0.97618834	-0.836117248	0.515559432	4.680581371	65.27283476
30	141	748.2035865	-0.978074247	-0.837485808	0.521675026	4.746392915	64.78801531
40	140	902.6606416	-0.981915332	-0.856755722	0.693620095	3.34593074	67.50478391
50	139	1123.629779	-	-	0.760772924	5.281561282	67.89411273

			0.984009602	0.872153977			
60	138	1155.490185	-0.969491879	-0.833949642	0.752996843	5.625920782	52.73701641
70	137	892.6286472	-0.979853681	-0.855049304	0.854191334	4.810601384	52.73073847
80	136	694.0507042	-0.981879718	-0.879292486	0.851645445	5.150036892	57.76071885
90	135	1031.776705	-0.977304953	-0.889925545	0.812475985	5.30479039	62.46265917
100	134	897.7251085	-0.960574962	-0.870191907	0.818724853	5.325209076	62.76190188
110	133	905.1135908	-0.963361968	-0.863785908	0.748179542	4.759932647	57.0692624
120	132	800.5516181	-0.976579002	-0.853463805	0.647205458	4.812587098	60.85435108
130	131	784.1283122	-0.963209537	-0.856325918	0.628737729	4.563004612	55.84297329
140	130	791.3260614	-0.925060483	-0.858751269	0.592856636	4.660454035	62.28812502
150	129	694.1815157	-0.955937349	-0.841630977	0.623677789	4.664957672	61.57138289
160	128	500.0873826	-0.984961268	-0.816185869	0.408685064	4.214593838	72.74706192
170	127	756.7756779	-0.974442235	-0.71600999	0.192468216	3.501607978	99.29887428
180	126	333.0871905	-0.948942355	-0.779202624	0.330173553	2.947596076	53.64338684
190	125	386.0068271	-0.956740106	-0.857717468	0.443476458	2.791021103	36.70456054
200	124	951.8867722	-0.954769626	-0.89297948	0.785488075	5.821873747	83.47362428
210	123	1156.209329	-0.981963159	-0.909386393	0.901210463	5.969926804	77.52756238
220	122	877.6106784	-0.948752807	-0.873945041	0.888679441	5.81487214	71.06604451
230	121	821.5105853	-0.941179183	-0.876063378	0.74139412	5.512268908	75.9863726
240	120	1498.037285	-0.977802563	-0.886915296	0.742680371	6.515936406	100.4787428
250	119	1498.037285	-0.977802563	-0.886915296	0.781332688	6.966020836	105.648707
260	118	1900.407585	-0.897462218	-0.887016735	0.584276179	6.259674264	95.65461235
270	117	1727.351396	-0.958184771	-0.844853328	0.54095619	5.305348398	88.36688353
280	116	1466.236216	-0.980939873	-0.874842916	0.617023343	5.36185371	87.38903871
290	115	1419.082164	-0.970769523	-0.868766391	0.585478682	4.840823193	75.79770868
300	114	1319.760914	-	-	0.60709741	5.097280698	77.95697518

			0.966956266	0.863401376			
310	113	1510.965387	-0.969631158	-0.856730467	0.461800497	4.876512494	87.84036328
320	112	3467.913533	-0.963426818	-0.865506754	0.379452571	4.413733689	99.469887
330	111	2180.855169	-0.982295226	-0.874626424	0.477431186	4.939846691	91.40305776
340	110	1648.106369	-0.963994083	-0.864937144	0.51811474	4.866910162	79.79826486
350	109	1362.040554	-0.966558619	-0.893042756	0.632791591	4.97767353	73.65058307
360	108	1373.686846	-0.962473672	-0.884343434	0.645260718	5.697434464	83.6169987
370	107	1134.901438	-0.962247162	-0.870026296	0.582043115	5.115479162	78.39966407
380	106	1390.751562	-0.963103251	-0.887373655	0.485090847	4.445683963	73.94293812
390	105	1557.144548	-0.966882838	-0.87147131	0.512438979	4.473426036	71.46942172
400	104	1901.473129	-0.991171455	-0.889725543	0.579193195	4.575434324	66.86217793
410	103	1531.322336	-0.994885195	-0.890286749	0.521267802	4.732271284	76.17813706
420	102	1063.66349	-0.987357552	-0.877383744	0.587685762	4.007984395	57.48821876
430	101	667.4828564	-0.972355032	-0.897864081	0.573197882	4.084740294	57.37538709
440	100	566.7396655	-0.975853633	-0.886558775	0.435080708	3.152483527	39.75314396
450	99	564.6777127	-0.966327197	-0.907724618	0.551704758	3.692875725	47.85046336
460	98	1406.064994	-0.988852022	-0.958875099	0.267692365	2.705658558	49.1831922
470	97	1315.266521	-0.971036248	-0.960083404	0.263974783	2.649823682	45.13426352
480	96	2388.211136	-0.994044106	-0.946460119	0.199168903	2.470828727	52.81075794
490	95	2963.101235	-0.99352837	-0.95778975	0.176519661	2.479043204	58.17467598
500	94	2806.207931	-0.994301563	-0.953396635	0.178843064	2.676205551	59.4466411
510	93	2893.112342	-0.994191563	-0.920992057	0.1912444	3.082400685	65.83403334
520	92	1893.267553	-0.990615589	-0.927159766	0.259303885	2.95687497	46.22459982
530	91	760.7705908	-0.974536493	-0.876609094	0.488032026	2.999276011	37.2132394
540	90	1108.523098	-0.986579169	-0.841039066	0.619318196	5.390081027	69.08489818
550	89	929.1806634	-0.991268571	-0.839472636	0.676251052	4.925696453	59.41995867

560	88	829.5723011	-0.979555119	-0.81913847	0.657425855	5.093290518	63.77313337
570	87	1133.98004	-0.979061217	-0.823585378	0.586240574	5.379785172	73.25351316
580	86	1663.91396	-0.980697844	-0.82786911	0.465851288	5.388641776	85.3761365
590	85	2902.873578	-0.984825267	-0.732653347	0.311804809	6.838747543	154.3271635
600	84	2031.44861	-0.982764053	-0.781087774	0.330047099	6.149954533	143.9011513
610	83	331.8423008	-0.923398964	-0.815981715	0.426526033	2.315013701	26.64125195
620	82	238.9185793	-0.948314312	-0.853204399	0.817701991	2.739080653	25.70334349
630	81	200.0289429	-0.947969861	-0.82833743	0.766688388	2.672128087	27.46541781
640	80	1113.235748	-0.973694359	-0.736852998	0.317036321	5.231700654	97.83183875
650	79	654.2275007	-0.981160918	-0.799479326	0.364062045	4.392762198	60.97416185
660	78	394.330513	-0.971850935	-0.813010885	0.528826821	4.03609651	50.8945386
670	77	1287.201073	-0.966130715	-0.882262176	0.720529343	7.525615109	90.34643194
680	76	750.8532011	-0.958513306	-0.868508225	0.706761244	3.027776249	36.66080915
690	75	770.0760413	-0.973086145	-0.894954939	0.941703638	4.63091693	54.48443458
700	74	378.483748	-0.964925445	-0.718930806	0.450480259	3.922677246	51.56600106
710	73	791.4228903	-0.966353164	-0.719076777	0.318204974	3.708502188	57.94163819
720	72	1976.192915	-0.99201392	-0.811610896	0.668988166	8.273415081	171.9456404
730	71	2352.066865	-0.991476422	-0.790599798	0.429892262	7.737263435	203.7264447
740	70	724.6330715	-0.984836644	-0.844965069	0.404745817	5.700403171	111.4504045
750	69	169.0212358	-0.934591863	-0.808080607	0.574245214	3.026983685	36.24538496
760	68	273.8475657	-0.975468239	-0.844931943	0.547528802	3.40009617	46.67912852
770	67	266.8745244	-0.944502822	-0.794806999	0.527165195	3.318844221	39.84075111
780	66	167.4357373	-0.941508823	-0.837632505	0.527334779	2.670913481	30.66837127
790	65	96.32963744	-0.862503553	-0.793875846	0.404273002	2.024652669	27.93578137
800	64	114.8040741	-0.936068616	-0.691983676	0.338405897	2.191456477	31.95996594

810	63	110.7542795	-0.99087205	-0.762617196	0.363608852	2.084599983	33.67656593
820	62	276.0403166	-0.993386563	-0.807320472	0.387828146	2.638463472	40.18159996
830	61	2207.719187	-0.987689672	-0.873442321	0.455517817	4.9592034	74.94626477
840	60	124.5052711	-0.989632688	-0.838987957	0.557648748	2.456525708	27.57032736
850	59	268.9215716	-0.993215779	-0.737108059	0.320729547	3.024293816	38.22707383
860	58	628.1868901	-0.959309473	-0.861972258	0.534305701	4.709210138	65.28601786
870	57	1130.988671	-0.986986977	-0.849485748	0.609482801	5.366602392	75.4979956
880	56	145.3613197	-0.989879188	-0.850977468	0.550363392	3.846835036	72.53092385
890	55	116.3719033	-0.989069678	-0.808046603	0.367537403	2.507142801	57.01537688
900	54	273.8560985	-0.933892832	-0.808022054	0.67413608	3.277827991	39.69873508
910	53	1045.845304	-0.949696235	-0.835240517	0.678567622	3.483699686	51.09240111
920	50	155.2846531	-0.934131295	-0.753165673	0.615292774	2.921732128	32.17124881
930	49	176.6944132	-0.933347303	-0.771599403	0.706539017	3.774029813	46.78224456
940	48	204.6279029	-0.95516594	-0.80420054	0.575067248	3.404657758	42.93772205
950	47	163.1957903	-0.957785971	-0.786524056	0.55506416	3.087021661	38.87754866
960	46	299.2143601	-0.944946278	-0.79793183	0.498909496	4.277372587	62.92015075
970	45	129.0716602	-0.945278825	-0.829317976	0.611626397	3.125480827	37.64285242
980	44	1828.449281	-0.970968633	-0.812047866	0.43906455	6.318837753	102.0115486
990	43	2240.04447	-0.959625768	-0.837360724	0.562209686	7.785078819	117.8035236
1000	42	486.1971326	-0.96106677	-0.830804917	0.491371804	7.054334007	114.7678193
1010	40	216.5388033	-0.954814216	-0.765336329	0.218726107	5.932858058	146.2000633
1020	39	2155.149701	-0.95419149	-0.798491427	0.31048561	5.243179694	93.70898611
1030	38	100.4674408	-0.964703637	-0.821644035	0.398464271	5.301012158	77.38873073
1040	37	2767.707517	-0.969826299	-0.854538109	0.552697168	8.131595442	165.2912599
1050	36	384.5171652	-0.96549226	-0.801218267	0.536218599	6.155701531	95.34226827
1060	35	1497.535978	-	-	0.522785218	5.883440129	91.85508825

			0.971222479	0.774867619			
1070	34	1430.051812	-0.944486326	-0.813336286	0.611958352	5.970392888	84.04567689
1080	33	549.7725893	-0.977529965	-0.818639016	0.526056135	5.206589845	84.94454913
1090	32	310.412491	-0.950944899	-0.831139357	0.606720422	4.614303111	72.08927224
1100	31	134.9236036	-0.951418504	-0.829756442	0.565371169	3.688630531	54.25612695
1110	30	253.2582454	-0.968297077	-0.839943706	0.614892232	4.32692638	60.55725667
1120	29	363.2091015	-0.960598627	-0.775601445	0.498772579	4.585564492	71.03890789
1130	28	198.185508	-0.970718456	-0.793962591	0.409480179	3.742229797	88.73105195
1140	27	33.10592602	-0.968761029	-0.580495566	0.478756382	3.68086191	63.92653266
1150	26	1367.061169	-0.987019078	-0.783436633	0.845895263	5.939420841	77.39690558
1160	25	1257.565932	-0.978822646	-0.780630954	0.826324933	6.018216473	82.36628936
1170	24	1303.720654	-0.975779809	-0.808057063	0.877444079	6.141271671	113.3209747
1180	23	2207.220188	-0.989805108	-0.844189516	0.973564661	6.97283333	94.41424473
1190	22	2460.135384	-0.993425855	-0.853801733	0.954435167	10.49256403	203.6168015
1200	21	4573.688705	-0.997317886	-0.868706325	0.789685151	10.46093646	263.5847747
1210	20	2064.281507	-0.978164818	-0.816384309	0.887232947	6.883949099	98.83759773
1220	19	1931.769036	-0.988265338	-0.84022485	0.862316662	7.733834371	120.6160039
1230	18	1914.83205	-0.990944131	-0.936333168	0.627415961	7.154643219	147.1216926
1240	17	1270.192217	-0.978972395	-0.903244855	0.669376926	6.76278884	133.4565027
1250	16	1330.575978	-0.806184374	-0.707496095	0.764940597	6.211637925	102.5277248
1260	15	1022.278014	-0.982609248	-0.881516408	1.034776591	5.811460179	88.76845767
1270	14	1535.178668	-0.956140699	-0.871008026	0.904156044	7.336424082	110.1119301
1280	13	1520.11865	-0.985625458	-0.868066779	0.833816582	7.55910548	112.059411
1290	12	1105.559753	-0.976041498	-0.848363622	0.721267548	6.747752013	108.8446436
1300	11	1518.806869	-0.988154351	-0.858349407	0.682363749	6.691403662	114.178317
1310	10	2091.538316	-	-	0.599657245	8.162084679	166.4464385

			0.994151684	0.825904193			
1320	9	1755.790361	-0.777790019	-0.79261672	0.572880497	7.942002874	150.0588743
1330	8	1819.89666	-0.987360462	-0.83789551	0.594220543	7.776771882	140.3189085
1340	7	1924.15885	-0.979484141	-0.84564943	0.599956042	7.473812334	129.8996089
1350	6	1434.001646	-0.980171426	-0.864911351	0.748198088	6.979426181	108.3158143
1360	5	1688.515757	-0.982047488	-0.84069366	0.610742521	7.867845716	149.7188376
1370	4	1475.892279	-0.978558039	-0.872954267	0.858533261	7.883313687	114.8773301
1380	3	2884.4132	-0.988947289	-0.888233918	0.659534408	8.284515457	141.7263752
1390	2	3223.591558	-0.971393643	-0.819894943	0.340720589	6.726817704	142.1950717
1400	1	2984.08444	-0.975091846	-0.796718187	0.343742489	7.207499525	150.6551199
1405	K50	2163.878312	-0.951553211	-0.886311163	0.43	6.35	153.2
1410	K48	4907.850193	-0.963293724	-0.782367728	0.23	5.16	146.98
1415	K47	517.2027417	-0.952833012	-0.894628337	0.41	4.2	80.29
1420	K46	210.7907445	-0.862748964	-0.718365438	0.32	2.83	46.29
1425	K45	704.3299643	-0.961026289	-0.843462323	0.4	4.96	83.86
1430	K44	318.5508986	-0.948365952	-0.821583526	0.62	5.13	91.63
1435	K43	114.509762	-0.89969477	-0.633274843	0.62	4.31	77.77
1440	K42	98.08149249	-0.897381559	-0.655841424	0.61	4.11	65.78
1445	K41	61.77509455	-0.88679682	-0.55664758	0.45	3.21	93.56
1450	K40	102.0725594	-0.90031582	-0.520652516	0.5	3.53	61.23
1455	K39	84.7054998	-0.859815293	-0.297973666	0.43	5.23	85.85
1460	K38	70.78278368	-0.865023411	-0.330872762	0.46	4.32	77.27
1465	K37	60.57550365	-0.868203852	-0.364851883	0.45	3.79	179.67
1470	K36	54.83705077	-0.842634003	-0.337238349	0.41	3.14	310.7
1475	K35	145.2191212	-0.926565221	-0.63700674	0.46	4.11	32.17
1480	K34	66.13600364	-0.867792826	-0.421666316	0.42	3.32	480.27

1485	K33	71.53585574	-0.91132155	-0.48871186	0.43	3.32	382.61
1490	K32	115.9085814	-0.938364768	-0.668163355	0.43	3.15	131.45
1495	K31	130.2090103	-0.909011749	-0.693829022	0.47	3.69	133.27
1500	K30	57.28452779	-0.943422808	-0.626550031	0.44	3.34	168.83
1505	K29	63.81509271	-0.942252167	-0.57008201	0.46	2.98	97.05
1510	K28	58.44965039	-0.894845538	-0.5250277	0.44	3.12	119.73
1515	K27	28.32204956	-0.888744438	-0.35728304	0.41	2.88	163.68
1520	K26	26.58158563	-0.862638118	-0.359689649	0.44	3.07	174.75
1525	K25	33.51706679	-0.883535375	-0.444027507	0.46	3.49	134.55
1530	K24	31.55732833	-0.852697078	-0.339203167	0.4	3.43	143.86
1535	K23	30.22810608	-0.806896365	-0.280331178	0.37	2.37	126.12
1540	K22	31.52711435	-0.833474637	-0.306870789	0.42	2.81	153.27
1545	K21	35.18529878	-0.830911087	-0.295407994	0.41	2.94	182
1550	K20	46.20698104	-0.816536766	-0.34093734	0.37	2.95	187.61
1555	K19	39.37157084	-0.830081191	-0.149649732	0.38	2.67	219.01
1560	K18	41.80132555	-0.687780451	-0.32518992	0.35	2.32	107.79
1565	K17	69.72555363	-0.787423048	-0.494598066	0.41	2.86	138.56
1570	K16	64.29651762	-0.743745252	-0.343934894	0.36	3.08	147.06
1575	K15	46.11785852	-0.702659497	-0.236599266	0.3	2.45	156.48
1580	K14	41.76688247	-0.703870776	-0.210766723	0.29	2.41	161.14
1585	K13	54.23336157	-0.726432152	-0.255197348	0.32	2.64	253.79
1590	K12	80.01879019	-0.737045598	-0.341593945	0.33	3	165.1
1595	K11	74.42715198	-0.754317937	-0.33646409	0.32	2.75	167.09
1600	K10	74.00916327	-0.751024607	-0.317437492	0.32	2.86	214.28
1605	K9	70.36053108	-0.763299589	-0.299786185	0.35	3.04	164.24
1610	K8	61.96064084	-	-	0.31	2.86	218.1

			0.720575321	0.252376899			
1615	K7	93.79162609	-0.767232305	-0.429111852	0.36	3.33	152.71
1620	K6	97.65353753	-0.771913342	-0.387041672	0.34	3.24	237.22
1625	K5	120.6088884	-0.815251046	-0.495442519	0.43	3.9	167.46
1630	K4	114.0536496	-0.777891647	-0.449426026	0.36	3.45	192.74
1635	K3	95.41646746	-0.813742164	-0.453750869	0.36	2.96	157.85
1640	K2	104.9162701	-0.873895795	-0.472292176	0.39	3.3	441.6
1645	K1	110.6341282	-0.816721595	-0.444608429	0.42	3.58	306.97
1650	KL63	857.8952527	-0.97963511	-0.87179173	0.78	9.38	196.88
1655	KL61	1255.952523	-0.989364663	-0.890354339	0.78	10.02	196.01
1660	KL59	1403.350726	-0.995172749	-0.866484457	0.63	8.93	182.04
1665	KL57	151.0850139	-0.974534634	-0.871597013	0.69	8.32	173.37
1670	KL53	589.7360197	-0.983027241	-0.852873509	0.76	8.64	162.4
1675	KL51	237.1789785	-0.889886002	-0.656281652	0.6	6.26	185.75
1680	KL49	324.118998	-0.922502773	-0.704492314	0.65	7.33	183.42
1685	KL47	373.7752277	-0.967985497	-0.797459629	0.83	7.99	175.61
1690	KL46	351.1695655	-0.836867707	-0.687689648	0.715796225	8.392205691	282.9036058
1695	KL45	423.2595827	-0.935984111	-0.758325505	1.01	11.58	241.81
1700	KL43	402.0160507	-0.918908161	-0.74031636	1.02	11.58	266.18
1705	KL41	658.650343	-0.911972049	-0.762750866	0.95	11.32	215.31
1710	KL40	509.4613208	-0.866207753	-0.782246652	1.218908807	12.5157898	251.0194951
1715	KL39	548.4120194	-0.879143311	-0.73944331	1.140674658	13.27980956	269.1143495
1720	KL37	424.5208892	-0.875981013	-0.730428701	1.117276162	12.75399403	294.3487576
1725	KL35	613.0626086	-0.965065816	-0.814346301	0.83	7.63	124.07
1730	KL33	496.6400908	-0.941224285	-0.765886009	1.17	12.43	203.28
1735	KL31	521.6102918	-0.88816755	-0.768160021	1.232254475	13.18659807	216.2944592

1740	KL30	442.322936	-0.95533577	-0.778951911	1.221167707	12.27430271	248.5691726
1745	KL29	408.0631142	-0.840119304	-0.70283653	1.136996778	11.76588306	288.9429358
1750	KL28	549.0386854	-0.867284033	-0.754905732	0.984903062	12.02582146	249.0565054
1755	KL27	592.3257754	-0.903363417	-0.742262454	1.0689637	12.04596874	211.2225018
1760	KL26	550.3882913	-0.978751606	-0.814127384	1.31	12.72	255.1
1765	KL25	566.0812607	-0.928818179	-0.743449348	1.205200242	13.83969979	320.3239918
1770	KL23	758.8160842	-0.928784397	-0.779483848	1.12	12.97	236.13
1775	KL20	538.1645988	-0.960512495	-0.818935291	1.14	12.84	289.71
1780	KL17	420.2500932	-0.972623021	-0.773632835	1.113435207	11.52891701	200.1005111
1785	KL16	439.0153744	-0.964165922	-0.811515602	1.291947065	12.87556032	229.7923925
1790	KL15	510.6201209	-0.909614294	-0.774301911	1.16	12.77	301.48
1795	KL13	451.6483096	-0.970427225	-0.816618956	1.292138117	13.49407659	295.204459
1800	KL11	516.5433929	-0.95791075	-0.792160825	1.19	12.58	261.8
1805	KL9	531.1307026	-0.973756206	-0.820938541	1.280076973	14.12762962	284.8163701
1810	KL7	553.3249797	-0.905589172	-0.815380357	1	10.67	216.96
1815	KL5	544.855992	-0.934038512	-0.785882385	1.15	13.52	291.24
1820	KL4	527.2503193	-0.956606807	-0.853263214	1.03280146	11.19953899	233.2117323
1825	KL3	529.967609	-0.953547246	-0.817651451	1.17	13.17	272.63
1830	KL1	484.6428041	-0.938728987	-0.798203375	1.19	13.18	280.8

APPENDIX 2 Major and trace element geochemistry

Depth cm	Sample	SiO2	Al2O3	CaO	K2O	Fe2O3	MnO	Ti2O3
0	144	31.424848	21.76704	1.280268	1.216646	19.415326	0.37109088	1.3302
10	143	31.702944	20.93566	1.2690744	1.2937404	19.658375	0.37341504	1.4482

20	142	34.697824	18.97058	1.2998568	1.4262464	19.029307	0.51351024	1.2775
30	141	37.286256	19.858645	0.9906336	1.3118094	16.884757	0.54049632	0.9856
40	140	34.65504	19.42406	1.0521984	1.3443336	18.142893	0.50718336	1.0897
50	139	36.066912	18.649365	1.161336	1.517796	18.414536	0.53985072	0.9872
60	138	35.061488	20.0287	1.0298112	1.3395152	19.086495	0.50085648	1.0721
70	137	35.959952	18.63047	1.021416	1.4190188	18.200081	0.58000704	0.9879
80	136	36.751456	18.44152	1.056396	1.4949086	18.843446	0.57058128	1.0299
90	135	37.64992	17.062185	1.0829808	1.8069	17.914141	0.49220544	1.0559
100	134	38.270288	15.928485	1.0745856	2.0586614	17.213588	0.60157008	1.1242
110	133	39.596592	17.57235	0.8591088	1.5467064	16.255689	0.49891968	0.9771
120	132	38.847872	17.477875	1.0032264	1.6153686	16.598817	0.54656496	1.0267
130	131	42.227808	15.26716	0.958452	1.7310102	15.269196	0.50640864	0.9808
140	130	41.521872	17.137765	0.9682464	1.379267	15.369275	0.5881416	0.9127
150	129	41.799968	17.099975	0.9668472	1.3901084	15.326384	0.53236176	0.8972
160	128	37.64992	19.34848	1.1725296	1.2744668	17.113509	0.49155984	1.0283
170	127	37.243472	19.254005	1.0885776	1.2515794	17.542419	0.51054048	1.1352
180	126	36.751456	19.00837	1.042404	1.1901448	18.171487	0.54837264	1.1469
190	125	38.39864	19.08395	0.9766416	1.1889402	17.199291	0.5532792	1.0067
200	124	34.33416	15.172685	1.4943456	1.3346968	21.030887	0.63772368	1.8265
210	123	36.815632	16.306385	1.2019128	1.300968	18.786258	0.77032992	1.3968
220	122	41.115424	15.45611	1.0647912	1.2190552	16.227095	0.64547088	1.0435
230	121	39.938864	17.72351	0.9752424	1.1720758	15.354978	0.5952432	0.9409
240	120	42.013888	16.722075	1.0647912	1.1347332	14.940365	0.4557936	0.882
250	119	41.350736	18.006935	0.888492	1.1178688	15.269196	0.52151568	0.8301
260	118	35.574896	23.713225	0.7877496	0.8335832	17.370855	0.5481144	0.6667
270	117	35.981344	24.431235	0.7247856	0.795036	16.555926	0.55508688	0.6123
280	116	34.826176	22.541735	0.8856936	0.9251328	17.756874	0.56980656	0.6589
290	115	34.97592	21.9182	0.9696456	1.029933	17.571013	0.76464864	0.7066
300	114	34.33416	22.2961	1.0410048	0.9010408	17.671092	0.6430176	0.6927
310	113	34.312768	22.390575	1.1025696	0.9528386	18.200081	0.73327248	0.7319
320	112	34.269984	21.634775	1.0270128	1.0552296	18.528912	0.68782224	0.7739
330	111	36.708672	19.08395	1.0521984	1.6153686	16.72749	0.6720696	0.8406
340	110	37.692704	19.707485	1.0521984	1.8803806	15.44076	0.58801248	0.8916
350	109	35.746032	23.08969	1.0661904	1.3286738	15.555136	0.57225984	0.745
360	108	42.955136	16.911025	1.0829808	2.9115182	11.137363	0.39743136	0.663
370	107	35.596288	21.861515	0.9808392	1.120278	16.355768	0.6920832	0.7768
380	106	34.97592	22.37168	1.0060248	1.3816762	15.841076	0.52732608	0.884
390	105	35.125664	22.25831	1.0270128	1.38529	16.269986	0.52074096	0.8906
400	104	36.216656	18.5171	1.5713016	2.1176868	15.698106	0.4235136	1.4126
410	103	35.574896	18.233675	1.4145912	2.4405196	16.041234	0.34487952	1.4687
420	102	36.708672	20.7845	1.1417472	1.5575478	16.026937	0.53223264	0.9835
430	101	37.436	21.143505	1.0885776	1.451543	14.683019	0.4248048	0.9322
440	100	38.847872	19.31069	1.1739288	1.5587524	14.58294	0.49039776	0.8592
450	99	33.713792	23.297535	0.9990288	0.7540796	17.242182	0.5442408	0.8366
460	98	34.612256	22.390575	1.0689888	0.7673302	17.01343	0.55418304	0.8098
470	97	34.54808	22.844055	1.0787832	0.728783	16.899054	0.5565072	0.8073
480	96	35.061488	22.37168	1.0829808	0.7239646	17.227885	0.48665328	0.8137
490	95	33.392912	21.69146	1.1837232	0.6553024	17.713983	0.47851872	0.8704
500	94	36.558928	22.503945	1.161336	0.7179416	15.783888	0.51660912	0.7387
510	93	35.446544	19.15953	1.2886632	0.7781716	17.999923	0.52693872	0.8037

520	92	39.46824	18.535995	0.881496	0.9167006	15.369275	0.50473008	0.7783
530	91	39.36128	18.44152	0.972444	1.048002	16.384362	0.51376848	0.804
540	90	35.746032	21.50251	1.1809248	0.9058592	16.770381	0.64534176	0.6981
550	89	35.8316	23.713225	1.0885776	0.7095094	15.283493	0.63630336	0.6349
560	88	35.125664	22.78737	1.4047968	0.7805808	15.640918	0.60983376	0.6663
570	87	36.066912	17.23224	1.0619928	1.3780624	18.943525	0.58388064	0.933
580	86	35.746032	19.480745	1.1585376	0.9118822	19.272356	0.65347632	0.7529
590	85	36.516144	20.047595	1.1669328	0.6673484	18.457427	0.5771664	0.6818
600	84	35.810208	18.876105	1.1865216	0.728783	19.115089	0.6998304	0.7058
610	83	43.554112	16.47644	0.9346656	1.0431836	14.640128	0.41718672	0.7838
620	82	36.04552	21.9182	1.0298112	0.8203326	17.227885	0.59601792	0.6468
630	81	36.516144	22.126045	1.2340944	0.758898	17.227885	0.71713248	0.6187
640	80	36.109696	21.521405	1.2676752	0.7083048	16.87046	0.71571216	0.6132
650	79	35.895776	21.408035	1.301256	0.7540796	16.927648	0.81500544	0.6338
660	78	37.821056	19.53743	1.301256	0.734806	17.699686	0.58697952	0.6555
670	77	37.32904	18.17699	1.2704736	0.8781534	18.44313	0.71028912	0.7157
680	76	37.86384	17.72351	1.2648768	0.8480384	17.1564	0.64327584	0.681
690	75	37.821056	17.87467	1.4369784	0.7685348	17.227885	0.6462456	0.672
700	74	37.928016	20.160965	1.0661904	0.9407926	16.484441	0.51363936	0.7085
710	73	38.869264	18.25257	1.1291544	1.8394242	14.797395	0.39756048	0.8129
720	72	40.259744	18.082515	1.0340088	1.933383	14.239812	0.2879376	0.7952
730	71	36.04552	19.858645	1.2410904	0.8227418	17.385152	0.52138656	0.7359
740	70	35.810208	19.254005	1.0270128	0.7757624	18.242972	0.42519216	0.7513
750	69	42.377552	17.137765	0.8898912	1.060048	14.683019	0.44339808	0.6677
760	68	48.089216	14.96484	0.671616	1.1347332	12.066668	0.4047912	0.5996
770	67	41.671616	17.931355	0.9752424	1.0684802	15.183414	0.47890608	0.7097
780	66	36.537536	19.87754	1.056396	0.8877902	17.656795	0.60144096	0.7711
790	65	36.837024	20.123175	1.1739288	1.0407744	17.771171	0.63707808	0.835
800	64	36.04552	20.312125	1.2676752	0.9299512	17.742577	0.49013952	0.8504
810	63	35.018704	20.74671	1.0507992	0.8986316	18.600397	0.60608928	0.7757
820	62	35.61768	20.916765	1.1557392	0.8962224	18.257269	0.53468592	0.7697
830	61	36.280832	21.20019	1.1249568	0.9239282	18.01422	0.51183168	0.7722
840	60	38.82648	17.969145	1.371216	1.2311012	16.112719	0.44920848	0.8272
850	59	40.559232	17.42119	1.1179608	1.5864582	14.983256	0.46960944	0.8109
860	58	42.420336	16.722075	0.9780408	1.1226872	14.282703	0.45049968	0.744
870	57	43.040704	16.268595	1.035408	0.9287466	14.01106	0.47283744	0.7332
880	56	42.655648	16.43865	1.0452024	0.819128	14.72591	0.47438688	0.7295
890	55	45.821664	14.96484	0.776556	1.0383652	13.86809	0.46186224	0.7099
900	54	45.393824	14.983735	0.7737576	1.2335104	13.882387	0.48471648	0.6814
910	53	35.8316	19.140635	0.8073384	1.2250782	18.857743	0.46302432	0.7306
920	50	40.302528	17.68572	0.8143344	2.613982	14.683019	0.53701008	0.5712
930	49	40.516448	16.70318	1.0256136	2.8175594	14.740207	0.46793088	0.5435
940	48	38.569776	17.27003	1.105368	2.4441334	16.212798	0.51531792	0.5969
950	47	38.099152	18.78163	0.8129352	1.7755804	17.44234	0.51764208	0.6172
960	46	38.377248	19.027265	0.7807536	1.8406288	16.756084	0.684336	0.6158
970	45	37.821056	18.66826	0.811536	1.1467792	17.999923	0.68846784	0.6223
980	44	36.451968	21.294665	0.8619072	1.0010226	18.786258	0.59433936	0.6532
990	43	36.494752	17.893565	0.94446	1.114255	19.186574	0.62468256	0.678
1000	42	36.922592	16.079645	0.993432	1.2202598	19.829939	0.70460784	0.7262
1010	40	41.778576	14.51136	0.8143344	1.4804534	17.042024	0.59085312	0.6363

1020	39	45.329648	14.114565	0.6184464	1.397336	14.854583	0.55366656	0.5886
1030	38	43.447152	15.323845	0.7093944	1.3346968	15.86967	0.68162448	0.5841
1040	37	45.13712	13.18871	0.678612	1.4551568	15.783888	0.51609264	0.6104
1050	36	44.794848	12.0928	0.7261848	1.56598	16.212798	0.56709504	0.6416
1060	35	40.944288	13.71777	0.776556	1.475635	18.571803	0.77459088	0.7153
1070	34	38.912048	14.54915	1.0326096	1.8165368	19.315247	0.83553552	0.9202
1080	33	42.698432	13.56661	0.7121928	1.644279	17.342261	0.88021104	0.7021
1090	32	38.227504	13.736665	1.0689888	1.9586796	18.486021	0.75767616	0.9583
1100	31	41.971104	13.33987	0.8563104	1.7924448	17.227885	0.80222256	0.7137
1110	30	42.398944	12.640755	0.8717016	1.6418698	17.642498	0.67607232	0.7135
1120	29	42.2492	13.245395	0.7877496	1.6876446	18.400239	0.68846784	0.7296
1130	28	42.548688	13.33987	0.776556	1.6972814	17.971329	0.66535536	0.7285
1140	27	43.404368	12.69744	0.7989432	1.6370514	16.412956	0.68136624	0.6814
1150	26	44.302832	12.62186	0.6828096	1.7334194	16.455847	0.703704	0.6696
1160	25	45.88584	12.225065	0.678612	1.7358286	16.069828	0.61667712	0.6584
1170	24	46.484816	11.091365	0.7051968	1.770762	15.283493	0.60337776	0.6384
1180	23	49.265776	10.600095	1.0242144	1.2419426	13.753714	0.57419664	0.5554
1190	22	46.014192	11.884955	0.8856936	1.1094366	16.613114	0.68962992	0.6455
1200	21	55.383888	8.068165	0.8143344	1.1106412	11.15166	0.56386704	0.4504
1210	20	58.314592	7.74695	0.5568816	0.8998362	9.536099	0.46986768	0.3872
1220	19	39.404064	14.85147	1.2508848	0.9263374	20.258849	0.44456016	0.721
1230	18	40.281136	14.152355	1.4075952	1.0275238	20.0158	0.55108416	0.7157
1240	17	40.131392	12.829705	1.8343512	1.1552114	19.715563	0.61990512	0.7238
1250	16	44.687888	11.922745	1.4117928	1.0383652	16.44155	0.5403672	0.6158
1260	15	49.501088	11.166945	0.8619072	1.035956	13.739417	0.52771344	0.5182
1270	14	49.09464	11.015785	0.8563104	1.0985952	13.524962	0.52371072	0.5117
1280	13	48.709584	11.07247	0.8381208	1.1118458	13.896684	0.51467232	0.5194
1290	12	49.158816	11.45037	0.8171328	1.1552114	13.86809	0.50176032	0.5184
1300	11	49.993104	11.393685	0.8003424	1.0997998	13.081755	0.4964664	0.4938
1310	10	50.399552	11.620425	0.8101368	0.9901812	12.910191	0.45217824	0.4935
1320	9	27.103664	17.49677	1.9560816	0.9383834	25.977649	0.23202864	2.9015
1330	8	26.290768	18.40373	1.7825808	0.7480566	26.721093	0.26043504	2.69
1340	7	28.408576	19.669695	1.7811816	0.7841946	23.761614	0.2543664	2.5299
1350	6	30.80448	19.23511	1.9043112	0.7215554	23.518565	0.56954832	2.2728
1360	5	32.344704	21.143505	1.4985432	1.3563796	18.700476	0.21537216	1.8655
1370	4	34.54808	25.489355	0.8339232	0.8600844	15.969749	0.58956192	0.7248
1380	3	39.168752	21.31356	0.9598512	1.035956	14.940365	0.448692	0.8245
1390	2	36.430576	25.01698	0.9836376	0.6962588	14.897474	0.50085648	0.8083
1400	1	37.093728	17.30782	1.3180464	1.9406106	16.970539	0.829596	1.0987
1405	K50	40.559232	18.384835	1.1921184	1.5105684	14.911771	0.31595664	1.0103
1410	K48	34.205808	21.067925	1.7098224	1.3527658	18.100002	0.22002048	1.863
1415	K47	37.286256	24.52571	0.797544	0.927542	15.469354	0.577812	0.7613
1420	K46	37.32904	24.60129	0.7443744	0.7336014	15.655215	0.658512	0.6118
1425	K45	38.890656	21.823725	1.126356	1.493704	14.697316	0.41679936	1.0876
1430	K44	41.864144	20.14207	1.0591944	1.5804352	13.310507	0.16230384	0.9858
1435	K43	48.474272	15.777325	0.958452	1.6912584	10.250949	0.15713904	0.7732
1440	K42	51.704464	14.076775	0.916476	1.6768032	9.021407	0.1246008	0.6889
1445	K41	52.987984	13.45324	0.9262704	1.7298056	8.649685	0.15868848	0.6677
1450	K40	52.175088	13.774455	0.8437176	1.6599388	8.878437	0.13066944	0.5736
1455	K39	62.507424	8.61612	0.5219016	2.1815306	3.359795	0.09503232	0.4559

1460	K38	58.143456	10.259985	0.762564	2.258625	5.504345	0.10988112	0.5962
1465	K37	55.105792	11.620425	0.8703024	2.1417788	7.177094	0.08547744	0.6155
1470	K36	53.90784	12.111695	0.9458592	2.1598478	8.106399	0.11698272	0.6519
1475	K35	52.816848	12.24396	0.993432	2.0707074	8.521012	0.11220528	0.6457
1480	K34	53.009376	12.65965	0.9948312	2.0695028	8.306557	0.11259264	0.6457
1485	K33	52.581536	13.07534	1.0242144	2.0430016	8.678279	0.14229024	0.6565
1490	K32	50.100064	14.152355	1.126356	1.915314	9.650475	0.1878696	0.6983
1495	K31	49.351344	14.492465	1.1585376	1.8803806	10.379622	0.16966368	0.7516
1500	K30	50.228416	14.454675	1.1081664	1.8683346	9.750554	0.1568808	0.6995
1505	K29	50.69904	14.114565	1.0857792	1.8623116	9.307347	0.2601768	0.6682
1510	K28	50.570688	14.114565	1.0955736	1.8659254	9.178674	0.15700992	0.6771
1515	K27	50.656256	13.396555	1.1067672	2.2200778	9.807742	0.21472656	0.7039
1520	K26	50.656256	13.64219	1.0927752	2.1574386	9.478911	0.2653416	0.7203
1525	K25	50.977136	13.64219	1.0787832	2.198395	8.992813	0.25449552	0.7002
1530	K24	51.169664	13.30208	1.08438	2.2429652	8.935625	0.2201496	0.7085
1535	K23	48.77376	12.640755	1.0815816	2.282717	12.166747	0.12046896	0.7091
1540	K22	48.944896	13.169815	1.0885776	2.3031952	10.86572	0.10794432	0.7351
1545	K21	49.436912	12.980865	1.1571384	2.3814942	10.72275	0.08095824	0.7287
1550	K20	48.538448	12.262855	1.2047112	2.4200414	12.023777	0.08922192	0.769
1555	K19	48.902112	13.056445	1.091376	2.1887582	11.795025	0.12873264	0.7078
1560	K18	46.09976	14.038985	1.2396912	2.0972086	13.43918	0.14526	0.9166
1565	K17	43.404368	15.399425	1.350228	1.8574932	14.668722	0.51157344	1.0731
1570	K16	41.243776	15.852905	1.4243856	1.8261736	15.483651	0.34784928	1.1888
1575	K15	39.831904	17.27003	1.5629064	1.9526566	16.055531	0.42196416	1.3488
1580	K14	39.275712	17.213345	1.6174752	1.9622934	15.497948	1.65480192	1.3418
1585	K13	38.93344	17.288925	1.6006848	2.0020452	15.7267	0.94012272	1.3445
1590	K12	39.104576	16.77876	1.5083376	1.9659072	16.198501	1.09338816	1.2716
1595	K11	39.36128	17.19445	1.5922896	2.0454108	16.141313	0.57019392	1.3402
1600	K10	39.019008	16.986605	1.5447168	1.9719302	16.355768	1.13599776	1.2747
1605	K9	38.912048	17.0055	1.5713016	2.0201142	16.141313	1.38055104	1.3162
1610	K8	39.382672	17.855775	1.5503136	2.0345694	15.712403	0.1271832	1.3487
1615	K7	39.489632	17.7613	1.43418	1.8936312	15.898264	0.1891608	1.2686
1620	K6	38.676736	17.53456	1.588092	2.0285464	16.44155	0.17650704	1.3911
1625	K5	40.388096	18.158095	1.4943456	1.945429	14.768801	0.17289168	1.3002
1630	K4	39.125968	17.742405	1.5587088	2.0032498	16.412956	0.2111112	1.369
1635	K3	38.71952	17.08108	1.5069384	1.9659072	16.455847	0.31156656	1.317
1640	K2	38.526992	17.15666	1.5852936	2.0562522	15.826779	1.3886856	1.3368
1645	K1	33.970496	15.04042	1.4635632	1.7358286	20.001503	4.00388208	1.2097
1650	KL63	37.585744	18.233675	1.140348	1.9887946	17.285073	0.60789696	1.0375
1655	KL61	37.821056	17.817985	1.098372	1.9743394	17.370855	0.57148512	1.1065
1660	KL59	38.270288	17.364505	1.1095656	2.053843	16.513035	0.61551504	1.1733
1665	KL57	36.879808	18.10141	1.1515416	1.8382196	17.828359	0.73365984	1.1655
1670	KL53	38.869264	16.92992	1.4075952	1.9309738	17.542419	0.83385696	1.1461
1675	KL51	36.088304	17.04329	1.6748424	2.0201142	19.15798	0.58220208	1.4526
1680	KL49	39.639376	15.90959	1.3838088	1.9490428	16.927648	0.92591952	1.1729
1685	KL47	35.2968	20.690025	1.2159048	1.3515612	17.928438	0.95071056	1.2247
1690	KL46	32.686976	21.370245	1.0885776	1.252784	20.759244	0.68343216	1.2633
1695	KL45	33.328736	22.503945	1.0549968	1.2274874	19.315247	0.6062184	1.2406
1700	KL43	30.569168	21.143505	0.8786976	1.1046182	23.475674	0.63036384	1.2317
1705	KL41	31.916864	20.97345	1.0242144	1.319037	21.331124	0.89570544	1.3335

1710	KL40	30.761696	21.634775	0.860508	1.1347332	23.046764	0.77071728	1.2338
1715	KL39	29.606528	20.36881	0.846516	1.096186	24.204821	1.30307904	1.2256
1720	KL37	31.061184	21.88041	0.8940888	1.132324	22.131756	1.04031984	1.2701
1725	KL35	38.441424	18.498205	0.9248712	1.5587524	17.528122	1.02146832	0.9533
1730	KL33	32.708368	21.483615	0.951456	1.1528022	20.30174	0.82133232	1.2535
1735	KL31	32.708368	23.39201	0.9850368	1.1600298	19.558296	0.80480496	1.2787
1740	KL30	30.16272	20.86008	0.8493144	1.0612526	23.246922	1.83518256	1.1698
1745	KL29	31.788512	22.59842	0.9262704	1.1130504	20.902214	0.800544	1.2409
1750	KL28	30.932832	21.46472	0.9570528	1.1154596	20.859323	2.02034064	1.2224
1755	KL27	31.938256	20.576655	0.9206736	1.1455746	22.031677	1.15588224	1.1701
1760	KL26	31.403456	22.14494	0.9752424	1.1118458	21.130966	1.2214752	1.2442
1765	KL25	29.73488	20.4066	0.8982864	1.0757078	23.947475	2.16237264	1.1447
1770	KL23	32.473056	23.12748	1.0396056	1.2033954	19.258059	0.45075792	1.2926
1775	KL20	30.954224	21.1624	0.9332664	1.1636436	21.802925	1.46848176	1.2014
1780	KL17	32.751152	21.65367	0.9822384	1.1853264	20.401819	0.86665344	1.2676
1785	KL16	32.002432	23.01411	0.9892344	1.1467792	19.386732	0.78324192	1.2853
1790	KL15	28.964768	19.442955	0.8731008	1.1118458	25.062641	2.09716704	1.1609
1795	KL13	29.62792	20.17986	0.8856936	1.0672756	23.547159	2.09213136	1.1351
1800	KL11	32.580016	20.992345	0.97944	1.1961678	20.501898	1.02805344	1.1802
1805	KL9	31.210928	21.937095	0.9808392	1.1515976	20.58768	1.14903888	1.2081
1810	KL7	30.761696	20.312125	0.9878352	1.2009862	22.632151	1.21811808	1.2282
1815	KL5	31.275104	21.256875	0.9752424	1.2214644	21.945895	1.1001024	1.2408
1820	KL4	31.103968	20.36881	0.9668472	1.2082138	22.889497	1.29907632	1.2356
1825	KL3	30.462208	20.878975	0.8563104	1.162439	23.146843	0.57122688	1.1448
1830	KL1	30.26968	20.82229	0.8227296	1.1347332	23.361298	0.7773024	1.0729

Depth cm	Sample	Ba (PPM)	V (PPM)	Cu (PPM)	Ga (PPM)	Pb (PPM)	Ni (PPM)	Nb (PPM)	Rb (PPM)	Sr (PPM)	Y (PPM)	Zn (PPM)	Zr (PPM)
0	144	326	236.2	28.3	39.6	28.3	40.1	234	90.5	43	111.9	434.5	960.5
10	143	387	97.1	29.2	36.4	24	26.2	219.2	100.3	38.6	175.8	425	948.9
20	142	379	138.7	34.4	39.4	39.9	36.6	258	121.2	32.4	182.1	498.2	1258
30	141	350	169.5	25.1	44	35.5	35.5	280	84.7	37.8	108.7	425.4	1218
40	140	410	119.3	36.2	37.1	37.6	41.1	257.7	102.1	31.1	145.2	493.5	1262.4
50	139	260	365.2	37.8	42.4	40.6	16.4	299	116	32.8	83.1	520.6	1479.3
60	138	363	239.3	39	43.9	43.3	42.1	290.1	103.6	30	131	531.5	1404.5
70	137	282	338.9	35.5	42	39.9	25.8	287.9	104.7	29.5	88.2	492.3	1414.6
80	136	234	310.2	42.3	41	43.9	15.9	288.4	116.3	30.4	85.3	532.8	1425.2
90	135	290	306	37.5	44.5	42.7	17.6	309.2	141	38.3	87.2	530.3	1488.2
100	134	357	253	32.7	37.5	46.9	17.2	277.4	147.3	47.6	90.3	449	1339.8
110	133	339	115.8	26.2	42	36.5	29.5	274.1	100.3	37.8	128.3	385.4	1274.5
120	132	294	202.8	31	36.9	32.4	24.5	249.5	109.8	28.2	107	420.2	1110.6
130	131	302	177	26.9	34.9	33.8	14.2	243.3	126.4	32.1	117	381.9	1128.1
140	130	279	154.6	29.9	34.8	32.9	19.4	248.5	117.1	28.6	119.5	411.9	1145.9
150	129	232	180.4	32.2	34.5	32.8	18.5	241.4	119.5	33.4	100.1	444.3	1056.9
160	128	251	210.5	31.5	40.6	26.3	26.6	240.3	97	29.8	107.2	462.8	960.2
170	127	239	217.5	28.9	43.5	34.2	21.5	236.5	111	32	127.4	456.6	975.6
180	126	262	209.2	32.5	37	33.7	30.2	236.7	114.2	19.1	170.4	482.2	1033
190	125	232	163.2	32.1	41.6	33.2	26.9	256.1	120.3	24.5	171.8	482.3	1139
200	124	365	273.2	27.9	31.7	29.8	33.2	204.9	120	21.5	165.1	460.8	879.2
210	123	318	227.1	30.9	32.1	30.6	42.9	229.3	128.8	18.6	176	495.3	1007.7
220	122	247	154	37.7	27.7	32	34.6	209.8	105.9	16.1	154.1	504	964.6
230	121	271	123.1	35.7	30.9	33.5	35.4	227.2	88	33.3	138	499.2	1003.6
240	120	222	134.9	33.3	32.2	31.2	32.1	218.2	79.4	26.5	129.4	461.8	979.8

250	119	231	30.4	40.2	30.2	33.8	19	283.5	82.9	18.2	136.1	509.3	1147.3
260	118	331	184.1	27.2	54.7	36.6	2.1	339	54.3	20.5	85.1	518.8	1268
270	117	264	177.5	25.5	49.3	37.8	-2.6	277.2	42.4	17.9	63.6	466.5	1115.4
280	116	205	230.5	34.1	43.9	31.6	2.4	273.1	54.1	21.2	57.7	543.3	1097
290	115	218	132.8	31	44.1	44.3	12.8	305.6	66.2	22.4	91.3	573	1219.2
300	114	226	73.1	32	40.8	38.3	16.2	306.4	51.4	25.4	93.3	580.4	1198.9
310	113	230	185.5	31.2	44.4	38.1	14.1	297.5	51.3	27.1	78.1	578.2	1136.4
320	112	276	247.9	33.5	39.9	32	22.1	291.5	59.4	31.9	73.6	586.3	1121
330	111	260	130.8	37.5	36.2	34	24.4	275.6	124.2	36.6	108.2	542.8	1129.7
340	110	348	234.1	35.6	34.8	42.6	22.7	271.7	146.3	48.6	90.5	578.1	1124.5
350	109	318	231.3	29.9	40.9	40.8	26.4	274.7	68.8	41.9	58.4	520.1	1137.8
360	108	375	128.8	25.6	34.3	27	14.3	242	175	112.1	80	334.5	1015
370	107	212	112.3	23.2	41	33	9.3	309.6	64	32.2	107.4	369.3	1272.8
380	106	348	165.5	25.1	39.7	31	8.9	276.2	72.4	48	102.9	307.1	1113.6
390	105	285	173.4	22.6	42	37.4	9.6	282.9	72.3	51	106.9	317.1	1138.9
400	104	1357	253.1	20.8	29.3	18.6	6.9	141.4	114	172.3	78.1	263.6	571.4
410	103	819	288.5	20.6	30.4	17.9	15.2	145.5	155.3	130.9	96.3	326.3	583.1
420	102	402	180.9	28.2	32.9	31.2	13	242.2	77.9	60.4	112.2	424.8	957.8
430	101	351	135.6	25	29.3	26.5	13.9	219.9	76	52.4	118.8	370.8	899.9
440	100	430	96.1	32.2	31.6	21.9	10	197.7	78.1	63.3	121.8	442.5	781.2
450	99	121	110.3	18.9	32.5	22.7	3	208.3	31.6	22.7	129.2	390.8	866.6
460	98	98	98.9	21.8	37.7	23.9	2.8	213	39.4	18.2	121.6	431.4	874.6
470	97	81	91.9	21.9	41.8	24.2	2.8	223	41	22.1	125.8	445.4	948.1
480	96	82	118.1	24.9	41.6	28.4	0.8	207.8	41.8	18.3	105.4	479.7	851.5
490	95	54	159.4	22.8	33.3	23.2	-1.8	205.7	33.2	15.5	121.9	366.6	838.5
500	94	84	82.2	26.9	39	27.2	0.5	191.8	41	16.7	101	496.7	798.5
510	93	71	112.5	26.9	35.1	27	7.5	221.9	50.9	10.5	155.6	551.6	898.5
520	92	118	134.2	30.4	32.1	29	7.5	219.9	50.2	13.8	159	445.3	953.6
530	91	137	137.3	38.1	30.3	26.5	9.1	231.9	62.3	28.3	125.6	586.5	928.5
540	90	123	108.1	33.8	40.7	34.3	5.4	248.4	50.6	26.7	96.7	674.2	940.7
550	89	78	69.7	22.6	47	32.4	-0.4	188.1	33.6	27	84.2	537.7	808.5
560	88	85	71.9	24.9	42.6	35.3	10.7	182.8	36.2	30.8	84.7	582.8	766.5
570	87	138	114.8	42.1	29.6	27.6	23.3	215.7	65.1	28	140.4	654.6	880
580	86	109	111	34.3	40.2	40.2	6.8	292.4	59.4	24.2	130	788.7	1106.2
590	85	57	7	24.9	45	36.8	-0.7	330.6	45.5	8.8	189.5	543.8	1276.9
600	84	65	21.9	25.2	39.5	35.6	-3.3	300.1	42.3	7.4	184.4	540.9	1172.9
610	83	131	88.1	43.7	29.4	33.1	13.9	236.4	69.3	32.2	130.7	524	942.9
620	82	122	101.4	28.7	47.3	43.4	4.8	307.1	54.2	28.1	95.6	697.9	1163.6
630	81	116	57.1	27.2	51	48.2	-0.6	250.9	46.4	40.3	100.8	706.7	1133.3
640	80	89	43.5	30.3	48.6	51.6	-5.7	271.9	57.5	41.3	100.1	702.4	1117.2
650	79	129	63.4	31.3	40	46.6	-4.2	278.7	56.1	40.2	110.3	713.5	1123.6
660	78	46	114.7	28.7	41.3	34.7	-5	276.1	57.3	18.7	144.2	605.4	1093.9
670	77	66	29.6	28.4	37.1	34.8	-2.6	268.7	57.2	20.1	156.5	565	1021.1
680	76	73	38.3	25.7	37.1	31.6	-1.2	258.6	56.1	19.9	174.2	493.7	1007.9
690	75	72	72.4	23.2	35.9	30.7	0.8	260	57.2	18.1	188.7	456.8	996.3
700	74	91	105	18	45	26.3	-0.3	246.7	58.2	27.3	159	356.8	1012.2
710	73	204	177	20.8	36.9	23.5	4.1	209.9	79.1	25.8	139.5	370.2	824.6
720	72	162	141.5	20.3	35.7	24.6	5.2	214.3	84.4	23.6	141.2	397.6	839.4
730	71	99	75.4	23.3	38	18.4	0.9	211.7	51	31.9	154.7	477.5	930.2
740	70	69	71.6	20.4	39.7	31.3	0.5	260.7	52.6	12.8	181.2	440.4	1229.5
750	69	81	61.8	27.8	31.6	41.8	13.5	316.6	84.7	21.3	176	516.5	1490.9
760	68	109	68.5	26.5	29.7	31.5	15.3	230.2	82	23	165.3	463	1010
770	67	121	80.5	34.2	35.7	26.8	13	237.3	72.1	30.3	110.7	654	943.6
780	66	95	100.2	25.1	39.9	26	2.3	235.9	63.4	24	137.3	615.2	949.6
790	65	125	102.5	25.7	40.6	26.5	7.2	210.7	66.3	34.2	111	718.9	814.2
800	64	116	103.6	25.1	32.2	19.3	0.2	193.7	58.9	27.9	132.3	553	772.1
810	63	87	131.8	30.4	42.1	26.2	3.8	248.8	67.6	19.6	111.6	725.5	968
820	62	82	152.3	32.7	39.3	27.2	2.3	232.8	69.4	26.6	97.5	716.2	901.8
830	61	121	110.4	30.3	40.5	23.2	0.6	177.9	66.8	29.3	94.1	690.8	747.5
840	60	206	114.4	23.9	35.1	22.8	2.9	203.1	89.8	42.3	154.4	513.4	809
850	59	216	115.2	19.4	31.4	22.4	7.4	188.1	91.7	29.8	172.1	434.1	774.5
860	58	120	109.1	17.8	30.4	26.9	16.5	197	78.1	24.9	201.4	455.9	815.5
870	57	106	87.9	17	31.8	21.2	22.1	188.2	74.2	26.7	211.3	448	791.7
880	56	72	102.6	19.1	28.3	25.5	17.1	193.5	68.4	27	191	445.3	815.4
890	55	86	50.5	22.6	29.7	24.2	17.5	192.4	92.3	24.8	162.5	475	827.4
900	54	71	54	24.2	31.3	22.8	12.4	199.8	105.9	24	139.1	504.7	818.2
910	53	57	153.3	34.6	46.8	29.8	8.8	293.9	69.3	18.8	98.6	613.3	1107.2

920	50	51	103.8	19.6	47.7	35.1	2.5	269.7	97.9	19	79	451.7	1022.1
930	49	67	93.4	21.6	40.7	31.3	1.4	271.3	100.1	16.9	82.1	437.1	1025.5
940	48	59	88.9	24	43.1	38.5	-2.4	314.2	103.4	21.7	97	529.5	1191.2
950	47	49	81.4	26	48.9	40.4	-1.9	339.5	91.8	17.8	110	576.2	1269.8
960	46	60	93.6	29.5	46.5	42.1	4.4	375.6	88.2	20.5	122.1	560.3	1454.1
970	45	114	211.8	31.5	51.7	45.8	0.2	362.8	73.4	23.8	97.1	706.4	1355.8
980	44	71	115	31.4	52.6	50.6	6.5	378.6	67.8	25	109	754.2	1463.2
990	43	81	107.1	32.1	50.8	46	5.3	386.1	76.6	33.4	132.5	693.4	1474
1000	42	82	47.1	32.2	46.5	48	5.5	437	87.5	39.7	173.2	686.7	1723.8
1010	40	83	93.6	23.9	41.5	36.3	7.4	363.8	99.3	37.1	162.2	483.1	1411.4
1020	39	111	168.7	26.9	42.3	48.8	1.1	387.1	96.7	24.2	125.7	489.3	1450.8
1030	38	79	94.8	23.2	46.9	58.2	7	400.8	92.1	29.1	117.8	539	1531.5
1040	37	130	181.4	24.7	43.9	38.2	1.1	314.1	108.4	30.1	115.6	462.2	1182
1050	36	116	155.4	24.7	42.6	32.2	2.9	304.4	112.1	25.5	124.2	467.3	1120.6
1060	35	163	198.4	27.7	47.6	45.9	5.1	366.2	114.2	23.8	122.3	554.9	1353.8
1070	34	398	261.8	25.2	46.6	51.9	5.6	352.1	131.1	44.7	106.3	532.9	1248.3
1080	33	175	212.1	20.6	44.7	36.3	7.2	314.8	122.1	26.3	108	482.9	1144.3
1090	32	419	238	24.3	42	43.3	9.2	295.7	148	45.8	95.6	488.3	1029.2
1100	31	377	203	26	43.3	41.1	1.4	328	132.6	42.6	101.5	486.1	1188.5
1110	30	264	233.8	25.5	45.1	36.4	7.7	336.9	115.3	27.6	108.3	494.7	1224.9
1120	29	146	242.9	23.4	43.7	39.9	4.8	326.4	114.2	25.9	105.8	513.5	1186.6
1130	28	158	219.9	27.6	44.2	37	-1.2	320.6	120.4	28.9	102.6	494.3	1156.9
1140	27	208	235.3	25.2	45.1	35.6	6.8	304.2	116.1	30.3	100.9	441.8	1121.8
1150	26	174	253.1	22.3	46.1	34.9	8.3	311.1	119.1	28.8	103	431.9	1135.6
1160	25	143	197.3	22.3	42.3	28.7	3.3	291.9	121.4	27.8	99.4	421.9	1088.8
1170	24	165	192	22.8	40.2	34.6	5.2	287.2	129.5	31.2	98.7	411.8	1077.8
1180	23	98	104.5	25	33	28	2.5	221.6	88.7	30.4	140.4	414.2	899.1
1190	22	58	111.1	23.4	39	29.4	2.8	249.3	91.1	21.8	173.9	494.1	986.8
1200	21	73	108.6	23.9	30.6	29.6	0.2	206.5	86.7	17	161.1	344	864.8
1210	20	56	70.5	21.1	30	24.5	-1.9	191	77.4	21.1	95.8	335.9	746.7
1220	19	39	128.3	27	47.2	30.5	-1.8	270.4	81.5	28.1	108.9	656.3	967.6
1230	18	46	104.9	23.1	50.3	29	-7.9	261.4	86.3	33.4	131	568.4	990.3
1240	17	85	154.4	22.7	40.5	20.1	-10	221	106	37.4	113.8	503.5	841.5
1250	16	33	76.9	17.9	43.3	24.1	-1	230.1	85.4	39.2	143	374.6	876.7
1260	15	53	108.6	16.6	41.5	25	0.1	211	70.1	34.1	138	362.6	789.2
1270	14	64	104.8	18	35.6	19.4	-4.2	194.3	62.6	33.6	125.9	363.5	743
1280	13	50	60.5	17.3	39.7	21.8	-1.6	194.7	73.5	32.5	127.5	378.3	757.5
1290	12	44	116.5	20	34.6	20.3	-3	200.7	71.5	35.4	134.1	391.1	771.6
1300	11	59	118.4	21.7	35.7	21.6	3.7	199.6	68.2	28.6	134.1	400.6	755.9
1310	10	59	60.6	23.1	35.2	25.9	-2.1	220.3	81.7	26.8	178	430	868.2
1320	9	366	443.1	51.7	28.6	12.1	40.4	97.7	59.9	25.8	80	366.3	414.1
1330	8	330	471.9	60.5	29.2	16.4	46.1	119.5	59.1	23.1	75.8	392.9	481.2
1340	7	491	451	51.9	27.9	20.2	43.8	101.9	60.1	36.4	73.5	338.3	417.1
1350	6	357	439.1	56.7	28.7	18.8	56.6	142.2	67.8	23.4	93.9	410.2	585.2
1360	5	595	251	47.3	28.9	9.2	28.8	119.6	92.1	51.8	95.9	328.6	501.5
1370	4	485	140.7	53	47	40.3	70.5	321.3	52.8	25.5	97.5	416.2	1223
1380	3	332	151.6	36.1	42.7	31	27.8	252.8	80.3	35.7	98.1	375.6	1157.9
1390	2	262	162.4	29.4	45.8	39.3	52.4	285	50.1	31.4	71.5	288.8	1094.6
1400	1	617	319.6	29.5	37.8	39.2	16.3	234.7	144.2	42.9	88.7	293	1038.8
1405	K50	333	176.7	36.7	42.4	33.6	32.9	270.9	134.4	57.8	120.7	380.6	1088.6
1410	K48	917	331.8	48.1	34.9	13.9	25.9	126.6	114.8	118.7	82.7	297.6	497
1415	K47	404	193.8	41.6	53.2	33.1	69.2	309.8	71.7	35.1	114.7	294.5	1224.6
1420	K46	366	200.5	36.7	55.5	45.8	78.8	404.9	57.2	36.5	122.3	260.9	1542.9
1425	K45	282	170	40.9	46.6	31.8	36.3	291.3	131.9	35.5	122.1	386.7	1212.3
1430	K44	215	155	40.6	47.3	36.5	27.9	291.9	146.4	35.5	132.4	379.9	1233.2
1435	K43	225	99.9	34.1	33.4	29.3	19.5	215.3	127.6	47	104.6	337.4	957.5
1440	K42	201	105.4	32.1	30.5	28.7	15.4	186.3	115.9	48.5	80.4	319.6	856.3
1445	K41	242	104.7	34.1	28	34.4	17.9	181.7	123.6	47.2	86	323.3	854
1450	K40	311	154.2	24.7	36.7	32	10	185.5	102.2	49.4	83.8	258	999.9
1455	K39	307	102.2	10.3	22.8	24.4	5.1	127.5	87.8	59.3	56.1	93.3	533.9
1460	K38	327	140.5	17.5	25.7	28.4	9.7	163.3	121	54.2	66	176.8	633
1465	K37	264	97	22.3	23.5	24.4	12.3	151.5	123.3	48.4	71.3	228.6	639.3
1470	K36	308	94.1	25.3	28.1	20.1	10.3	166.9	134.6	49	81.1	267.1	705.8
1475	K35	309	99.1	23.7	27.8	23.6	14	166.1	132.2	52.6	86.7	272.9	711.9
1480	K34	303	79.5	23.9	27.8	17.4	13.2	155.3	125.2	54.9	76.5	264.1	706.5
1485	K33	312	91.5	24.2	28.1	23.7	16.9	159.6	127	51.6	78.9	287.9	698.7
1490	K32	301	106.7	27.2	30	23.6	16.7	172	128.2	49.3	81.5	315.8	739.4

1495	K31	252	107.9	30.9	29.2	28.1	20.5	189.7	139.3	46.9	96	335.6	825.8
1500	K30	294	118.3	27.2	30.3	23.4	14.7	179.3	127.5	50.3	83.5	303.1	767.3
1505	K29	379	117.7	23.3	31.2	27.9	17.8	171.1	117.5	62	76.1	270.2	757
1510	K28	374	124	25.7	29	22.5	14.9	167.1	113.6	53.7	79.1	260.8	720.1
1515	K27	399	142	26.6	29.1	23.8	16.4	154.5	134.3	62.9	86.8	297.5	692.5
1520	K26	419	144.8	26.1	27.9	22.8	15.8	152.5	129	54.9	93.7	303.4	673.3
1525	K25	496	162.3	26.7	27.9	21.9	16.1	154.5	132.8	58.4	96.2	290.5	700.9
1530	K24	840	185.9	26.4	26	21.5	15.2	151.8	133.7	63.8	91	288.3	691.2
1535	K23	351	129.6	25.2	23.7	19	14	128.5	122.9	60.8	72.4	288.9	618.4
1540	K22	384	127.7	24.2	27.7	19.6	14.8	150.9	135.8	65.3	144.6	294.5	738.9
1545	K21	444	126.6	24.3	26.4	19.5	17	143	128.2	71.6	145	278.4	697.1
1550	K20	426	119.5	28.2	25.9	18.1	16.8	137.1	125.9	67.1	139.4	299.5	680.7
1555	K19	391	161.8	24.2	26.4	20.8	13	153.9	135.7	66.6	135.2	283.2	731.3
1560	K18	428	190.2	30.1	30.2	23.1	17	182.5	144	53.9	195.8	305.1	812.6
1565	K17	830	224.4	32.5	30.3	28.5	27.4	188.5	132.4	60.8	110.7	312.5	764.5
1570	K16	651	237.2	31	33.2	31.9	24.5	207.1	143.4	64.2	132.4	324.3	831.2
1575	K15	726	296	34.4	36.5	24.7	28.5	211.6	146.9	69.1	142.7	368.9	836.7
1580	K14	1300	306.2	37.6	34.2	40.1	39.2	202.7	138.8	74.8	129.1	375.1	806.1
1585	K13	972	282	34.9	30.3	24	34.9	191.6	127.6	67.4	120.2	354.8	744.8
1590	K12	1248	271.3	33.9	33.7	26.2	35	199.6	135.9	84.1	127.3	333.1	796.8
1595	K11	717	295.7	34.6	32.1	23.3	30.9	190.6	130.1	76.4	109.3	341.5	746
1600	K10	1266	281.2	37.2	32.6	22	32.4	188.8	128.8	80.4	102.5	340.6	729.9
1605	K9	1487	299	41.4	32.4	37.3	31	212.3	139.5	81.6	120.5	369.2	819
1610	K8	540	295.4	37	37	30.6	28.1	217.2	146.8	79.3	113.1	351	840.1
1615	K7	568	289.8	34.8	36.4	33	24.6	207.1	139.9	73.6	106.9	336.9	811.1
1620	K6	625	320.2	38.6	34.2	33	29.4	203.3	136.4	76.3	95.2	359.3	792.6
1625	K5	481	247	36.2	35.2	29.3	23.2	189.4	126.3	82.1	87.4	323.3	749.8
1630	K4	580	285.7	38.1	36	27.3	27.9	202.6	130.3	79.3	90.8	348.8	773
1635	K3	613	313.3	38.3	31.2	33	28.7	192.5	125.4	82.8	101.5	339.5	758.1
1640	K2	2011	335	38.7	34.8	27.9	34.8	202.3	130.8	93.1	100.1	355.4	777.4
1645	K1	4900	378.4	46.6	30.7	31.3	49.2	189.2	126.2	91.9	101.3	409.8	736.7
1650	KL63	378	245.2	34.3	43.2	43.3	46.8	255.5	111.1	35.2	103.4	440.6	1015
1655	KL61	402	240.6	34.4	38.3	57.4	39.8	260.4	112.7	28.6	142.3	511.2	1055.3
1660	KL59	433	283.6	31.7	39.7	40.9	50	262.5	121	28.1	103.6	403.7	1046.5
1665	KL57	432	330.9	37.9	33.7	51.3	45	259.1	121.8	31.9	115.8	403.1	1053.7
1670	KL53	527	244.6	37.7	34.7	41.5	43.3	256.3	113.4	33.5	111.1	434.6	1020.1
1675	KL51	567	224.6	47	32.9	33.7	44.2	272.9	123.7	35.4	108.9	411.2	1085.9
1680	KL49	582	248.2	37.4	31.2	44.1	43	263.5	115.1	32.2	100.6	432.4	1027.9
1685	KL47	574	273.3	39.9	37.4	46.6	47.4	244.6	111.6	30.1	102.8	441.8	1008.4
1690	KL46	409	301.6	44.9	42	34.9	51	243	110.5	24.8	129.7	418.3	984.9
1695	KL45	433	338.4	47.5	43.1	37.9	45.7	268.1	116.7	28.1	93.7	435.5	1052.5
1700	KL43	382	336.4	46.1	40	44.8	33.2	262.6	110.7	28.9	123.2	501.6	1051.5
1705	KL41	585	297.4	49.7	39.7	38.1	45.4	260.7	118.9	29.7	109.8	447.3	1013.9
1710	KL40	457	265.3	45.1	47.1	40.1	51.8	267.6	121.8	30.4	107.8	407.4	1066.1
1715	KL39	895	292.2	49.5	40.4	37.4	32.1	263.3	126.7	33.3	88.7	409.6	1029.6
1720	KL37	651	208.8	47.3	43.7	44.2	41.8	267.9	125.3	22.8	152.5	423	1093.8
1725	KL35	471	296.8	38.6	43.8	48.2	43.1	260.7	118.9	28.1	131.3	426.8	1037.8
1730	KL33	562	304.2	49.3	41.2	57.6	39.8	268.5	119.3	35.9	123.4	499.6	1080.2
1735	KL31	559	279.6	44	45.3	44.6	42.8	261.4	123.8	28.2	124.1	425.2	1055
1740	KL30	1528	429.8	51.4	40.1	41.2	38.2	238.9	118.3	35.4	123	400	959.2
1745	KL29	535	299.9	51.6	46.3	40.3	44.3	252.8	118.4	30.4	107.8	417.7	1019
1750	KL28	1498	331.7	45.9	38.7	34.3	41.3	235.9	122.3	33	116.3	413.2	967.4
1755	KL27	558	308.6	51.9	41.6	36.9	44	226.1	119.9	37.9	116.2	407.6	918.6
1760	KL26	732	337.7	50.1	43.9	34.9	23.2	218.1	126.3	54.4	117.7	407.1	895.2
1765	KL25	1392	386.5	50.3	43.2	43.3	44.4	283.6	121.8	34.1	128.2	521.5	1158.3
1770	KL23	431	338.2	47.6	44.4	29.4	25.7	205.8	125.3	63.2	119.1	421.9	824.6
1775	KL20	1051	339.1	54.6	39.3	29.3	25.2	215.8	133.6	52.4	121.3	425.1	883
1780	KL17	630	312.5	48.8	42.2	37.6	23.3	217	119.5	46.9	71.8	397.2	869.6
1785	KL16	486	289.8	44.4	44.3	35.7	17.4	249.1	125.7	48.3	91.5	349.5	1002.4
1790	KL15	1412	396	56.1	38.5	36.1	18.6	259	124.9	46.5	99.2	402.6	1038.6
1795	KL13	1473	414.5	50.6	39.9	32.1	23.5	272.8	131.9	39.7	114	435.7	1098.4
1800	KL11	611	228.9	45.2	42.8	52.1	42.4	266.1	115.5	35.3	123.5	498.5	1063.7
1805	KL9	703	335.3	53.7	44.7	45.5	32.7	286.6	114.1	31.3	109.6	555.3	1139.6
1810	KL7	907	264.2	46.2	43.1	40	36.4	271.4	118	31	103.4	472.7	1058.3
1815	KL5	635	227.1	52.6	42.9	53	47.5	261.6	114.5	37.5	111.4	454.1	1062.5
1820	KL4	1086	299.5	54.8	40.6	49.7	43.9	254.9	117.7	29.3	113.5	396	1026.2
1825	KL3	342	249.8	48	38.8	53.5	44.4	265.3	121.5	28.7	119.1	424.5	1037.3

1830	KL1	431	333.8	54.2	40.9	47.3	42.1	271.9	116.2	36.8	98.9	434.5	1098.4

Depth cm	Sample	CIA	Si/Al	CaO/Al	Zr/Rb	Ti/Al	Ti/Zr
0	144	74.55130654	2.563915541	0.110793479	10.61325967	0.11546875	13.84903696
10	143	73.70804353	2.669757358	0.116670056	9.460618146	0.130703971	15.26188218
20	142	72.68252011	3.141499218	0.126944495	10.37953795	0.127241036	10.15500795
30	141	76.45361519	3.214269347	0.098778621	14.38016529	0.093777355	8.091954023
40	140	69.45442824	3.074193872	0.104643813	12.36434868	0.106001946	8.631970849
50	139	71.68063995	3.298754307	0.121885395	12.75258621	0.100020263	6.673426621
60	138	80.9929918	3.023880655	0.105601319	13.55694981	0.101141509	7.633321467
70	137	69.57094478	3.293088959	0.112850652	13.51098376	0.100192698	6.983599604
80	136	76.97100979	3.387062648	0.117732625	12.25451419	0.105522541	7.226354196
90	135	67.5818206	3.307469948	0.134096068	10.55460993	0.116932447	7.095148502
100	134	62.60846021	3.601254013	0.135804042	9.095723014	0.133357058	8.390804598
110	133	71.43553219	3.377493015	0.094752302	12.70687936	0.105064516	7.666535896
120	132	68.68344831	3.331540528	0.1140684	10.1147541	0.110994595	9.244552494
130	131	65.7395215	4.14578501	0.123010108	8.924841772	0.121386139	8.694264693
140	130	71.96488029	3.631526668	0.113258479	9.785653288	0.100628445	7.964918405
150	129	74.44917236	3.663928327	0.11973669	8.844351464	0.099138122	8.488977197
160	128	77.90880285	2.916645862	0.123518157	9.898969072	0.100419922	10.70922724
170	127	75.91750589	2.899316162	0.118057787	8.789189189	0.111403337	11.63591636
180	126	76.59881494	2.897985233	0.114161468	9.045534151	0.114005964	11.10261375
190	125	81.13126221	3.015880078	0.103988545	9.467996675	0.099673267	8.838454785
200	124	62.35955004	3.391801913	0.204305953	7.326666667	0.227459527	20.77456779

210	123	67.57296849	3.38408345	0.153794793	7.823757764	0.161853998	13.86126823
220	122	70.61284757	3.987227987	0.133434681	9.108593012	0.127567237	10.81795563
230	121	70.70473845	3.377633076	0.10912773	11.40454545	0.100309168	9.375249103
240	120	75.63055332	3.765903629	0.119634915	12.34005038	0.099661017	9.00183711
250	119	81.51245966	3.441992683	0.097235062	13.83956574	0.087103882	7.235247974
260	118	88.49531663	3.24863783	0.069007583	23.35174954	0.053123506	5.257886435
270	117	88.43010243	3.207488531	0.061589283	26.30660377	0.047354988	5.48951049
280	116	81.23951112	3.315714133	0.084024004	20.27726433	0.055230511	6.006381039
290	115	78.43493184	3.391832469	0.093049542	18.41691843	0.060913793	5.795603675
300	114	77.00206618	3.308149946	0.093424117	23.32490272	0.05870339	5.777796313
310	113	82.50163357	3.296978885	0.09819541	22.15204678	0.061763713	6.440513904
320	112	79.46248861	3.374258571	0.102366839	18.87205387	0.06758952	6.903657449
330	111	69.76342877	3.883147752	0.110529082	9.095813205	0.083227723	7.440913517
340	110	69.59679423	3.866768244	0.110808913	7.686261107	0.08548418	7.92885727
350	109	77.22315597	3.320471471	0.093585595	16.5377907	0.06096563	6.547723677
360	108	56.80663138	4.807252342	0.126153159	5.8	0.074078212	6.532019704
370	107	75.51485012	3.440568223	0.089362226	19.8875	0.067139153	6.103079824
380	106	73.27799619	3.343349378	0.09029323	15.38121547	0.074662162	7.938218391
390	105	75.84408601	3.365368733	0.08992997	15.75242047	0.075602716	7.819826148
400	104	61.83363796	3.931580821	0.177980747	5.012280702	0.144142857	24.72173609
410	103	59.76979278	3.924394276	0.16454409	3.754668384	0.152196891	25.1877894
420	102	76.16750509	3.647253845	0.115369844	12.29525032	0.089409091	10.26832324
430	101	75.3775085	3.653865762	0.107182534	11.84078947	0.083306524	10.35892877
440	100	71.83331455	4.015337562	0.119846051	10.00256082	0.08407045	10.9984639
450	99	81.5648099	3.169022844	0.085672733	27.42405063	0.06785077	9.653819525

460	98	77.78509059	3.317027329	0.098297697	22.19796954	0.068337553	9.25908987
470	97	80.42792188	3.266820936	0.095293686	23.12439024	0.066774194	8.514924586
480	96	83.45010202	3.349082343	0.104471929	20.3708134	0.068724662	9.55607751
490	95	75.50614312	2.307448434	0.112604897	25.2560241	0.075818815	10.38044126
500	94	80.87798155	2.435013036	0.107674339	19.47560976	0.06202351	9.251095805
510	93	72.67348462	2.773036224	0.133462446	17.65225933	0.079260355	8.94490818
520	92	75.8595283	3.191525748	0.085007597	18.99601594	0.079337411	8.16170302
530	91	80.73808536	3.199182347	0.105003095	14.90369181	0.082377049	8.659127625
540	90	77.83719652	2.491754075	0.109120917	18.59090909	0.061344464	7.421069416
550	89	80.73250592	2.264863719	0.096098733	24.0625	0.050589641	7.852813853
560	88	78.99622307	2.310451382	0.117692258	21.17403315	0.055248756	8.692759295
570	87	74.94685927	3.137138708	0.122738375	13.51766513	0.102302632	10.60227273
580	86	80.72458816	2.750355128	0.125795012	18.62289562	0.073026188	6.80618333
590	85	81.92765727	2.730166457	0.11755424	28.06373626	0.064260132	5.339494087
600	84	78.11053163	2.843550561	0.125759883	27.72813239	0.070650651	6.017563305
610	83	76.44762973	3.962162453	0.108143749	13.60606061	0.089885321	8.312652455
620	82	79.12483582	2.464977193	0.098169618	21.46863469	0.055758621	5.558611207
630	81	85.03455153	2.47370334	0.114947618	24.42456897	0.052835184	5.459278214
640	80	74.8130229	2.514894132	0.130574733	19.42956522	0.053836699	5.488721805
650	79	75.12297348	2.513234634	0.133405843	20.0285205	0.055939982	5.640797437
660	78	81.90698584	2.901567721	0.142720625	19.09075044	0.063394584	5.992321053
670	77	76.11478909	3.078161122	0.147984509	17.8513986	0.074397089	7.009107825
680	76	68.37708179	3.202148123	0.144469867	17.96613191	0.072601279	6.756622681
690	75	71.86564273	3.171480998	0.158495476	17.41783217	0.071035941	6.744956338
700	74	79.37715523	2.819780517	0.103488541	17.39175258	0.066401125	6.999604821

710	73	65.5884623	3.191896424	0.125350673	10.42477876	0.084151139	9.858113024
720	72	68.10229903	3.337172612	0.114940479	9.94549763	0.083092999	9.473433405
730	71	73.33525573	2.72062183	0.124208493	18.23921569	0.070019029	7.911201892
740	70	73.94789957	2.787739951	0.101464274	23.37452471	0.073729146	6.110614071
750	69	78.05642082	3.70636493	0.081786654	17.60212515	0.073616318	4.478502918
760	68	74.84939516	4.816617006	0.082643154	12.31707317	0.075707071	5.936633663
770	67	79.59851543	3.483322856	0.104861303	13.08737864	0.074783983	7.521195422
780	66	74.58396752	2.755136472	0.114815328	14.97791798	0.073298479	8.120261163
790	65	81.25840466	2.743813122	0.122746424	12.28054299	0.078403756	10.25546549
800	64	77.91453715	2.659882366	0.130737626	13.10865874	0.079106977	11.01411734
810	63	76.17665943	2.529981402	0.108846102	14.31952663	0.07064663	8.013429752
820	62	78.39973784	2.552334591	0.11360012	12.99423631	0.069530262	8.535151918
830	61	81.92471732	2.565098108	0.118779279	11.19011976	0.068823529	10.33043478
840	60	67.97173282	3.238673008	0.168049771	9.008908686	0.086982124	10.2249691
850	59	69.3640424	3.489622121	0.138957622	8.446019629	0.087950108	10.46998063
860	58	70.87702069	3.802335487	0.122168683	10.44174136	0.084067797	9.123237278
870	57	71.97162521	3.965480461	0.126277972	10.66981132	0.085156794	9.261083744
880	56	72.51363499	3.889348781	0.139391454	11.92105263	0.083850575	8.946529311
890	55	76.38849356	4.589498944	0.108201315	8.964247021	0.089633838	8.579888808
900	54	70.3898748	4.540913003	0.104549322	7.726156752	0.08592686	8.328037155
910	53	71.05677783	2.805926918	0.085911896	15.97691198	0.072122409	6.598627168
920	50	63.21489907	3.415671052	0.095439894	10.44024515	0.061025641	5.588494276
930	49	62.57507033	3.635789231	0.116273808	10.24475524	0.0614819	5.29985373
940	48	63.60545624	3.347499496	0.126713475	11.52030948	0.065306346	5.010913365
950	47	71.66356943	3.04052462	0.09090747	13.83224401	0.062092555	4.86060797

960	46	73.98516155	3.023179664	0.081187803	16.48639456	0.061151936	4.234921945
970	45	73.64677203	3.036660955	0.0903554	18.47138965	0.06298583	4.589910016
980	44	89.40245944	2.565763743	0.07813579	21.58112094	0.057959184	4.464188081
990	43	68.05401746	3.057032369	0.111802429	19.24281984	0.071594509	4.59972863
1000	42	67.36699531	3.441772979	0.11971442	19.70057143	0.0853349	4.212785706
1010	40	63.50508837	4.315310128	0.114423465	14.21349446	0.082851563	4.508289641
1020	39	66.97611136	4.813725755	0.087134871	15.00310238	0.078795181	4.05707196
1030	38	72.35794656	4.249717473	0.092140493	16.6286645	0.072022195	3.813907933
1040	37	65.00780137	5.129771519	0.108185967	10.90405904	0.087449857	5.164128596
1050	36	57.84174034	5.552233124	0.118274406	9.996431757	0.10025	5.725504194
1060	35	63.26472657	4.47379729	0.117036063	11.85464098	0.098526171	5.283646033
1070	34	62.8298772	4.008786833	0.157415532	9.52173913	0.119506494	7.371625411
1080	33	65.07240304	4.71744757	0.108717568	9.371826372	0.097785515	6.135628769
1090	32	51.83471051	4.171201125	0.16439205	6.954054054	0.131815681	9.311115429
1100	31	58.42055258	4.715907644	0.13872188	8.963046757	0.101090652	6.00504838
1110	30	58.81554622	5.027458817	0.135432653	10.62359063	0.106651719	5.824965303
1120	29	68.14400004	4.781014616	0.12207451	10.39054291	0.104079886	6.148660037
1130	28	64.90101887	4.780805456	0.124386141	9.608803987	0.103186969	6.297000605
1140	27	56.89498909	5.123700827	0.124997771	9.662360034	0.10139881	6.074166518
1150	26	61.61652662	5.261076609	0.116401481	9.534844668	0.100239521	5.896442409
1160	25	65.05454449	5.625925868	0.120647935	8.968698517	0.101761978	6.047024247
1170	24	55.19350908	6.281923082	0.125959243	8.322779923	0.108756388	5.923176842
1180	23	59.53451307	6.966298282	0.190457361	10.13641488	0.099001783	6.1772884
1190	22	68.66665682	5.803109351	0.153969408	10.83205269	0.102623211	6.541345764
1200	21	58.90887244	10.28904732	0.17486027	9.974625144	0.105480094	5.208140611

1210	20	58.64990656	11.28269853	0.134661309	9.647286822	0.094439024	5.185482791
1220	19	67.84033404	3.976839549	0.186055746	11.87239264	0.09173028	7.451426209
1230	18	69.84635936	4.266183107	0.218388305	11.47508691	0.095554072	7.227102898
1240	17	61.64033471	4.68850139	0.311950522	7.938679245	0.106597938	8.60130719
1250	16	60.99405426	5.617978465	0.243956654	10.26580796	0.097591125	7.024067526
1260	15	63.566759	6.644263739	0.162331105	11.25820257	0.087681895	6.56614293
1270	14	60.04020495	6.680133234	0.15478699	11.86900958	0.087770154	6.886944818
1280	13	58.34714433	6.593809622	0.153167193	10.30612245	0.088634812	6.856765677
1290	12	65.08246054	6.434997604	0.142611718	10.79160839	0.085544554	6.718506998
1300	11	64.48954146	6.576765994	0.141210608	11.08357771	0.081890547	6.532610134
1310	10	65.71978466	6.500865184	0.136188752	10.62668299	0.080243902	5.684174153
1320	9	68.95287635	2.321863143	0.243728882	6.913188648	0.313336933	70.06761652
1330	8	74.62699782	2.141232938	0.211868538	8.14213198	0.276180698	55.90191189
1340	7	71.8292556	2.16480277	0.194913999	6.940099834	0.243025937	60.6545193
1350	6	85.09256573	2.400411526	0.213308097	8.631268437	0.223261297	38.8380041
1360	5	71.33627212	2.292940018	0.151756169	5.445168295	0.166711349	37.19840479
1370	4	83.86712495	2.031568949	0.063120828	23.16287879	0.053728688	5.926410466
1380	3	82.07232566	2.754547298	0.089241907	14.41967621	0.073093972	7.120649452
1390	2	87.95186881	2.182718112	0.078548448	21.84830339	0.061049849	7.384432669
1400	1	65.28859095	3.212362954	0.138346084	7.203883495	0.119945415	10.57662688
1405	K50	69.07122812	3.306712843	0.140892564	8.099702381	0.103833505	9.28072754
1410	K48	77.11018631	2.433574162	0.181923648	4.329268293	0.167085202	37.48490946
1415	K47	89.96453873	2.278734271	0.066347979	17.07949791	0.058651772	6.216723828
1420	K46	87.98490052	2.274340245	0.059394742	26.97377622	0.046989247	3.965260224
1425	K45	80.96730147	2.671055328	0.107462337	9.191053829	0.094164502	8.971376722

1430	K44	77.77492541	3.115333967	0.109327745	8.423497268	0.092476548	7.993837172
1435	K43	67.31611482	4.605156773	0.128177718	7.503918495	0.092598802	8.075195822
1440	K42	65.13862364	5.505431546	0.138618639	7.388265746	0.092469799	8.04507766
1445	K41	66.42414379	5.903601063	0.148533272	6.909385113	0.09377809	7.818501171
1450	K40	62.89117764	5.677475403	0.130437879	9.783757339	0.078683128	5.736573657
1455	K39	48.88052719	10.87392563	0.136095393	6.080865604	0.09997807	8.539052257
1460	K38	52.45086914	8.49416342	0.166189346	5.231404959	0.109797422	9.41864139
1465	K37	57.26395913	7.107906925	0.163189995	5.184914842	0.100081301	9.627717816
1470	K36	59.02329729	6.671346542	0.170752876	5.243684993	0.101700468	9.236327572
1475	K35	57.63042453	6.46572268	0.173865212	5.385022693	0.099645062	9.070094114
1480	K34	59.46779052	6.27621032	0.173221696	5.642971246	0.096373134	9.139419674
1485	K33	62.8972318	6.027632605	0.170079293	5.501574803	0.094869942	9.396021182
1490	K32	61.76360284	5.30610772	0.174047145	5.767550702	0.093230975	9.4441439
1495	K31	65.28566935	5.104147544	0.172017003	5.928212491	0.097992177	9.101477355
1500	K30	66.40398136	5.208439775	0.166049723	6.018039216	0.091437908	9.116382119
1505	K29	63.5184053	5.38392168	0.167535855	6.442553191	0.089451138	8.826948481
1510	K28	62.03920501	5.370291498	0.169401871	6.338908451	0.09064257	9.402860714
1515	K27	61.03397287	5.667694752	0.178395759	5.156366344	0.099280677	10.16462094
1520	K26	62.4470662	5.565644847	0.171070566	5.219379845	0.099764543	10.69805436
1525	K25	60.66478962	5.600900199	0.16972752	5.277861446	0.096980609	9.990012841
1530	K24	60.20235293	5.765799093	0.173808884	5.169783096	0.100639205	10.25028935
1535	K23	58.67548011	5.783353231	0.178825456	5.031733116	0.105994021	11.46668823
1540	K22	57.31441955	5.570500677	0.164598604	5.441089838	0.105466284	9.948572202
1545	K21	59.7725928	5.708397375	0.179521301	5.437597504	0.106069869	10.45330656
1550	K20	57.83166556	5.932814758	0.198903863	5.406671962	0.118489985	11.29719406

1555	K19	59.36536349	5.613958114	0.168922129	5.389093589	0.102431259	9.678654451
1560	K18	63.05722229	4.921862197	0.179449469	5.643055556	0.123364738	11.27984248
1565	K17	65.7712429	4.224695651	0.184417607	5.774169184	0.131668712	14.03662525
1570	K16	62.03337668	3.899564051	0.183115166	5.79637378	0.141692491	14.30221367
1575	K15	68.13364813	3.457040523	0.183936777	5.695711368	0.147571116	16.12047329
1580	K14	69.23978244	3.419993568	0.19472094	5.807636888	0.147288694	16.64557747
1585	K13	65.20052906	3.375369201	0.191485242	5.836990596	0.146939891	18.05182599
1590	K12	65.96569028	3.493286576	0.178061253	5.863134658	0.143198198	15.95883534
1595	K11	66.88973386	3.431210957	0.195401111	5.73405073	0.147274725	17.96514745
1600	K10	67.31368831	3.442992936	0.184174422	5.666925466	0.141790879	17.46403617
1605	K9	69.43147414	3.429739846	0.189222215	5.870967742	0.146244444	16.07081807
1610	K8	65.94457852	3.305924792	0.180211633	5.722752044	0.142719577	16.05404119
1615	K7	67.21609721	3.332535868	0.157959788	5.797712652	0.134957447	15.64048823
1620	K6	66.35019838	3.306141517	0.188410956	5.81085044	0.149903017	17.55109765
1625	K5	68.09551778	3.333877144	0.170211073	5.936658749	0.135296566	17.34062417
1630	K4	70.18551511	3.305362553	0.178781464	5.932463546	0.145793397	17.71021992
1635	K3	63.18800632	3.397669516	0.172429213	6.045454545	0.145685841	17.37237831
1640	K2	66.00023563	3.365881745	0.18301636	5.943425076	0.14722467	17.19578081
1645	K1	67.6473005	3.38538776	0.156232938	5.837559429	0.151972362	16.42052396
1650	KL63	67.94944467	3.089693772	0.13647111	9.135913591	0.107512953	10.22167488
1655	KL61	67.25147188	3.181570545	0.134834833	9.363797693	0.117338282	10.48517009
1660	KL59	63.54567744	3.303435401	0.140136651	8.648760331	0.127671382	11.21165791
1665	KL57	67.19239761	3.053815125	0.142402724	8.651067323	0.121659708	11.06102306
1670	KL53	71.45890731	3.441263333	0.181882579	8.995590829	0.127912946	11.23517302
1675	KL51	67.32603115	3.173799844	0.211109586	8.778496362	0.161042129	13.37692237

1680	KL49	66.29350964	3.734515937	0.191028048	8.930495222	0.139299287	11.41064306
1685	KL47	78.44524742	2.557059386	0.115785952	9.035842294	0.111844749	12.14498215
1690	KL46	82.58676295	2.292618215	0.088040656	8.913122172	0.111697613	12.82668291
1695	KL45	85.45668868	2.2198656	0.0734282	9.018851757	0.104164568	11.7871734
1700	KL43	86.58204394	2.167070956	0.039807561	9.498644986	0.110071492	11.71374227
1705	KL41	83.63023181	2.280955611	0.065245902	8.527333894	0.120135135	13.15218463
1710	KL40	89.61782878	2.131200889	0.044037854	8.752873563	0.107755459	11.57302317
1715	KL39	84.28362858	2.178654275	0.03710509	8.126282557	0.113692022	11.9036519
1720	KL37	89.32511712	2.127791386	0.045846254	8.729449322	0.109680484	11.61181203
1725	KL35	77.02864575	3.114844529	0.094652721	8.728343146	0.097374872	9.185777606
1730	KL33	82.46257796	2.282012453	0.065135695	9.054484493	0.110246262	11.60433253
1735	KL31	92.82714196	2.095838578	0.062171506	8.52180937	0.103287561	12.12037915
1740	KL30	87.14456077	2.167309969	0.043257902	8.108199493	0.105960145	12.19557965
1745	KL29	87.87301432	2.108427243	0.053004021	8.606418919	0.103754181	12.17762512
1750	KL28	80.8935502	2.160035809	0.063965995	7.910057236	0.107605634	12.63593136
1755	KL27	81.88063903	2.326499252	0.066337131	7.661384487	0.107447199	12.73786196
1760	KL26	87.00827255	2.125540739	0.064069599	7.087885986	0.10616041	13.89857015
1765	KL25	87.75593027	2.184047272	0.056115722	9.509852217	0.105990741	9.882586549
1770	KL23	82.62594905	2.104560152	0.070854351	6.581005587	0.105604575	15.67547902
1775	KL20	81.35011185	2.192408604	0.060983761	6.609281437	0.107267857	13.60588901
1780	KL17	84.77685134	2.267052421	0.06652798	7.276987448	0.11061082	14.57681693
1785	KL16	82.24469482	2.084276321	0.06239626	7.974542562	0.105525452	12.82222666
1790	KL15	83.78585606	2.232925734	0.050062423	8.315452362	0.11281827	11.1775467
1795	KL13	81.03385502	2.200642571	0.057994653	8.327520849	0.106282772	10.33412236
1800	KL11	77.31098595	2.326252398	0.079752008	9.20952381	0.106228623	11.09523362

1805	KL9	79.37977105	2.132524658	0.064363428	9.987730061	0.104056848	10.6010881
1810	KL7	77.24785823	2.269976761	0.080900601	8.968644068	0.114251163	11.60540489
1815	KL5	83.93807779	2.205290667	0.073318558	9.279475983	0.110293333	11.67811765
1820	KL4	83.38367107	2.288846326	0.075671895	8.718776551	0.114619666	12.04053791
1825	KL3	78.9409503	2.186848518	0.054626751	8.53744856	0.10360181	11.03634436
1830	KL1	77.44141894	2.178942825	0.050980777	9.452667814	0.097359347	9.767844137

Appendix 3 Loss on ignition

Sample	Depth cm	LOI%
144	0	8.66379443
143	10	6.825112108
142	20	5.012235818
141	30	3.566398732
140	40	3.002964581
139	50	5.401140114
138	60	5.489698891
137	70	6.860847018
136	80	6.996219282
135	90	4.668055349
134	100	5.909949165
133	110	5.146446176
132	120	6.764722947
131	130	2.556973163
130	140	6.420701169
129	150	6.661898318
128	160	6.284248173
127	170	5.860736299
126	180	8.631463146
125	190	11.1222539
124	200	5.31405378
123	210	5.230876217
122	220	9.354244352
121	230	6.638888889
120	240	4.994967093

119	250	5.861564263
118	260	6.209498148
117	270	5.38381201
116	280	6.182484519
115	290	6.940507768
114	300	6.037220352
113	310	4.857461024
112	320	2.91558112
111	330	4.656934307
110	340	4.547667343
109	350	7.147632312
108	360	6.37481136
107	370	6.699538844
106	380	4.637616149
105	390	7.266752815
104	400	5.798294029
103	410	7.706051873
102	420	15.72115156
101	430	10.55562513
100	440	14.00557103
99	450	5.260188088
98	460	10.25487945
97	470	8.411238825
96	480	4.442969722
95	490	4.347772468
94	500	2.903954802
93	510	9.992424242
92	520	7.986498926
91	530	11.89227108
90	540	9.232102825
89	550	11.49570362
88	560	11.81940618
87	570	10.98909812
86	580	8.225165563
85	590	8.032732232
84	600	10.2155215
83	610	13.40165787
82	620	9.168719395
81	630	8.889880952
80	640	10.40621476
79	650	11.12835685
78	660	7.62461156
77	670	8.239529941
76	680	7.044576523
75	690	6.170300077
74	700	11.76620616
73	710	9.894583576
72	720	4.549734748
71	730	6.971185167
70	740	11.39012264

69	750	12.75064711
68	760	14.25861155
67	770	15.16939891
66	780	13.95990257
65	790	13.3755001
64	800	12.98360656
63	810	13.64502165
62	820	13.1097054
61	830	7.807722616
60	840	13.92621015
59	850	13.30718954
58	860	13.1952862
57	870	12.64104467
56	880	13.98001817
55	890	14.25358739
54	900	13.01640008
53	910	9.331589274
50	920	15.3463035
49	930	14.33488241
48	940	14.63493026
47	950	14.27704752
46	960	15.79203165
45	970	15.49924585
44	980	7.300546448
43	990	8.649153532
42	1000	8.437762036
40	1010	8.675739335
39	1020	8.771346121
38	1030	11.96191136
37	1040	4.806401401
36	1050	4.528457076
35	1060	6.474800611
34	1070	9.762565304
33	1080	13.10502738
32	1090	12.8560436
31	1100	13.78532009
30	1110	12.24400331
29	1120	11.79312763
28	1130	12.74455631
27	1140	10.96406276
26	1150	9.331471879
25	1160	10.17330211
24	1170	10.28254848
23	1180	9.370892019
22	1190	12.04337051
21	1200	9.922746781
20	1210	10.17198486
19	1220	8.952460616
18	1230	8.5434
17	1240	8.349697774

16	1250	7.805515239
15	1260	7.057817999
14	1270	6.102193995
13	1280	7.614145879
12	1290	7.467775468
11	1300	6.249471459
10	1310	4.067659682
9	1320	4.736413694
8	1330	6.916481719
7	1340	4.590069435
6	1350	5.702702703
5	1360	10.03020768
4	1370	8.889880952
3	1380	7.473766641
2	1390	8.977472773
1	1400	8.254319281
K50	1410	7.83879896
K47	1420	8.8935
K45	1430	8.668013128
K43	1440	6.834224599
K41	1450	7.762154076
K39	1460	1.336432702
K37	1470	5.07343159
K35	1480	5.7956
K33	1490	6.68788084
K30	1500	6.5738
K27	1510	6.102535369
K25	1520	5.798679868
K23	1530	6.150337111
K21	1540	5.170018282
K19	1550	6.09591094
K17	1560	8.154048716
K15	1570	8.149471129
K13	1580	7.9876
K11	1590	7.664070437
K9	1600	7.5698
K7	1610	7.916540975
K5	1620	7.169726489
K3	1630	7.2567
K1	1640	7.342588308
KL63	1650	5.72693754
KL59	1660	4.722971479
KL53	1670	6.055541137
KL47	1680	5.413446268
KL45	1690	3.692379038
KL41	1700	4.481908162
KL39	1710	6.759170654
KL35	1720	7.141876073
KL31	1730	7.412791674
KL29	1740	6.853907135

KL27	1750	6.461166724
KL25	1760	8.07912234
KL20	1770	8.271588662
KL16	1780	8.076715023
KL13	1790	8.372186869
KL9	1800	8.132901135
KL5	1810	8.1628
KL3	1820	8.3056
KL1	1830	8.4072

Appendix 4 Granulometry

Sample	RC 7 (very fine silt) MUD	BC2 (clay) MUD	BC2 (clay) MUD	YGC 3 (mud) MUD	GGC (mud) MUD
Facies					
Sorting	poorly	moderate	moderate	poorly	poorly
Mode	polymodal	polymodal	polymodal	polymodal	polymodal
Sorting	1.2	0.8	0.8	1.3	1.04
Mean	8.8	10	10	8.7	9.03
Skewness & kurtosis	-0.405 v coarse, platykurtic	-0.41 v coarse, 0.76 platykurtic	-0.41 v coarse, 0.76 platykurtic	-0.464, v coarse, 0.742 platykurtic	-0.426 v coarse, 0.749 platykurtic
Fine sand					
V fine sand					
V coarse silt				1.4%	
Coarse silt	6%			11.7%	1.4%
Medium silt	7.1%				7.8%
Fine silt	14.3%	5.4%	5.4%	14.3%	16.5%
V fine silt	21.4%	7.7%	7.7%	28.9%	23.2%
Clay	51.1%	86.9%	86.9%	43.7%	51.1%
Sample	**Palaeosol 5 (mud) MUD**	**Wt6 (mud) MUD**	**TC7 (mud) MUD**	**BT8 (v fine silt) MUD**	**3BT (sandymud) FINESANDYV FINE SILT**
Facies					
Sorting	poorly	moderate	moderate	poorly	V poorly

Mode	polymodal	polymodal	polymodal	polymodal	Polymodal
Sorting	1.08	0.98	0.988	1.16	2.894
Mean	9.032	8.9	9.167	8.001	6.027
Skewness & kurtosis	-0.441 v coarse, 0.807 platykurtic	-0.392 v coarse, 0.775 platykurtic	-0.282 coarse, 0.774 platykurtic	-0.308, v coarse, 0.642 platykurtic	-0.391 v coarse, 0.567 v platykurtic
Coarse sand					11.7%
Fine sand					
V fine sand					14.3%
V coarse silt				1.4%	
Coarse silt	1.4%	1.4%	1.4%	11.7%	121.4%
Medium silt	7.8%	7.8%	4.6%	14.3%	24%
Fine silt	16.5%	16.5%	7.1%	21.4%	
V fine silt	23.2%	23.2%	20.9%	24%	27.1%
Clay	51.1%	51.1%	65.9%	27.1%	

Sample	**FHC 4 (mud) MUD**	**FHC 9 (v fine silt) MUD**	**FHC 14 (v fine silt) MUD**	**FHC 19 (v fine silt) MUD**	**FHC 24 (v fine silt) MUD**
Facies					
Sorting	poorly	poorly	poorly	poorly	poorly
Mode	polymodal	polymodal	polymodal	polymodal	polymodal
Sorting	1.293	1.5	1.65	1.4	1.5
Mean	8.898	8.135	7.956	7.866	8.001
Skewness & kurtosis	-0.437 v coarse, 0. 884 platykurtic	-0.396 v coarse, 0.664 v platykurtic	-0.386 v coarse, 0.617 v platykurtic	-0.654, v coarse, 0.689 platykurtic	-0.396 v coarse, 0.664 v platykurtic
Fine sand					
V fine sand		1.4%	1.4%	1.4%	1.4%
V coarse silt	1.4%	4.6%	11.7%	11.7%	4.6%
Coarse silt	4.6%	7.1%	0.2%		7.1%
Medium silt	7.1%	14.3%	14%	14.3%	14.3%
Fine silt	14.3%	18.8%	21.4%	121.4%	21.4%
V fine silt	21.4%	26.6%	24%	32.4%	24%
Clay	51.1%	27.1%	27.1%	18.7%	27.1%
Sample	**FHC 29 (mud) MUD**	**FHC 34 (v fine silt) MUD**	**FHC 39 (v fine silt) MUD**	**FHC 44 (fine silt) MUD**	**FHC 49 (fine silt) MUD**
Facies					
Sorting		poorly	poorly	poorly	poorly
Mode		polymodal	polymodal	polymodal	Polymodal
Sorting		1.556	1.3	1.7	1.4

Mean		7.821	8.584	7.597	7.597
Skewness & kurtosis		-0.340 v coarse, 0.701 platykurtic	-0.414 v coarse, 0.746 platykurtic	-0.357, v coarse, 0.641 v platykurtic	-0.299 coarse, 0.676 platykurtic
Coarse sand					
Fine sand					
V fine sand		1.4%		6%	1.4%
V coarse silt		11.7%	1.4%	7.1%	11.7%
Coarse silt			11.7%	14.3%	0.2%
Medium silt		14.3%			14
Fine silt		21.4%	14.3%	42.5%	45.4%
V fine silt		24%	45.4%	2.9%	8.4%
Clay		27.1%	27.1%	27.1%	18.7%

Sample	**FHC 54 (fine silt) MUD**	**FHC 59 (fine silt) MUD**	**FHC 64 (fine silt) MUD**	**FHC 69 (v fine sandy silt) SANDY MUD**	**FHC 74 (v fine silt) SANDY MUD**
Facies					
Sorting	poorly	poorly	poorly	poorly	V poorly
Mode	polymodal	polymodal	polymodal	polymodal	polymodal
Grain size mean	7.328	7.507	7.731	7.014	6.610
Sorting	1.732	1.387	1.441	1.826	2.076
Skewness & kurtosis	-0.350 v coarse, 0. 625 v platykurtic	-0.263 coarse, 0.669 v platykurtic	-0.292 coarse, 0.656 v platykurtic	-0.382, v coarse, 0.647 v platykurtic	-0.408 v coarse, 0.598 v platykurtic
Medium sand				0.4%	1.4%
Fine sand	1.4%			4.3%	11.7%
V fine sand	5.7%	1.4%	1.4%	8.4%	0
V coarse silt	6%	8.8%	8.8%	8.4%	14.3%
Coarse silt	14.3%	3.2%	3%	5.9%	0
Medium silt	9.6%	14%	14.3%	21.4%	21.4%
Fine silt	35.8%	45.4%	42.5%	24%	24%
V fine silt	8.4%	27.1%	2.9%	27.1%	27.1%
Clay	18.7%	0	27.1%	0	0%
Sample	**FHC 79 (fine silt) MUD**	**FHC 84 (v fine sandy silt) SANDY**	**FHC 89 (v fine silt) MUD**	**FHC 94 (fine silt) MUD**	**FHC 99 (v fine silt) MUD**

		MUD			
Facies					
Sorting	Poorly	V poorly	poorly	poorly	poorly
Mode	polymodal	polymodal	polymodal	polymodal	Polymodal
Grain size	7.373	5.893	7.552	7.373	8.458
Sorting	1.698	2.428	1.698	1.678	1.212
Skewness & kurtosis	-0.336 v coarse, 0.650 v platykurtic	-0.405 v coarse, 0.617 v platykurtic	-0.399 v coarse, 0.650 v platykurtic	-0.329, v coarse, 0.634 v platykurtic	-0.167 coarse, 1.89 leptokurtic
V coarse sand		0.6%			
Coarse sand		5.4%			
Medium sand		7.1%			
Fine sand	1.4%			1%	
V fine sand	4.6%	35.7%	6%	5%	1.7%
V coarse silt	7.1%		7.1%	7.1%	10.2%
Coarse silt	14.3%		14.3%	14.3%	3.4%
Medium silt	9.6%	24%	0	9.6%	0
Fine silt	35.8%		42.5%	35.8%	25.%
V fine silt	8.4%	27.1%	2.9%	8.4%	28%
Clay	18.7%	0	27.1%	18.7%	31.7%

Sample	**FHC 104 (v fine silt) MUD**	**FHC 109 (v fine silt) MUD**	**FHC 114 (v fine silt) MUD**	**FHC 119 (v fine sandy silt) MUD**	**FHC 124 (v fine silt) MUD**
Facies					
Sorting	poorly	poorly	poorly	poorly	poorly
Mode	polymodal	polymodal	polymodal	polymodal	polymodal
Grain size mean	7.732	8.359	8.404	8.270	8.279
Sorting	1.786	1.448	1.536	1.516	1.151
Skewness & kurtosis	-0.430 v coarse, 0. 617 v platykurtic	-0.138 coarse, 0.729 platykurtic	-0.403 v coarse, 0.682 platykurtic	-0.396, v coarse, 0.664 v platykurtic	-0.043 symmetrical 1.094 mesokurtic
Medium sand					0
Fine sand	0			0	0
V fine sand	6%	0	0.2%	0.2%	1.7%
V coarse silt	7.1%	4.1%	5.8%	5.8%	5.3%
Coarse silt	14.3%	9%	7.1%	7.1%	8.3%
Medium silt	0	6.4%	14.3%	14.3%	0

Fine silt	21.4%	7.9%	0	18.8%	25%
V fine silt	24%	45.4%	45.4%	26.6%	28%
Clay	27.1%	27.1%	27.1%	27.1%	31.7%
Sample	**FHC 129 (fine silt) MUD**	**FHC 134 (fine silt) MUD**	**FHC 139 (v fine sandy silt) SANDY MUD**	**FHC 144 (fine sandy silt) SANDY MUD**	
Facies					
Sorting	Poorly	poorly	V poorly	V poorly	
Mode	polymodal	polymodal	polymodal	trimodal	
Grain size	7.373	7.507	7.107	6.919	
Sorting	1.637	1.698	2.015	2.248	
Skewness & kurtosis	-0.314 v coarse, 0.601 v platykurtic	-0.336 v coarse, 0.650 v platykurtic	-0.388 v coarse, 0.653 v platykurtic	-0.419, v coarse, 0.681 platykurtic	
V coarse sand					
Coarse sand				1.4%	
Medium sand			1.4%	4.6%	
Fine sand	0	1%	4.6%	7.1%	
V fine sand	2.1%	5%	7.1%	0	
V coarse silt	11%	7.1%	14.3%	14.3%	
Coarse silt	14.3%	14.3%	0	0	
Medium silt	9.6%	9.6%	21.4%	21.4%	
Fine silt	35.8%	35.8%	24	24%	
V fine silt	8.4%	20	8.9%	19.7%	
Clay	18.7%	27.1%	18.3%	7.5%	